Summer 7-31-2024

Excited State Processes in Radical Elaborated Platinum Donor-Acceptor Complexes

Sangita Paudel

Sangita Paudel

Candidate

Chemistry and Chemical Biology

Department

This dissertation is approved, and it is acceptable in quality and form for publication:

Approved by the Dissertation Committee:

Prof. Martin L Kirk Chairperson

Prof. Victor Acosta

Prof. Terefe Habteyes

Prof. Dongchang Chen

Excited State Processes in Radical Elaborated Platinum Donor-Acceptor Complexes

By

Sangita Paudel

MS Chemistry, New Mexico Tech, 2007

Dissertation

Submitted in Partial Fulfillment of the

Requirement for Degree of

Doctor of Philosophy

Chemistry

The University of New Mexico

Albuquerque, New Mexico

August, 2023

.

Dedication

To my late mother, Bhagawati Sapkota who always supported and inspired me.

ACKNOWLEDGEMENTS

First, I would like to sincerely thank my research advisor, Professor Martin Kirk for the opportunity, guidance, encouragement, and support. Thank you for mentoring and guiding me throughout this long academic journey. I always enjoyed the research chat with him.

I would like to thank the members of my research group, Dr. Jing Yang, Caroline Mangione, Dr. Ju Chen, Shiyue Gao, Dr. Ranjana Dangi, Jesse Lepluart, Joshua Mengell, Dr. Khadanand KC, Dr. Amrit Pokhrel, Dr. Munendra Yadav, Dr. Dominic Kerci and Dr. Laura Ingersol for their help and support. I am grateful to Dr. Jing Yang for helping me in data collection. I also want to thank Rajani Thapa Magar for her help and emotional support as my family has already moved to NC.

I would like to extend my sincere thanks to my committee members Prof. Victor Acosta, Prof. Terefe Habteyes and Prof. Dongchang Chen for their time, support, and suggestions to serve on my committee.

I thank my family, my husband Dr. Keshab Paudel, my kids Aseem Paudel and Abiral Paudel and my father Prem Raj Sapkota for their love and unconditional support.

Finally, I would like to acknowledge to The University of New Mexico, Department of Chemistry and Chemical Biology for the study opportunity and financial support.

Excited State Processes in Radical Elaborated Platinum Donor-Acceptor Complexes

By

Sangita Paudel

MS Chemistry, New Mexico Tech, 2007

PhD Chemistry, The University of New Mexico, 2023

ABSTRACT

Organo-transition metal complexes are being widely studied to understand their photophysical properties for their wide range of applications as efficient emitters in organic light emitting diodes (OLEDs), light emitting electrochemical cells (LEECs), etc. Cyclometalated organo-transition metal complexes such as cyclometalated square planar platinum(II) complexes are becoming suitable candidates for such applications because of their highly efficient luminescence. Understanding the excited properties of such complexes is useful in designing highly efficient and color tunable phosphors with desired excited state lifetimes. We aim to explore the influence of radical substituents on electronic structure, luminescence quantum efficiencies, and excited state lifetimes by synthesizing new radical elaborated donor-acceptor molecular frameworks built on cyclometalated square planar platinum(II) dithiolate and catecholate complexes. The novel radical elaborated molecular frameworks are designed, synthesized, characterized, and studied by numerous spectroscopic and computational methods. This study has explored the effect of an appended radical substituent on the photophysical properties of cyclometalated platinum dithiolate and catecholate complexes with respect to how the S = ½ spin doublet radical interacts with the triplet chromophore and affects the excited state lifetimes through the addition of a new exchange interaction yielding a three-spin excited state manifold. The results of experiments on the cyclometalated platinum(II) dithiolate series with two different cyclometalating ligands showed that emissive

properties of these radical substituted complexes are not lost. However, their emission lifetimes are decreased. The results of cyclometalated platinum(II) catecholate complexes demonstrated that their lifetimes are longer than that of the cyclometalated platinum(II) dithiolate series. The variation of the donors and acceptors in Donor-Acceptor Platinum(II) complexes were studied to explore their excited state properties.

Contents

List of Figures

List of Tables

Glossary

Bpy Bipyridine

Ppy Phenylpyridine

Tpy Thienylpyridine

Bdt Benzenedithiol

Cat Catechol

ND Napthalene-1,2-diol

IN Iminonitroxide

NN Nitronylnitroxide

DCM Dichloromethane

ACN Acetonitrile

EPR Electron Paramagnetic Resonance

TREPR Time Resolved Electron Paramagnetic Resonance

VT Variable Temperature

MCD Magnetic Circular Dichroism

DFT Density Functional Theory

TD-DFT Time Dependent-Density Functional Theory

CASSCF Complete Active space self-consistent field

ISC Intersystem Crossing

IC Internal Conversion

LLCT Ligand-to-ligand Charge Transfer

MLCT Metal-to-ligand Charge Transfer

ILCT Intra-ligand Charge Transfer

MC Metal Centered

LF Ligand Field

PL Photoluminescence

Chapter 1

Introduction, Statement of Research Problem, Research Design and Strategy

1.1 Introduction

A significant research effort has been given in the field of cyclometalated square planer Platinum (II) complexes for their wide range of applications as emissive probes for photochemical and electrochemical devices as well as photosensitizers, chemosensors etc.[1,2,3,4]

Cyclometalated Pt(II) complexes are also widely being investigated because of their strong emissive behavior and long luminescent lifetimes from low lying triplet states.[1,3] These cyclometalated Pt(II) complexes were first investigated during the discovery of many other compound families possessing interesting photophysical properties.[2] Von Zelewsky et al. investigated the first emissive cyclometalated platinum/palladium complexes which were homoleptic in nature[2]. Transition metal salts of Pt(II) and Pd(II) easily undergo ortho-metalation reactions with cyclometalating ligands and form five membered metallocycles[4]. Later, many luminescent heteroleptic cyclometalated metal complexes with various ligands were studied in detail.[1,3,5-7,10-13] The cyclometalation effect and heavy atom effect make them suitable candidates as very efficient phosphorescent luminophores.[3,5,6,7] In general, due to the strong σ-donor and π-acceptor abilities of cyclometalated ligands bound to Pt ions, their electronic spectra have bands usually located in the near UV region of the spectrum and their energies are a function of the strong ligand field of Pt(II) complexes with Pt-C bonds. Strong Pt spin-orbit coupling (SOC)

allows for efficient intersystem crossing (ISC) to low-lying triplet states that display a high photoluminescence quantum yield.[5] This same SOC can ultimately be used to modulate radiative and non-radiative excited state lifetimes. As a result of their excited state electronic structure, they are found to be important for many applications such as solar cells[7], chemical sensors and electroluminescent emitters in organic light emitting diodes (OLEDs).[1,5] Currently, these organic light emitting diodes (OLEDs) are increasingly a leading target in the field of organic displays and lighting technologies, with the aim of utilizing all the electrogenerated excitons.[1,8,9] The thermally activated delayed fluorescence (TADF) mechanism[8,9] is recently being explored as an alternative OLED light emitting mechanism to harvest all generated triplet and singlet excitons from the lowest excited singlet state in transition metal complexes (Figure 1.1).

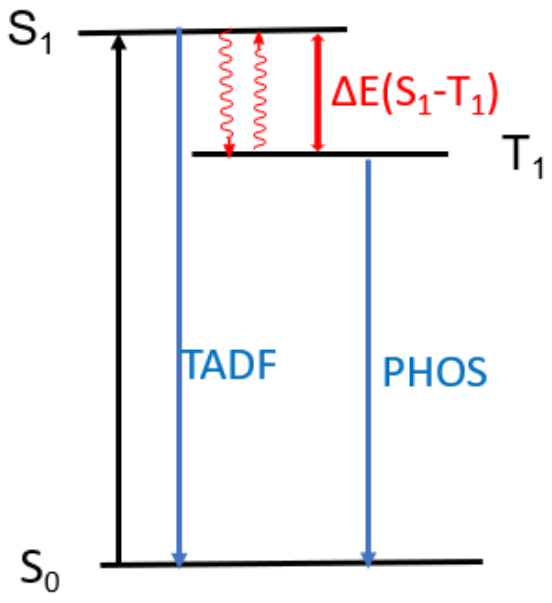

Figure 1.1: Mechanism based on thermally activated delayed fluorescence (TADF). A small energy gap (ΔE) between singlet and triplet states facilitates the TADF process over phosphorescence (PHOS).

The most studied square planar cyclometalated Pt(II) complexes are those with the general formula (C^N)Pt(O^O), where C^N represents 2-phenylpyridine or 2-thienylpyridine, and O^O represents a diketonate ligand.[12] These cyclometalated platinum complexes with diketonate ligands are primarily investigated because of their thermal stability and tunable photophysical properties that depend on the nature of the cyclometalating ligand. Many of these heteroleptic cyclometalated square planar platinum complexes are strongly emissive in solution at room temperature, with long emission decay times (microseconds).[5] There are very few examples of anionic cyclometalated (C^N) complexes with dithiolates and catecholates as donor ligands.[10,12,13] One major advantage of such cyclometalated complexes is that they have relatively high energy metal centered (MC) or ligand field (LF) excited states that conspire to enhance their luminous efficiency compared to diimine (N^N) platinum complex analogs[11](Figure1.2).

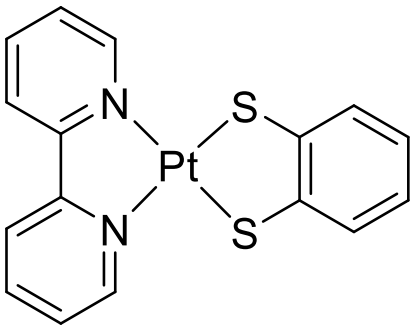

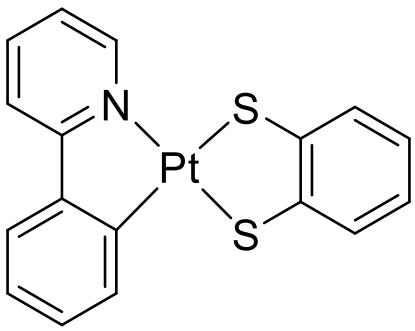

Figure 1.2: Diimine (N^N) platinum dithiolate complexes (left) and the analogous cyclometalated (C^N) platinum dithiolate complexes (right).

In (N^N)Pt(dichalcogenolene) complexes, the diamine (N^N) moiety (e.g. bipyridine) is the acceptor group, and dichalcogenolene (e.g. dithiolates, catecholates, etc.) are the donor ligands. If the emitting state (either intraligand, interligand, or MLCT) and the MC states are close in energy, the emission process will typically be quenched by fast radiation-less decay through the MC states due to thermal equilibrium between these states. Thus, a small energy gap between the lowest emitting state and a metal centered d-d or LF state is not favored for emission efficiency. The cyclometalation effect raises the energy of non-emitting MC states and thereby improves the luminescent efficiencies of these molecules (Figure1.3).

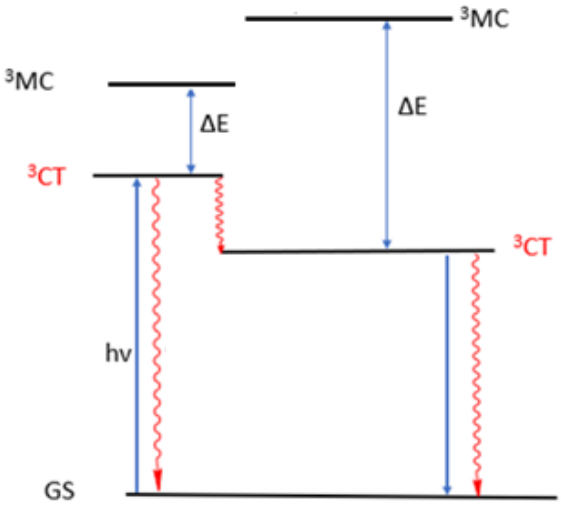

Figure 1.3: A generic diagram showing the effect of cyclometalation on increasing the ^{3}MC - ^{3}CT energy gap on metal complexes. For Pt(II) complexes, the MC states lie above the charge transfer (CT) states.[5]

Another advantage of using cyclometalating ligands with highly conjugated pyrimidinic aromatic systems is that they allow for emission tuning through molecular aggregation (i.e., π-π interactions, and hydrogen bonding). Sometimes, these anionic cyclometalated complexes with their counter-cation help to tune the photophysical properties of these molecules and increase their solubility in aqueous media for biological applications.[13]

There is also an emerging interest in the spin manipulation of dynamic processes that involve photomagnetic materials, and this includes the area of molecular spintronic.[14,15,16] Radical elaborated molecules can be used to understand electron spin-polarized states that reflect a non-Boltzmann population of m_s levels which may be useful for quantum information science (QIS) applications.[17,18,24,26] Markedly little research has focused on radical elaborated Pt (II) complexes, including the effect of an organic radical on excited state properties. Earlier studies in our laboratory have focused on radical elaborated donor-acceptor and donor-bridge-acceptor dyads with bipyridine acceptor ligands.[19,20,21,22,23] Furthermore, in the (bpy)Pt(dioxolene) complexes studied to date, the radical was placed on the donor (dioxolene) side of the complexes.[24,25,26] The parent compound of these systems using catechol donor ligands is observed to be non-photoluminescent, as shown by prior detailed studies on their photophysical properties.

Earlier studies in our laboratory principally focused on radical-elaborated forms of the (bpy)Pt(Cat) system (Figure 1.4). In this Donor-Acceptor dyad, the two lowest energy charge transfer bands are of the LL'CT type, and they involve one-electron promotions from the catechol HOMO and catechol HOMO-1 to the bipyridine LUMO.[23,27]

In the parent molecules of these systems, these excited state configurations lead to two singlet and two triplet excited states. The incorporation of an additional spin center in the radical elaborated forms of these complexes results in the singlet-triplet pair being converted into two doublets (D_{sing} (IS_i, 1/2>) and D_{trip} (IT_i, 1/2>)) states and a quartet state (IT_i, 3/2>) shown in Figure 1.5.

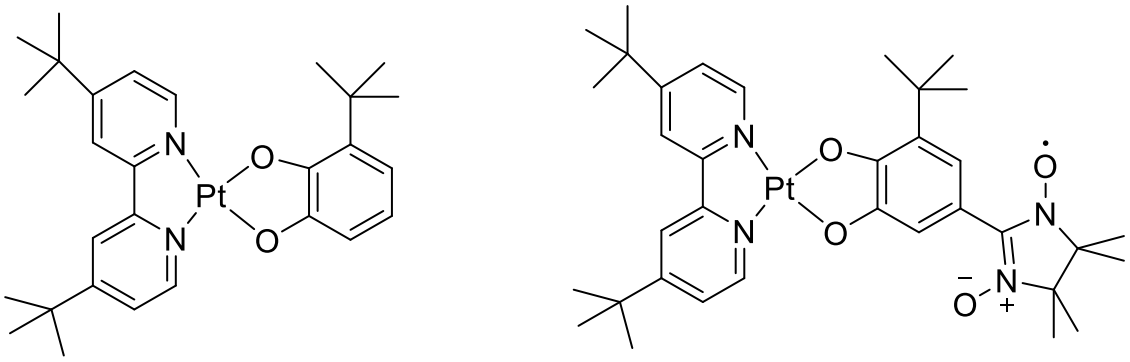

Figure 1.4: Radical elaborated systems previously studied by Kirk and Shultz groups.[24,25]

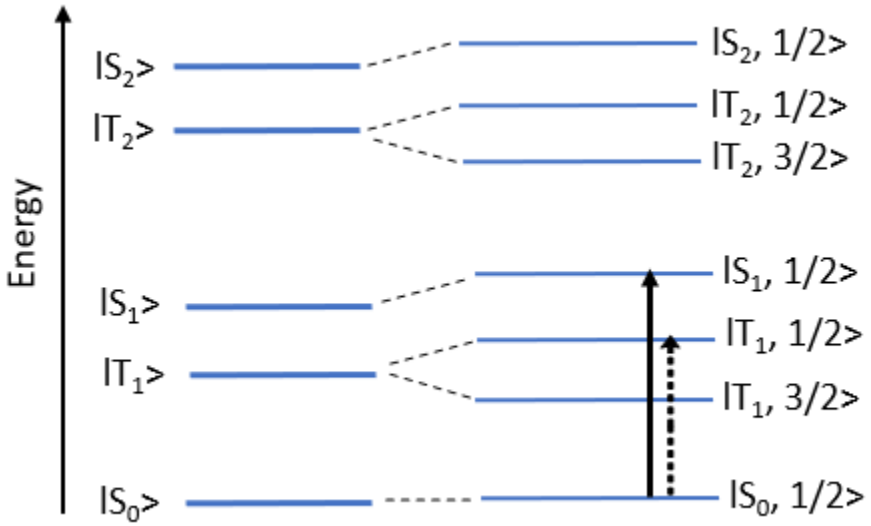

Figure 1.5: Excited state manifold for the parent molecules (left) and the radical elaborated three spin system (right) previously studied by the Kirk and Shultz groups.[24,25] Here, in the Figure, “1/2” and “3/2” indicate the total spins of the states.

Magnetic circular dichroism (MCD) spectroscopy, coupled with theoretical calculations, on the (bpy)Pt(Cat-NN) system have provided tremendous insight into the nature of their ground and excited state electronic structures, including a dramatic power-law dependence on their ground state recovery rates from the low-lying trip-doublet excited state. In marked contrast to the (bpy)Pt(dithiolene) systems, both (bpy) Pt(Cat-NN) and the parent (bpy)Pt(Cat) systems are non-emissive in nature as described in Figure 1.6.

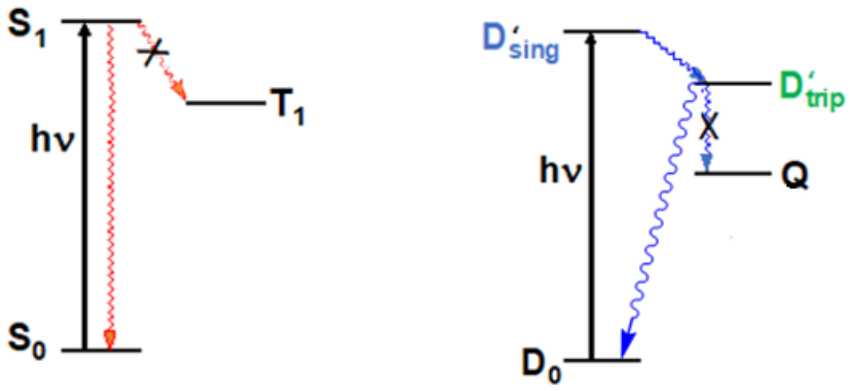

Figure 1.6: Decay mechanisms in the nonemissive parent and related radical elaborated systems, respectively.

This work on the (bpy)Pt(Cat) and (bpy)Pt(Cat-NN) systems probed their electronic structure and their excited state magnetic exchange couplings[5,24,25]. In the radical elaborated systems, due to large chromophore singlet-triplet splitting (2J), the

overall mixing of sing-doublet and trip-doublet states mediated by the nitronylnitroxide-semiquinone (NN-SQ) excited state exchange interaction was found to be very small[24]. The charge recombination lifetimes of these radical elaborated systems with different bridge fragments (e.g., phenylene, thiophene, etc. as shown in Figure 1.7) are found to be inversely proportional to mixing between the sing-doublet and trip-doublet states.

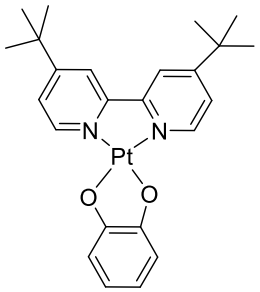

1-t-Bu
(t-Bu_2Bpy)Pt(Cat)

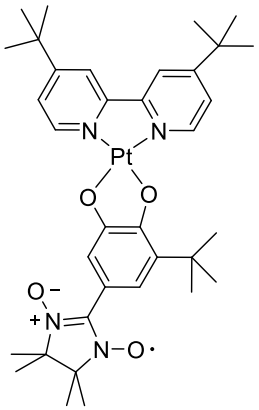

1-NN
(t-Bu_2Bpy)Pt(Cat-NN)

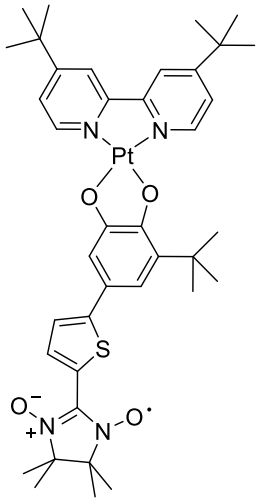

1-Th-NN
(t-Bu_2Bpy)Pt(Cat-Th-NN)

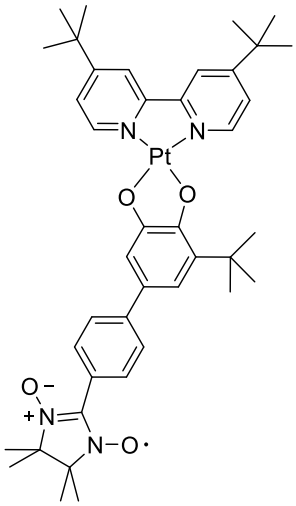

1-Ph-NN
(t-Bu_2Bpy)Pt(Cat-Ph-NN)

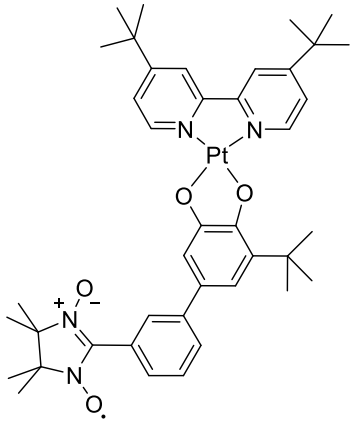

1-m-Ph-NN
(t-Bu_2Bpy)Pt(Cat-m-Ph-NN)

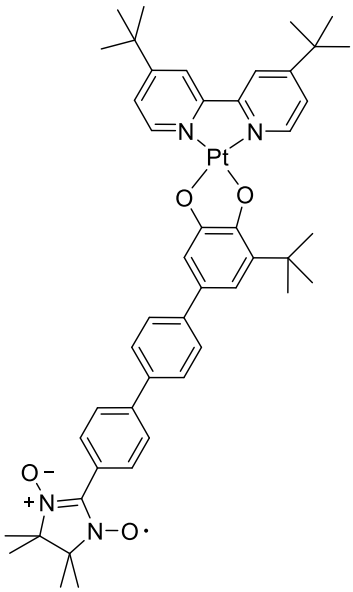

1-Ph-Ph-NN
(t-Bu_2Bpy)Pt(Cat-Ph-Ph-NN)

Figure 1.7: Radical elaborated systems, (bpy)Pt(Cat-B-NN), with different bridge (B) fragments previously studied by the Kirk and Shultz research groups.[24,25]

Here, the nitronylnitroxide-semiquinone (NN-SQ) excited state exchange interaction ($J_{SQ\text{-}NN}$) for all these radical elaborated complexes (Figure 1.7) was equated with the magnetic exchange coupling determined by magnetic susceptibility measurements for the ground state $Tp^{cum,Me}Zn$(SQ-NN) analogs.[19] The bipyridine-semiquinone (bpy-SQ) excited state exchange interaction ($J_{bpy\text{-}SQ}$ = ±1400 cm^{-1}) for the molecules in figure 1.7A was determined by MCD spectroscopy.[24] In this study, a spin Hamiltonian for this three-spin system, including two different J (exchange interaction) values, is shown in Equation 1.1. In this Equation, S_{SQ}, S_{bpy}, S_{NN} represent the three spin operators associated with the donor (SQ), the acceptor (bpy) and the nitronylnitroxide radical (NN), respectively.

$$H = -2JS_{SQ}S_{bpy} - 2JS_{SQ}S_{NN} \quad (1.1)$$

The D_{sing} and the D_{trip} wavefunctions can only mix via the exchange interaction because there is no direct spin-orbit coupling matrix elements to connect them. Once these two pairwise exchange interactions are known, the mixing coefficient (λ) of the D_{sing} and D_{trip} functions can be calculated by using a following Equation 1.2.

$$\lambda = \frac{1}{2}\ tan^{-1}\ \frac{\sqrt{3}\ J_{SQ-NN}}{2\ J_{SQ-NN} - J_{SQ-bpy}} \quad (1.2)$$

The wavefunction mixing parameters for the radical elaborated molecules were previously determined using Equation 1.1 and are presented again in Table 1.1 below.

Radical-elaborated Complex	$J_{SQ\text{-}B\text{-}NN}$ (cm^{-1})	$\lvert\lambda\rvert$	% $(\sin\lambda)^2$	D_{trip} Lifetime (ps)
1-NN	550	11.5	3.97	250
1-Th-NN	220	4.25	0.55	410
1-Ph-NN	100	1.83	0.102	640
1-m-Ph-NN	-32	0.63	0.012	790
1-Ph-Ph-NN	20	0.36	0.004	1010

Table 1.1: Wavefunction mixing parameters and D_{trip} Lifetimes for nitronylnitroxide elaborated (bpy)Pt(Cat) systems.[25]

Table 1.1 shows that the excited state exchange interaction between semiquinone (SQ) and nitronylnitroxide (NN) are different with different bridge fragments and different SQ-NN distances. The longer the distance between the semiquinone and the pendent radical, the smaller the exchange and the mixing parameters.

The experimentally measured D_{trip} lifetimes as a function of $(\sin\lambda)^2$have been fit to a phenomenological power law function shown in 1.3.

$$Y = Kx^n \qquad 1.3$$

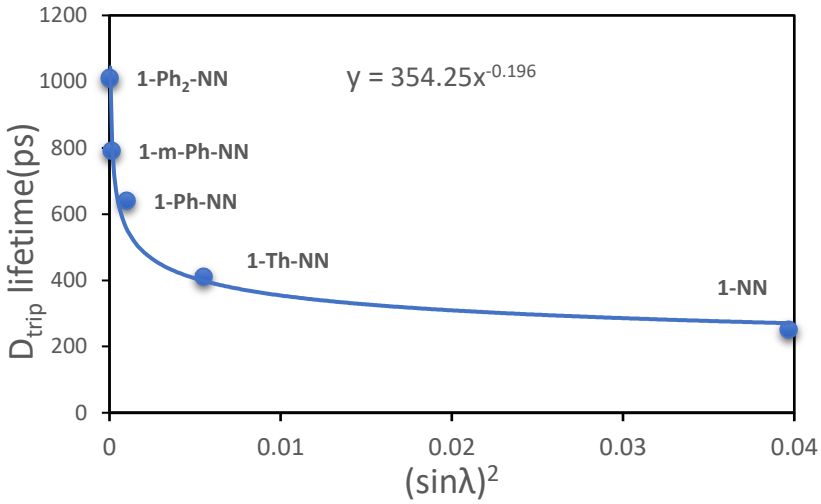

Figure 1.8: Experimentally measured D_{trip} lifetimes are shown fit to a power law function with $(\sin\lambda)^2$ for (bpy)Pt(Cat-B-NN) systems.[25]

Figure 1.8 indicates that when there is no bridge between the semiquinone and the appended radical, the D_{trip} lifetime is short. The D_{trip} lifetime increases as a function of increasing bridge length, where we observe the smallest exchange couplings between the semiquinone and the appended radical in this radical elaborated series. When the wavefunction mixing becomes very small or negligible (*i.e.* no mixing between D_{sing} and D_{trip}), then these molecules decay fast from D_{sing} state as they cannot access to the D_{trip} state by an exchange interaction mediated internal conversion (enhanced intersystem crossing[4,25,32,33]. In this case, the off-diagonal matrix element that connects the D_{sing} and D_{trip} becomes small, and the effect of pendent radical on lifetime becomes negligible.

The (bpy)Pt(Cat-B-NN) system (Figure 1.8) shows that an exchange interaction as small as 20 cm^{-1} between the pendent radical and the triplet state of the chromophore

can dramatically alter decay rates of the radical elaborated donor-acceptor molecules relative to their parent molecules. Thus, the pairwise magnetic exchange interactions in radical elaborated complexes can enable magnetic exchange coupling dependent wave function mixing, ultimately allowing for a novel mechanism to modulate excited state lifetimes.

In the case of our newly proposed radical-elaborated systems, their parent molecules are emissive in nature. We have included 1,2-benzene-dithiol (bdt) and catechol (Cat) as donor ligands to the square planar cyclometalated Pt(II) complexes in order to probe the effect of a radical on their dominant LL'CT excited states and their photoluminescent properties.

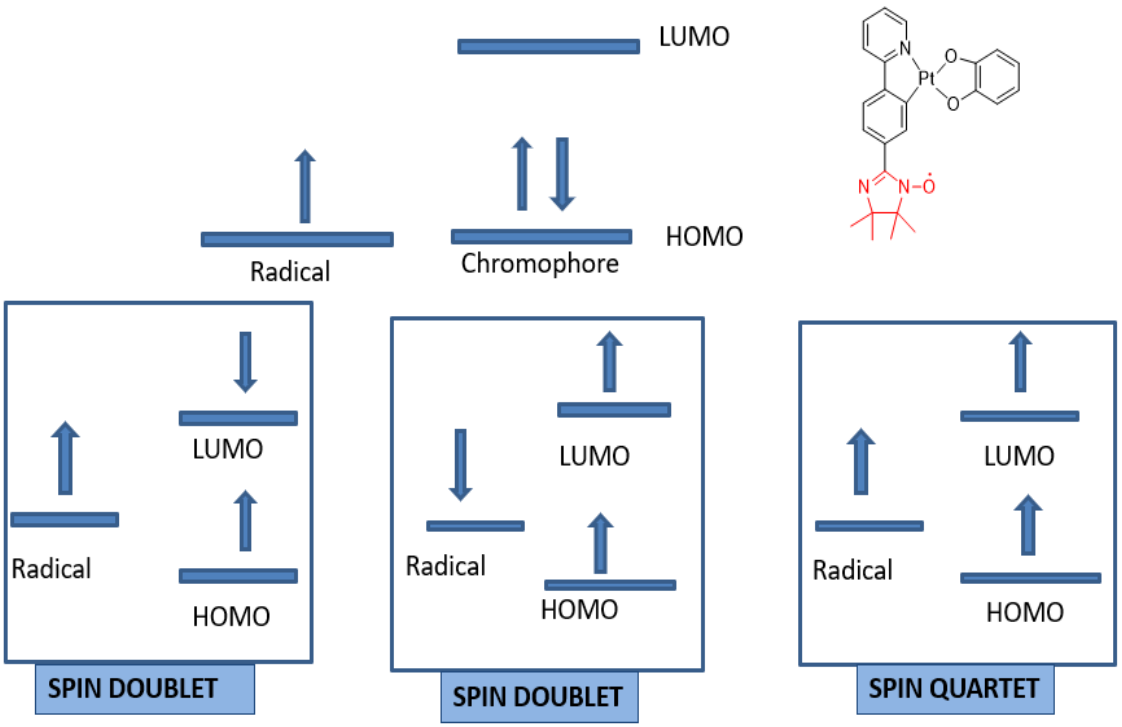

Figure 1.9: Excited state configurations when an additional spin interacts with the singlet and triplet states of a chromophore. The two spin doublets are D_{sing} and D_{trip}. There is one quartet state.

Another particularly interesting feature of our new multispin system is that the pendent radical has been placed on the acceptor (LUMO) portion of the molecule, and not on the donor side as in earlier studies.[24,25,28] Similarly, cyclometalated ligands have not yet been employed as components of radical elaborated LL'CT molecules. Thus, the spin dependent photophysical properties of cyclometalated platinum complexes have not yet been explored. We aim to understand the effect of a pendent radical on the excited state properties of these molecular charge transfer systems that consist of a localized radical covalently bound to acceptor ligand side of the cyclometalated complex. Here, we wish to explore whether the excited state spin exchange interaction will facilitate and enhance intersystem crossing rates and affect their excited state lifetimes. Another key objective of our study is to determine whether spin-orbit and spin-vibronic coupling effects[27] will play a dominant role in controlling the excited state lifetimes of cyclometalated Pt(II) dioxolenes, in addition to how an extra spin added to these complexes affects their photophysical properties and the magnitude of the excited state magnetic exchange coupling.

We have synthesized these molecules, characterized them, and determined their ground and excited state electronic structure by various spectroscopic methods such as

electronic absorption, EPR, and photoluminescence spectroscopies that have been coupled with, theoretical calculations.

1.2 Statement of Research Problem

Probe the excited state electronic structure, dynamics, and photoluminescent lifetimes of cyclometalated Pt(II) complexes that contain peripherally elaborated localized spins.

Understanding the nature of the lowest triplet excited states of cyclometalated square planar Pt(II) complexes is very useful in designing highly luminescent and color tunable phosphors with desired excited state lifetimes. We have proposed a study of new radical elaborated molecular frameworks for determining the effect of new excited exchange interactions that emerge with the presence of a pendent radical, with the added benefit of being able to probe these states with paramagnetic spectroscopic techniques.

These radical elaborated, cyclometalated, square planar Pt(II) complexes are paramagnetic with S = ½ ground states and will therefore be EPR and MCD active. As a result, we will be able to obtain detailed insight into the excited state electronic structure through spectroscopic band assignments. When these complexes are photoexcited, the radical spin will interact with the singlet and triplet excited states of the chromophore to create new excited state exchange interactions. In our study, where a pendent iminonitroxide radical is attached to a cyclometalating acceptor ligand, the spin Hamiltonian for this three-spin system is given by Equation 1.4,

$$H = -2JS_DS_A - 2JS_AS_{IN} \quad 1.4$$

Where there are two different J values that describe the $D^{+\bullet}$- $A^{-\bullet}$ and $A^{-\bullet}$- $IN^{\bullet}$ exchange interactions. Here, the S_D, S_A, S_{IN} represent the spin operators the donor, acceptor and the iminonitroxide moieties. Here, we have ignored the weaker magnetic exchange interaction between the donor ligand (dithiolate or catecholate) and the pendent iminonitroxide radical because of the large distance between the spin on the donor ligand and the spin on the pendent iminonitroxide radical.

We expect that the addition of the acceptor-radical excited state exchange interaction will allow for dramatic control over intersystem crossing rates and allow us to modify the photophysical properties of these complexes (*e.g.* lifetimes and quantum yields). Overall, our interest is to manipulate the excited state electronic structure through the incorporation of an additional spin center covalently attached to the acceptor moiety of these cyclometalated donor-acceptor platinum complexes and determine how this affects excited state lifetimes.

1.3 Research Significance, Design and Strategy

A unique strategy to explore the electronic structure and spectroscopy of luminescent systems is to elaborate them with pendant radicals. Here, we have synthesized new radical elaborated molecular frameworks built on sparsely studied cyclometalated square planar Pt(II) complexes. These molecules have been subjected to a combined spectroscopic approach utilizing EPR, electronic absorption, and various other spectroscopic methods. These combined spectroscopies are used to probe both the ground and excited state electronic structures, and are used to calibrate the results of

spectroscopic, and bonding calculations using DFT. Slightly different radical elaborated molecular frameworks[24,25,26,28] have previously been used in our laboratories to address the influence of a pendent radical on excited state properties. However, these prior systems did not undergo intersystem crossing[25,26,27]. This limits our understanding of excited states of differing spin than the ground state. This study shows that the radical elaborated cyclometalated anionic complexes are phosphorescent in nature, providing an interesting example of emission from a Kramer's spin system.[29]

Similarly, the study of these new radical-elaborated, cyclometalated Pt(II) complexes can also be used to exploit the quantum properties of molecular spin systems for molecular quantum information science (QIS) applications.[17,18,24,26] These radical-elaborated chromophores, upon photoexcitation, will allow for the S = ½ radical qubit to be exchange coupled with the open-shell spins of the photoexcited chromophores.

Our proposed research plan will also contribute to an underexplored field that involves radical elaborated molecular frameworks of emissive molecular systems. Earlier studies from our laboratories involved radical elaborated forms of the (diimine)Pt(L) series, where the diimine is a bipyridine acceptor ligand and L is a catechol (Cat) donor ligand. Here, the initial photoexcited state is a LL'CT type charge transfer state. When using a Cat ligand as the donor, these molecules do not undergo intersystem crossing to the states of different multiplicity, and they are not luminescent.[27] The prior studies also probed the electronic ground and excited state electronic structure.[24,25,26,28] However, due to the non-emissive nature of the CAT containing systems, photoluminescence measurements could not be performed to obtain a more advanced understanding of their

excited state properties. In contrast to (bpy)Pt(Cat) systems, which are non-emissive and do not undergo intersystem-crossing, cyclometalated acceptor ligands in complexes of the type, (C^N)Pt(Cat), are photoluminescent.[12,13] The cyclometalation effect[5,10,12] also provides increased thermal stability and promotes photoluminescence. Additionally, the proper choice of ancillary ligands around the metal is important[5,34]. Thus, the cyclometalation effect[5,10,12] coupled with the heavy atom effect[5,7] is expected to make our molecules better candidates for studying the role of excited state exchange interactions on the excited processes using techniques such as MCD, magneto-photoluminescence, and EPR spectroscopies. Similarly, in the radical-elaborated complexes of the type, (N^N)Pt(Cat), the excited state singlet-triplet splitting of the parent molecule was large and hence the overall mixing of the sing-doublet and trip-doublet states due to the presence of the extra spin was small.[28] We will address energy gap issues by using cyclometalated acceptor ligands to tune the relative energy gap between the trip-doublet and quartet states. Additionally, due to the LL'CT and MLCT contributions to the lowest lying charge transfer state, our radical elaborated molecular frameworks may be able to probe the effects of different pendent radicals on excited states properties. Here, we are incorporating the iminonitroxide (IN) radical as the pendent organic radical that is covalently to the monoanionic cyclometalating ligand of the emissive molecular complex. The presence of iminonitroxide radicals were accidentally discovered as byproduct[30] during the synthesis of the nitronylnitroxide (NN) radical by oxidizing the precursor molecule using sodium bicarbonate or lead oxide (PbO_2). Some studies show that the iminonitroxide radical has greater thermal stability

than the nitronylnitroxide radical.[30] Deoxygenation of nitronylnitroxide to iminonitroxide occurs easily by simply heating or with any acid derivatives (*e.g.* acid chlorides and acid anhydrides).[30]

Figure 1.10 shows the SOMO (singly occupied molecular orbital) for both iminonitroxide and nitronylnitroxide radicals. The SOMO electron density of the iminonitroxide radical is primarily delocalized within the NCNO fragment, and for the nitronylnitroxide radical delocalization is primarily within the ONCNO fragment. The Lewis structure is thus asymmetric in iminonitroxide radical and symmetric for the two dominantly contributing resonance structures of the nitronylnitroxide radical. Although their SOMO orbitals look somewhat similar, the differences in their delocalized π-system illustrate their different electronic structures.[31] The computed spin populations (Mulliken spin population analysis) on methine carbon atom of the free iminonitroxide radical and free nitronylnitroxide radical are -0.141 and -0.089 respectively (Figure 1.10). Since the magnitude of spin population on the methine carbon is slightly higher in iminonitroxide than for the nitronylnitroxide, it can be expected that there will be a larger magnetic exchange interaction between the pendent iminonitroxide radical, and excited chromophore compared to that of a covalently attached nitronyl nitroxide.[34] However, when these pendent radicals are covalently attached to donor or acceptor ligands, their position of substitution can also play a role in modifying the effective overlap between these radicals and the chromophore.[23] with an expected change in them nature of any radical-chromophore magnetic exchange interactions.

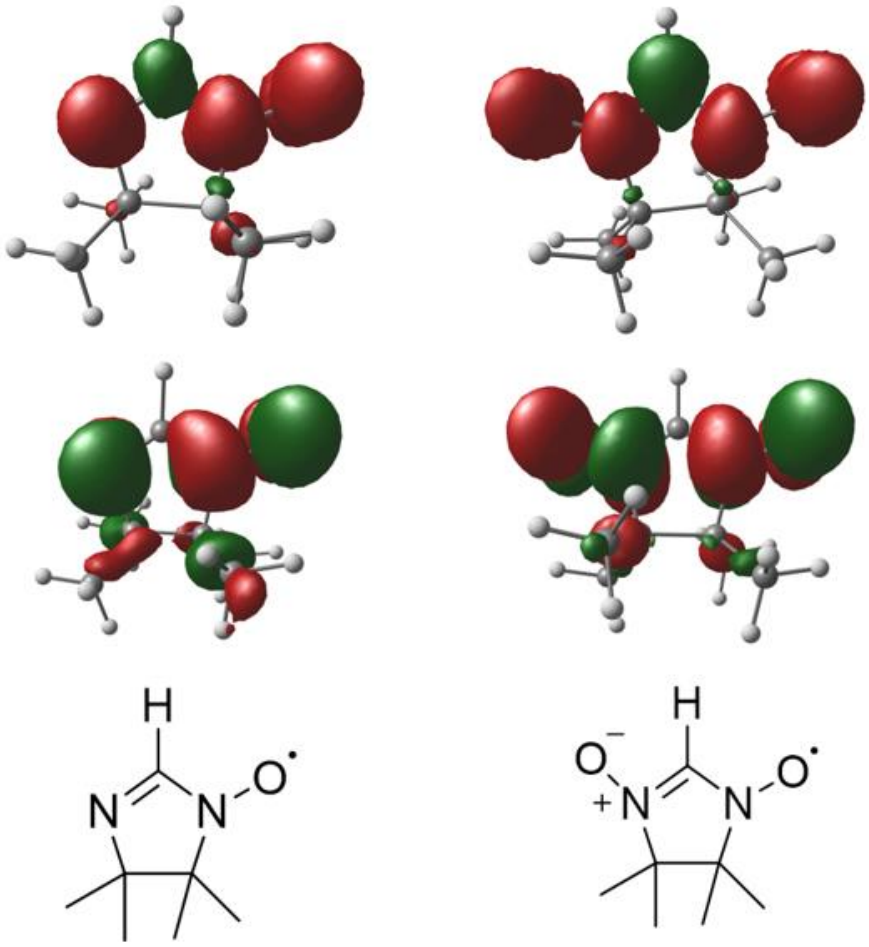

Figure 1.10: DFT computed spin densities (top; negative spin density in green, positive spin density in red) and the SOMO orbitals (middle; alpha majority orbitals) for the iminonitroxide radical (left) and the nitronylnitroxide radical (right). Bond line drawings (bottom) for iminonitroxide and nitronylnitroxide radicals.

Studies in our laboratories have incorporated a NN radical as a substituent on the donor side of non-emissive molecular complexes.[24,25,28] Here, we are incorporating a pendent IN radical as a substituent on the acceptor side of these emissive cyclometalated complexes. Building upon this concept, we are trying to explore the novel and very

interesting interactions between a doublet spin and triplet chromophore, by adding a stable organic radical on the acceptor side of these donor-acceptor LL'CT complexes.

The design criteria for our novel radical elaborated complexes is based on the parent molecular framework having thermal stability, reduced non-radiative decay rates, and varied emission properties. One of the parent molecules (molecules without a radical substituent) is already known to be a triplet emitter with a long emission lifetime (*e.g.* microseconds) in degassed room temperature solutions.[15]

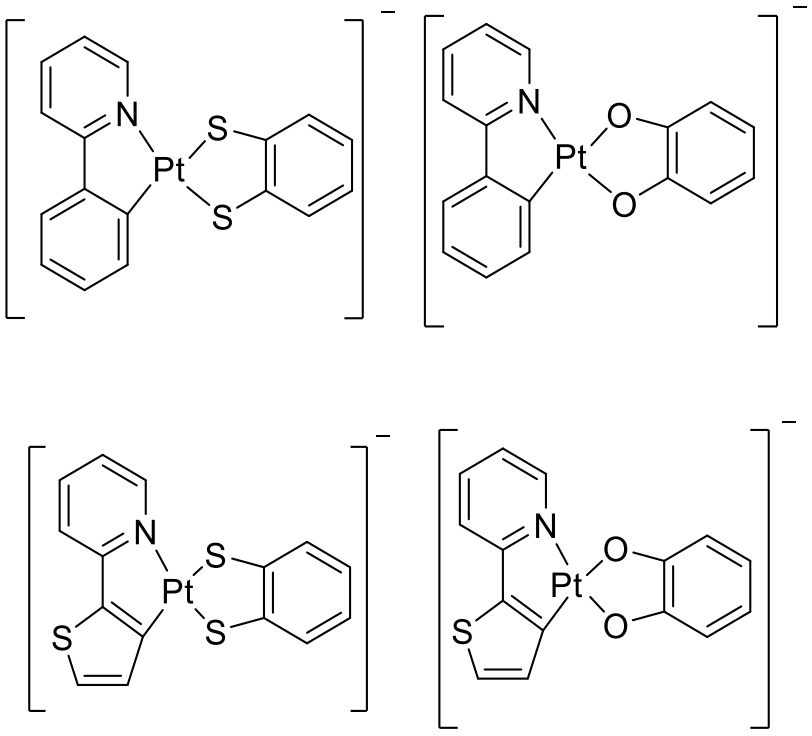

Figure 1.11: Molecular frameworks prior to radical elaboration.

We have chosen a class of complexes that have dominant LL'CT character by using strong donor ligands (*e.g.* bdt and Cat) as shown in Figure 1.11. Here, in our donor-acceptor complexes, the acceptor ligand is either a 2-phenylpyridine (Ppy) or 2-thienylpyridine

(Tpy) monoanionic cyclometalating ligand. These cyclometalating ligands form strong M-C covalent bonds with the Pt ion and this raises the energy of higher lying d-d excited states relative to their diimine counterparts.[35,36,37] Hence, our interest in these donor-acceptor types of cyclometalated compounds are also motivated in part by their improved stability[5,10] and increased luminescence efficiency due to the cyclometalation effect.

As mentioned earlier, to create charge separated excited states and study their interactions with pendent radicals, we have synthesized a new series of radical-elaborated, cyclometalated, square planar Pt(II) molecular frameworks with dithiolates and catecholates as donor ligands (Figure 1.12). We also included radical-elaborated cyclometalated platinum diketonate (acac) complexes in our computational studies (CASSCF) for comparison to our novel radical substituted cyclometalated Pt-bdt/Cat series.

Detailed studies of these iminonitroxide-elaborated, NBu_4^+ salts of anionic cyclometalated Pt(II) complexes with the dithiolate and catecholate ligands are presented in Chapters 2 and 3, respectively.

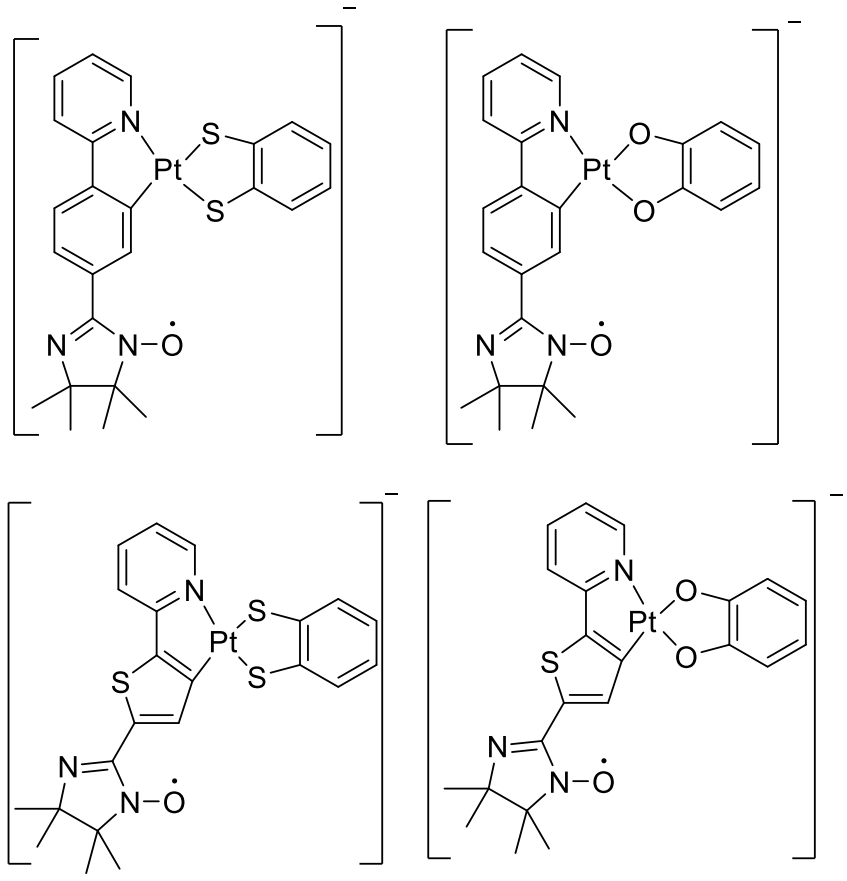

Figure 1.12: Radical elaborated target molecules under study.

1.4 References.

1. Yersin, H.; Rausch, A. F.; Czerwienic, R.; Hofbeck, T. and Fisher, T. The Triplet State of Organo-Transition Metal Compounds. Triplet Harvesting and Singlet Harvesting for Efficient OLEDs. *Coordination Chemistry Reviews.* **2011,** 255, 2622-2652.

2. Maestri, M.; Sandrini, D.; Balzani, V.; Chassot, L.; Jolliet, P. and Zelewsky, A. V. Luminescence Orthometallated Platinum(II) Complexes; *Chemical Physics Letters* .**1985**,122,375-379
3. Yersin, H.: Triplet Emitters for OLED Applications. Mechanisms of Exciton Trapping and Control of Emission Properties. *Top Curr. Chem.,* **2004**, 241, 1-26.
4. Mdleleni, M. M.; Bridgewater, J. S.; Watts, R. J.; Ford, P.C. Synthesis, Structure, and Spectroscopic Properties of Ortho-Metalated Platinum(II) Complexes. *Inorg. Chem.* **1995**, 34, 2334-2342
5. Brooks, J.; Babayan, Y.; Lamansky, S.; Djurovich, P.; Tsyba, I.; Bau, R. and Thompson, M. Synthesis and Characterization of Phosphorescent Cyclometalated Platinum Complexes. *Inorganic Chemistry* **2002,** 41, 3055-3066.
6. Bossi, A.; Rausch, A.; Leitl, M.; Czerwieniec, R.; Whited, M.; Djurovich, P.; Yersin, H. and Thompson, M. Photophysical Properties of Cyclometalated Pt(II) Complexes: Counterintuitive Blue Shift in Emission with an Expanded Ligand Pi System. *Inorganic Chemistry*, **2013**, 52, 12403-12415
7. Kozhevnikov, D.; Kozhevnikov, V.; ShafiKov, M.; Prokhorov, A.; Bruce, D. and Willams, J. Phosphorescence vs Fluorescence in Cyclometalated Platinum(II) and Iridium(III) Complexes of (Oligo)thienylpyridines. *Inorg. Chem.* **2011**, 50, 3804-3815.
8. Xu, S.; Yang, Q.; Wan, Y.; Chen, R.; Wang, S.; Si, Y.; Yang, B.; Liu, D.; Zheng, C. and Huang, W. Predicting intersystem crossing efficiencies of organic molecules for thermally activated delayed fluorescence. *J. Mater.Chem. C.* **2019**,7,9523-9530.

9. Pander, P.; Zaytsev, A. V.; Sil, A.; Williams, J. A.; Lanoe, P-H.; Kozhevnikov, V. N. and Dias, F. B. The role of dinuclearity in promoting thermally activated delayed fluorescence (TADF) in cyclometalated N^C^N-coordinated platinum(II) complexes. *J. Mater.Chem. C.* **2021**, 9, 10276-10287.
10. Julia, F.; Jones, J. and P. Gonzalez-Herrero. Synthesis and Photophysical Properties of Cyclometalated Platinum(II) 1,2-Benzenedithiolate Complexes and Heterometallic Derivatives Obtained from the Addition of $[Au(PCy_3)]+$ Units. *Inorg. Chem*. **2012**,51, 5037-5049
11. Moussa, J.; Chamoreau, L.; Esposti, A.; Gullo, M.; Barbieri, A. and Amouri, H. Tuning Excited States of Bipyridy; Platinum(II) Chromophores with Pi-Bonded Catecholate Organometallic Ligands: Synthesis , Structure, TD-DFT Calculations, and Photophysical Properties. *Inorg. Chem.* **2014,** 53, 6624-6633.
12. Mousa, J.; Loch, A.; Chamoreau, L.; Esposti, A.; Bandini, E.; Barbieri, A. and Amouri, H. Luminescent Cyclometalate Platinum Complexes with Pi-binded Catecholate Organometallic Ligands. *Inorg. Chem.* **2017**,56, 2050-2059.
13. Ricciard, L.; Deda, M. L.;Lonescu, A.; Godbert, N.; Aiello, L. and Ghedini, M. Anionic cyclometallated Pt(II) square-planar complexes: new sets of highly luminescent compounds*, Dalton Trans*.,**2017**, 46, 12625-12635
14. Wolf, S. A.; Awschalom, D. D.; Buhrman, R. A.; Daughton, J. M.; von Molnar, S.; Roukes, M. L.; Chtchelknova, A. Y. and Treger, D. M. Spintronics: A Spin-Based Electronics Vision for the Future. *Science* **2001**, 294, 1488-1495.

15. Herrmann, C. and Elmisz, J. Electronic communications through molecular bridges. *Chemm. Commun*. 2013,,49, 10456-10458.
16. Shultz, D. A. and Kirk, M. L. Molecular spintronics: a web themed issue. *Chem. Commun* , **2014**, 50, 7401.
17. Wasielewski, M. R.; Forbes, M. D. E.; Frank, N. L.; Kowalski, K.; Scholes, G. D.; Yuen-Zhou, J.; Baldo, M. A.; Freedman, D. E.; Goldsmith, R. H.; Goodson, T.; Kirk, M. L.; McCusker, J. K.; Ogilvie, J. P.; Shultz, D. A.; Stoll, S. and Whaley, K. B. Exploiting chemistry and molecular systems for quantum information science. *Nat. Rev. Chem*. **2020**, 4, 490-504.
18. Harvey, S. M. and Wasielewski, M. R. Photogenerated Spin-Correlated Radical Pairs: From Photosynthetic Energy Transduction to Quantum Information Science. J. Am. Chem. Soc. 2021, 143, 15508-15529.
19. Kirk, ML.; Shultz, DA.; Stasiw, DE.; Lewis, GF.; Wang,GB.; Brannen, CL. *et al.* Superexchange Contributions to Distance Dependence of Electron Transfer/Transport: Exchange and Electronic Coupling in Oligo(para-Phenylene)- and Oligo(2,5-Thiophene)-Bridged-Donor-Bridge Acceptor Biradical Complexes. *J Am. Chem. Soc.* **2013**, 135(45)**,** 17144-17154.
20. Kirk, ML.; Shultz, DA.; Habel-Rodriguez, D.; Schmidt, RD. and Sullivan, U. Hyperfine Interaction, Spin Polarization, and Spin Delocalization as Probes of Donor-Bridge-Acceptor Interactions in Exchange-Coupled Biradicals. *Journal of Physical Chemistry B,* **2010**, 114(45), 14712-14716.

21. Kirk, ML.; Shultz, DA.; Depperman, EC.; Habel-Rodriguez, D. and Schmidt, RD. Spectroscopic Studies of Bridge Contributions to Electronic Coupling in a Donor-Bridge-Acceptor Biradical System. *J. Am. Chem. Soc.* **2012**, 134(18),7812-7819.

22. Kirk, ML.; Shultz, DA.; Depperman, EC. and Brannen, CL. Donor-Acceptor Biradicals as Ground State Analogues of Photoinduced Charge Separated States. *J. Am. Chem. Soc.* **2007**, 129(7)**,**1937-1943.

23. Kirk, ML and Shultz, DA. Transition Metal Complexes of Donor-Acceptor Biradicals*. Coordination Chemistry Reviews* **2013**, 257, 218-233.

24. Stein, B. W.; Tichnell, C. R.; Chen, J.; Shultz, DA and Kirk, ML. Excited State Magnetic Exchange Interactions Enables Large Spin Polarization Effects; *J. Am. Chem. Soc.* **2018**, 140, 2221-2228

25. Tichnell, C.R.; Daley, D.R.; Stein, B.W.; Stultz, DA.; Kirk, M L., and Danilov, E.O.; Wave Function Control of Charge-Separated Excited-State Lifetimes. *J. Am. Chem*. *Soc*. **2019**, 141, 9,3986-3992

26. Kirk, M. L.; Shultz D, A.; Chen, J.; Hewitt, P.; Daley, D.; Paudel, S.; Est, A. Vd. Metal Ion Control of Photoinduced Electron Spin Polarization in Electronic Ground States*. J. Am. Chem. Soc*.**2021**, 143, 10519-10523.

27. Yang, J.; Kersi, D. K.; Giles, L. J.; Stein, B. W.; Feng, C.; Tichnell, C. R.; Shultz, DA and Kirk, ML. Ligand control of donor-acceptor excited -state lifetimes. *Inorg. Chem*. **2014**, 53, 4791-4793.

28. Stein, B.W. The Electronic Structure of the Pyranopterin Dithiolene Cofactor and Radical Reporters of Excited state Interactions. Disseration, 2015.

29. Cho, E.; Coropceanu, V. and Breadas, J.-L. Organic Neutral Radical Emiiers: Impacts of Chemical Substitution and Electronic-State Hybridization on the Luminescence Properties. *J. Am. Chem*. *Soc.* **2020**, 142, 17782-17786.

30. Ullman, E.F; Call L. and Osiecki J. H.; Stable free radicals. VIII. New imino, amidino, and carbamoyl nitroxies. *J. Org. Chem*. **1970**, 35, 3623.

31. Beaulac, R.; Luneau, D.; Reber C.; The emitting state of the imino nitroxide radical. *Chem. Phys. Lett*. **2005**,405, 153-158

32. Teki, Y.; Excited-State Dynamics of Non-Luminescent and Luminescent π-Radicals. *Chem. Eur. J*. **2019,** 25, 1-18.

33. Wang, J.; Zhao, J.; Barbon, A.; Toffoletti, A.; Liu, Y.; An, Y.; Xu, L.; Karatay, A.; Yaglioglu, H. G.; Yildiz, E. A. and Hayvali, M. Radical-Enhanced Intersystem Crossing in New Bodipy Derivatives and Applications for Efficient Triplet-Triplet Annihilation. *J. Am. Chem*. *Soc*. **2017**,139, 7831-7842

34. Khan, O. Molecular Magnetism. **1993,** VCH, New York.

35. Sesolis, H.; Moussa, J.; Gontard, G.; Utand, A.; Gullo, M. P.; Barberi, A. and Amouri, H. A unique class of neutral cyclometalated platinum(II) complexes with π-bonded benzenedithiolate: synthesis, molecular structures and tuning of luminescence properties. *Dalton Trans. Comm.* **2015**, 44, 2973-2977

36. Culham, S.; Lanoe, P-H.; Whittle, V.L.; Durant, M. C.; Williams, J. A. G.; and Kozhenikove, V. N. Highly Luminescent Dinuclear Platinum(II) Complexes Incorporating Bis-Cyclometallating Pyrazine-Based Ligands: A Versatile Approach to Efficient Red Phosphors. *Inorg. Chem*. **2013**, 52, 10992-11003.

37. Leal, J.; Dura, G.; Jalon, F. A.; Zafon, E.; Massaguer, A.; CueVas,J. V.; Santos, L.; Rodriguez, A. M. and Manzano, B. R. Luminescent cyclometalated platinum compounds with N, P, and O^O ligands: Density-functional theory studies and analysis of the anticancer potential. Appl. *Organomet. Chem*. **2023**, 37, e6983.

Chapter 2

Cyclometalated Square Planar Pt(II) Benzene-dithiolate Complexes and their Radical Elaboration

2.1 Background

Although cyclometalated square planar platinum complexes have been studied for a long time,[1,2,3,4] very few studies have been done on cyclometalated platinum(II) benzene-dithiolate complexes. Most of the prior studies were focused on (diimine)Pt(II)(dithiolate) complexes because of the presence of low-lying charge-transfer absorption bands, long-lived excited states and efficient photoluminescence.[5,36] These Donor-Acceptor type complexes are interesting due to their charge separated excited state having open shell biradical character.[1,5,27] The d^8 transition metal complexes such as Pt(II), Pd(II), and Ir(I) with diimine ligands have been extensively investigated due to their emissive nature.[5,6,7,36] Many of these metal complexes are in the form of (diimine)M(dithiolate) with the dithiolate ligands being mnt (maleonitrile dithiolate), tdt (toluene-dithiolate) or ecda (1-(ethoxycarbonyl)-1-cyanoethylen-2, 2-dithiolate).[7] The dithiolate ligands are good metal chelating agents with strong σ and π donating abilities. Only a very few cyclometalated dithiolates have been reported so far.[8,9,11,12] Among them, some neutral and some anionic Iridium cyclometalated dithiolates are known. [8,9,11,12] The electronic structure of the cyclometalated gold complex with mnt ligand was explored by density functional theory (DFT) computations to investigate the electronic structure.[7]

Anionic cyclometalated iridium(III) dithiolates were studied to investigate the effect of sulfur deoxygenation on excited state properties.[10] Platinum(II) complexes with cyclometalating ligands such as 2-phenylpyridine and 2-thienylpyridine have been studied in detail by the Yersin group because of their suitability as phosphors in organic light emitting diodes (OLEDs).[13] However, cyclometalated Pt(II) complexes with dithiolates are rarely touched upon. We can find only one study of cyclometalated dithiolate complexes where Pt(II) is involved with Ir(II) as hybrid luminescent complexes.[14] The purpose of the study was to conjoin two different chromophores for red or near-IR emission from the interchromophore charge transfer excited state. Neutral cyclometalated platinum complexes with a benzene dithiolate ligand were investigated by Sesolis, et al., but in their system, the benzene dithiolate unit was coordinated to a cyclopentadienyl-ruthenium (Cp*Ru) fragment.[15] To our best knowledge, there is only one study on mononuclear anionic cyclometalated Pt(II) dithiolate complexes by Julia, et al., where the cyclometalating ligand is phenylpyridine.[16] This research group has reported synthesis and brief photo-physics of anionic cyclometalated Pt(II) complexes with the benzene 1,2-dithiolate ligand, and phenylpyridine as cyclometalating ligand. This cyclometalated Pt(II) dithiolate complex by Julia, et al. has an intense absorption peak around 474nm assigned as π-π* transition with mixed MLCT and LL'CT character.[16]

In our study, we are the first to report the synthesis and detailed study of cyclometalated platinum dithiolate complexes with pendent organic radicals. Recently, many organic radical groups have been investigated for their application as functional magnetic materials, where nitronylnitroxide and iminonitroxide are popular radicals for

their stability and suitability to different purposes in molecular magnetism.[21,22] During our synthetic procedures, we also found that for cyclometalation reactions, iminonitroxide is the more stable radical. At the same time, cyclometalated platinum complexes have also emerged for their technological applications, which include organic light emitting devices.[13,16] It is these advances that allowed us to realize the utility of merging these two molecular systems to develop a novel radical elaborated molecular system with unique excited properties and control of the spin polarization. In this chapter, we are studying the iminonitroxide appended cyclometalated platinum dithiolate complexes shown in Figure 2.1.

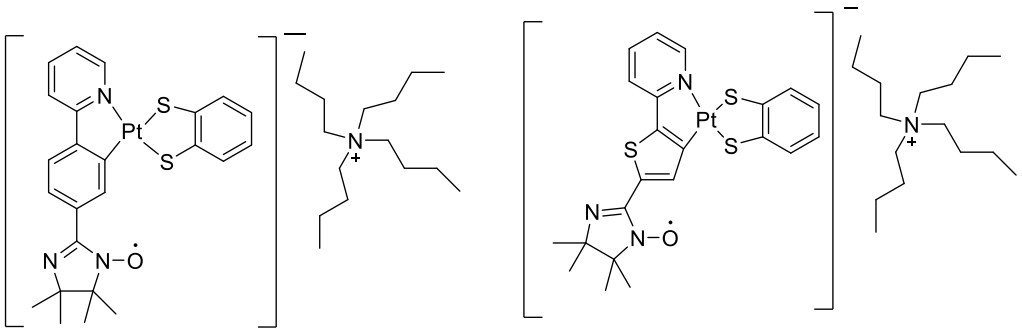

Figure 2.1: Radical elaborated cyclometalated platinum dithiolates with two different cyclometalating ligands.

2.2 Synthesis and Characterization

Cyclometalating ligands can undergo orthometalation reactions[2,3,17] with transition metal salts to form five membered metallocycles that yield a higher stability for these complexes. When these heteroaromatic cyclometalating ligands react with

platinum metal salts, they form halo-bridged dinuclear complexes, mononuclear complexes, or possibly a mixture of both. To synthesize cyclometalated square planar platinum dithiolate complexes, we have chosen two different cyclometalating ligands; 2-phenylpyridine (Ppy) and 2-thienylpyridine (Tpy). These are paired with benzene'1,2-dithiolate (bdt) as a dianionic thiolate ligand.

The Ppy and Tpy ligands are the most commonly used cyclometalating ligands to prepare cyclometalated metal complexes.[17] First, Pt(II)-dichloro-bridged dimers or monomer were prepared by using previously reported literature procedures.[16,17,18,19] These precursors for cyclometalated complexes were synthesized by heating potassium tetrachloroplatinate salt (K_2PtCl_4) with cyclometalating ligands in a 1:3 mixture of water and 2-ethoxyethanol overnight.[16,17,18,19,20] These precursors (monomer, dimer, or mixture of both) can be isolated as a yellow precipitate in water and washed several times with diethyl ether and cold chloroform. We did not characterize these precursors because of their complexity as a mixture and directly used them for the next step to synthesize the cyclometalated anionic complexes with donor ligands. Figure 2.2 shows the cyclometalating acceptor ligands and benzene dithiolate ligands for the synthesis of radical-elaborated cyclometalated donor-acceptor complexes.

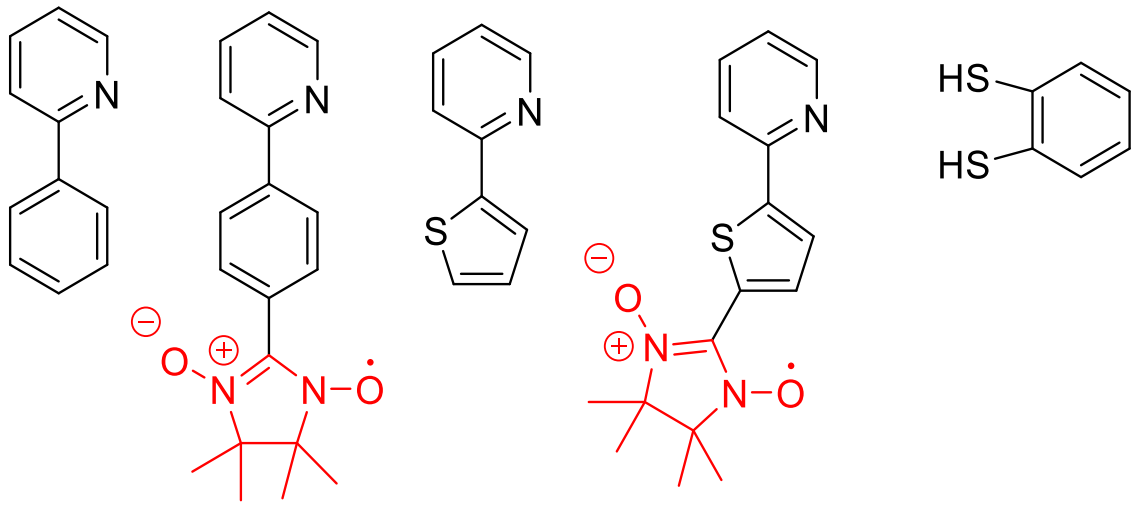

Figure 2.2: Ligands involved in our synthetic procedures.

For the radical elaborated complexes, we used radical elaborated cyclometalating ligands. We first synthesized the nitronylnitroxide elaborated ligands with 2-phenylpyridine and 2-thienylpyridine, and then these ligands were used for the cyclometalation reaction to prepare the dimer/monomer precursors. These precursors are used for the next reaction with benzene-dithiolate to obtain the final complexes. When the electron paramagnetic resonance (EPR) study of the final complexes was performed, we found that the radical species present in these complexes were iminonitroxide and not nitronylnitroxide. In all sample reactions, we found that the reaction products were the anionic complexes with an iminonitroxide radical. So, we followed the same procedures for all radical elaborated complexes to get the Pt(II) complexes with iminonitroxide radicals. From the literature, we also found that nitronylnitroxide radicals could easily be converted to iminonitroxide radicals in presence of heat, water, and acid derivatives.[21] So, we directly used cyclometalating ligands with nitronylnitroxide radicals to synthesize the iminonitroxide elaborated cyclometalated

platinum dithiolate complexes. These radical elaborated platinum complexes were purified by column chromatography using alumina, and characterized by mass spectrometry, EPR spectroscopy, and elemental analysis. These complexes were found to be stable in the solid state. These complexes are unstable in solution for longer times and the solutions are observed to become discolored after few days. Detailed synthetic procedures and sample characterization can be found in the experimental section (Appendix B).

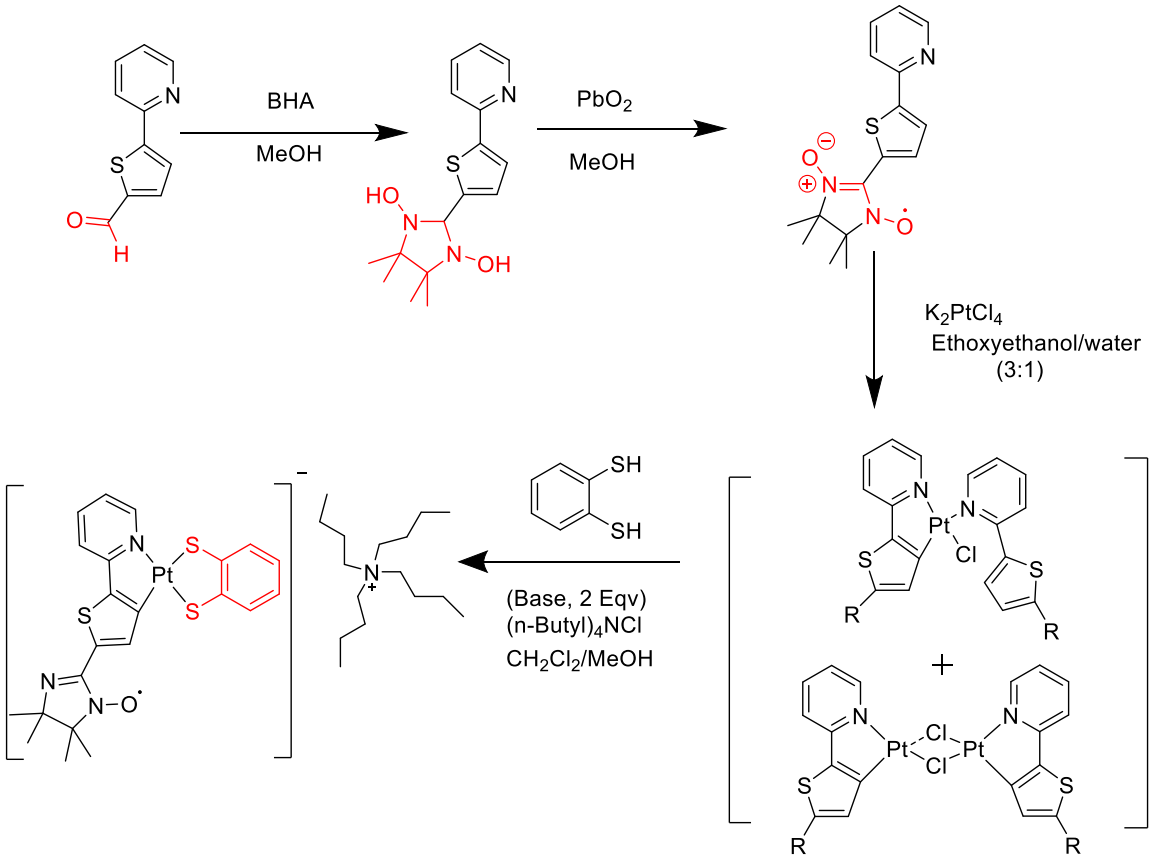

Figure 2.3: Synthetic scheme of cyclometalated platinum dithiolate complexes. (Here, R represents a radical fragment).

2.3 Electronic Absorption Spectra

Room temperature electronic absorption data for $[(PpyIN)Pt(bdt)]^{1-}$ and $[(TpyIN)Pt(bdt)]^{1-}$ have been collected in dichloromethane. The $[(PpyIN)Pt(bdt)]^{1-}$ complex has a weaker absorption band at ~19,100 cm^{-1} with a molar extinction coefficient of 2,450 $M^{-1}cm^{-1}$ as shown in Figure 2.4. The $[(TpyIN)Pt(bdt)]^{1-}$ derivative has a less intense lowest energy absorption peak around 1,880 cm^{-1} with a molar extinction coefficient of 3,000 $M^{-1}cm^{-1}$ as shown in Figure 2.5.

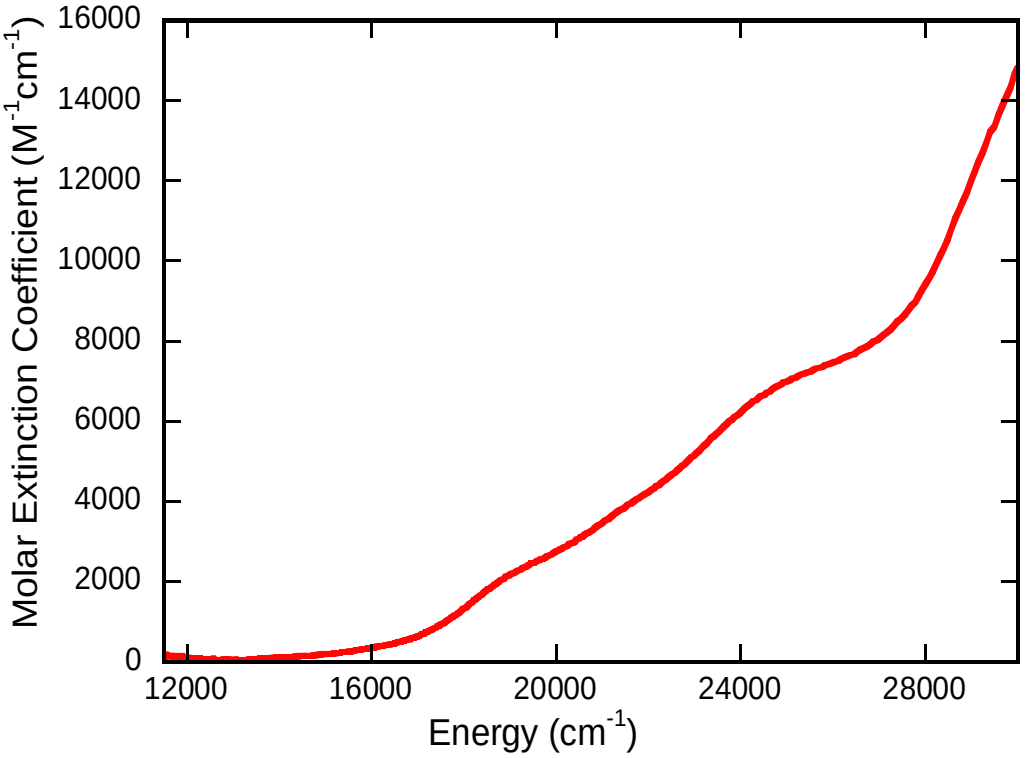

Figure 2.4: Room temperature electronic absorption spectrum for $[(PpyIN)Pt(bdt)]^{1-}$ complex in dichloromethane.

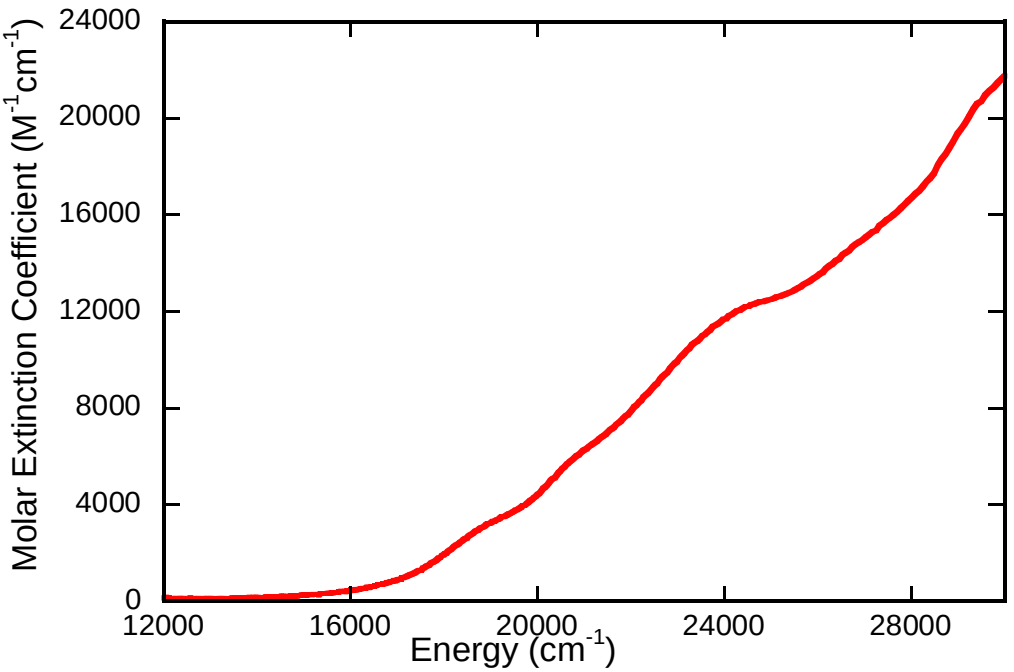

Figure 2.5: Room temperature electronic absorption spectrum for $[(TpyIN)Pt(bdt)]^{1-}$ complex in dichloromethane.

The room temperature electronic absorption spectra for $[(PpyIN)Pt(bdt)]^{1-}$ and $[(TpyIN)Pt(bdt)]^{1-}$ are slightly red shifted when compared to their parent molecules $[(Ppy)Pt(bdt)]^{1-}$ and $[(Tpy)Pt(bdt)]^{1-}$ as shown in Figures 2.6A and 2.6B, respectively. The lowest energy bands are also less intense when compared to their parent molecules. The parent molecules have low energy bands at ~475 nm (~21,000 cm^{-1}), but these bands are red shifted to ~525 nm (~19,000 cm^{-1}) when the cyclometalating ligand is appended with an iminonitroxide radical as seen in the overlays of Figures 2.6 A and 2.6B.

Thus, the lowest energy absorption bands in both $[(PpyIN)Pt(bdt)]^{1-}$ and $[(TpyIN)Pt(bdt)]^{1-}$ were clearly tuned by the presence of a radical substituent. The π-π*

transitions from the cyclometalating ligand[2] can be seen as an intense absorption band around 250 nm - 350 nm.

For the complexes that contain strongly donating dithiolate ligands, we observe that their lowest lying emitting states are dominantly LL'CT (L'= C^N and L = bdt) in character with partial MLCT character[16].

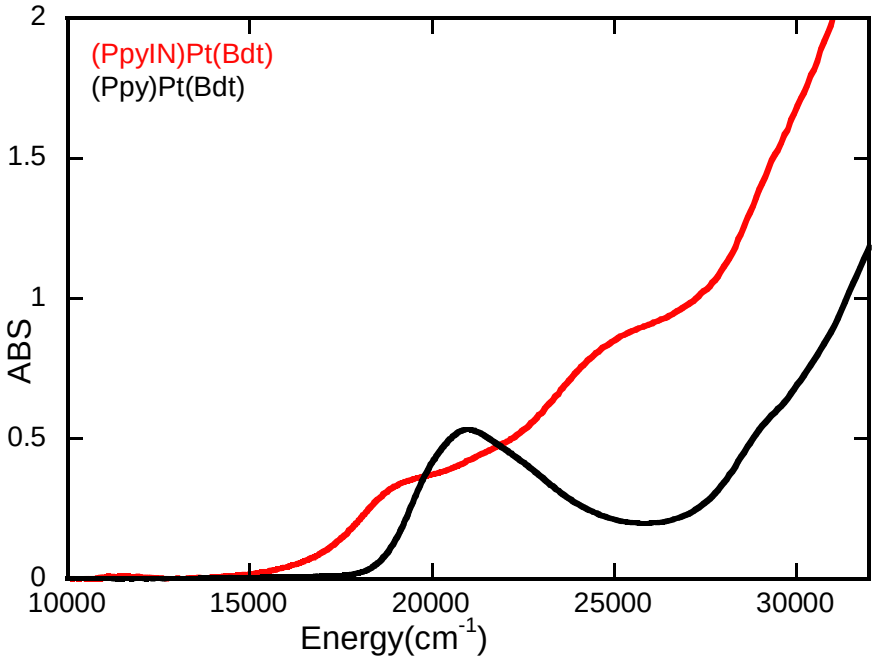

Figure 2.6A: An overlay of the room temperature electronic absorption spectra for[(PpyIN)Pt(bdt)]$^{1-}$ (red) and [(Ppy)Pt(bdt)]$^{1-}$ (black) in DCM.

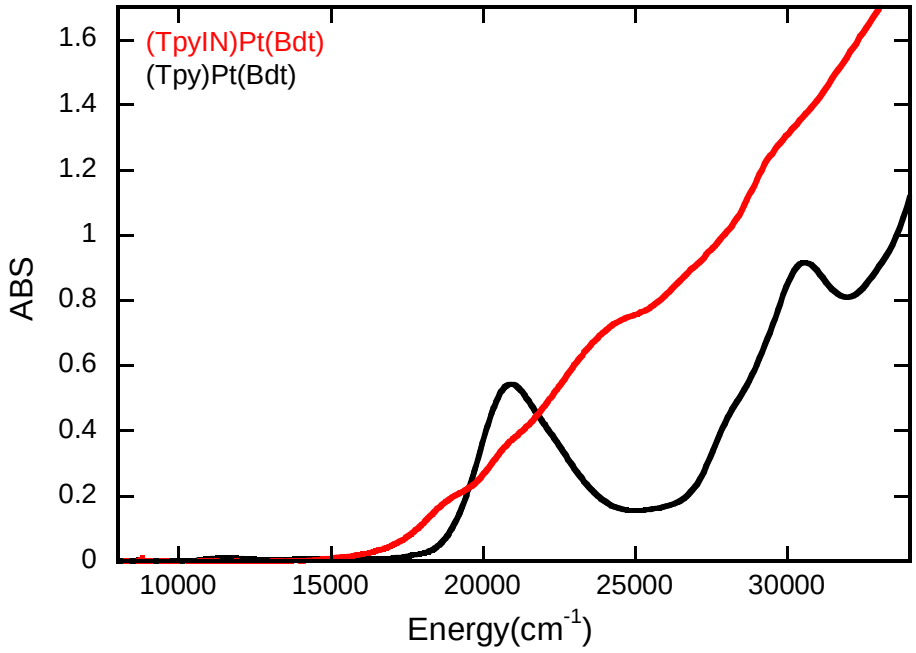

Figure 2.6B: An overlay of the room temperature electronic absorption spectra for $[(TpyIN)Pt(bdt)]^{1-}$ (red) and $[(Tpy)Pt(bdt)]^{1-}$ (black) in DCM.

Considering the UV-Vis spectrum in the 400 nm - 540 nm region of the phenyl-iminonitroxide molecule (PhIN) found in literature,[39] it can be predicted that there is π-conjugation between the cyclometalating ligand moiety and the pendent iminonitroxide radical in both the $[(PpyIN)Pt(bdt)]^{1-}$ and $[(TpyIN)Pt(bdt)]^{1-}$ complexes.

Electron density difference maps (EDDM) were computed in order to understand the nature of the lowest energy absorption bands. Calculating the EDDMs is a simple way to understand electron density changes in an electronic transition occurring between donor and acceptor parts of a donor-acceptor molecules. The EDDMS of the lowest energy transitions with higher oscillator strengths (electronic transitions 4 and 5 in TD-

DFT calculations for $[(PpyIN)Pt(bdt)]^{1-}$ and $[(TpyIN)Pt(bdt)]^{1-}$, respectively) are presented in Figure 2.7 for the cyclometalated platinum(II) dithiolate complexes.

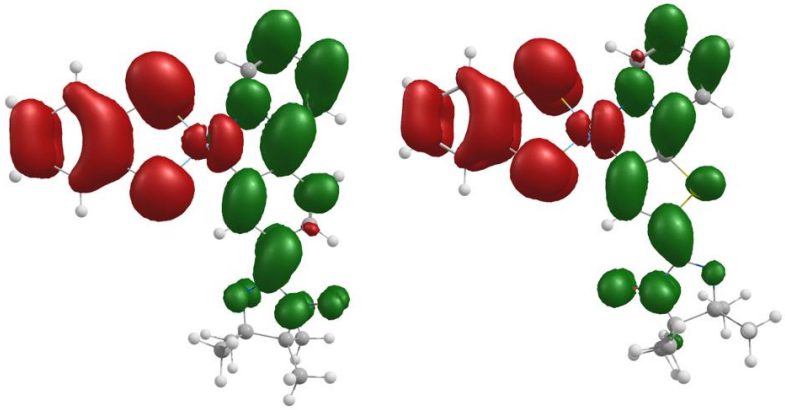

Figure 2.7: Computed EDDMs of $[(PpyIN)Pt(bdt)]^{1-}$ and $[(TpyIN)Pt(bdt)]^{1-}$ for electronic transitions 4 and 5 at a contour value of 0.0006, respectively. Here, the red and green regions indicate the loss and the gain of electron densities, respectively, in the computed transition.

The calculated electron density difference maps (EDDMs) for $[(PpyIN)Pt(bdt)]^{1-}$ and $[(TpyIN)Pt(bdt)]^{1-}$ with higher oscillator strengths at lower energies indicate that electron densities are lost from the HOMO (Highest Occupied Molecular Orbital) to the LUMO (Lowest Unoccupied Molecular Orbital) as shown in Figure 2.7.

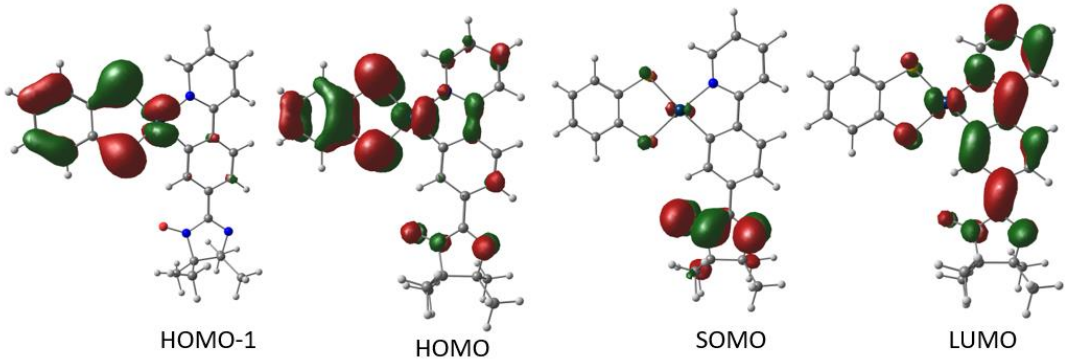

Figure 2.8A: DFT computed frontier molecular orbitals for $[(PpyIN)Pt(bdt)]^{1-}$.

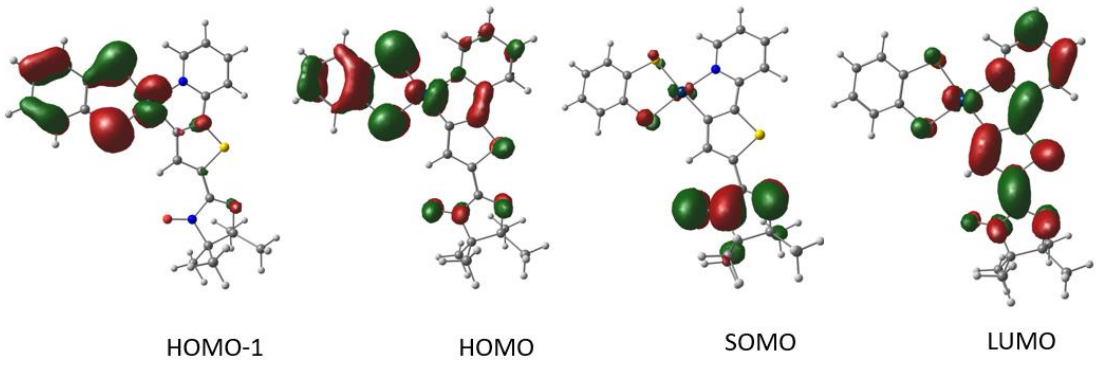

Figure 2.8B: DFT computed frontier molecular orbitals for $[(TpyIN)Pt(bdt)]^{1-}$.

A broad but less intense lowest energy absorption band of the radical-elaborated dithiolate complexes is found around 19000 cm^{-1}, and can be assigned as a charge transfer transition from the dithiolate HOMO to the π* LUMO of Ppy or Tpy. Based on the previous studies of similar phenylpyridine dithiolate complexes such as $[Pt(Ppy)(S\text{^}S)]^{-}$, we can predict that the HOMO has some Pt metal character as well. Thus, the charge transfer bands for these radical elaborated Ppy/Tpy Pt(II) dithiolates can be proposed as a mixed MLCT/LL'CT state with a dominant LL'CT character.

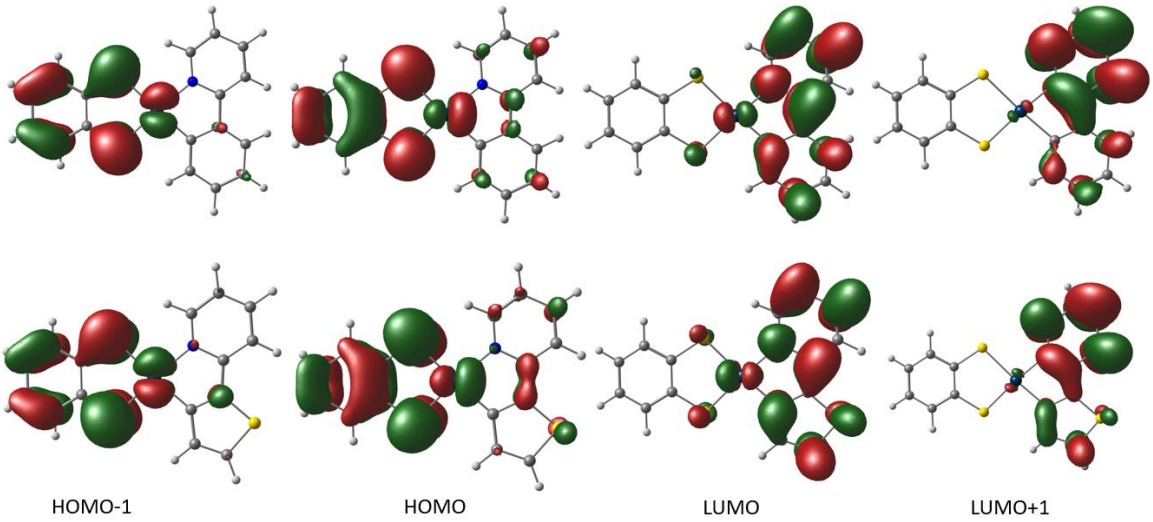

Figure 2.9: Frontier molecular orbitals of the parent molecules $[(Ppy)Pt(bdt)]^{1-}$ (top) and $[(Tpy)Pt(bdt)]^{1-}$ (bottom), respectively.

The frontier molecular orbitals for the radical-elaborated molecules $[(PpyIN)Pt(bdt)]^{1-}$ and $[(TpyIN)Pt(bdt)]^{1-}$ show that the iminonitroxide moiety is a dominant constituent of LUMO (Figures 2.8A and 2.8B, respectively). Similarly, EDDMs of both radical elaborated molecules involve the iminonitroxide moiety as an electron accepting group. This also indicates that there is some degree of π-conjugation between the iminonitroxide moiety and the cyclometalating ligand moiety, and this conjugation can be correlated with the observation of a red shift in the UV-Vis spectra of the radical elaborated molecules.

Figure 2.8A and Figure 2.8B show DFT computed frontier molecular orbitals that indicate the SOMO (Singly Occupied Molecular Orbital) is predominantly localized on the IN fragment. The nature of the SOMO leads to the paramagnetic doublet ground state

configuration in these radical elaborated molecules. The closed shell diamagnetic parent molecules naturally lack this SOMO orbital.

2.4 EPR Spectra

Electron paramagnetic resonance (EPR) spectroscopy is a powerful tool to identify and study radical species. It is similar to nuclear magnetic resonance spectroscopy but only samples that have unpaired electron spins are detected. A single unpaired electron can have two degenerate spin states ($m_s = \pm½$) in absence of an external field. When an external field is applied, these two m_s states are no longer degenerate. When the microwave energy is equal to the energy separation between the two m_s states in an applied magnetic field, this energy is absorbed and gives rise to an EPR transition. The selection rules for EPR are $\Delta m_s = \pm 1$. The resulting spectral pattern (number, spacing and amplitude of lines) helps to identify the radical species present in the sample. The number of hyperfine lines can be predicted with respect to the number of equivalent and non-equivalent magnetic nuclei present near the spin center. The number of EPR hyperfine lines is equal to (2NI) +1, where N is the number of equivalent nuclei, and I is the nuclear spin. For iminonitroxide radical (IN), there are two nonequivalent nitrogen nuclei, hence seven spectral lines are expected with an intensity pattern of 1:1:2:1:2:1:1.

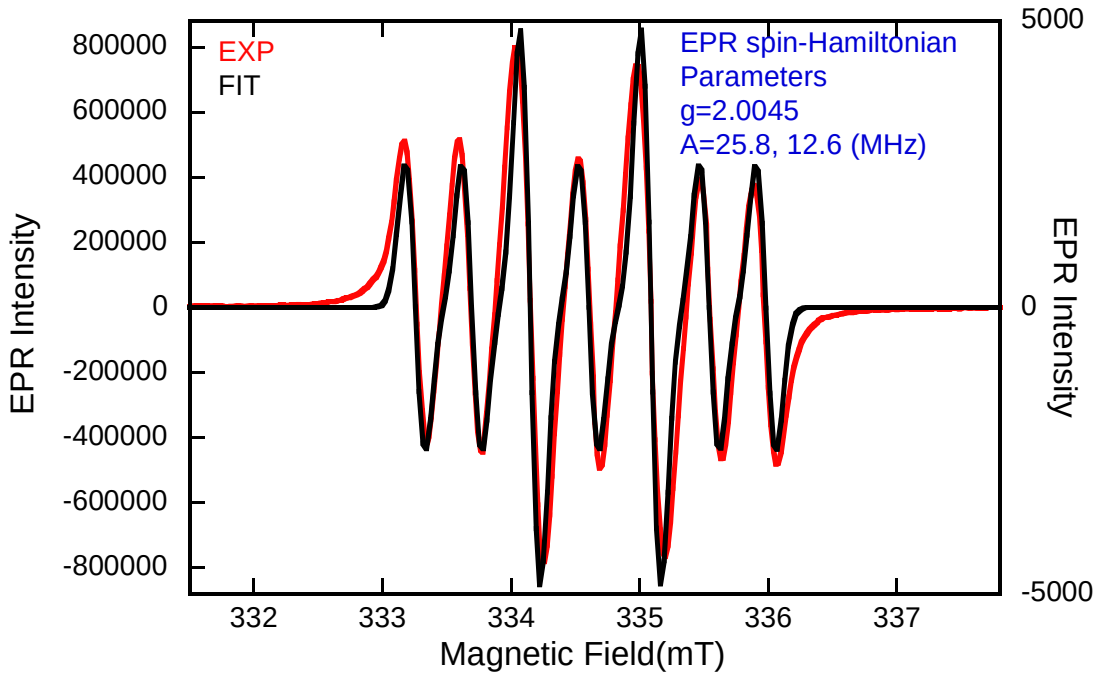

Figure 2.10: Room temperature X-band EPR spectrum for $[(PpyIN)Pt(bdt)]^{1-}$ in DCM and corresponding spectral simulation.

We have collected room temperature EPR spectra for the synthesized cyclometalated platinum(II) dithiolate complexes. The room temperature EPR spectra of these iminonitroxide elaborated cyclometalated complexes show the characteristic features of the iminonitroxide radicals, with no evidence of hyperfine coupling to the ^{195}Pt I =1/2 nucleus (Figure 2.10 and Figure 2.11). All EPR data represent a seven-line pattern with intensities ratios of 1:1:2:1:2:1:1 due to the interaction of a single unpaired electron with two nonequivalent nitrogen nuclei.

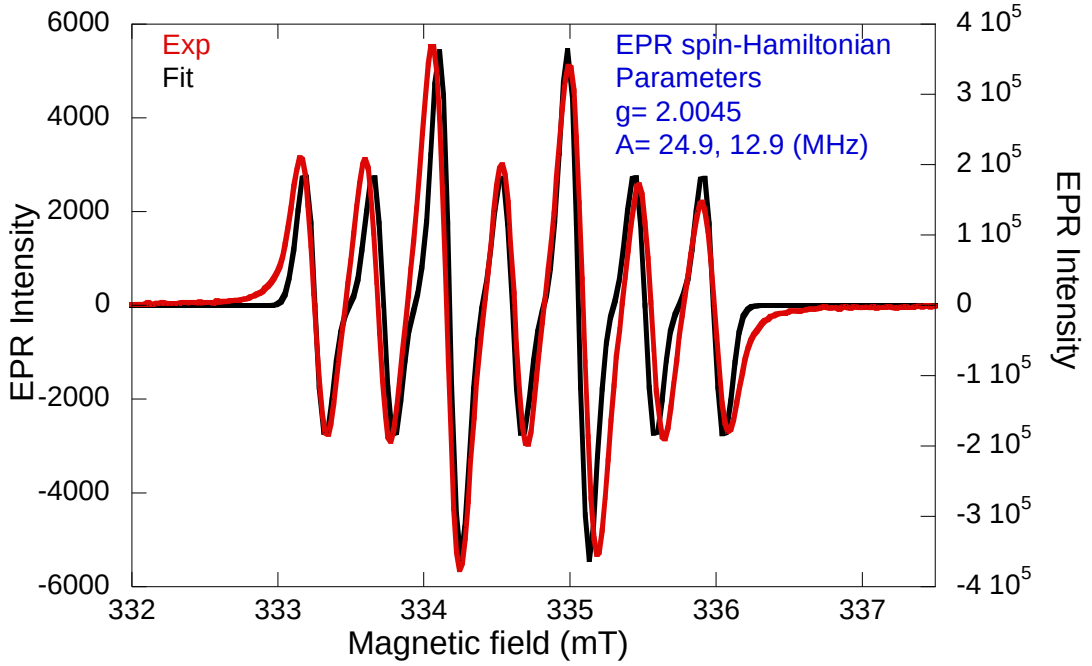

Figure 2.11: Room Temperature X-band EPR spectrum of $[(TpyIN)Pt(bdt)]^{1-}$ in DCM and corresponding spectral simulation.

Spectral simulations of the EPR spectra for these complexes (Figure 2.10 and Figure 2.11) yield an isotropic g value very similar to that of the free iminonitroxide radical.[39,42] The isotropic g-value for $[(PpyIN)Pt(bdt)]^{1-}$ was found to be 2.0045 and the isotropic hyperfine interactions with two non-equivalent nitrogen nuclei were determined to be 25.8 MHz and 12.6 MHz. Similarly, the isotropic g-value for $[(TpyIN)Pt(bdt)]^{1-}$ was found to be 2.0045 and the hyperfine interactions with two non-equivalent nitrogen nuclei were determined to be 24.9 MHz and 12.9 MHz. The hyperfine coupling constants for these radical elaborated complexes also match the hyperfine coupling constants of free iminonitroxide radicals.[39,42] Thus, these data indicate that the spin density on radicals is not dramatically perturbed by their attachment to the

chromophore. This is shown in the computed spin densities of the doublet ground states for these molecules. Note that there is negative spin density on methine carbon atom as can be seen in Figure 2.12.

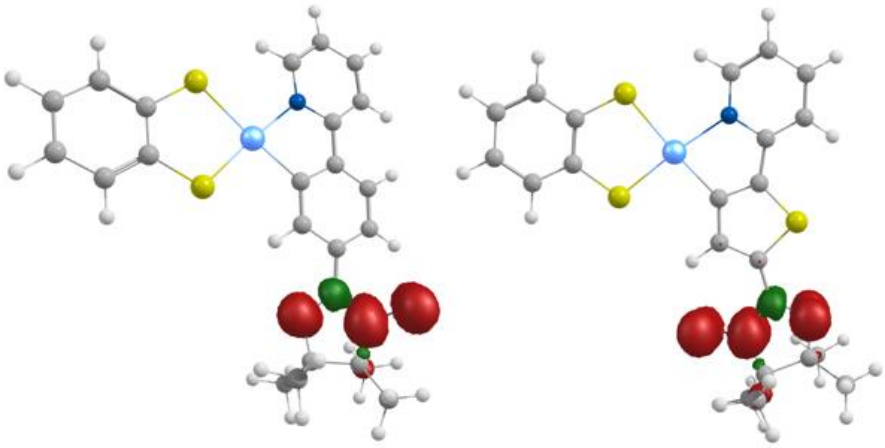

Figure 2.12: DFT computed spin densities for $[(PpyIN)Pt(bdt)]^{1-}$ and $[(TpyIN)Pt(bdt)]^{1-}$ at a 0.0031 contour values. Positive spin density (red), negative spin density (green).

The Mulliken spin population analysis for both iminonitroxide and nitronylnitroxide radical appended complexes has been completed for comparison purposes. The magnitude of the spin densities on the methine carbons for these iminonitroxide radical-elaborated bdt containing complexes are comparable with the complexes when they are substituted with nitronylnitroxide radicals (NN substituted complexes). The Mulliken spin populations on the methine carbons in $[(PpyIN)Pt(bdt)]^{1-}$ and $[(PpyNN)Pt(bdt)]^{1-}$ are -0.0996 and -0.0968 respectively. Similarly, Mulliken spin populations on the methine carbons of $[(TpyIN)Pt(bdt)]^{1-}$ and $[(TpyNN)Pt(bdt)]^{1-}$ are -0.0869 and -0.1110 respectively.

2.5 Emission Spectra and Lifetimes

The choice of the ligand plays an important role in tuning the photophysical behavior of cyclometalated square planar Pt(II) complexes[15]. The cyclometalating ligand 2-phenylpyridine (Ppy) is itself nonemissive at room temperature, and the proper choice of a the acceptor ligand helps to induce photoemission in these complexes at room temperature.[15] In contrast to, 2-thienylpyridine (Tpy) is an emissive ligand and the choice of ligands helps to tune the emission wavelength. We are introducing the iminonitroxide radical as a functional group covalently bound to the cyclometalating ligand to study the effect of this radical substituent on the electronic structure of these Pt donor-accpetor complexes. There are very limited studies about the effects of organic radical substituents on emissive metal complexes.[23,24,25,26]

Room temperature steady state emission spectra of the cyclometalated Pt(II) complexes were collected in degassed dichloromethane solutions. The sample solutions were degassed by purging using a flow of nitrogen gas for fifteen minutes.

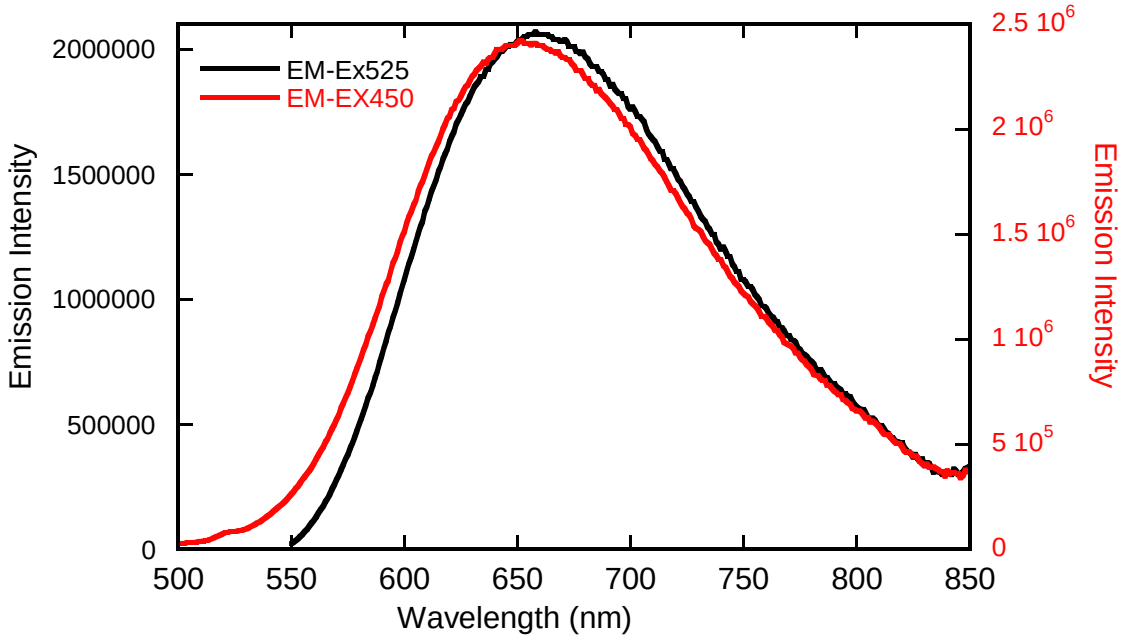

Figure 2.13: Steady state room temperature emission spectra of $[(PpyIN)Pt(bdt)]^{1-}$ in DCM using 450 nm (red) and 525 nm (black) excitation.

These radical substituted anionic complexes are found to be emissive in nature. For these donor-acceptor type complexes, they show a broad band emission band (Figure 2.13 and Figure 2.14) that derives from a dominantly LL'CT type emitting state. The emissive properties of the parent molecules were not lost upon radical elaboration on the acceptor side of these anionic cyclometalated square planar Pt(II) dithiolates.

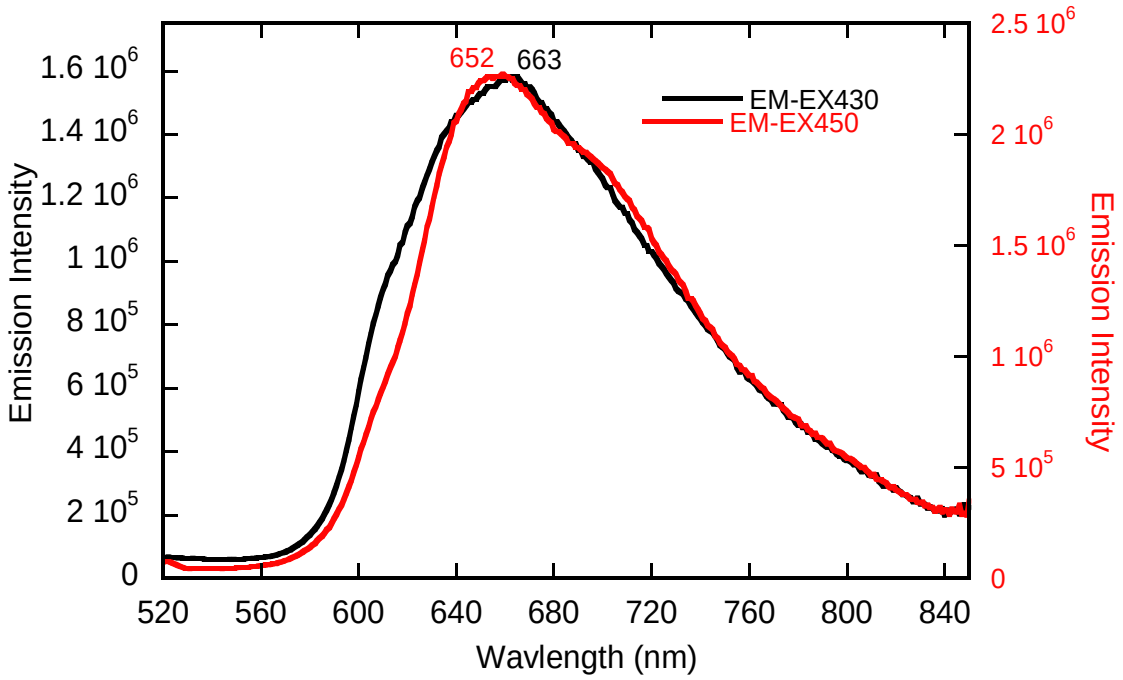

Figure 2.14: Steady state room temperature emission spectra of (TpyIN)Pt(bdt) in DCM using 430 nm (black) and 450 nm (red) excitation.

The emission spectra of $[(PpyIN)Pt(bdt)]^{1-}$ in degassed dichloromethane solution (Figure 2.13) has a broad band with a emission peak maximum at 659 nm (15,175 cm^{-1}) when excited at 525 nm. When the same molecule is excited at 450 nm (Figure 2.13), it gave a emission maximum at 649 nm (15,400 cm^{-1}). However, the emission spectra of $[(TpyIN)Pt(bdt)]^{1-}$ in degassed dichloromethane solution has a structured band with a emission maximum at 652 nm (15,340 cm^{-1}) when excited at 450 nm (Figure2.14). This molecule gave an emission maximum at 663 nm (15,050 cm^{-1}) upon excitation at 430 nm. The $[(TpyIN)Pt(bdt)]^{1-}$ derivative shows evidence of possible vibronic structure in its emission spectrum.

Prior studies on (diimine)Pt(bdt) and related complexes show that these molecular systems undergo intersystem crossing from their S_1 to T_1 states.[5,27,28,36] Therefore, we expect that these new radical elaborated complexes discussed here will also undergo intersystem crossing. These radical elaborated molecules possess a spin allowed LL'CT transitions from their $^2S_0$ doublet ground state to a $^2S_1$ excited state. Due to the exchange interaction between the appended radical and the chromophore, there is an enhanced intersystem crossing that leads to a rapid relaxation to a lower lying $^2T_1$ trip-doublet state. The Pt(II) ion ensures a large spin orbit coupling to promote intersystem crossing to a $^4T_1$ trip-quartet state. The relaxation process from the $^4T_1$ state to the $^2S_0$ ground state doublet is spin forbidden and expected to be slow. Hence, we can expect a long-lived emission from these radical elaborated systems.

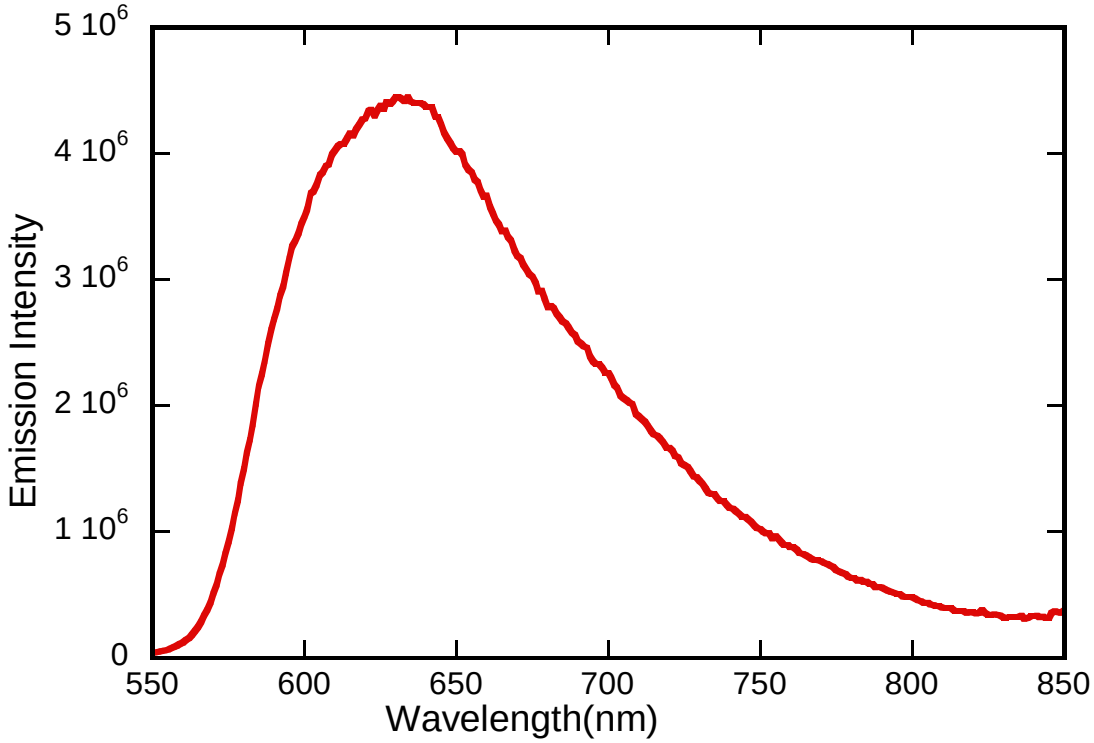

Figure 2.15: Steady state emission spectrum for $[(PpyIN)Pt(bdt)]^{1-}$ in degassed butyronitrile at 77K (Cryogen = liquid nitrogen) using 525 nm excitation.

We have also collected 77K emission spectra for both $[(PpyIN)Pt(bdt)]^{1-}$ and $[(TpyIN)Pt(bdt)]^{1-}$ complexes dissolved in optical glasses. The emission spectrum of $[(PpyIN)Pt(bdt)]^{1-}$ in butyronitrile at 77K has an emission band with an emission maximum at 635 nm (15,750 cm^{-1}) using an excitation wavelength at 525 nm (Figure 2.15). For the $[(PpyIN)Pt(bdt)]^{1-}$ complex, the emission spectrum is blue shifted when temperature is lowered to 77K .

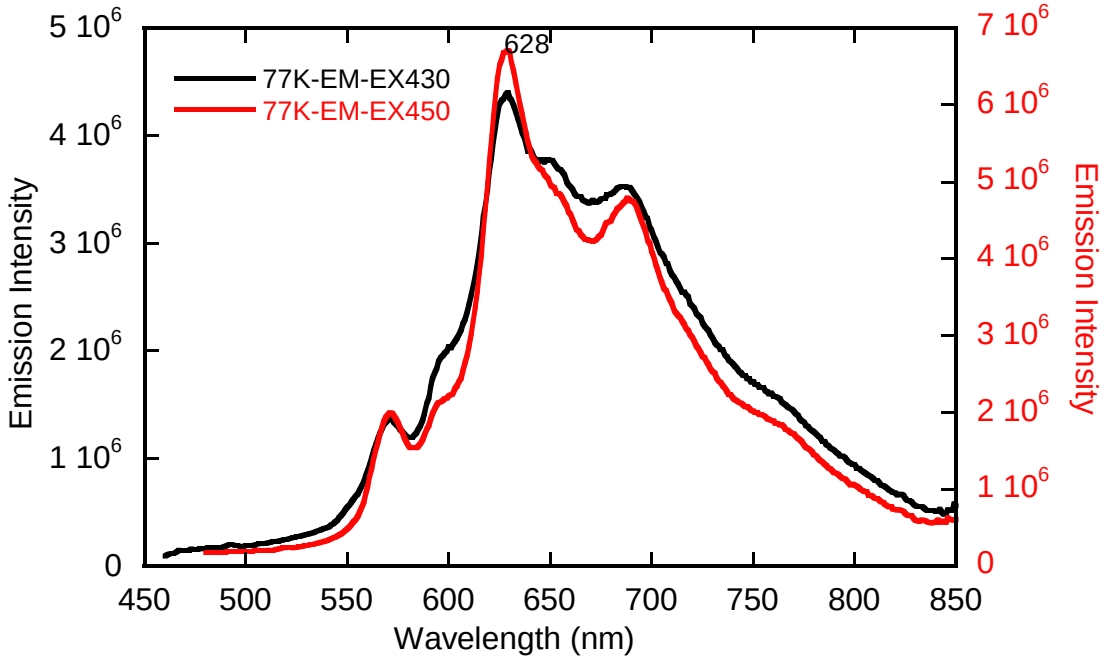

Figure 2.16A: Steady state emission spectra for $[(TpyIN)Pt(bdt)]^{1-}$ in degassed butyronitrile at 77K (Cryogen = liquid nitrogen) using 430 nm (black) and 450 nm (red) excitation.

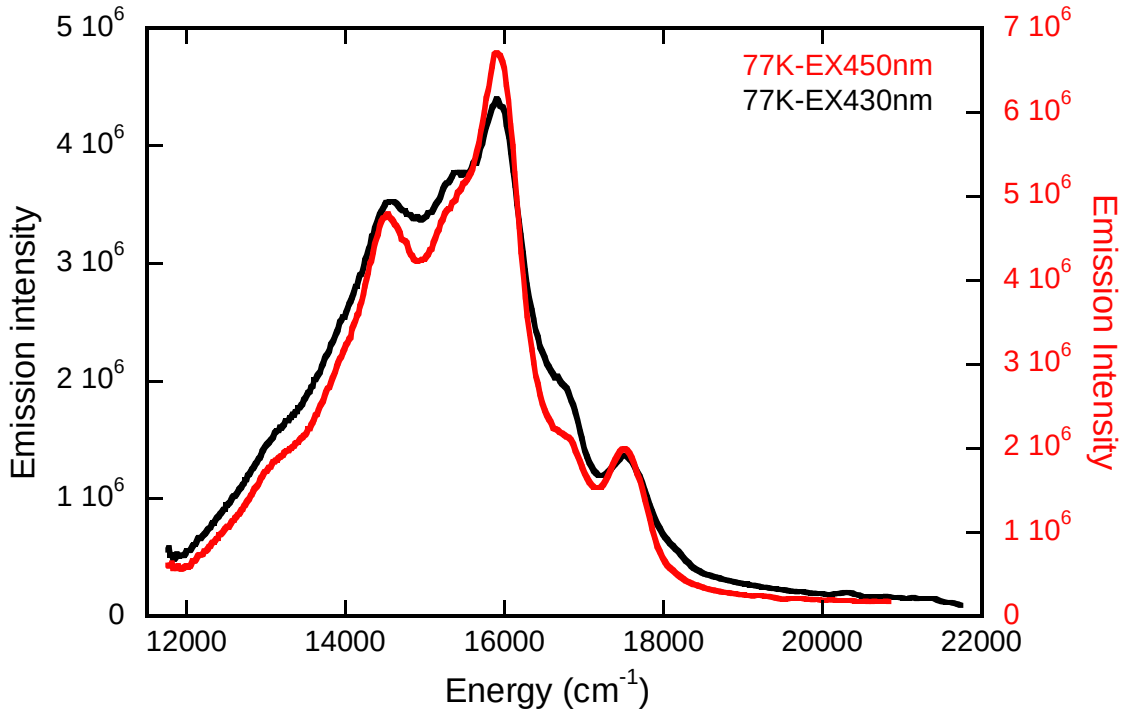

Figure 2.16B: Steady state emission spectra for $[(TpyIN)Pt(bdt)]^{1-}$ complex in degassed butyronitrile at 77K (Cryogen = liquid nitrogen) using 430 nm (black) and 450 nm (red) excitation.

The $[(TpyIN)Pt(bdt)]^{1-}$ complex gives a structured band with an emission maximum at 628 nm (15,900 cm^{-1}) using an excitation wavelength at 450 nm (Figure 2.16). In the 77K emission spectra of $[(TpyIN)Pt(bdt)]^{1-}$, evidence of possible vibronic structure can clearly be seen (Figure 2.16). Similarly, the emission maxima are also slightly blue shifted at 77K for $[(TpyIN)Pt(bdt)]^{1-}$.

When we measured the emission lifetimes of these two complexes in dichloromethane solutions at room temperature, both $[(PpyIN)Pt(bdt)]^{1-}$ (Figure 2.17)

and [(TpyIN)Pt(bdt)]$^{1-}$ had lifetimes that are shorter than the instrument response time of ~600ps (Figure 2.18).

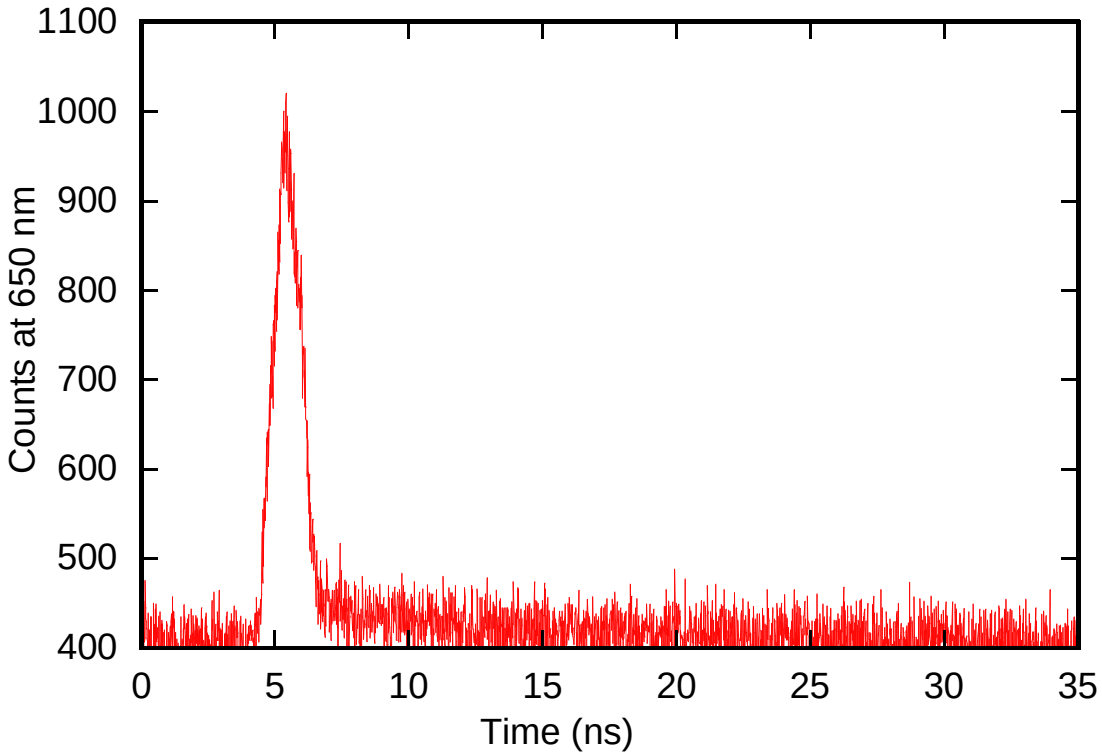

Figure 2.17: Room temperature PL decay for [(PpyIN)Pt(bdt)]$^{1-}$ in degassed DCM at 650 nm emission using a 450 nm diode laser. Here, the lifetime of this complex is shorter than the instrument response time of ~600ps.

$$R(t) = A + B_i \,.\, exp^{(-t/t_i)} \qquad 2.1$$

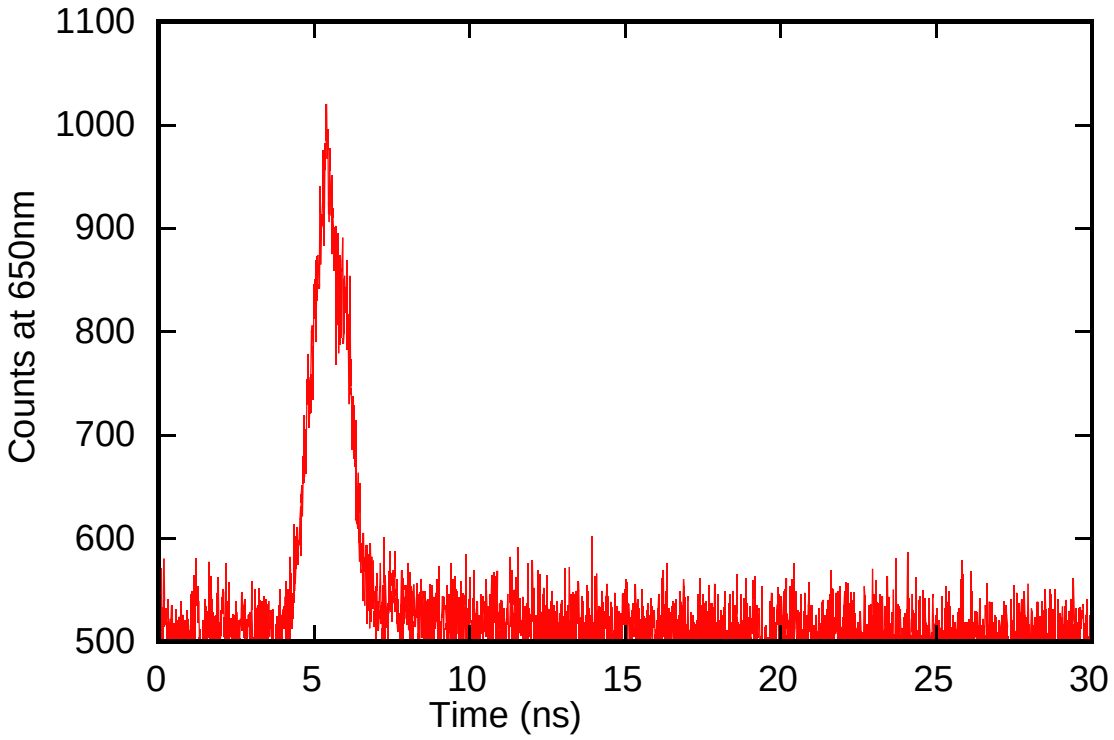

Figure 2.18: Room Temperature emission decay of $[(TpyIN)Pt(bdt)]^{1-}$ in degassed DCM measured at 650 nm using a 450 nm diode laser. Here, the lifetime of this complex is shorter than the instrument response time of ~600 ps.

The PL lifetime of $[(PpyIN)Pt(bdt)]^{1-}$ at 77K was found to be 1.32 ns and that of $[(TpyIN)Pt(bdt)]^{1-}$ was 1.31 ns as showm in Figure 2.19 and Figure 2.20, respectively (see Eqn. 2.1). We used butyronitrile to dissolve the samples and form an optical glass in order to study their decay rates at liquid nitrogen temperature (77K). Samples were degassed with a nitrogen flow before the temperature was reduced to 77K.

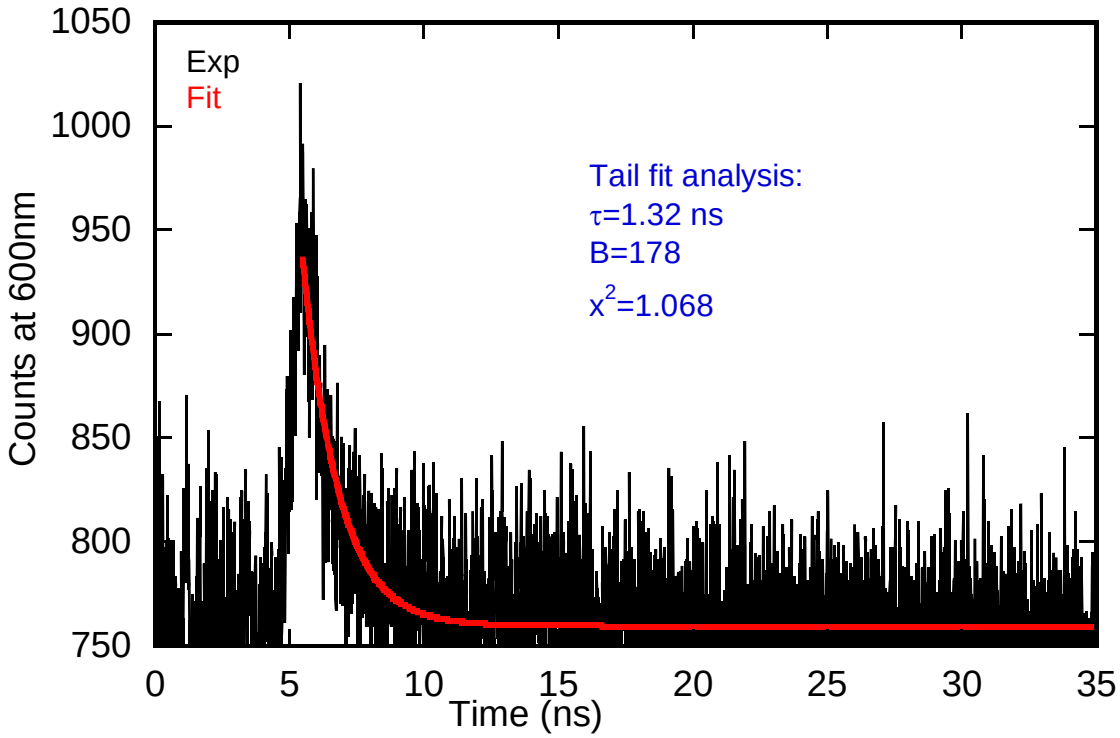

Figure 2.19: Emission decay of $[(PpyIN)Pt(bdt)]^{1-}$ at 77K in degassed butyronitrile, measured at 600 nm using a 450 nm diode laser.

The photoluminescence (PL) lifetimes of the radical elaborated complexs are quite short (< 600ps) and had lifetimes of ~1.3 ns when the temperature was reduced to 77K. Their decay rates are expected to be many times slower than the rooom temperature decay rates.

At 77K, both complexes display a blue shift in ther emission maxima. Generally, we can expect a red shift at lower temperature if thermally activated delayed fluorescence is occurring.[40] So, this blue shift in emission maxima at lower temperature indicates that these complexes are not behaving as TADF materials.

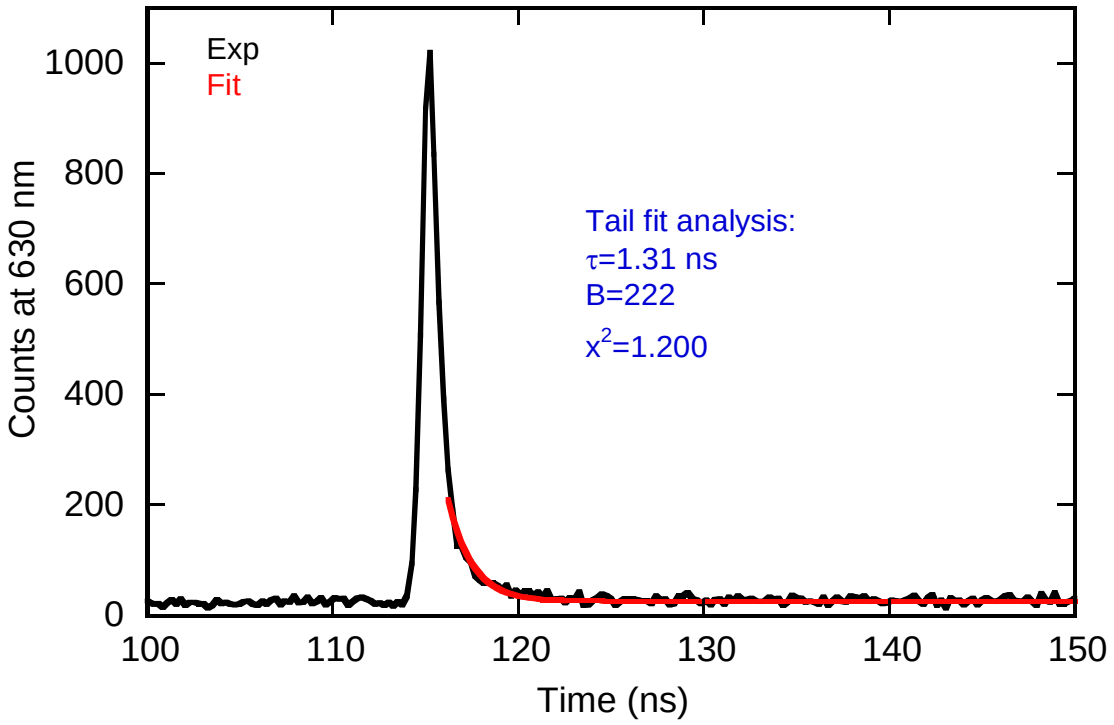

Figure 2.20: PL decay for $[(TpyIN)Pt(bdt)]^{1-}$ at 77K in butyronitrile, measured at 630 nm emission using a 450 nm diode laser.

We also measured the variable temperature photoluminescence lifetimes of these radical elaborated complexes in a thin polymer film matrix prepared using polystyrene/DCM. These lifetimes are presented in Section 2.6 later in this Chapter.

To compare the emisssion properties of these radical elaborated anionic cyclometalated square planar Pt(II) benzene-dithiolate molecules, the parent molecules (molecules without a pendent iminonitroxide radical) were also synthesized and spectroscopically studied. Photoluminescence of these parent molecules were examined in dichloromethane solution at room temperature.

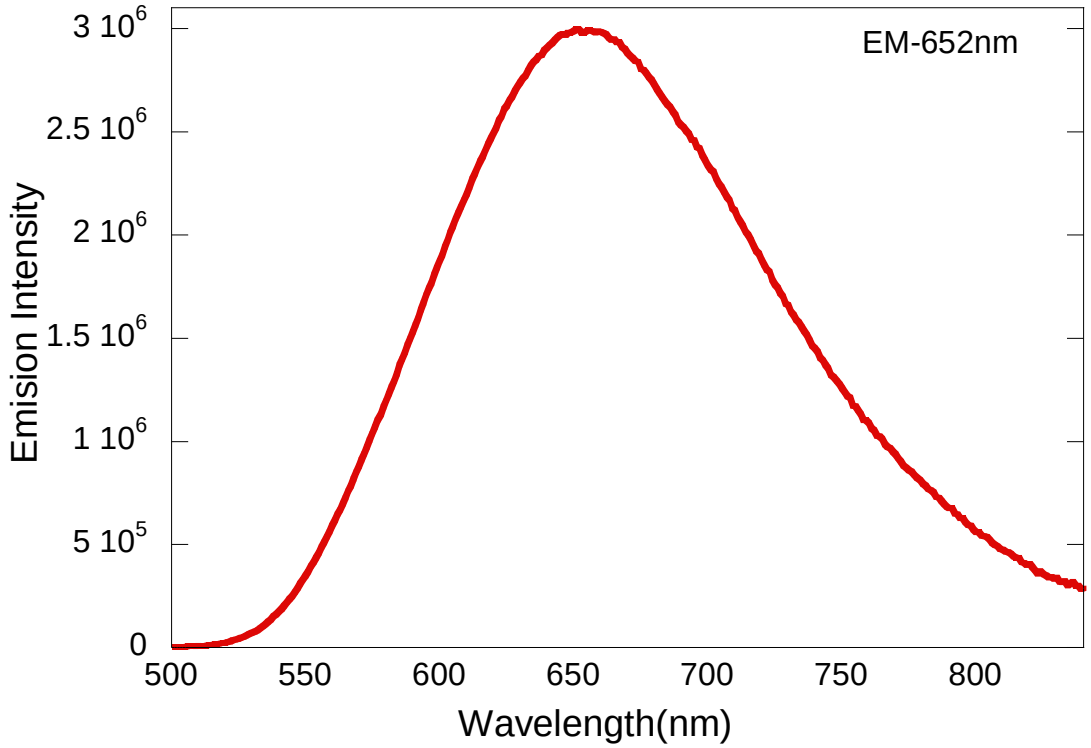

Figure 2.21: Room temperature emission spectrum for $[(Ppy)Pt(bdt)]^{1-}$ in degassed DCM using 470 nm excitation.

The $[(Ppy)Pt(bdt)]^{1-}$ and $[(Tpy)Pt(bdt)]^{1-}$ parent molecules are both emissive in dichloromethane solution. The $[(Ppy)Pt(bdt)]^{1-}$ complex has an emission maximum at 652 nm (15,300cm^{-1}) using an excitation wavelength at 470 nm in dichloromethane solution (Figure 2.21). This is consistent with the $[(Ppy)Pt(bdt)]^{1-}$ parent molecule being reported as emissive in literature and the lowest lying emitting state being characterized as triplet with dominantly LL'CT and partial MLCT character.[16]

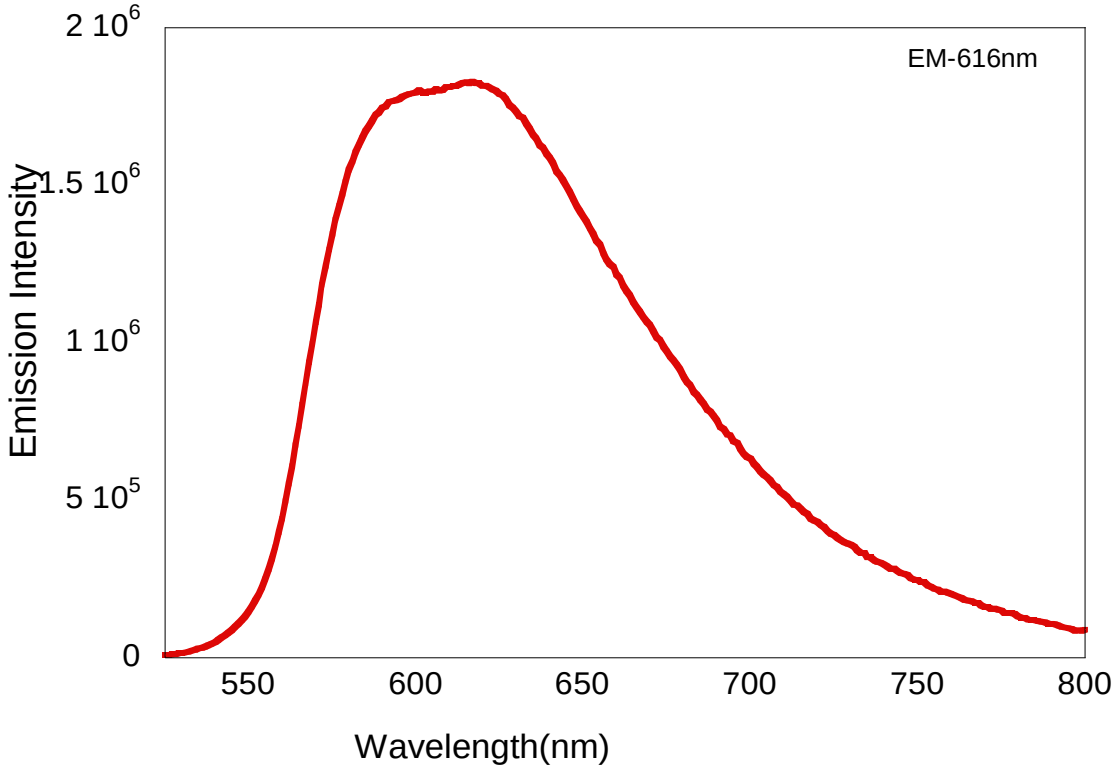

Figure 2.22: Room Temperature emission spectrum for $[(Tpy)Pt(bdt)]^{1-}$ in degassed DCM using 470 nm excitation.

Similarly, $[(Tpy)Pt(bdt)]^{1-}$ has an emission maximum at 616 nm (16234 cm^{-1}) using an excitation wavelength at 470 nm in degassed dichloromethane solution as shown in Figure 2.22. The $[(Tpy)Pt(bdt)]^{1-}$ complex also gave a broad and featureless emission spectrum in degassed dichloromethane solution (Figure 2.22). Based on this observation, the lowest lying emitting state can be assigned as a triplet that is dominantly comprised of LL'CT and partial MLCT character[16]. The PL lifetimes of these two parent molecules, $[(Ppy)Pt(bdt)]^{1-}$ and $[(Tpy)Pt(bdt)]^{1-}$, are 548 ns and 718 ns respectively (Figure 2.23 and Figure 2.24).

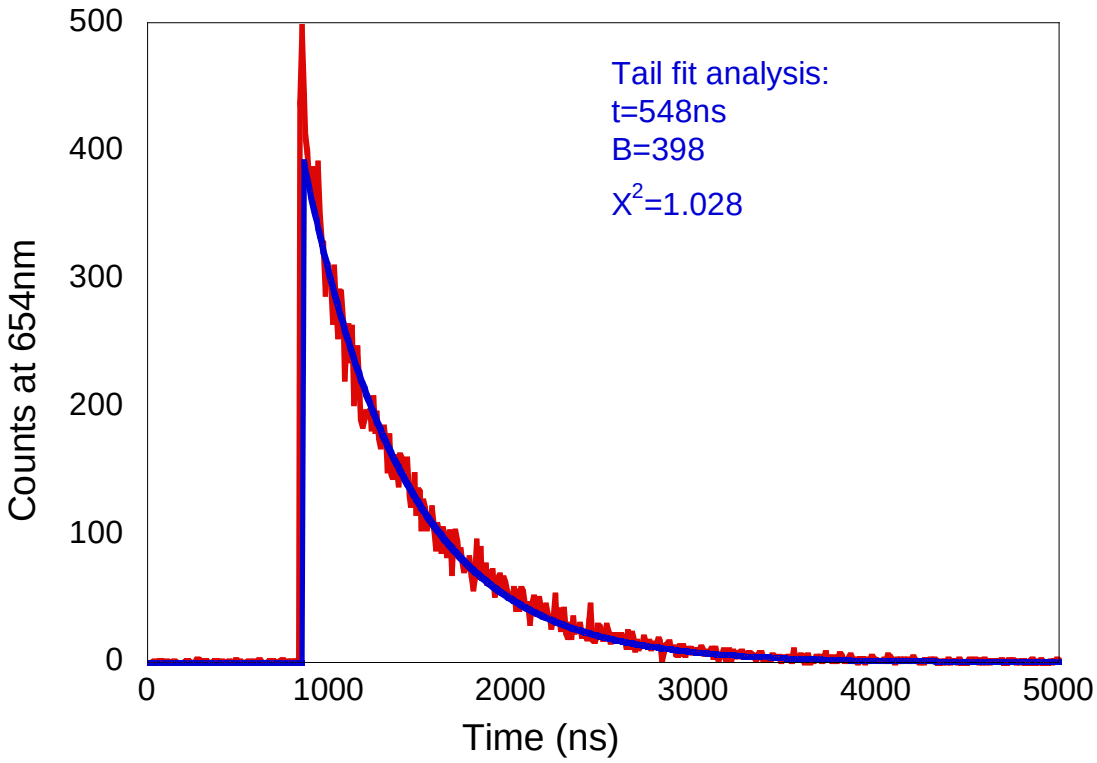

Figure 2.23: Room Temperature PL decay for $[(Ppy)Pt(bdt)]^{1-}$ in degassed DCM at 654nm using a 450 nm diode laser.

Spin orbit coupling (SOC) matrix elements for the T_1 to S_0 process in the parent molecules were computed using CASSCF methods to understand how the non-radiative decay pathways can be enhanced by SOC. The computed SOC matrix elements for the parent molecules $[(Ppy)Pt(bdt)]^{1-}$ and $[(Tpy)Pt(bdt)]^{1-}$ are 47.14 cm^{-1} and 77.90 cm^{-1}, respectively.

Compared to the parent molecule emission lifetimes, the radical elaborated molecule emission lifetimes were decreased. One of the reasons behind these drastically shortened lifetimes for radical elaborated molecules could be SOC-mediated enhanced non-radiative decay pathways. Symmetry restrictions can affect the out-of-state SOC

contributions to nonradiative decay mechanisms via ISC.[27,28] The observed shorter lifetimes for the radical elaborated molecules in solution compared to that of parent molecules could be due to thermal population of the D_{trip} state, with a small energy gap between D_{trip} and quartet but we donot have experimental evidence to support it.[37]

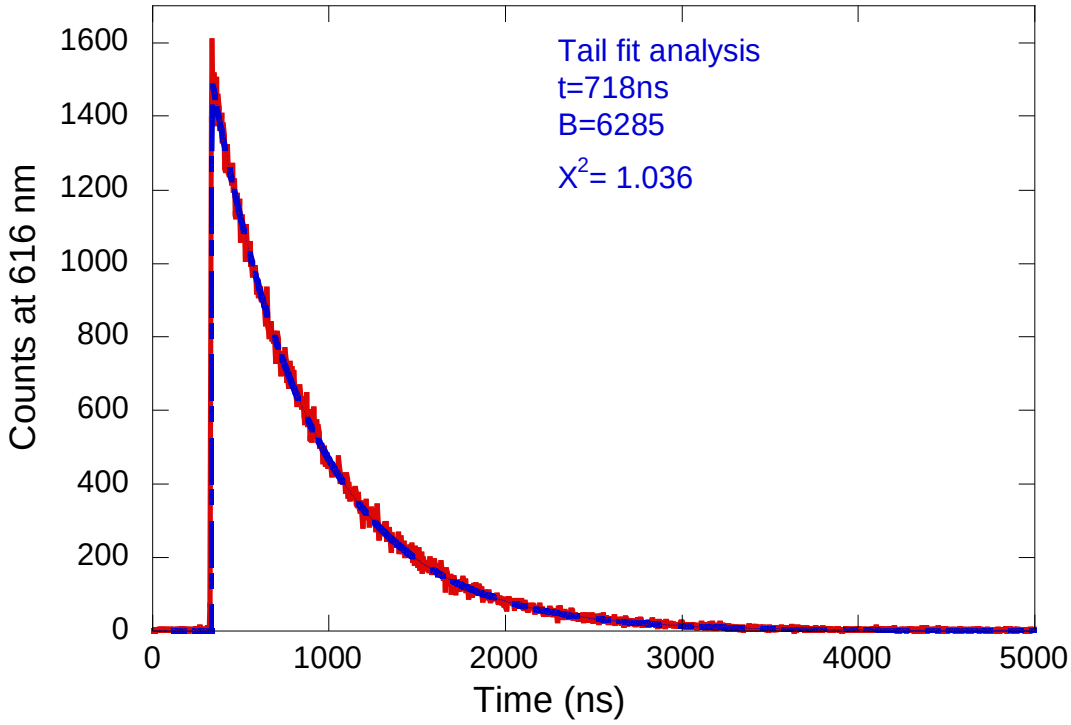

Figure 2.24: Room Temperature PL decay for $[(Tpy)Pt(bdt)]^{1-}$ in degassed DCM at 616 nm using a 450 nm diode laser.

We have also checked the emissive properties of these radical elaborated cyclometalated platinum benzene-dithiolate complexes in solid state. Solid state

emissive phosphors are of interest for many optoelectronic applications such as OLEDs (organic light emitting diodes) and solid-state lasers.[38] Photophysical properties in the solid state are affected by different factors, such as molecular aggregation, π-π stacking, rigidity, etc. Development of solid-state organic emitters is becoming an emerging field for their potential applications in OLEDS, sensing, lighting etc and, their compatibility in soild state.

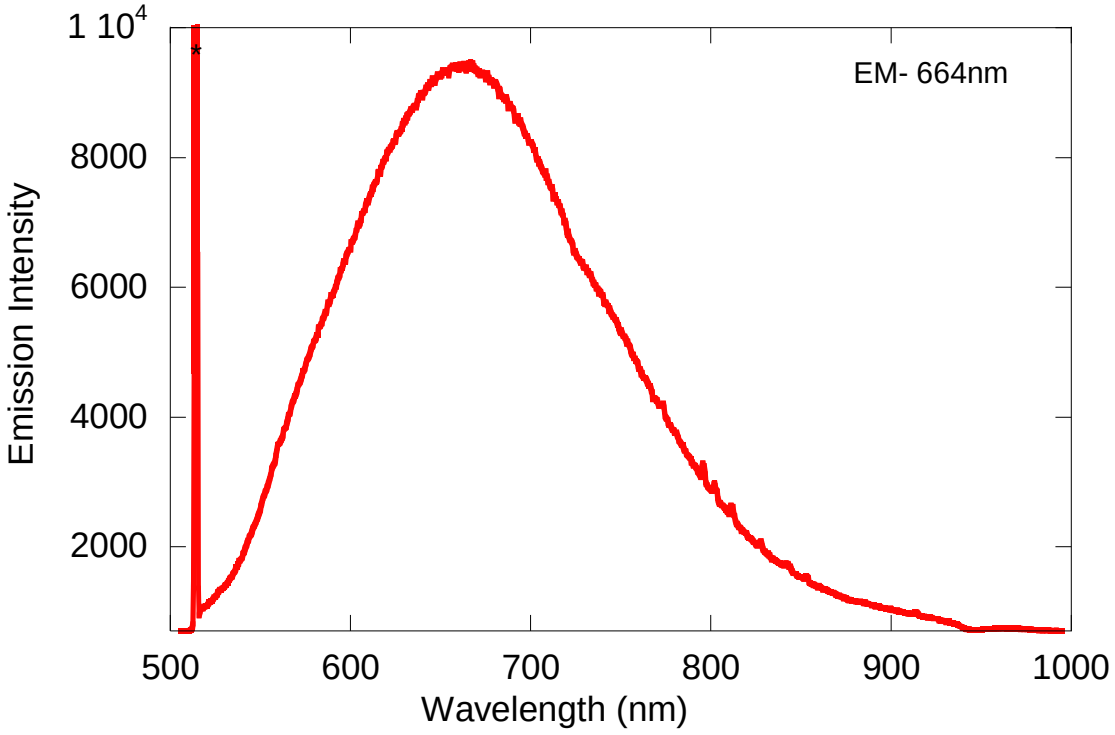

Figure 2.25: Solid state emission spectrum for $[(PpyIN)Pt(bdt)]^{1-}$ using 514 nm excitation.

We found that these radical elaborated cyclometalated Pt(II) dithiolate complexes are emissive in the solid state. Emission bands in the solid state are slightly red shifted compared to those dissolved in dichloromethane solutions. However, the spectral

shapes are similar in both the solid state and in dichloromethane solutions. The spectral band shapes of the solid state emission bands for $[(PpyIN)Pt(bdt)]^{1-}$ and $[(TpyIN)Pt(bdt)]^{1-}$ complexes are also broad and featureless, as shown in Figure 2.25 and Figure 2.26, respectively.

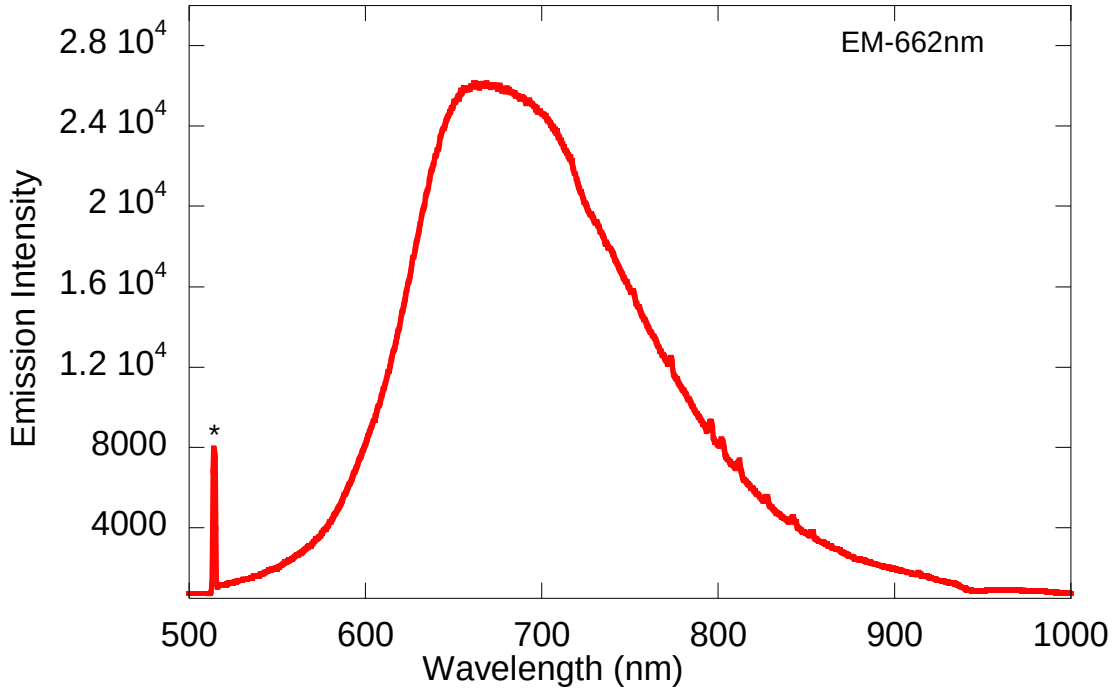

Figure 2.26: Solid state emission spectrum for $[(TpyIN)Pt(bdt)]^{1-}$ using 514 nm excitation.

We have also collected photoluminescence data for these complexes in polystyrene thin films. Details of the thin film studies of these iminonitroxide substituted anionic cyclometalated platinum dithiolate complexes are presented in Section 2.6. Film thickness, phosphor concentration, experimental parameters, and detection efficiencies

of the instrument can give complex emission response with various emission mechanisms such as aggregation induced emission.[18,45,47] Here, thin film emission spectra for $[(PpyIN)Pt(bdt)]^{1-}$ and $[(TpyIN)Pt(bdt)]^{1-}$ at room temperature are shown in Figure 2.27 and Figure 2.28, respectively. The emission band of $[(PpyIN)Pt(bdt)]^{1-}$ is slightly blue shifted in the polystyrene thin film when compared with the solid-state emission, while the emission band of $[(TpyIN)Pt(bdt)]^{1-}$ has similar λ_{max} in both solid state and the polystyrene thin films.

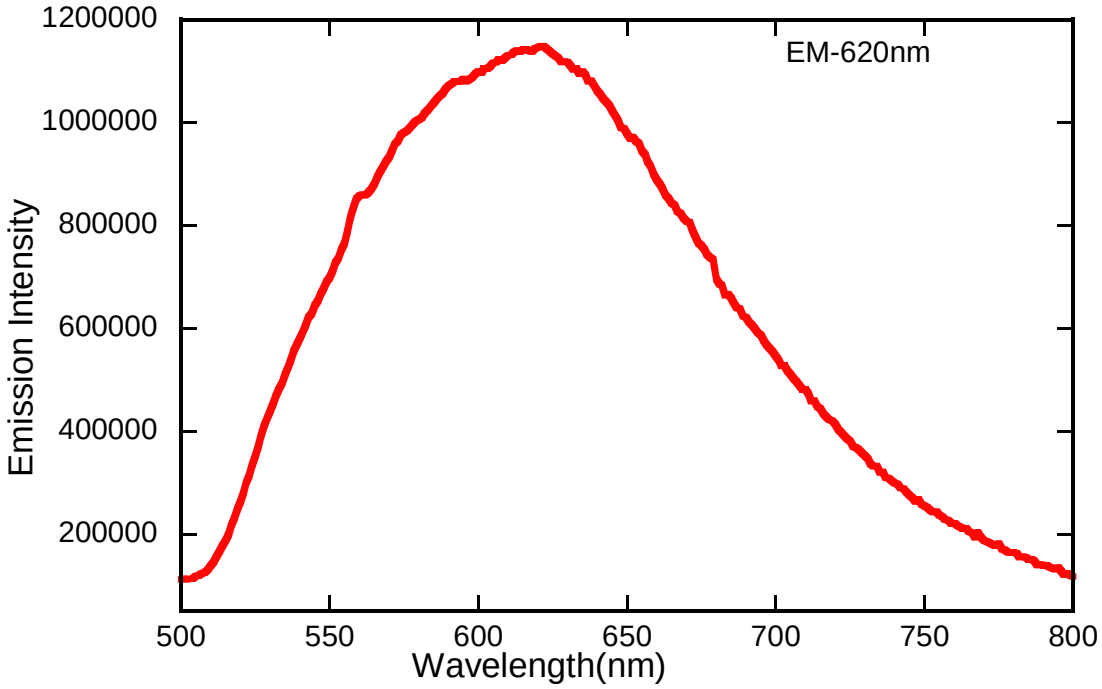

Figure 2.27: Room temperature emission spectrum for $[(PpyIN)Pt(bdt)]^{1-}$ collected in a polystyrene thin film using 450 nm excitation.

All of the room temperature emission spectra these radical-elaborated cyclometalated platinum dithiolate complexes (solution, solid and thin film) were usually observed as broad, featureless bands. This indicates that their emitting states could be described as predominantly LL'CT character with partially mixed MLCT character.[16]

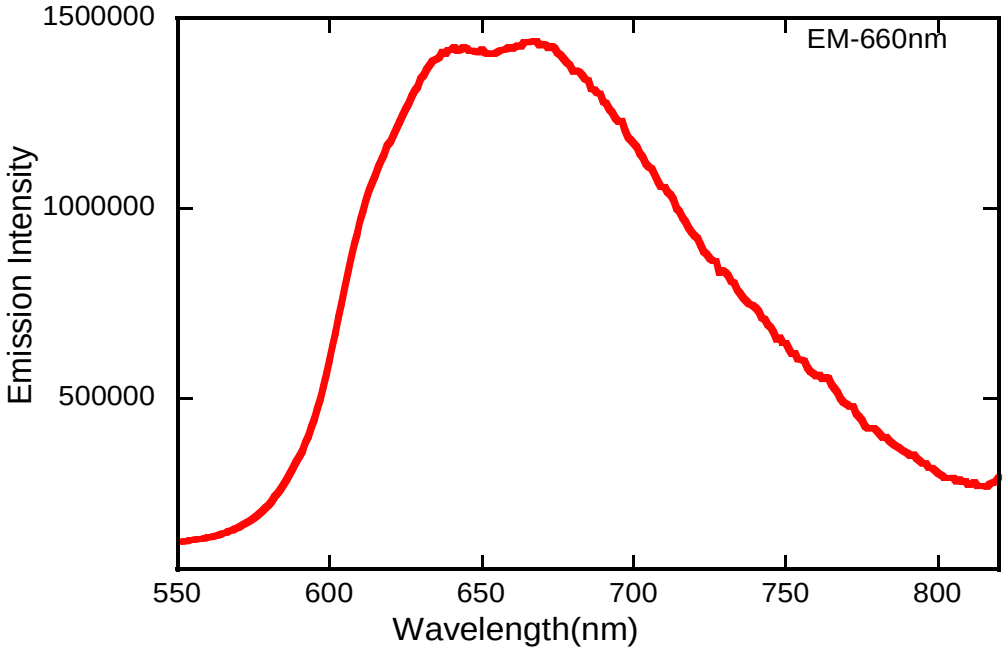

Figure 2.28: Room temperature emission spectrum for $[(TpyIN)Pt(bdt)]^{1-}$ collected in a polystyrene thin film using 430 nm excitation.

We have determined the relative quantum yields of these complexes by using tris(bipyridine)ruthenium(II)chloride $[Ru(bpy)_3Cl_2]$ as a standard. The relative quantum yield method is that two solutions that have the same absorbance at a given excitation wavelength can be assumed to be absorbing the same number of photons. The quantum yield of $[Ru(bpy)_3]^{++}$ is 0.095 in acetonitrile under degassed conditions at room temperature.[29]

The quantum yield formulas are given below:

$$Qs = Qr \left(\frac{Ar}{As}\right) \left(\frac{Es}{Er}\right) \quad 2.2$$

$$Qs = Qr \left(\frac{Ar}{As}\right) \left(\frac{Es}{Er}\right) \left(\frac{\eta s}{\eta r}\right)^2 \quad 2.3$$

Here, the subscripts s and r are for sample and reference respectively, Qs = Quantum yield of Sample, Qr = Quantum yield of Reference, Ar = Absorbance of reference, As = Absorbance of sample, Es = Integrated emission area of sample and Er = Integrated emission area of reference, ηs = refractive index of solvent of sample, ηs = refractive index of solvent of reference.

By observing quantum yields of radical elaborated molecules compared to the parent molecules (molecules without iminonitroxide substituents), we found that phosphorescence efficiencies are quenched by a factor of 10 with the radical attachment on the acceptor side of these molecules (Table 2.1).

Compound	ϕ (ACN)	ϕ (DCM)
$[(Ppy)Pt(bdt)]^{1-}$	0.0236	0.0309
$[(Tpy)Pt(bdt)]^{1-}$	0.0161	0.0154
$[(PpyIN)Pt(bdt)]^{1-}$	0.0026	0.0088
$[(TpyIN)Pt(bdt)]^{1-}$	0.0029	0.0018

Table 2.1: Quantum yields of compounds with and without iminonitroxide radical substituents measured in acetonitrile (ACN) and dichloromethane (DCM).

The radiative decay rate constants (k_r) of these complexes with radical substituents and without radical substituents were evaluated from their emission quantum yield (ϕ_{em}) and emission decay rates (τ_{em}) using the following equations.

$$Q_{em} = k_r/(k_r + k_{nr}) \quad 2.3$$

$$t_{em} = 1/(k_r + k_{nr}) \quad 2.4$$

$$k_r = Q_{em}/t_{em} \quad 2.5$$

Using the above equations, the calculated radiative rate constants are presented in Table 2.2.

Complex	Stokes shift (cm^{-1})	τ(ns)	ϕ	k_r (s^{-1})	k_{nr} (s^{-1})
$[(Ppy)Pt(bdt)]^{1-}$	5630	548	0.0309	5.66×10^{4}	176.8×10^{4}
$[(Tpy)Pt(bdt)]^{1-}$	4643	718	0.0154	1.40×10^{4}	137.6×10^{4}
$[(PpyIN)Pt(bdt)]^{1-}$	3896	0.62	0.0088	1.42×10^{7}	159.6×10^{7}
$[(TpyIN)Pt(bdt)]^{1-}$	3786	0.68	0.0018	2.6×10^{6}	146.8×10^{7}

Table 2.2: Photophysical properties of cyclometalated platinum dithiolate complexes with and without iminonitroxide radical substituents.

The quantum yields of cyclometalated Pt(II)dithiolate complexes without radical substituents ([(Ppy)Pt(bdt)]$^{1-}$ and [(Tpy)Pt(bdt)]$^{1-}$) are found to be higher than the Pt(II) diimine analogs[36], and, the iminonitroxide radical substituted cyclometalated platinum(II) complexes have a comparable quantum yield with these Pt(II)(diamin)(dithiolate) complexes.[36]

We may assume that quenching of the phosphorescence emission and the very short lifetimes of radical elaborated complexes is an indication of either small energy gaps between D_{trip} and quartet states and, reverse intersystem crossing to the D_{trip} states is happening, or there is a SOC-enhanced nonradiative decay mechanism[27,28] via IC. The D_{trip} to doublet ground state recovery is fast and favored by D_{sing} to D_{trip} mixing via exchange coupled interactions and partially spin allowed overall doublet character (see Figure 2.43).

2.6 Variable Temperature Photoluminescence and Lifetimes

To further investigate photoluminescence behavior of these cyclometalated square planar platinum complexes that incorporate a benzene-dithiolate ligand, we have performed variable temperature photoluminescence experiments. We prepared thin film samples of these complexes by dissolving the compounds and polystyrene in dichloromethane solvent and allowing them to dry. Doped polymer films are reported to increase the photoluminescence efficiency of various Pt complexes compared to solution phases[45] This temperature dependent study also helps to detect if there is any presence

of thermally activated delayed fluorescence[40] (TADF) in these complexes. It is important to study TADF behavior in these molecules because they exhibit very short decay rates at room temperature in solution. We have observed a very small energy gap between the trip-doub and quartet states from our CASSCF calculations, and our initial hypothesis was that this small energy gap might facilitate TADF behavior. Hence, to check the photophysical behavior at low temperature, we have examined the emission spectra and decay rates from room temperature to 4K using an Oxford cryostat cooled with liquid helium. To the best of our knowledge, we are reporting the first emissive properties of cyclometalated Pt(II)dithiolate complexes in a polystyrene thin film matrix. The procedure for variable temperature photoluminescence and lifetime measurements are detailed in Appendix A (A9).

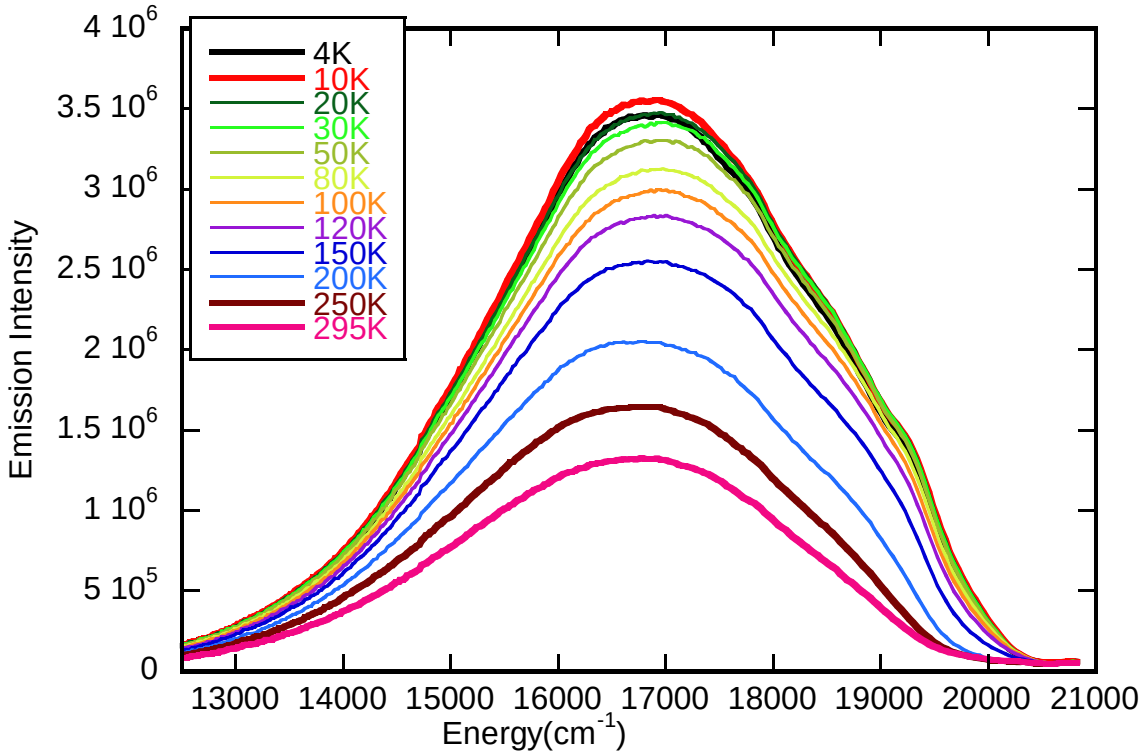

Figure 2.29A: Variable-temperature emission spectra of $[(PpyIN)Pt(bdt)]^{1-}$ collected in a polystyrene thin film using an excitation wavelength of 450 nm.

When we decrease the temperature from 295K to 10K in these cyclometalated Pt(II)dithiolate complexes with two different cyclometalating ligands (Ppy and Tpy), there is a regular increase in emission intensities (Figures 2.29A and 2.29B, respectively). Also, the emission peak at λ_{max} is very slightly blue shifted when the temperature is decreased. Generally, we can expect a red shift in emission maxima at lower temperature if thermally activated delayed fluorescence is happening.[40]

For the $[(PpyIN)Pt(bdt)]^{1-}$ complex, we observed a consistent peak shape with a slight blue shift of ~5 nm from 600 nm (16,650 cm^{-1}) to 595 nm (16,800 cm^{-1}) upon cooling

to 4K as shown in Figure 2.29A. We also observed broad shoulders at 520 nm (19,231 cm^{-1}), 540 nm (18,519 cm^{-1}) and 565 nm (17,700 cm^{-1}) at very low temperatures (below 20K) as shown in Figure 2.29A. Unfortunately, the low resolution of these spectra, even at 4K, does not permit a detailed analysis of these spectral features.

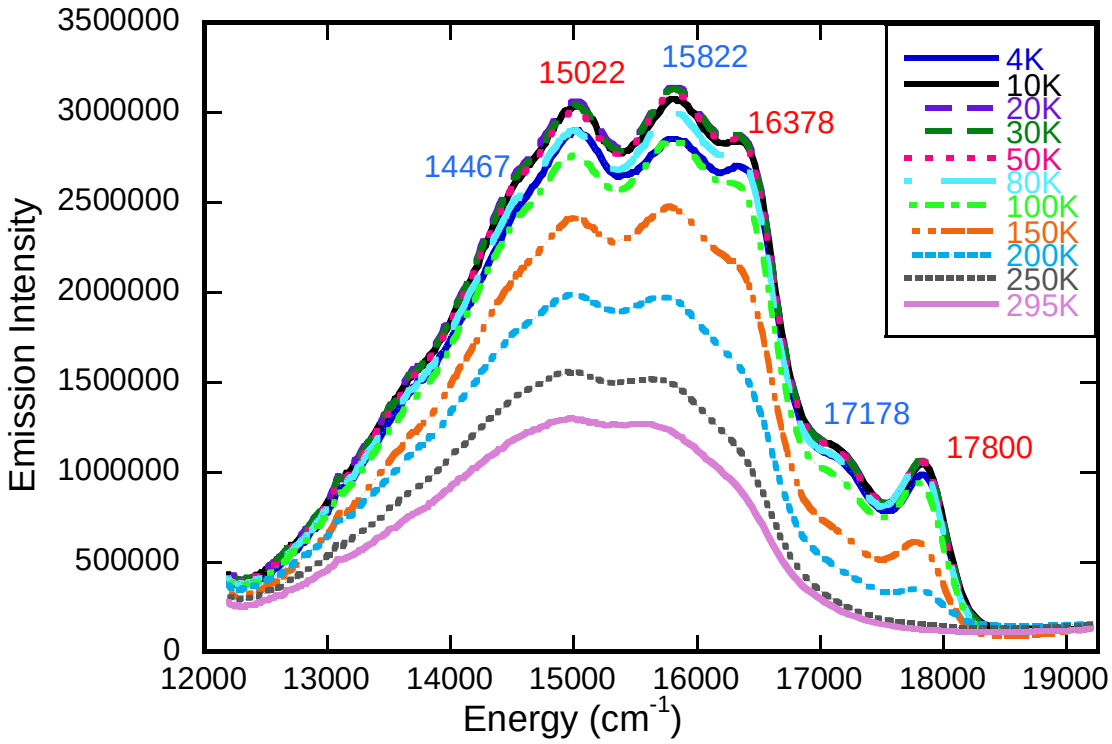

Figure 2.29B: Variable-temperature emission spectra of $[(TpyIN)Pt(bdt)]^{1-}$ collected in a polystyrene thin film using an excitation wavelength of 430 nm.

For the $[(TpyIN)Pt(bdt)]^{1-}$ complex, we previously observed complex vibronic structure in the steady state emission spectrum at 77K (degassed butyronitrile glass). Here, we also observe vibronic structure in the variable temperature emission spectra where the complex has now been imbedded in a polystyrene polymer matrix. We observe

only broad peaks at 640 nm (15,625 cm^{-1}) and 666 nm (15,015 cm^{-1}) in both the room temperature and 250K data sets (Figure 2.29B). However, upon lowering the temperature further the room temperature peak at 640 nm is blue shifted to 633 nm (15,822 cm^{-1}) while the peak at 666 nm is blue shifted to 663 nm (15,083 cm^{-1}). Starting from 200K, peaks are also observed at 562 nm (17,800 cm^{-1}), 584 nm (17,178cm^{-1}), 612 nm (16,378cm^{-1}), 633 nm (15,822cm^{-1}) and 666 nm (15,015 cm^{-1}). The intensities of these bands gradually increase with decreasing temperature. However, the intensity of the spectrum at 4K is reduced, and is nearly the same as the intensity recorded at 80K. The origin of this intensity reduction is not fully understood at this time but may derive from weak intermolecular exchange interactions between some of the chromophores.

The highest energy peak in Figure 2.29B is observed at ~17,800 cm^{-1} and has the appearance of an inhomogeneously broadened zero-phonon line (ZPL). Evidence for a ZPL assignment derives from the fact that the intensity distribution between the ZPL and the phonon side band is very temperature dependent. If the chromophores are strongly coupled to phonons in the polymer matrix, there are likely to be a large number of phonons that are excited at room temperature. This typically has the effect of dramatically reducing the intensity of the ZPL such that it is not observed at higher temperatures. The two bands at ~16,378 cm^{-1} and ~15,022 cm^{-1} may be assigned as vibronic transitions associated with the origin at ~17,800 cm^{-1}. Thus, the band displays a progression in an apparent vibrational mode with an ~1,390 cm^{-1} energy spacing. The band at 17,178 could either be a second inhomogeneously broadened zero-phonon line, deriving from a different subset of chromophores in the polymer matrix, or a 622 cm^{-1}

vibronic origin with an ~1,360 cm^{-1} progression forming mode that is very similar the ~1,390 cm^{-1} vibration responsible for the progression built on the ~17,800 cm^{-1} origin. The two sets of the vibronic progressions support the idea of aggregate formation[18] in the polymer thin film matrix, which leads to two different chromophoric environments. Since these are emission spectra, the vibrational spacings correlate with the ground state vibrations of the molecule. DFT frequency computations for $[(TpyIN)Pt(bdt)]^{1-}$ reveal three vibrational modes, depicted in Figure 2.30, that could be associated with the progressions observed in the low-temperature emission spectra of the $[(TpyIN)Pt(bdt)]^{1-}$ complex.

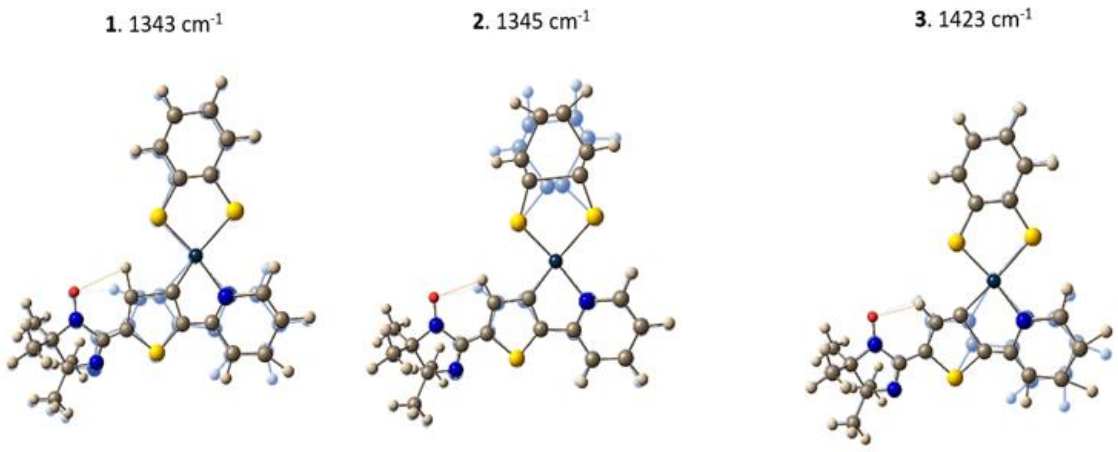

Figure 2.30: Results of a DFT frequency calculation for $[(TpyIN)Pt(bdt)]^{1-}$ showing the most probable vibrational modes that could correspond to the experimental progressions observed in the low-temperature emission spectra of this complex. Here, we observe thiophene carbon-carbon stretching (1), symmetric phenyl ring stretching (2) and inter-ring thiophene-pyridine carbon-carbon stretching (3) modes, whose energies are close to the energy intervals observed in the emission spectrum (Figure 2.29).

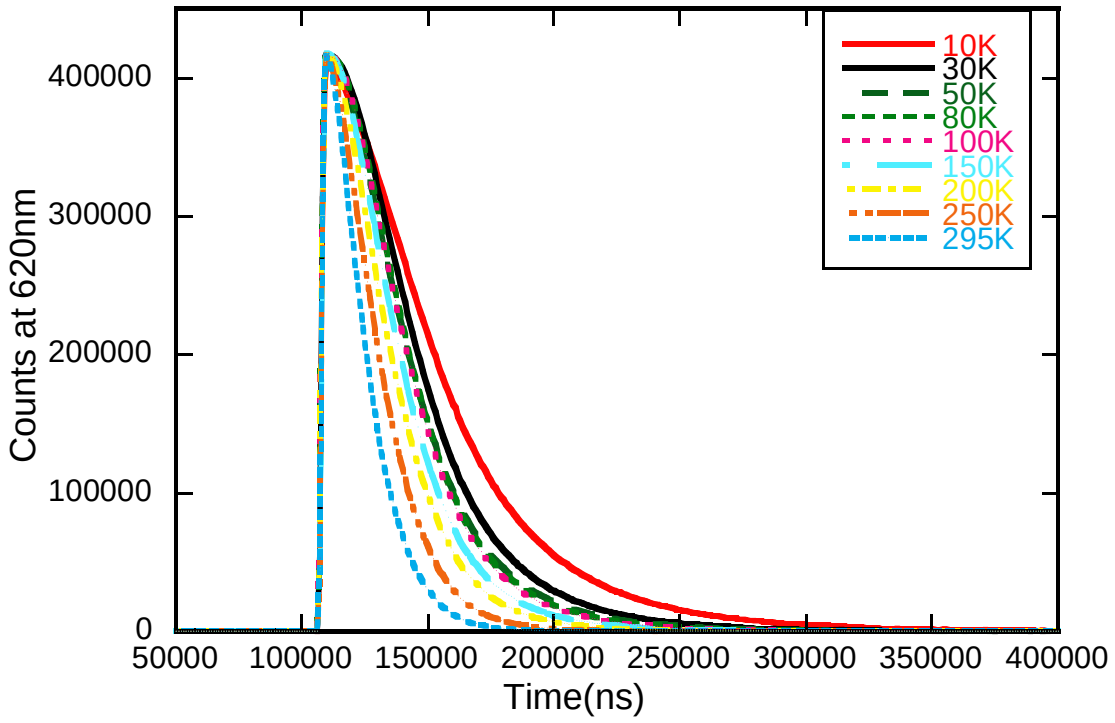

Figure 2.31A: A variable-temperature (10 – 295K) overlay of emission decay traces at 620 nm for $[(PpyIN)Pt(bdt)]^{1-}$ in a polystyrene thin film.

Additionally, these cyclometalated Pt(II)dithiolate complexes show multiexponential decay times in polystyrene thin films. The emission lifetimes of the $[(PpyIN)Pt(bdt)]^{1-}$ and $[(TpyIN)Pt(bdt)]^{1-}$ complexes were best fit by a tri-exponential function (Table 2.3A and Table 2.4). Table 2.3B shows the biexponential fitting for $[(PpyIN)Pt(bdt)]^{1-}$ complex, however the fitting is better using a tri-exponential function. An exponential tail fit analysis was used, and the χ^2 values are close to unity, indicative of the goodness of fit.

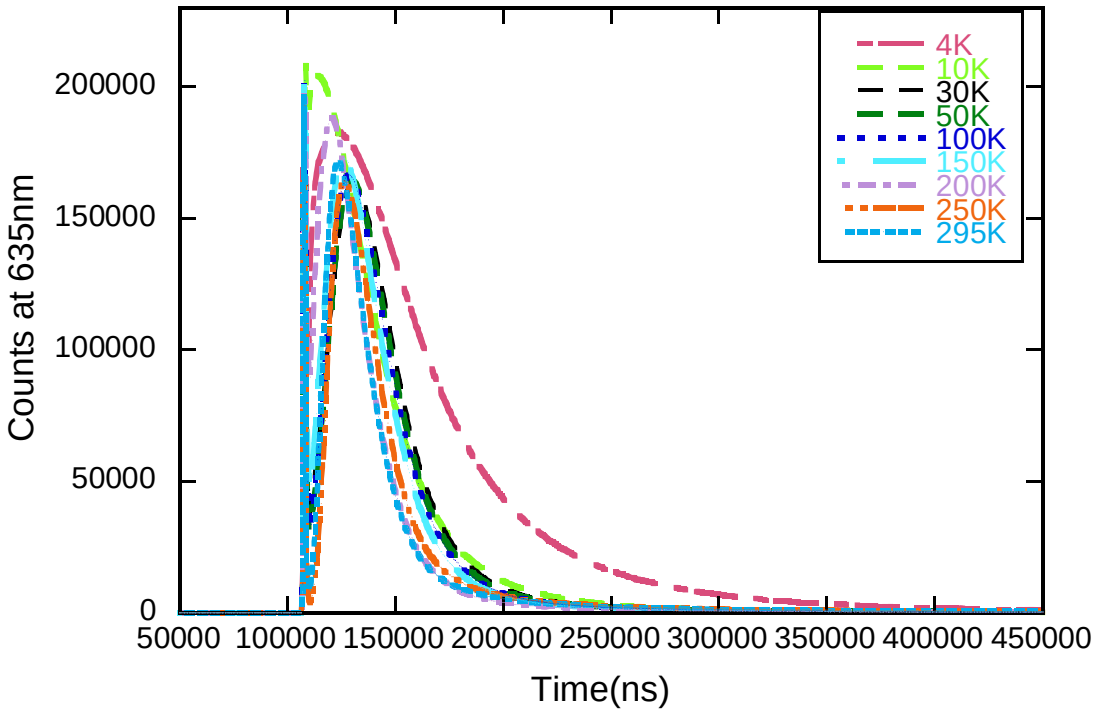

Figure 2.31B: A variable-temperature (10 – 295K) overlay of emission decay traces at 635 nm for $[(TpyIN)Pt(bdt)]^{1-}$ in a polystyrene thin film.

These types of cyclometalated platinum complexes are known for aggregation induced emission at higher concentrations and in solid state, and exhibit longer and multiexponential lifetimes because these molecules can exhibit different aggregation modes.[18,45] Aggregation induced emission usually results in longer lifetimes, and different modes of aggregation can give multiexponential decay rates.[18,45] The multiexponential emission decays in a thin film matrix can also indicate their complex photophysical behavior.

T (K)	τ_1(μs)	B1	τ_2(μs)	B2	τ_3(μs)	B3	X^2
10	**32.7082**	92839.5	**53.2481**	33926.0	**468.2121**	120.1	1.147
20	**28.6675**	135470.3	**51.5271**	17080.3	**468.6093**	114.7	1.435
30	**25.8219**	114236.9	**46.6297**	177757.1	**442.6090**	123.7	1.234
50	**27.5370**	134206.4	**64.4072**	3855.1	**473.6305**	144.5	1.321
100	**24.5318**	120067.3	**61.0006**	3337.3	**444.0884**	162.7	1.257
150	**21.6187**	108215.4	**53.9945**	3440.8	**435.5354**	150.6	1.260
200	**19.3318**	116704.5	**74.6160**	1082.2	**496.1677**	117.0	1.357
250	**14.9736**	78949.0	**90.5970**	504.3	**544.6853**	82.4	1.197
295	**11.8158**	58037.1	**95.4225**	360.99	**543.4042**	67.4	1.243

Table 2.3A: The variable temperature lifetime parameters for $[(PpyIN)Pt(bdt)]^{1-}$ complex at 600 nm emission collected in a polystyrene thin film. These data are fit with tri-exponential functions.

T (K)	τ_1(μs)	B1	τ_2(μs)	B2	X^2
4	**55.1343**	155067.5	**583.1226**	167.9	2.041
10	**39.7777**	90546.1	**300.3589**	296.5	2.665
30	**30.4435**	65893.1	**336.8729**	215.5	2.484
50	**29.1949**	80705.0	**359.5188**	254.8	2.226
100	**26.0604**	77792.7	**343.1495**	278.3	2.245
150	**23.2770**	66062.5	**345.1750**	245.0	2.304
200	**20.1591**	54951.0	**342.5403**	223.9	2.050
250	**15.5413**	34090.8	**328.7004**	189.9	1.942
295	**12.3958**	16821.4	**309.7409**	169.0	1.979

Table 2.3B: The variable temperature lifetime parameters for $[(PpyIN)Pt(bdt)]^{1-}$ complex at 600 nm emission collected in a polystyrene thin film. These data are fit with bi-exponential functions.

T (K)	τ_1(μs)	B1	τ_2(μs)	B2	τ_3(μs)	B3	X^2
4	**37.5027**	11619.2	**89.5638**	24855.3	**589.3043**	226.1	1.276
10	**22.1614**	71888.1	**63.2441**	11033.9	**479.1187**	177.3	1.341
30	**18.9310**	100423.7	**88.1609**	4500.5	**515.2904**	289.6	1.329
50	**18.1296**	94192.5	**86.3248**	4544.4	**508.1328**	299.1	1.355
100	**17.6427**	88274.0	**85.8088**	4388.1	**510.1572**	291.0	1.326
150	**16.8850**	77588.4	**81.2047**	4320.8	**481.9554**	281.6	1.373
200	**14.6981**	45911.2	**74.2973**	4206.1	**460.3903**	263.5	1.389
250	**14.2529**	53915.9	**75.2830**	8204.2	**429.2454**	542.5	1.686
295	**13.4818**	39147.8	**73.8416**	7625.5	**426.8501**	522.7	1.707

Table 2.4: The variable temperature lifetime parameters for $[(TpyIN)Pt(bdt)]^{1-}$ complex at 633 nm emission collected in a polystyrene thin film. These data are fit with tri-exponential functions.

There is a regular increase in integrated emission area (calculated using Kaleidagraph software) as shown in Figures 2.32A and 2.32B, respectively, and an increase in emission intensities (emission peak intensities as shown in Figure E5 and Figure E6 in appendix E) on lowering the temperature from 295K to 10K. Both the $[(PpyIN)Pt(bdt)]^{1-}$ and $[(TpyIN)Pt(bdt)]^{1-}$ complexes have non-linear integrated intensities as a function of temperature as shown in Figure 2.32A and Figure 2.32B, respectively.

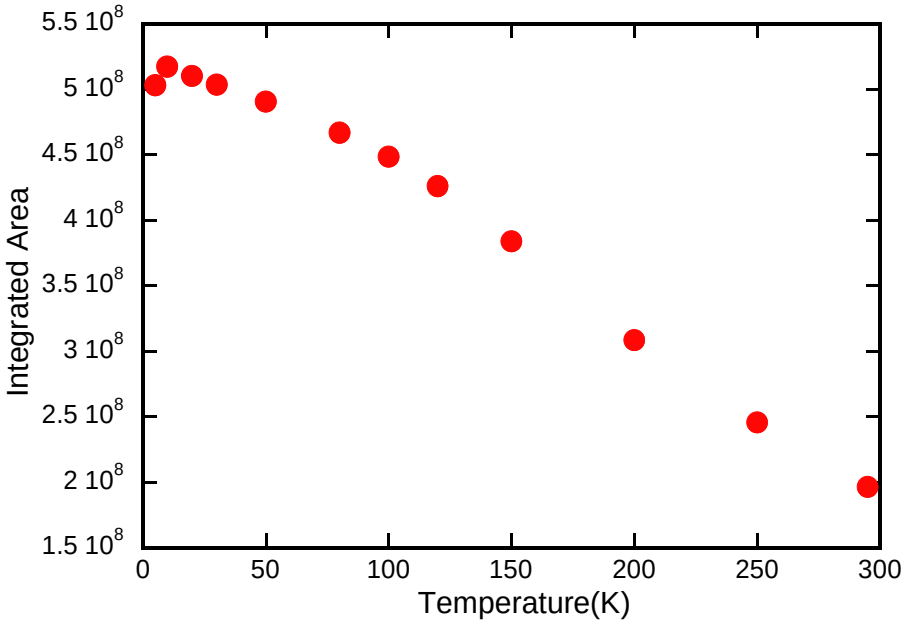

Figure 2.32A: Integrated area of emission versus temperature for $[(PpyIN)Pt(bdt)]^{1-}$ in a polystyrene thin film.

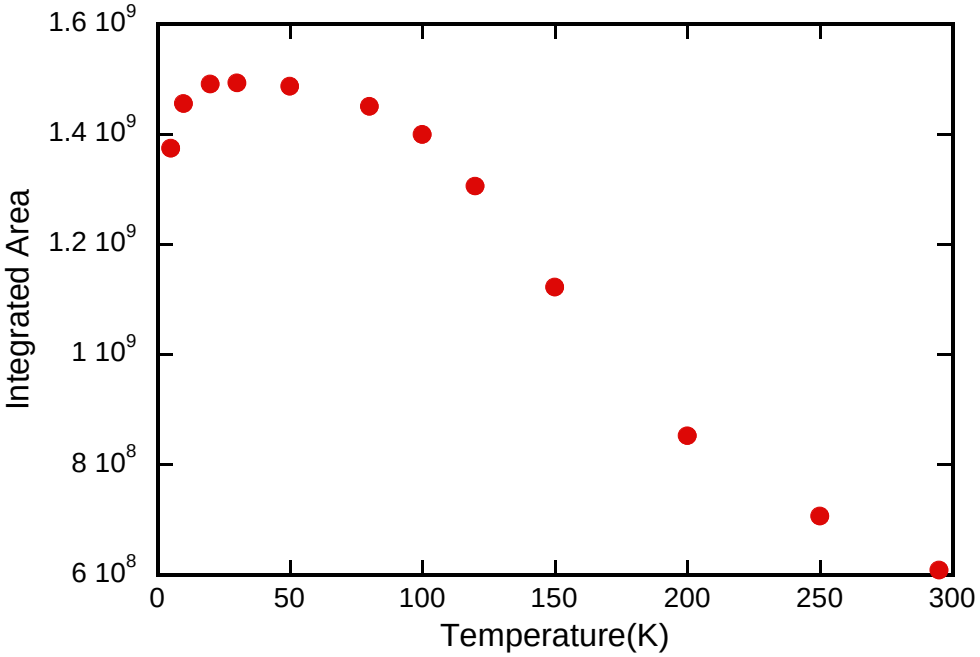

Figure 2.32B: Integrated area of emission versus temperature for $[(TpyIN)Pt(bdt)]^{1-}$ in a polystyrene thin film.

The variable temperature photoluminescence of the parent complexes $[(Ppy)Pt(bdt)]^{1-}$ and $[(Tpy)Pt(bdt)]^{1-}$ were also collected in polystyrene thin films. Variable temperature experiments were performed on the non-radical-elaborated parent molecules to obtain better insight into the photophysical behavior of their radical-elaborated forms. When the temperature is cooled down from 295K to 4K, there is an irregular change in emission intensities for both the $[(Ppy)Pt(bdt)]^{1-}$ and $[(Tpy)Pt(bdt)]^{1-}$ compounds as shown in Figures 2.33A and 2.34A, respectively.

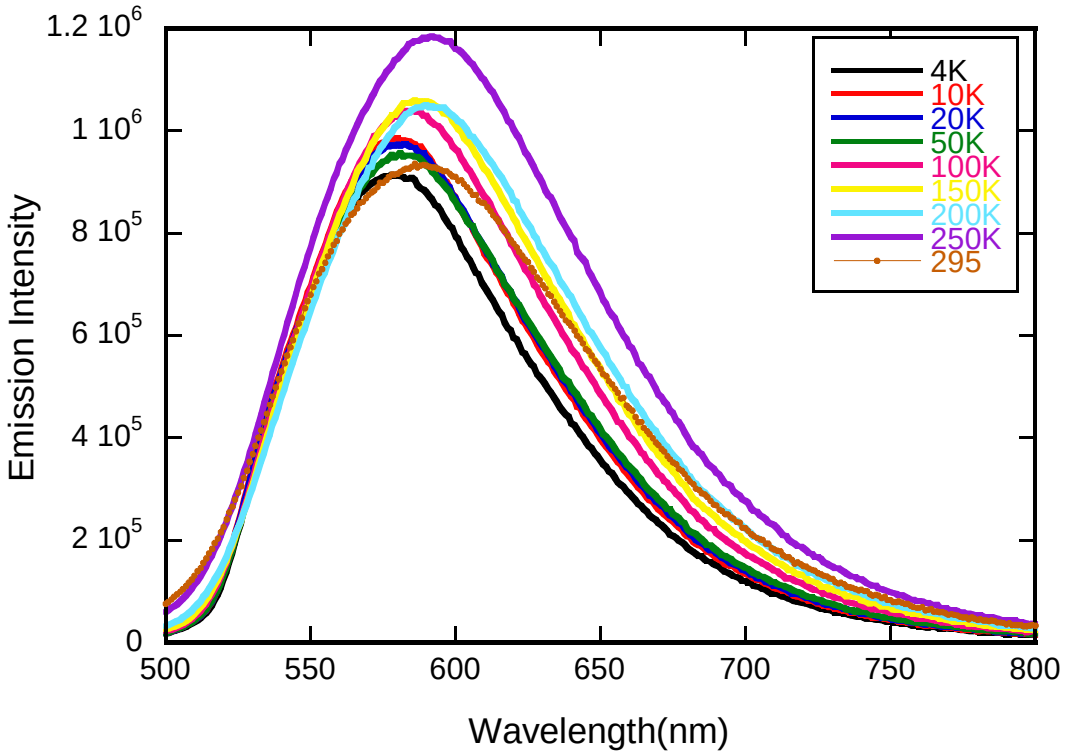

Figure 2.33A: Variable-temperature emission spectra of $[(Ppy)Pt(bdt)]^{1-}$ collected in a polystyrene thin film using an excitation wavelength of 470 nm.

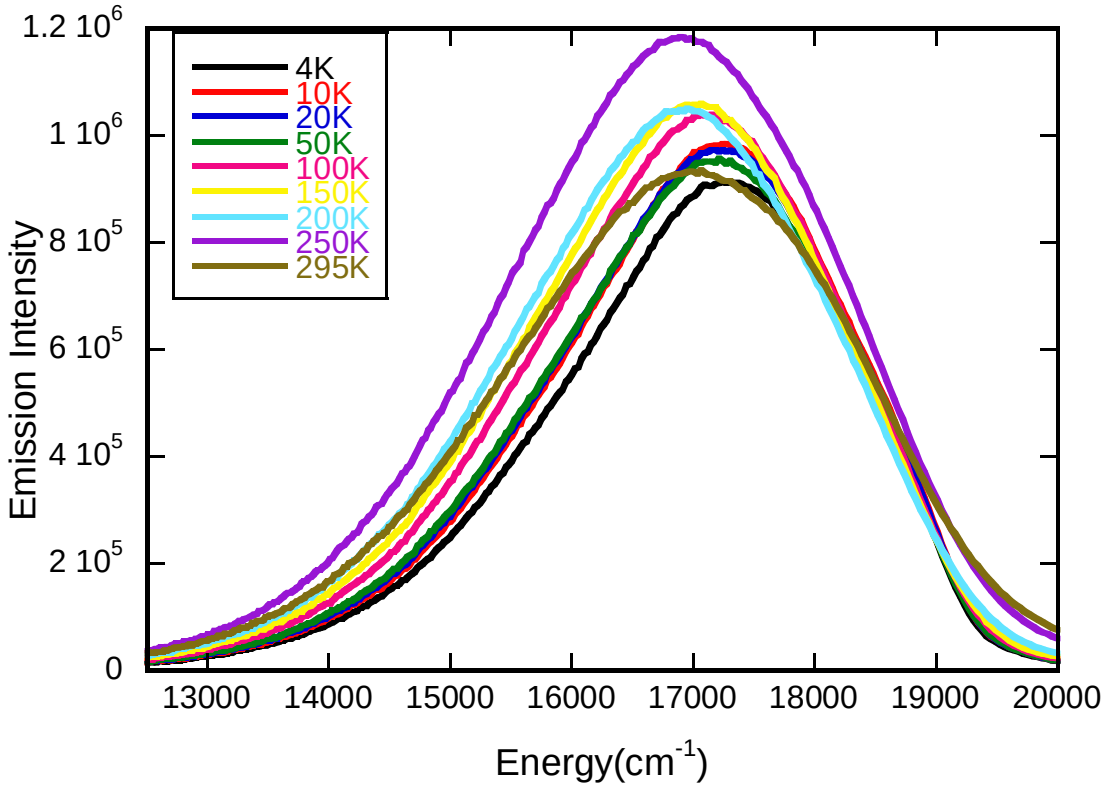

Figure 2.33B: Variable-temperature emission spectra of $[(Ppy)Pt(bdt)]^{1-}$ collected in a polystyrene thin film using an excitation wavelength of 470 nm.

The emission band of the $[(Ppy)Pt(bdt)]^{1-}$ complex is slightly blue slightly from 588 nm to 581 nm upon cooling from 295K to 4K, and an irregular change was observed in emission intensities with the lowest emission intensity occuring at 4K as seen in Figure 2.33A. Similarly, the emission band of the $[(Tpy)Pt(bdt)]^{1-}$ complex is blue shifted from

591 nm to 589 nm with a similar irregular change in emission intensities as shown in Figure 2.34A. For the $[Tpy)Pt(bdt)]^{1-}$ complex, the lowest integrated emission intensity was observed at 50K.

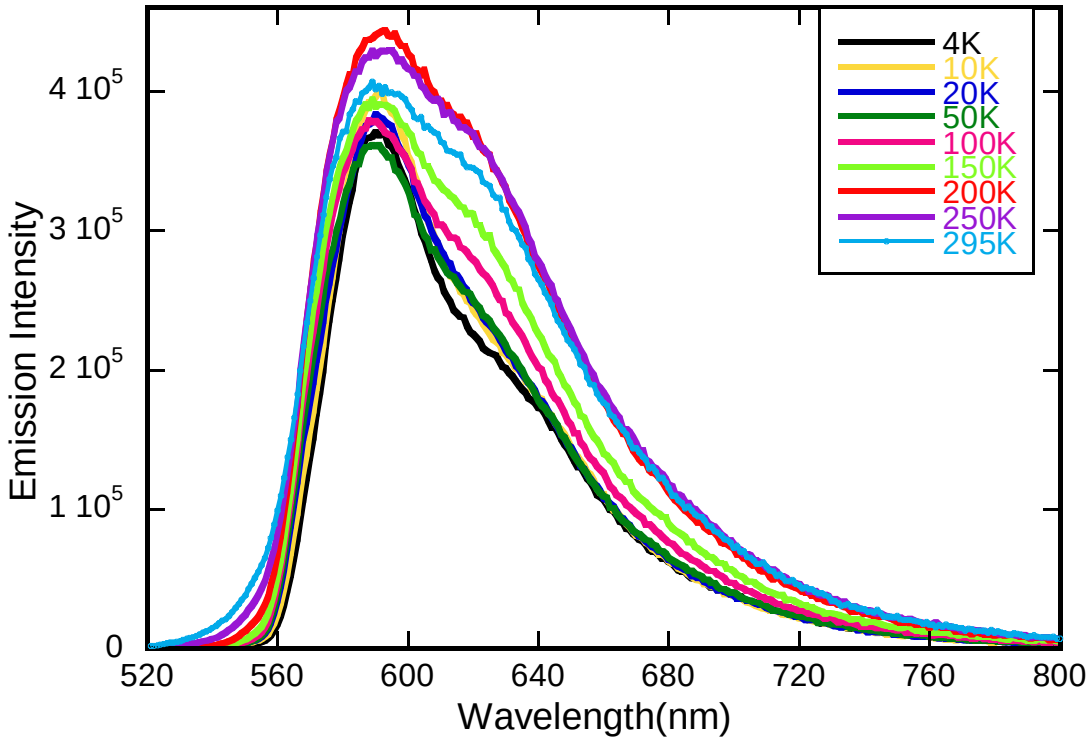

Figure 2.34A: Variable-temperature emission spectra of $[(Tpy)Pt(bdt)]^{1-}$ collected in a polystyrene thin film using an excitation wavelength of 485 nm.

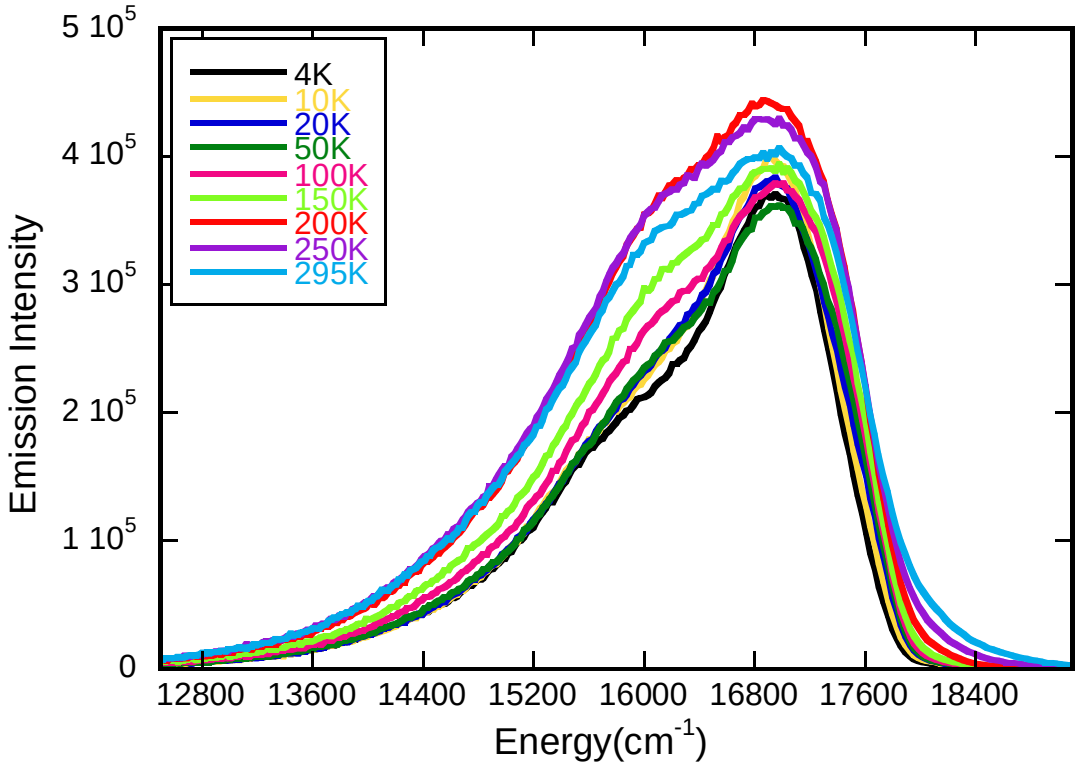

Figure 2.34B: Variable-temperature emission spectra of $[(Tpy)Pt(bdt)]^{1-}$ collected in a polystyrene thin film using an excitation wavelength of 485 nm.

In terms of photoluminescence lifetimes in polystyrene thin films, the lifetime data for both parent molecules, $[(Ppy)Pt(bdt)]^{1-}$ and $[(Tpy)Pt(bdt)]^{1-}$, were best fit with bi-exponential decay functions. $[(Ppy)Pt(bdt)]^{1-}$ parent complex had a short component lifetime of 13.83 μs at 295K, and upon decreasing the temperature to 4K, the lifetime was increased to 81.35 μs (Table 2.5A). The $[(Ppy)Pt(bdt)]^{1-}$ parent complex had a long component lifetime of 362.67 μs at 295K, and upon decreasing the temperature to 4K, the lifetime was increased to 591.73 μs (Table 2.5A). Similarly, $[(Tpy)Pt(bdt)]^{1-}$ had a short component lifetime of 12.29 μs at 295K, and upon decreasing the temperature to 4K, the lifetime was increased to 86.98 μs (Table 2.5B). The $[(Tpy)Pt(bdt)]^{1-}$ had a long component

lifetime of 240.07 μs at 295K, and upon decreasing the temperature to 4K, the lifetime was increased to 1137.24 μs (Table 2.5B). The short and long component lifetimes of both parent complexes are increasing with decreasing the temperatures from 295K to 4K.

Temperature (K)	τ_1 (μs)	B_1	τ_2 (μs)	B_2	X^2
4	**81.35**	379915	**591.73**	721	2.958
10	**38.13**	352315	**441.81**	922	2.957
20	**27.55**	374639	**455.10**	860	3.228
30	**25.21**	337142	**435.24**	847	3.133
50	**23.52**	306569	**432.58**	857	3.215
100	**21.78**	266025	**417.64**	874	3.175
150	**20.83**	239626	**441.67**	801	3.142
200	**19.83**	318513	**422.94**	690	2.985
250	**17.45**	261412	**398.83**	706	3.170
295	**13.83**	142367	**362.67**	661	3.494

Table 2.5A: Variable temperature lifetime parameters for the $[(Ppy)Pt(bdt)]^{1-}$ complex in a polystyrene thin film monitored at 588 nm. These data are fit with bi-exponential decay functions.

Temperature (K)	τ_1 (μs)	B_1	τ_2 (μs)	B_2	X^2
4	**86.98**	453786.09	**1137.24**	546.33	2.319
10	**61.56**	360153.56	**1088.37**	549.92	2.141

20	**42.71**	146607.66	**882.37**	643.99	3.50
30	**32.92**	114291.83	**465.91**	556.45	2.806
50	**24.31**	235123.84	**246.86**	643.46	3.108
100	**17.74**	168088.69	**232.99**	662.16	2.983
150	**16.03**	140062.45	**232.11**	622.79	2.682
200	**15.09**	127839.26	**240.42**	607.94	2.456
250	**13.78**	104587.03	**242.10**	537.51	2.199
295	**12.29**	72140.82	**240.07**	448.79	2.092

Table 2.5B: Variable temperature lifetime parameters for the $[(Tpy)Pt(bdt)]^{1-}$ complex in a polystyrene thin film monitored at 591 nm. These data are fit with bi-exponential decay functions.

Compared to the lifetime measurements in thin polymer films of the radical-elaborated cyclometalated dithiolate complexes, the polymer film lifetimes of the corresponding parent molecules were slightly longer at lower temperatures (4K). The thin film lifetime of $[(PpyIN)Pt(bdt)]^{1-}$ was 55.13 μs at 4K while that of $[(Ppy)Pt(bdt)]^{1-}$ was 81.35 μs at 4K. Similarly, the thin film lifetime of $[(TpyIN)Pt(bdt)]^{1-}$ was 37.50 μs at 4K while that of $[(Tpy)Pt(bdt)]^{1-}$ was 86.98 μs at 4K. These long-lived emission lifetimes in the thin film samples showed that the radical-elaborated cyclometalated anionic complexes were phosphorescent in nature, supporting the idea that doped film encourages predominantly phophorescece.[45] However, the room temperature (295K) lifetimes of

radical-elaborated complexes and their associated non-radical elaborated parent molecules in thin film matrices were similar to those obtained at low-temperature. This indicates that concentration dependent thin film studies are now necessary to interpret these results due to the potential for aggregate formation in the polymers. From the VT photoluminescence data of these cyclometalated Pt(II) complexes, it can be rationalized that the photophysics of the cyclometalated Pt(II) systems is markedly more complex in polymer thin films than in frozen glasses.

2.7 Time Resolved EPR Spectroscopy

Time Resolved Electron Paramagnetic Resonance (TREPR) spectroscopy is a useful technique to explore different electronic structure-function relationships in the short-lived excited states of paramagnetic molecules.[32,33,48] TREPR methods can also be used to detect and characterize triplet-doublet pairs (*e.g.* higher spin states such as quartets) that are created by an excited state magnetic exchange interaction between a persistent organic radical and the singlet and triplet charge separated excited states of a donor-accepter complex[32]. Another important application of TREPR spectroscopy is that photoinduced electron spin polarization (ESP) can be measured in short lived excited states of the chromophore as well as in the electronic ground state. This ESP can be observed in systems where a stable radical or paramagnetic metal is appended to a chromophore.[33,34,48,49] The nature of the observed ESP helps us to obtain important details about the spin dynamics and photoexcited state properties of a variety of

complexes. When an appended radical interacts with a chromophore photoexcited state, ESP (resulting from a non-Boltzmann spin population of GS/ES Zeeman split m_s levels) can be produced under specific conditions and detected by TREPR. With respect to the detected ESP in an S=1/2 GS, if the lower m_s level (β) is more populated than expected from Boltzmann statistics than the upper m_s level (α), there is a net absorption that is referred to as "A polarization". For the opposite case, when the population of upper m_s level α is greater than that of the m_s level β, a net emission is observed, and this is referred to as "E polarization". A variety of different mechanisms can be operating for the generation of ESP, including reversed quartet (RQM), modified reversed quartet, radical-triplet pair, radical-quartet pair mechanisms etc.[33,34,48,49,50,51]

Prior studies,[33,48,49,50] in collaboration with Professor David Shultz (NC State University) and Professor Art Van der Est (Brock University, Canada), of radical elaborated donor-acceptor complexes showed that spin polarization is observed in the doublet ground state of Pt/Pd donor-acceptor complexes. Furthermore, this work showed that the nature of the metal ion was controlling the type (i.e., A or E) of photo-induced GS ESP.[32] This study indicated that small energy gaps between the trip-doub and quartet states, in addition to metal-mediated spin orbit coupling, play critical roles in producing ESP in the ground and excited states of these systems.[33]

As a result of these early studies, we hypothesized whether we could observe GS or ES ESP in our two anionic cyclometalated platinum(II) dithiolate complexes that are elaborated with a pendent iminonitroxide radical. Initial interpretations of TREPR data

indicate that the quartet state is populated at low temperature. Our initial TREPR data indicate that emissive spin polarization (E polarization) can be observed in these systems.

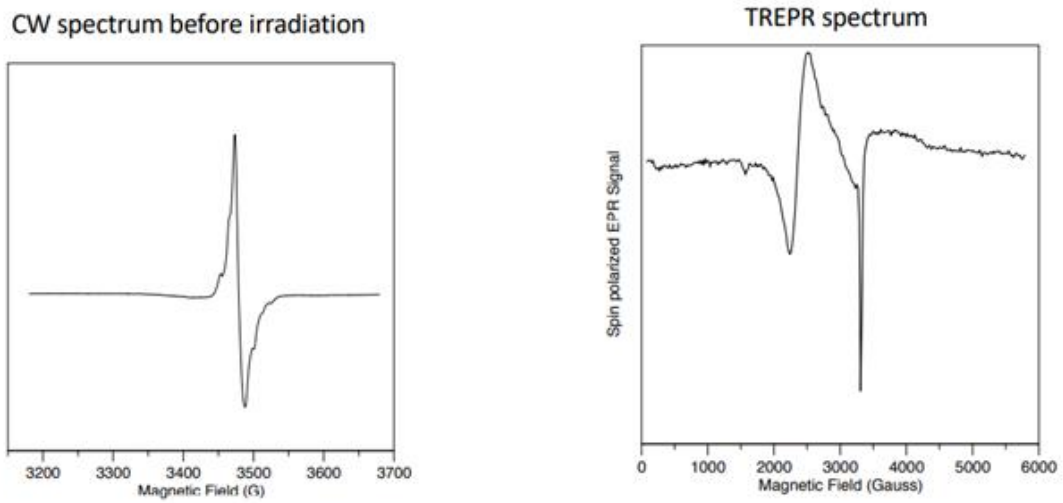

Figure 2.35: CW and TREPR spectra of $[(PpyIN)Pt(bdt)]^{1-}$, DCM, 20K, 5 mJ pulse, 532 nm, 34 dB (Data collected at Brock University - Canada in the laboratory of Prof. Art van der Est). Here, the CW spectrum derives from an S = ½ iminonitroxide center with ^{14}N hyperfine coupling. The TREPR spectrum features characteristics that could arise from an excited quartet state with strong g-tensor anisotropy. The sharp peak observed at g ~ 2 might be from the S=1/2 ground state doublet, but it could also be the part of the excited quartet state.

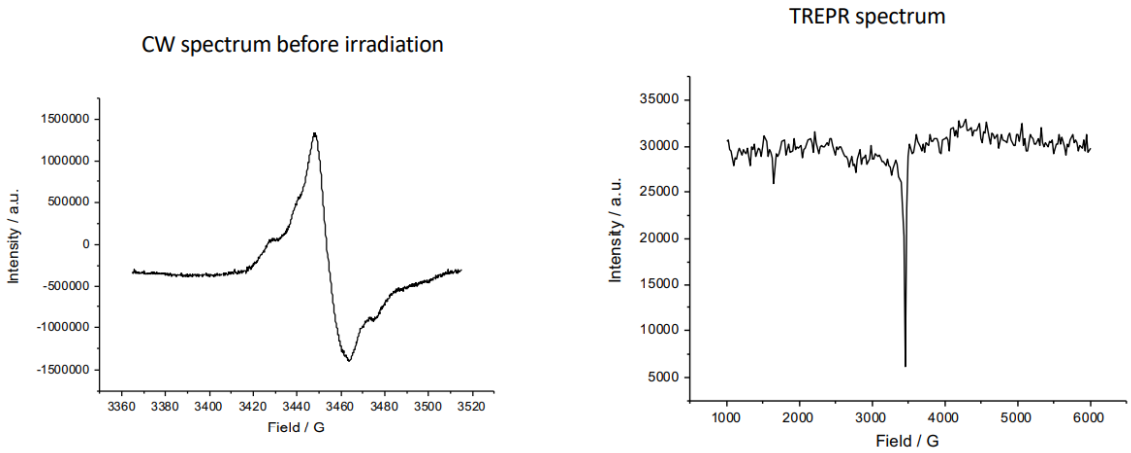

Figure 2.36: CW spectrum and TREPR spectrum of $[(PpyIN)Pt(bdt)]^{1-}$, DCM, 80K, 4.75 mJ pulse, 525nm, 25dB (Data was collected at facilities in Padua, Italy). Here, the CW spectrum is similar to the CW spectrum at 20K. However, only the sharp g_{obs} ~ 2 and weaker sharp g_{obs} ~ 4 features of the TREPR spectrum[52,53] are clearly visible at 80K.

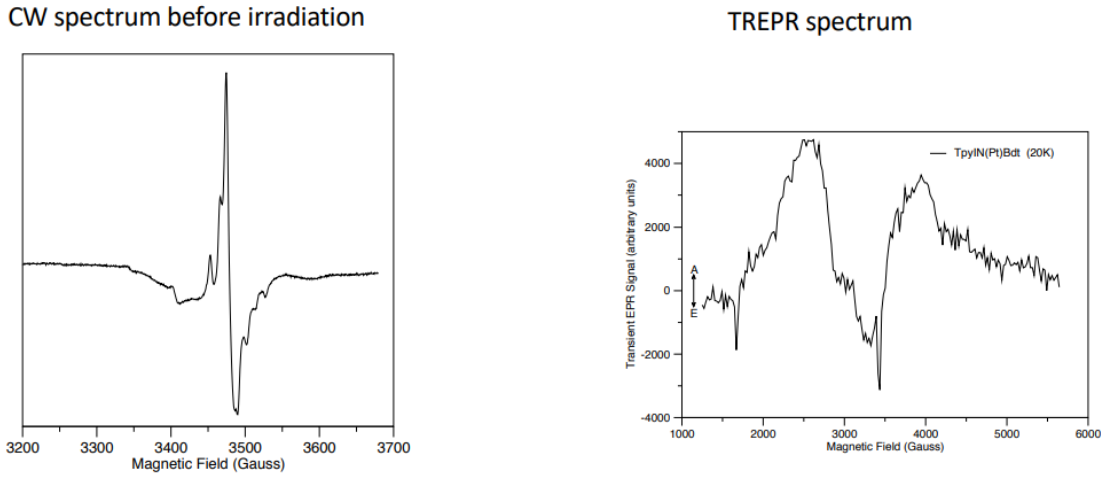

Figure 2.37: CW spectrum and TREPR spectrum of $[(TpyIN)Pt(bdt)]^{1-}$, DCM, 20K, 5 mJ, 532 nm, 34 dB. (Data collected at Brock University - Canada in the laboratory of Prof. Art van der Est). Here, the CW spectrum derives from an S = ½ center with ^{14}N hyperfine coupling.

The wide features in the wings probably derive from the resonator. The TREPR spectrum shows features characteristics of a quartet state with strong g-anisotropy (e.g. sharp features at g_{obs} ~ 2 and g_{obs} ~ 4).[52,53] The sharp peak in the middle of the spectrum might be from the ground state but could also be part of the quartet state.

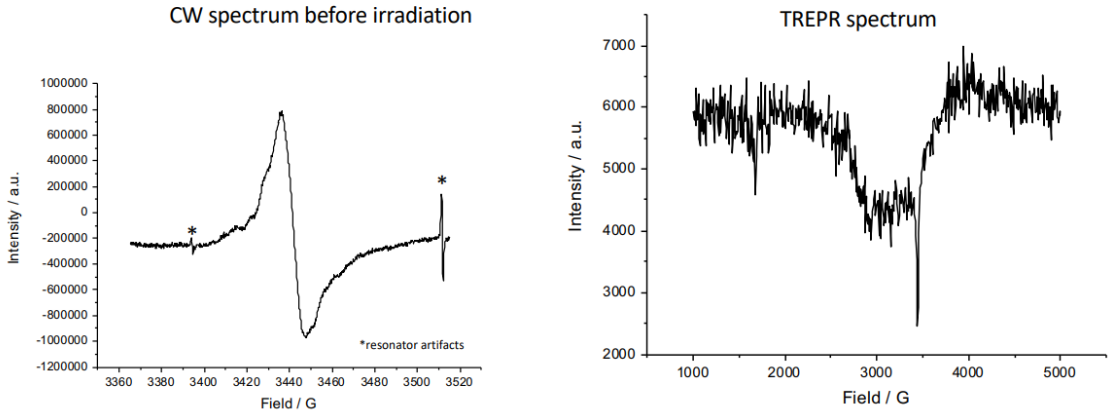

Figure 2.38: CW spectrum and TREPR spectrum of $[(TpyIN)Pt(bdt)]^{1-}$, DCM, 80K, 4.7 mJ, 525 nm, 25 dB (Data was collected at facilities in Padua, Italy). CW spectrum does not show as much structure because the signal may be overmodulated. The TREPR spectrum is similar to that at 20K but has less background signal. The shape of the broad features seems to be different than observed at 20K. Sharp features are observed at g_{obs} ~ 2 and g_{obs} ~ 4, indicating they derive from an excited S = 3/2 quartet state.[52,53]

Although we have not yet simulated these ground state EPR or the TREPR data, based on the initial data we have collected we can suggest that these anionic cyclometalated Pt(II) dithiolates with persistent radicals are displaying emissive ESP characteristic of a quartet spin state at low temperatures. Unfortunately, we do not have

TREPR lifetime data for these systems, and this remains a goal of future studies. Looking at these initial data, we observe both g = 2 and g = 4 EPR transitions. The g = 2 signal could be from the ground state doublet, the excited state D_{trip}, or the $m_s = \pm 1/2$ levels of the excited S = 3/2 quartet state from molecules oriented in the z-direction with respect to the applied field. However, the g = 4 signal can only arise from the $m_s = \pm 1/2$ levels of the S = 3/2 quartet state in the perpendicular direction. From our earlier studies, we can consider two different quartets being involved in the reversed quartet mechanism, with one deriving from the quartet state of the localized radical[33] and the other from the exchange coupling of three unpaired spins in the excited state manifold.[33,48,49,50] Here, we assume the quartet involved in generating the observed spin polarization is from the three-spin exchange coupled system, where the chromophore triplet has some platinum character and a spin orbit coupling contribution that is large enough to have a zero-field splitting greater than or equal to the microwave quantum at X-band (~ 0.33 cm^{-1}).[52,53] These initial TREPR data are encouraging for us to explore the reversed quartet, modified reversed quartet, and J-modulation[35] mechanisms for the generation of ground and excited state ESP in these and related systems.

For the reversed quartet mechanism to be plausible, the quartet state must be populated, which requires a small energy gap between the D_{trip} (trip-doublet) and quartet states.[34] Based on the very short fluorescence decay emission lifetimes for these molecules in frozen glass matrices, we can assume that these molecules have a small

energy gap between the D_{trip} and quartet states, with decay to the ground state originating from the D_{trip} state in a mechanism reminiscent of TADF.[40]

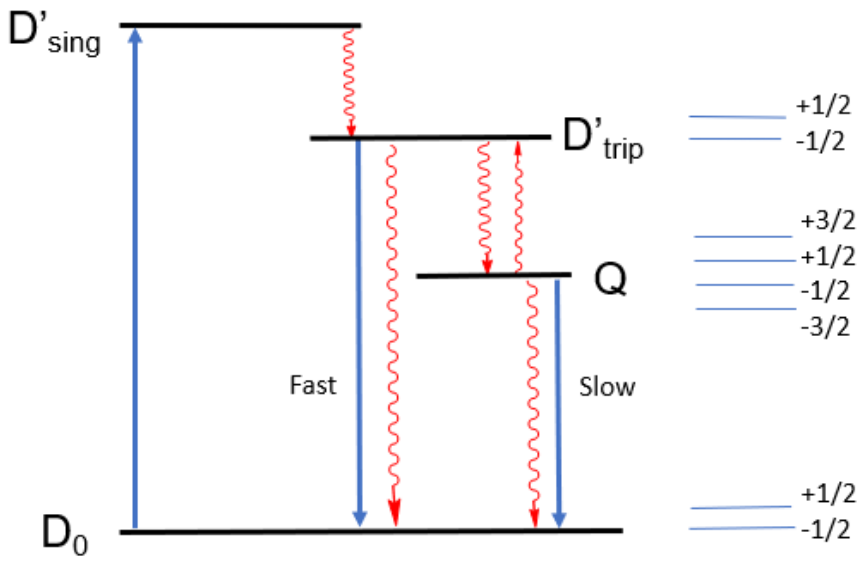

Figure 2.39: A schematic diagram that spin polarization can happen within the energy levels of quartet and doublet spin systems during ground state recovery.

J-modulation[35] may play a role in dynamically changing the magnitude of the D_{trip} – quartet energy gap. J-modulation involves distortions about a torsional energy barrier, where the bond torsions can affect the magnitude of the exchange coupling between the spin containing group (*e.g.* IN) and the chromophoric fragment (*e.g.* $[(Tpy)Pt(bdt)]^{1-}$). Thus, the bond torsion between Tpy/Ppy and IN can modulate the π-interaction between the radical (iminonitroxide) and the Tpy/Ppy ligand fragments to control the intraligand chromophore-radical exchange coupling.[35]

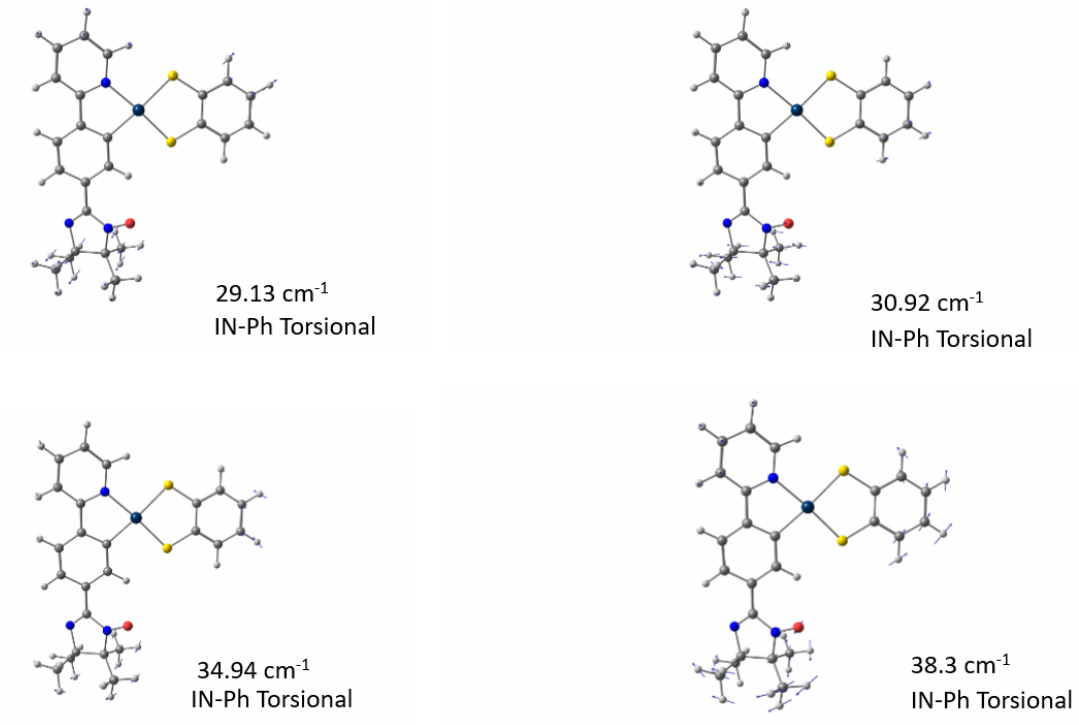

Figure 2.40: The four lowest energy vibrational modes of $[(PpyIN)Pt(bdt)]^{1-}$. Here, the vibrational mode at 30.92 cm^{-1} has the largest IN-Ph bond torsion contribution. These vibrational modes were obtained from a DFT frequency calculation.

IN-Ph and IN-Tp bond torsions that reduce the radical-chromophore exchange coupling function to enhance the mixing between D_{trip} and quartet states. These bond torsions result in a decrease in the energy gap between D_{trip} and quartet. Thus, J-modulation can facilitate transitions between these two states to generate ESP by the reversed quartet mechanism.[33,34,35]

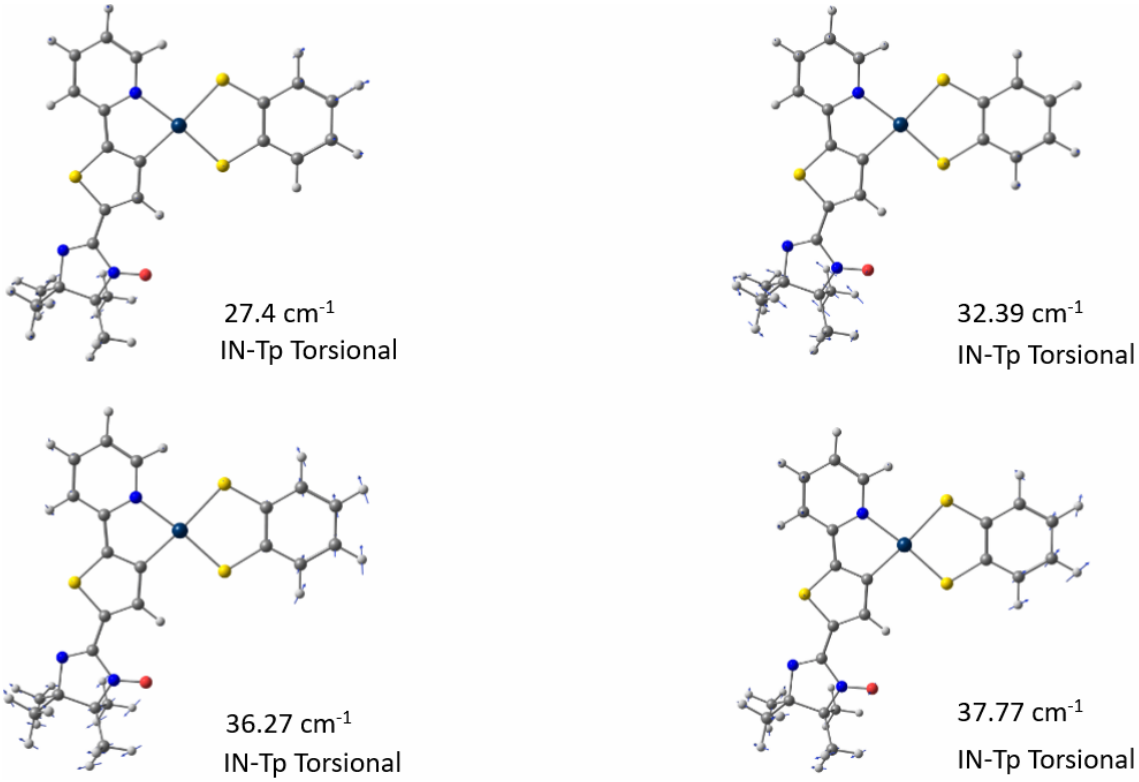

Figure 2.41: The four lowest energy vibrational modes of $[(TpyIN)Pt(bdt)]^{1-}$. Here, the vibrational mode at 32.39 cm^{-1} has the largest IN-Tp bond torsion contribution. These vibrational modes were obtained from a DFT frequency calculation.

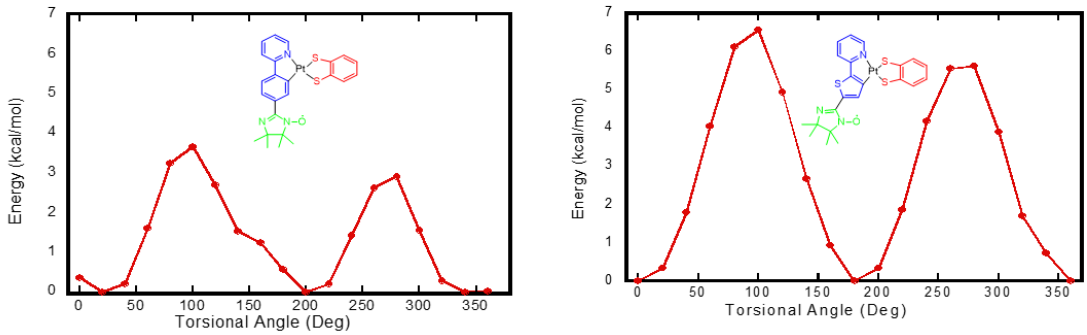

Figure 2.42: Torsional angle between Ppy/Tpy ligand and IN radical vs Energy for $[(PpyIN)Pt(bdt)]^{1-}$ and $[(TpyIN)Pt(bdt)]^{1-}$, respectively.[55]

In summary, when the torsional energy barrier becomes low, the J value (exchange coupling) decreases and thus the energy gap between D_{trip} and quartet decreases. And, at a small energy gap, these states can mix, and ESP can occur. From the calculation, the overall torsional energy barrier for $[(PpyIN)Pt(bdt)]^{1-}$ is lower than torsional energy barrier for $[(TpyIN)Pt(bdt)]^{1-}$ as shown in Figure 2.42. Lower torsional energy barrier is favorable for effective mixing between the pendent radical moiety and the ligand chromophore. This calculation indicates that $[(PpyIN)Pt(bdt)]^{1-}$ has a more favorable molecular structure for mixing between D_{trip} and quartet states compared to that of $[(TpyIN)Pt(bdt)]^{1-}$ as shown in Figure 2.42. We will explore the possible mechanisms for spin polarization generation in detail for these cyclometalated Pt(II) complexes in future work.

2.8 Discussions

We have synthesized and studied the excited state properties of the benzene dithiolate derivatives of cyclometalated square planar platinum complexes with and without iminonitroxide radicals. We aimed to study the effect of a localized pendent radical on the photophysical properties of cyclometalated platinum dithiolate complexes.

The photoexcitation of these radical elaborated platinum dithiolates results in a spin allowed doublet ground state to sing-doub excited state transition with a concomitant charge transfer from the dithiolate ligand to cyclometalating ligand. This charge transfer transition results in a three-spin entangled system (triradical character). As these systems

can intersystem cross to the quartet state, the quartet should be involved in the emission process. We found that molecules are emissive in the presence of a stable iminonitroxide radical substituent. Although the radical elaborated molecules are emissive, their emission lifetimes are highly affected by the presence of the radical substituent. Their photoluminescence decay rates are drastically shortened in solution in the presence of a pendent radical. Similarly, the presence of this organic radical substituent has lowered the quantum efficiencies (quantum yield) of these cyclometalated platinum complexes in solution.

Low temperature time resolved EPR data from our collaborators in Canada and Italy show that doublet and quartet states are both are spin polarized. The quartet is detected at low temperature, however, emission decay rates of these molecules in solution do not support decay from the quartet state. Short emission lifetimes in solution at room temperature suggest the decay pathway can be assumed to be indirect through D_{trip}, though the quartet is still involved in the decay mechanism. However, the microsecond long emission lifetimes in thin film samples supports spin forbidden decay from the quartet state.

The CASSCF calculations indicate a small energy gap between the D_{trip} (trip-doub) and Quartet states, which may favor thermally activated decay via the D_{trip} state. The energy gaps between the D_{trip} and quartet states for $[(PpyIN)Pt(bdt)]^{1-}$ and $[(TpyIN)Pt(bdt)]^{1-}$ from CASSCF computations are $123cm^{-1}$ and $46cm^{-1}$ respectively.

State	Multiplicity	Energy (cm^{-1})
GS(0)	2	0
1	4	14541.8
2	2	14664.9
3	2	17077.5

Table2.5: CASSCF(3,3) transition energies for $[(PpyIN)Pt(bdt)]^{1-}$ complex.

State	Multiplicity	Energies (cm^{-1})
GS(0)	2	0
1	2	14043.3
2	4	14098.9
3	2	17195.3

Table 2.6: CASSCF(3,3) transition energies for $[(TpyIN)Pt(bdt)]^{1-}$ complex.

There are pairwise exchange interactions in these three spin systems. Here, one spin is on the iminonitroxide radical, one spin is on the cyclometalating ligand (LUMO) and one spin is localized on the dithiolene donor ligand (HOMO). The exchange interaction between iminonitroxide radical and the spin in the LUMO of the acceptor ligand can control the mixing between D_{sing} and D_{trip}. Because of small energy gaps between D_{trip} and the Quartet state, it can be expected that the decay pathways can be from the D_{trip} (trip-doublet) and quartet states to the doublet ground state.[43] The decay pathway from

the quartet to doublet ground state represents a slow process because of the spin forbiddenness of the processes, while the D_{trip} to doublet ground state transition is expected to be fast because of the doublet character in both of these states. However, due to the very short emission decay rates in solution, the D_{trip} to doublet ground state transition is the only possible major decay pathway, with quartet emission becoming an indirect pathway via the D_{trip} state. There is also significant phosphorescence quenching in solution due to the presence of the iminonitroxide radical, which also supports D_{trip} decay.

Thus, the D_{sing} character admixed into the D_{trip} due to the exchange interaction, coupled with the small energy gap between D_{trip} and quartet favor fast relaxation from D_{trip} to ground state doublet in solution. Based on this consideration, we can propose that the radical elaborated cyclometalated platinum dithiolates are decaying from the trip-doub (D_{trip}) state in solution.

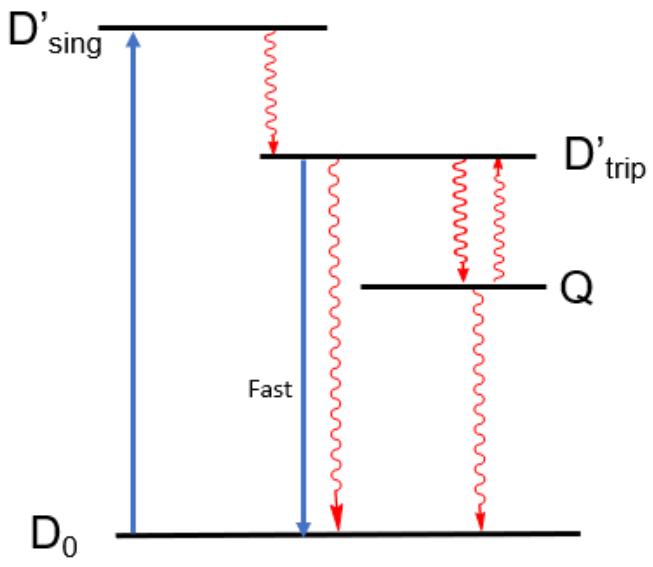

Figure 2.43: Schematic diagram for possible decay pathways of cyclometalated bdt complexes with a pendent radical in solution.

The variable temperature emission lifetimes of these molecules in polystyrene thin films shows that the lifetimes of these radical elaborated molecules can be fit by multiexponential functions and are in the microsecond range (Table 2.3A and Table 2.4). Similarly, the variable temperature photoluminescence lifetimes of the parent molecules in polystyrene thin films are also fit by bi-exponential functions and are in in the microsecond time range (Table 2.5A and Table 2.5B). The lifetime of the shortest component in these radical elaborated molecules slightly increases with decreasing temperature, and it may be a result of quartet decay rate because the parent molecules emitting from the triplet states are also showing the similar behavior in the thin film photoluminescence lifetime studies. Here, multiexponential emission lifetimes in polystyrene thin films could be from different aggregation modes because these types of complexes are known for aggregate formation.[18] Expanding on the temperature

dependent photoluminescence behavior, concentration dependent photoluminescence studies are necessary to explore the intermolecular aggregation behavior (multiexponential lifetime in thin films).

Compared to the room temperature solution phase emission decay measurements of radical elaborated cyclometalated dithiolate complexes in dichloromethane (the lifetimes for these $[(PpyIN)Pt(bdt)]^{1-}$ and $[(TpyIN)Pt(bdt)]^{1-}$complexes are shorter than the instrument response time of ~600ps, the emission lifetimes in polystyrene thin films were increased to microsecond range for both complexes and, were best fit with multiexponential functions.

In the solution phase, their lifetimes are very short and close to the instrument response time (~600ps) and no long-time phosphorescence was observed, although time resolved EPR data showed the quartet state was observed, so it must be at least transiently populated. This could be possible because of the exchange-mediated wave function mixing between D_{sing} and D_{trip} and, the enhanced nonradiative decay due to the small energy gap between the D_{trip} and quartet states. In the case of thin film phase photoluminescence experiments, the appearance of long-lived lifetimes may be interpreted as aggregation behavior and bulk phenomena.[18,41,45,47] Thin film samples are also known as solid solution samples and the long-lived emission in thin films could be favored by high concentration, rigidity and immobilization, and film thickness leading to a suppression of all intramolecular processes and minimizing the nonradiative decay in the excited state. The longer lifetimes indicate that the thin polystyrene film encourages phosphorescence in aggregate forms.[45,47]

Based upon the results presented in thin film and solution phases, the following mechanism is proposed for the excited state decay pathways for iminonitroxide elaborated cyclometalated platinum benzene dithiolates $[(PpyIN)Pt(bdt)]^{1-}$ and $[(TpyIN)Pt(bdt)]^{1-}$. This project is relatively new and a rarely touched field. Hence, more experiments such as concentration dependent emission studies and MCD studies are necessary to accurately assign the decay mechanisms.

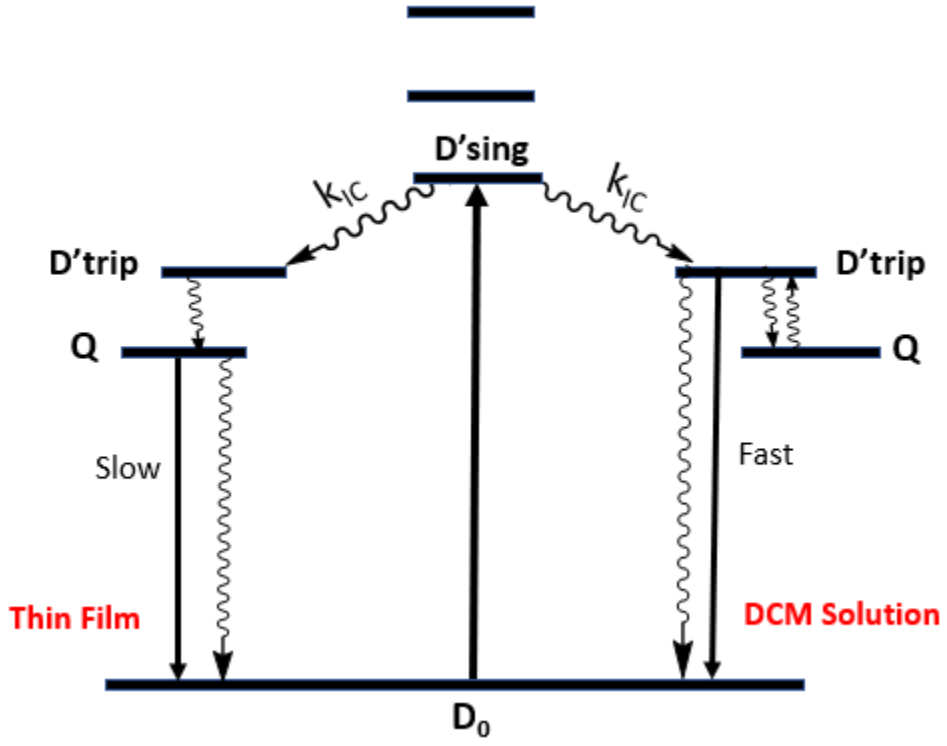

Figure 2.44: A schematic diagram showing the favored decay pathways for thin film and solution phases. Based on the results, quartet emission is favored in thin films, while D_{trip} emission occurs in the solution phase.

Thus, the introduction of the stable radical substituents to the Donor-Acceptor cyclometalated platinum dithiolates is a unique method for the modification of

photophysical properties without a large donor or acceptor ligand variation. The low energy and long-lived emissions of these anionic cyclometalated Pt(II) complexes in polymer thin films, due to predominantly aggregate-induced phenomenon, are also promising results for future photo functional applications.[45,47]

2.9 Conclusions and future directions:

In this project, an important goal of our proposed research was to create a new platform to study the role of iminonitroxide radicals on the excited state electronic structure, excited-state dynamics, and photoluminescent lifetimes of cyclometalated Pt (II) complexes that contain peripherally elaborated localized spins.

The attachment of a persistent radical onto the emissive $[(Ppy/Tpy)Pt(bdt)]^{1-}$ chromophore does lead to radical elaborated molecules that are still emissive. However, the photoluminescence efficiency (quantum yields) of these radical elaborated dithiolate complexes is reduced in solution. Similarly, the lifetimes of these radical elaborated molecules are orders of magnitude shorter in the solution phase compared to their parent chromophores. The origin of this drastic decrease in their lifetimes could be due to the magnetic exchange coupling interaction between the pendent radical and chromophore, and the enhanced nonradiative decay due to a smaller energy gap between D_{trip} and quartet states. Due to a radical-chromophore exchange interaction, D_{sing} mixes with D_{trip}

and can affect the IC and ISC rates.[43,44] Thus, the D_{trip} to doublet ground state transition is a partially spin favored process due to D_{sing} character in D_{trip}.

The thin film studies (solid solution) showed that the radical elaborated cyclometalated anionic complexes were still phosphorescent in nature even though they contain radical substituents, providing a rare example of emission from a Kramer's spin system.[54] The origin of this long-lived emission could be predominantly from aggregate formation, along with immobilization in solid solution forms while minimizing the nonradiative decay processes and encouraging the phosphorescence.[18,38,45,46,47]

In future studies, magnetic circular dichroism (MCD) spectroscopy coupled with theoretical calculations needs to be performed for detailed analysis of the doublet excited state manifold and band assignments as these radical elaborated molecules are expected to be accelerated by MCD studies. To better understand how the exchange interaction between the pendent radical and cyclometalating moiety can change spin dynamics and excited state lifetimes, we can add bridging units such as para-phenyl, meta-phenyl, and thiophene groups between the cyclometalating ligand and the radical moieties. Further, we can extend this project by synthesizing the iminonitroxide radicals on the donor side of these cyclometalated complexes (Figure 2.45) and compare their excited state properties with that of the radical elaborations on acceptor side of molecules.

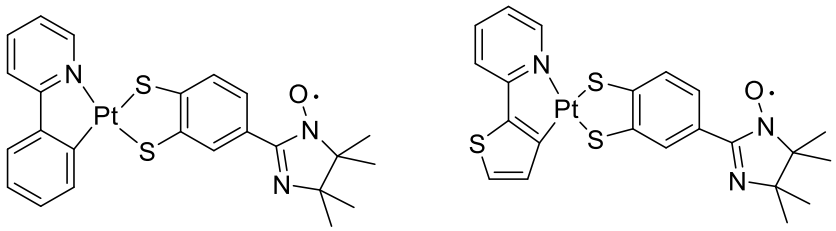

Figure 2.45: Proposed cyclometalated platinum dithiolates with pendent radical on donor side of the molecules.

2.9 References

1. Kvam, P.; Engebretsen, T.; Maartmann-Moe, K.; and Songstad, J. Crystal Structure of Bu4N[Pt(ppy)Cl2], Et4N[(Pt(tpy)Cl2] and [Pt(ppy)en]Cl (ppy= N,C'-Chelated 2-Phenylpyridinate, tpy=N,C'-Chelated 2-(2'-Thienyl)pyridinate, en= N,N'-Chelated 1,2-Diaminoethane). *Acta Chemica Scandinavica*, **1996**,50,107-113.

2. Maestri, M.; Sandrini, D.; Balzani, V.; Chassot, L.; Jolliet, P. and Zelewsky, A. V. Luminescence Orthometallated Platinum(II) Complexes; *Chemical Physics Letters* .**1985**,122,375-379 .

3. Mdleleni, M. M.; Bridgewater, J. S.; Watts, R. J.; Ford, P.C. Synthesis, Structure, and Spectroscopic Properties of Ortho-Metalated Platinum(II) Complexes. *Inorg. Chem.* **1995**, 34, 2334-2342.

4. Balashev, K.P.; Puzyk, M.V.; Kotlyar, V.S.; and Kulikova, M. V. Photophysics, photochemistry and electrochemistry of mixed-ligand platinum(II) complexes with 2-phenylpyridine and 2-(2'-thienyl)pyridine as cyclometalating ligands. *Coordination*

Chemistry Reviews, **1997**, 159,109-120

5. (a) Zuleta, J.A.; Burberry, M.S. and Eisenberg, R. Platinum(II) diimine dithiolates. New solution luminescent complexes. *Coordination Chemistry Review*, **1990**, 97, 47-64. (b) Lazarides, T.; McCormick, T. M.; Wilson, K. C.; Lee, S.; McCamant. D. W. and Eisenberg, E. Sensitizing the Sensitizer: The Synthesis ad Photophysical Study of Bodipy-Pt(II)(diimine)(dithiolate) Conjugates. *J. Am. Chem. Soc.* **2011**, 133, 350-364.

6. Suardi, G.; Cleary B.; Duckett, Simon.; Sleigh C.; Rau, M.; Reed, E. W.; Lohman, J. A. and Eisenberg, R. Luminescent Iridium(I) Diethyldithiocarbamate Complexes: Synthesis, Structure, and Reactivity Including Stereoselective Hydrogen Oxidative Addition. *J Am. Chem. Soc.* **1997**, 119, 33, 7716-7725

7. Pintus, A.; Aragoni, M. C.; Cinellu, M. A; Maiore, L.; Isaia, Francesco, Lippolis, V.; Orru, G.; Tuveri, E.; Zucca, A.; Arca, M. [Au(py^b-H)(mnt): A novel gold(III) 1,2-dithiolene cyclometalated complex with antimicrobial activity(py^b-H = C-deprotonated 2-benzylpyridine ; mnt = 1,2-dicyanoethene-1,2-dithiolate). *J. Inorg. Biochem*. **2017**, 170, 188-194

8. Chen, L.; Yang, C.; Qin, J.; Gao, J; Ma, D. Luminescent iridium (III) complexes with mixed 2-phenylpyridinato-C2, N and dithionate ligands for dopant emitter in OLEDs. *Synthetic metals*. **2005**, 152, 225-228

9. Chen, L.; You, H.; Yang, C.; Ma, D.; Qin, J. Novel, highly efficient blue-emitting heteroleptic iridium(III) complexes based on fluorinated 1,3,4-oxadiazole: tuning to blue by dithiolate ancillary ligands. *J. Chem Comm*. **2007**, 13, 1352-

10. Nguyen, V. H.; Chew, H.Q.; Su, B.; Yip, J.H. Synthesis and Spectroscopy of Anionic Cyclometalated Iridium (III)-Dithiolate and Sulfinates-Effects of Sulfur Deoxygenation on Electronic Structure and Luminescence. *Inorg. Chem*. **2014**, 53(18), 9739-9750

11. Wang, X. M.; Qiang J. Y.; Ai-Quan, J.; Tong, B.; Zhang, Q.F. Synthesis, crystal structure and phosphorescent properties of cyclometalated iridium (III) bis(pyridylbenzaldehyde) complexes with dithiolate ligands. *A J. Chem. Sci*. **2017**, 72, 941-946.

12. Sie, W. S., Jian, J. Y.; Shiu, K. B. Synthesis, Characterization and Photophysical properties of Iridium(III) Bis-cyclometallated Complexes Containing 1,1- Dithiolates. *Journal of the Chinese Chemical Society.* **2011**, 58, 611-616

13. Yersin, H.; Rausch, A. F.; Czerwienic, R.; Hofbeck, T. and Fisher, T. The Triplet State of Organo-Transition Metal Compounds. Triplet Harvesting and Singlet Harvesting for Efficient OLEDs. *Coordination Chemistry Reviews.* **2011,** 255, 2622-2652.

14. Nguyen, H. A.; Kandasamy, B.; Yip, J. H. K. Coupling d^6 Ir(III) and d^8 Pt(II) Chromophore. Inorg. Chem. **2018**, 57, 4699-4718

15. Sesolis, H.; Moussa, J.; Gontard, G.; Utand, A.; Gullo, M. P.; Barberi, A. and Amouri, H. A unique class of neutral cyclometalated platinum(II) complexes with π-bonded benzenedithiolate: synthesis, molecular structures and tuning of luminescence properties. *Dalton Trans. Comm.* **2015**, 44, 2973-2977

16. Julia, F.; Jones, P.G.; Gonzalez-Herrero, P. Synthesis and photophysical Properties of Cyclometalated Platinum(II) 1,2-Benzenedithiolate Complexes and Heterometallic

Derivatives Obtained from the Addition of [Au(PCy_3)]+ Units. *Inorg. Chem*. **2012**, 51, 5037-5049

17. Brooks, J.; Babayan, Y.; Lamansky, S.; Djurovich, P.I.; Tsyba, I.; Bau, r.; and Thompson, M.E. Synthesis and Characterization of Phosphorescent Cyclometalated Platinum Complexes. *Inorg. Chem.* **2002**, 41, 3055-3036

18. Ricciardi, L.; Deda, M. L.; Lonescu, A.; Godbert, N.; Aiello, I.; and Ghedini, M. Anionic cyclometallated Pt(II) square-planar complexes: new sets of highly luminescent compounds. *Dalton Trans.* **2017**,46, 12625-12635

19. Xing, Y.; Liu, C.; Song, X. and Li, J. Photostable trifluoromethyl-substituted platinum (II) emitters for continuous monitoring of molecular oxygen. *Journal of Materials Chemistry C*. **2015**, 3, 2166-2174

20. Cho, J. Y.; Suponitsky, K. Y.; Li, J.; Timofeeva, T.V.; Barlow, S. and Marder, S. R. Cyclometalated platinum complexes: High-yield synthesis, characterization, and a crystal structure. Journal of *Organometallic Chemistry*, **2005**, 690, 4090-4093.

21. Ullman, E.F; Call L. and Osiecki J. H.; Stable free radicals. VIII. New imino, amidino, and carbamoyl nitroxies. *J. Org. Chem*. **1970**, 35, 3623.

22. Hirel, C.; Vostrikova, K. E.; Pecaut, J.; Ovcharenko, V. I and Rey, P. Nitronyl and Imino Nitroxide: Improvement of Ullman's Procedure and Report on a New Synthetic Route. *Chem. Eur. J*. **2001**, 9, 2007-2015.

23. Katayama, K; Hirotsu, M.; Kinoshita, L.; Teki, Y.; Design, synthesis, magnetic properties of a π-radical ligand with photo-excited high-spin state and its Fe(II) complex. The first stage of a new strategy for LIESST materials. *Dalton Trans*. **2012**, 41, 13465-13473

24. Ito, A; Kobayashi, N.; Teki, Y.; Low-Energy and Long-Lived Emission from Polypyridyl Ruthenium(II) Complexes Having A Stable-Radical Substituent. *Inorg. Chem*. **2017**, 56, 3794-3808

25. Hattori, Y.; Kusamoto, T.; Nishihara, H. Enhanced Luminescent Properties of an Open-Shell (3,5-Dichloro-4-pyridyl)bis(2,4,6-trichlorophenyl)methyl Radical by Coordination to Gold. *Angew. Chem. Int. Ed*. **2015**, 54, 3731-3734

26. Yoshikawa, H.; Kobayashi, M.; Takahashi, T.; Awaga, K. A Novel Free Radical Probe Based on a Preluminescent Iridium Complex Bearing a Nitronyl Radical Moiety. *Bull. Chem. Soc. Jpn*. **2010**, 83, 762-766

27. Yang, J.; Kersi, D.K.; Giles, L. J.; Stein, B. W.; Feng, C.; Tichnell, C. R.; Shultz D. A. and Kirk, M. L. Ligand control of donor-acceptor excited -state lifetimes. *Inorg. Chem*. **2014**, 53,4791-4793.

28. Yang, J.; Kersi, D.K.; Richers, C. P.: Giles, L. J.; Dangi, R.: Stein, B. W.; Feng, C.; Tichnell, C. R.; Shultz D. A. and Kirk, M. L. Ground State Nuclear Magnetic Resonance Chemical Shifts Predicts Charge-Separated Excited State Lifetimes. *Inorg. Chem*. **2018**, 57, 13470-13476.

29. Suzuki, K.; Kobayashi, A.; Kaneko, S.; Takehira, K.; Yoshihara, T.; Ishida, H.; Shiina, Y.; Oishi, S.; Tobita, S. Reevaluation of absolute luminescence quantum yields of standard solutions using a spectrometer with an integrating sphere and a back-thinned CCD detector. *Phys. Chem. Chem. Phys*. **2009**, 11, 9850−9860.

30. Stein, B. W.; Tichnell, C. R.; Chen, J.; Shultz, DA and Kirk, ML. Excited State Magnetic Exchange Interactions Enables Large Spin Polarization Effects; *J. Am. Chem. Soc.* **2018**, 140, 2221-2228

31. Tichnell, C.R.; Daley, D.R.; Stein, B.W.; Stultz, DA.; Kirk, M L., and Danilov, E.O.; Wave Function Control of Charge-Separated Excited-State Lifetimes. *J. Am. Chem*. *Soc*. **2019**, 141, 9,3986-3992

32. Till Biskup, Frontiers in chemistry (**2019**), 7, Article 10 Doi: 10.3389/fchem.2019.00010

33. Kirk, M. L.; Shultz D, A.; Chen, J.; Hewitt, P.; Daley, D.; Paudel, S.; Est, A. Vd. Metal Ion Control of Photoinduced Electron Spin Polarization in Electronic Ground States. *J. Am. Chem. Soc*. **2021**, 143, 10519-10523

34. Rozenshtein, V.; Berg, A.; Stavitski, E.; Levanon, H.; Franco, L.; and Corvaja, C. Electron Spin Polarization of Functionalized Fullerenes. Reversed Quartet Mechanism. *J. Phys. Chem. A*. **2005**, 109, 11144-11154

35. Shultz, A. D.; Fico, R. M.; Lee, H.; Kampf, J. W.; Kirschbaum, K.; Pinkerton, A.A.; and Boyle, P.D. Mechanisms of Exchange Modulation in Trimethylenemethane-type

Biradicals: The Roles of Conformation and Spin Density. *J Am. Chem. Soc*. **2003**, 125,15426-15432

36. Cummings, S. and Eisenberg, R. Tuning the Excited-State Properties of Platinum (II) Diimine Dithiolate Complexes. *J. Am. Chem. Soc*. **1996,** 118, 1949-1960

37. Ito, A.; Hinoshita, M.; Kato, K. and Teki, Y. Excited-state Dynamics and Spin-exchange Coupling of Anthracene-Verdazyl Radical in Frozen Glass Matrix Investigated by Transient Absorption Spectroscopy. *Chem. Lett*. **2016**, 45, 1324–1326.

38. Grolleau, J.; Petrov, R.; Allain, M.; Skene, W. G. and Frere, P. Solid-State Emission Enhancement via Molecular Engineering of Benzofuran Derivatives. *ACS Omega*. **2018**, 3, 12, 18542-18552.

39. Nishida, S.; Morita, Y.; Kobayashi, T.; Fukui, K.; Ueda, A.; Sato, K.; Shiomi, D.; Takui, T. and Nakasuji, K. Spin delocalization on curved π-system: Corannulene with iminonitroxide. *Polyhedron*. **2005**,24,2200-2204.

40. Deaton, J.C.; Switalski, S. C.; Kondakov, D. Y.; Young, R. H.; Pawlik, T. D.; Giesen, D. J.; Harkins, S. B.; Miller, A. J. M.; Mickenberg, S. F. and Peters, J. C. E-Type Delayed Fluorescence of a Phosphine-Supported $Cu_2(\mu\text{-}Nar_2)_2$ Diamond Core: Harvesting Singlet and Triplet Excitons in OLEDs. *J. Am. Chem. Soc*. **2010,** 132, 9499-9508.

41. Byrne,H. J.; Maser, W.;Ruehle, W. W.; Mittelbach, A.; Hoenle, W.; von Schnering ,H. G.; Movaghar, B.; Roth, S.; Time-resolved photoluminescence of solid state fullerenes. Chemical Physics Letters. **1993**, 204, 461-466.

42. Fidan, I.; Onal, E.; Luneau, D.; Ahsen, V. and Hirel, C. Synthesis and Straightforward Quantification Methods of Imino Nitroxide-Based Hexaradical Architecture on a Cyclotriphosphagene Scafold. *Inorg. Chem.* **2016,** 55, 11447-11453.

43. Teki, Y.; Excited-State Dynamics of Non-Luminescent and Luminescent π-Radicals. *Chem. Eur. J*. **2019,** 25, 1-18.

44. Wang, J.; Zhao, J.; Barbon, A.; Toffoletti, A.; Liu, Y.; An, Y.; Xu, L.; Karatay, A.; Yaglioglu, H. G.; Yildiz, E. A. and Hayvali, M. Radical-Enhanced Intersystem Crossing in New Bodipy Derivatives and Applications for Efficient Triplet-Triplet Annihilation. *J. Am. Chem*. *Soc*. **2017**,139, 7831-7842.

45. Coffey, B.; Clough, L.; Bartkus, D. D.; McClellan, I. C.; Greenberg, M. W.; LaFratta, C. N.; Tanaski, J. M and Anderson, C. M. Photophysical Properties of Cyclometalated Platinum(II) Diphosphine Compounds in the Solid State and in PMMA Films. *ACS Omega.* **2021**, 6, 28316-28325.

46. Chi, C.; Im C. and Wagner, G. Lifetime determination of fluorescence and phosphorescence of a series of oligofluorenes. J. Chem. Phys. **2006**,124, 024907.

47. Alam, P.; Climent, C.; Alemany, P. and Laskar, I. R. "Aggregation-induced emission" of transition metal compounds: Design, mechanistic insights, and applications. *Journal of Photochemistry and Photobiology C: Photochemistry Reviews*. **2019**, 41, 100317.

48. Kirk, M. L.; Shultz D. A.; Hewitt, P.; Stasiw, D. E.; Chen, J.; and Est, A.v.d. Chromophore-radical excited state antiferromagnetic exchange controls the sign of photoinduced ground state spin polarization. *Chem. Sci*. **2021**,12,13704-13710.

49. Kirk, M. L.; Shultz D. A.; Hewitt, P.; Chen, J.; and Est, A.v.d. Excited State Magneto-Structural Correlations Related to Photoinduced Electron Spin Polarization. *J. Am. Chem. Soc*. **2022,** 144, 28, 12781-12788.

50. Kirk, M. L.; Shultz D. A.; Hewitt and Est, A.v.d. Excited State Exchange Control of Photoinduced Electron Spin Polarization in Electronic Ground States. *J. Phys. Chem. Lett.* **2022,** 13, 3, 872-878

51. Kandrashkin, Y. E. and Est, A. v.d. The triplet mechanism of electron spin polarization in moderately coupled triplet-doublet rigid complexes as a source of the enhanced +1/2 ↔ −1/2 transitions. *J. Chem. Phys*. **2019**, 151, 184301.

52. Weltner, W. Magnetic atoms and Molecules. Dover publication, **1989**.

53. Stoll, S. and Goldfarb, D. EPR Spectroscopy: Fundamentals and Methods. Wiley Publisher, **2018**.

54. Cho, E.; Coropceanu, V. and Breadas, J.-L. Organic Neutral Radical Emitters: Impacts of Chemical Substitution and Electronic-State Hybridization on the Luminescence Properties. *J. Am. Chem*. *Soc.* **2020**, 142, 17782-17786.

55. The Orca 4.0.0.2 software program was used for computations. The input files were generated using the molecular builder function in the Gaussview 03 software. For ring

torsion energy computations, optimized geometry cartesian coordinates were used as starting point and a relaxed surface scan was used for a series of constrained geometry optimizations. For each computation, the dihedral angles between the Ph/Tp ring of cyclometalating ligands, and the iminonitroxide ring were constrained from 0 degree to 360 degrees using 20 degree increments. The final single point energies obtained from each fully optimized constrained geometry were plotted against the torsional angles from 0 degree to 360 degrees. I appreciate the assistance of Dr. Ju Chen in this computation.

Chapter 3

Radical Elaborated Cyclometalated Square Planar Pt(II) Catecholate Complexes

3.1 Background

Cyclometalated metal complexes are known to us and have been studied due to their superior photoluminescence efficiency and thermal stability compared to non-cyclometalated analogs such as metal diimine complexes. Cyclometalated complexes with different metals such as Ir, Rh, Pt and Pd have been studied for their charge-transfer transitions at low energies[1]. The first emissive cyclometalated platinum/palladium complexes were studied by the Von Zelewsky group[2]. Later, there were many examples of emissive cyclometalated metal complexes with a variety of ancillary ligands. Cyclometalated complexes containing platinum and iridium are gaining much attention due to their applications in advanced technologies such as organic light emitting devices (OLEDs and PHOLEDs)[3]. The Yersin group has explored many cyclometalated phosphorescent complexes in detail for the development of efficient triplet emitters for electroluminescent devices[4,5]. However, studies on cyclometalated metal complexes with catecholate ligands are limited. Cyclometalated gold catecholates were studied in 2003 by Cameron Evans, et al. to investigate their biological activity toward leukemia cells[6]. Anionic cyclometalated iridium catecholates were investigated by Mauro Ghedini, et al., where their redox phenomena and photophysical properties were specifically explored[7]. Similarly, Thomson, et al. studied the cyclometalated iridium and platinum complexes with di-tert-butyl-catechol ligands, where the catechol ligand was in semiquinone form.[8]

Cyclometalated platinum complex with a catecholate ligand π-bonded to organometallic moiety such as a cyclopentadienyl-rhodium fragment were reported by Jamal Moussa, et al. to tune the excited state properties of the complex[9]. Recently, the Ghedini group in 2017 had studied anionic cyclometalated Pt(II) complexes with tetrabromo-catecholate as highly luminescent complexes.[10] These represent the few photophysical studies on cyclometalated platinum complexes with dianionic catecholate.

To the best of our knowledge, we are the first to report the synthesis and photophysical properties of cyclometalated square planar Pt(II) catecholate complexes with a radical substituent on cyclometalating ligand (Figure 3.1).

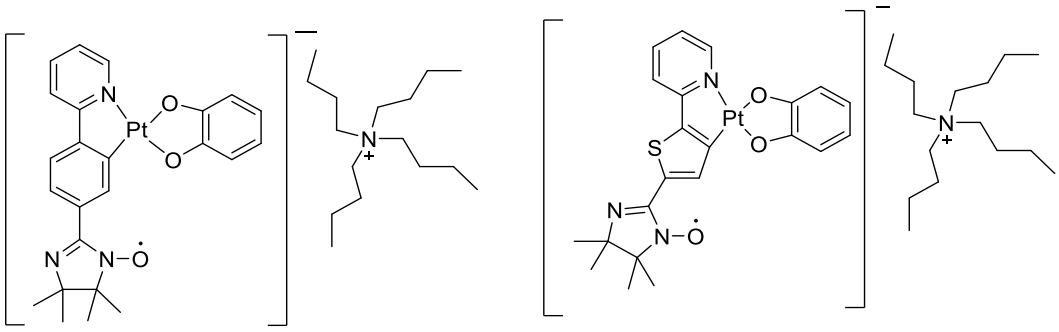

Figure 3.1: Radical elaborated cyclometalated platinum catecholates with two different cyclometalating ligands.

3.2 Synthesis and Characterization

The novel radical elaborated anionic platinum catecholate complexes were synthesized using the same precursors as outlined in Chapter 2 for the synthesis of radical elaborated anionic platinum dithiolate complexes. Many reported procedures [10,11,12,13]

have shown that these precursors could be dimers, monomers, or a mixture of both as discussed earlier in Chapter 2. Because of the complexity of the molecular structures and the possibility of mixtures of monomer and dimer formation, we directly used them for the next step of the reaction without characterization. We obtained these precursors as yellow/orange solids and found them to be insoluble in water and many less polar solvents (ether, chloroform). Using this to our advantage, we washed these precursors with water and then with less polar solvents (diethyl ether, cold chloroform, and cold dichloromethane) many times to remove any excess soluble cyclometalating ligands used in prior reactions. These complexes were purified by alumina chromatography and characterized by EPR, mass spectrometry, and elemental analysis. Synthetic procedures and characterizations are presented in the experimental section (Appendix B).

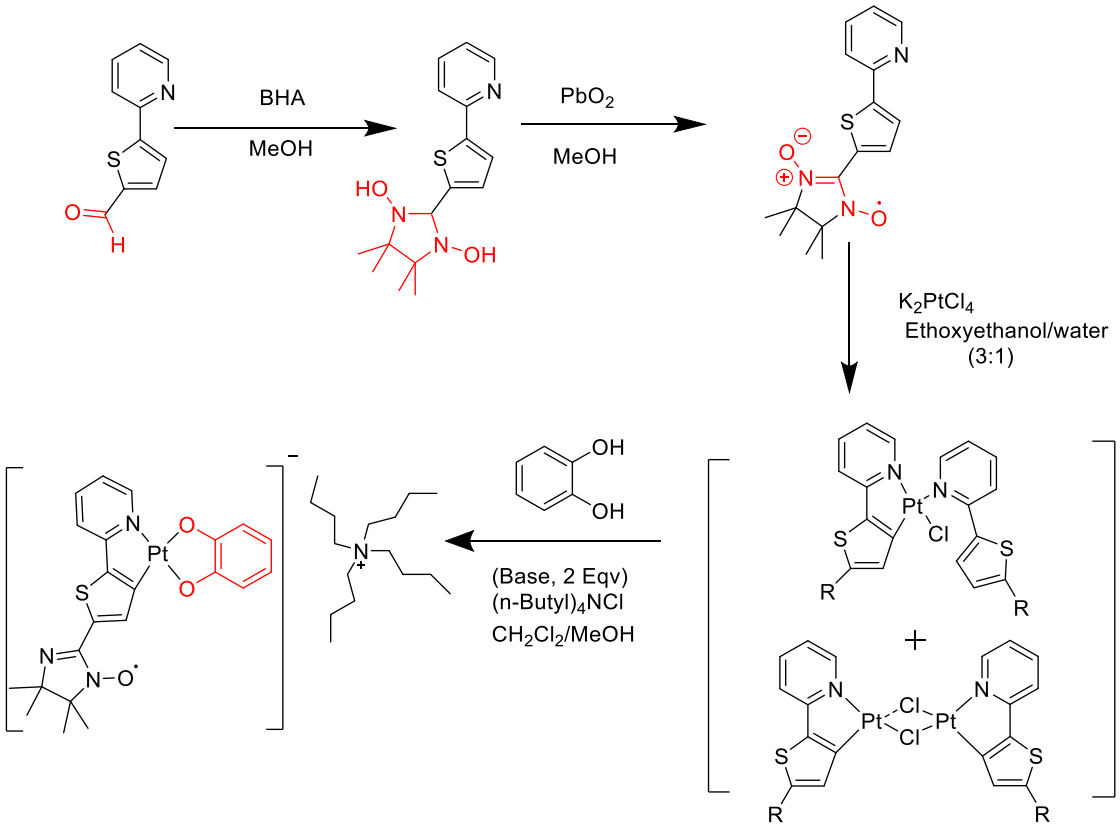

Figure 3.2: Synthetic scheme for cyclometalated platinum catecholate complexes. (Here, R represents a radical fragment).

3.3 Electronic Absorption Spectra

Room temperature electronic absorption spectra for $[(PpyIN)Pt(Cat)]^{1-}$ and $[(TpyIN)Pt(Cat)]^{1-}$ have been collected in dichloromethane. The charge transfer absorption maxima, which are the lowest energy bands, for $[(PpyIN)Pt(Cat)]^{1-}$ and $[(TpyIN)Pt(Cat)]^{1-}$ are at 19,400 cm^{-1} (520 nm) and 18,700 cm^{-1} (527 nm), respectively (Figure 3.3 and Figure 3.4).

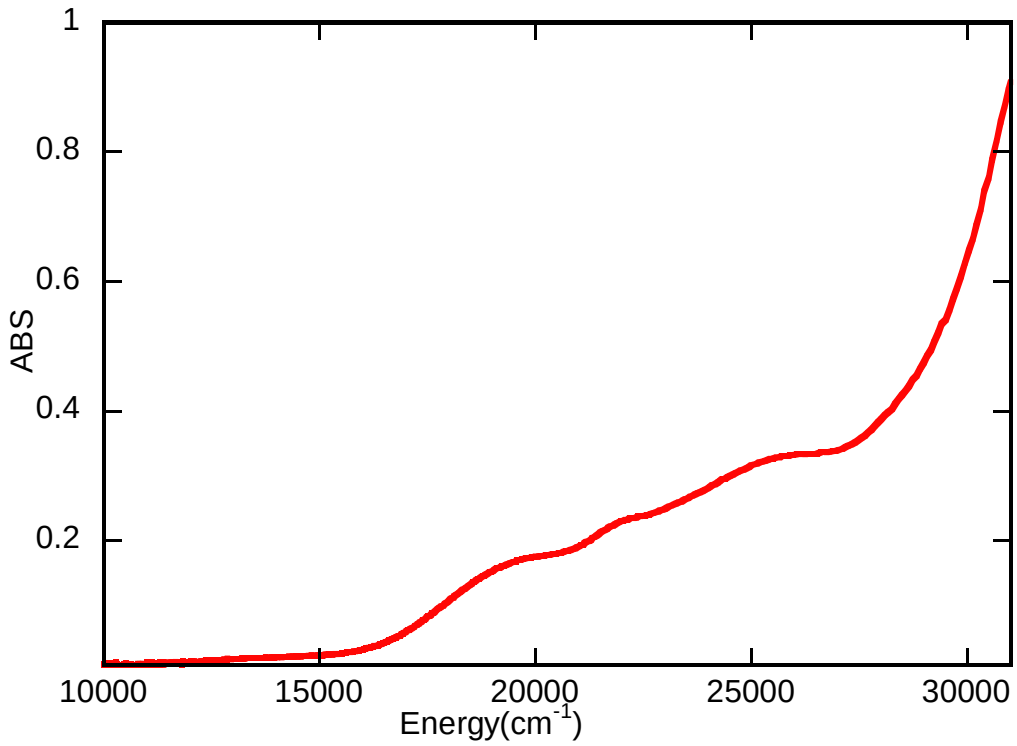

Figure 3.3: Room temperature electronic absorption spectrum for $[(PpyIN)Pt(Cat)]^{1-}$ complex in DCM.

The lowest energy band maximum for platinum catecholate complexes with 2-phenypyridine as a cyclometalating ligand is at slightly higher energy than the corresponding complexes with 2-thienylpyridine as the cyclometalating ligand.

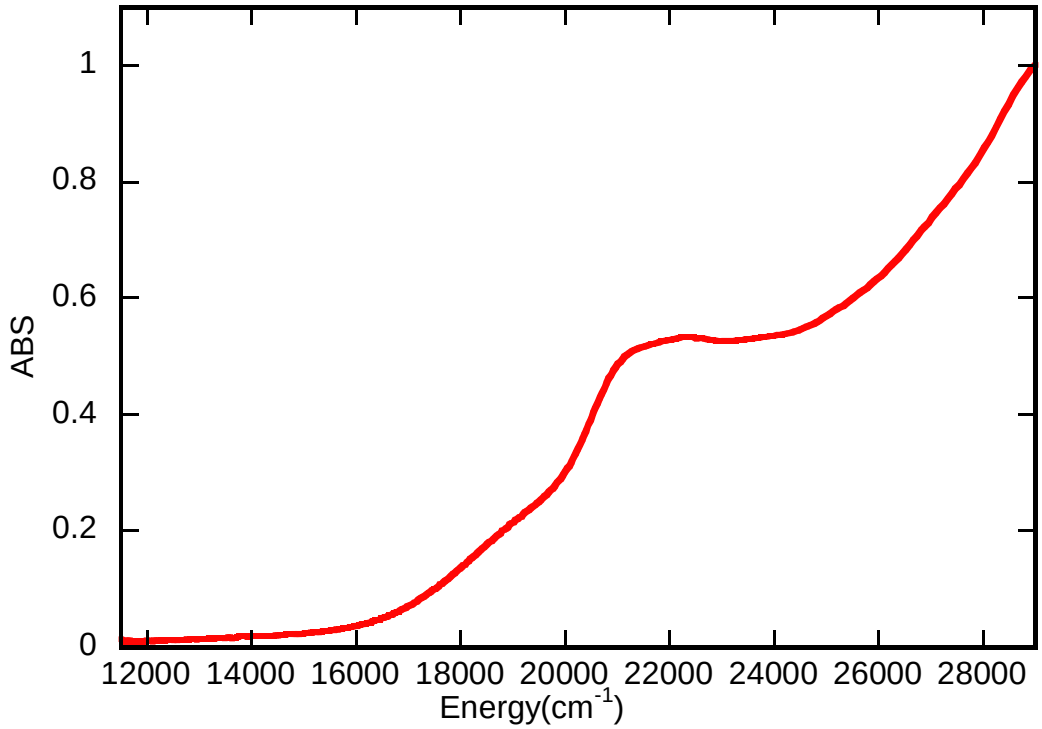

Figure 3.4: Room temperature electronic absorption spectrum for $[(TpyIN)Pt(Cat)]^{1-}$ in DCM.

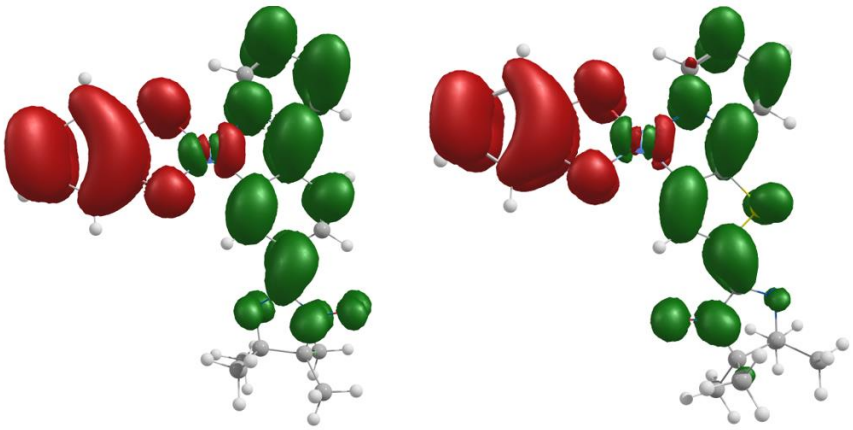

Figure 3.5: Computed EDDMs of $[(PpyIN)Pt(Cat)]^{1-}$ and $[(TpyIN)Pt(Cat)]^{1-}$ for electronic transition 4 at a contour value of 0.0006. Here, the red and the green regions indicate the loss and the gain of electron densities, respectively, in the computed transition.

The calculated electron density difference maps (EDDMs) for computed transition 4 in $[(PpyIN)Pt(Cat)]^{1-}$ and $[(TpyIN)Pt(Cat)]^{1-}$ indicate that these are LL'CT transitions since electron density is lost from the HOMO (Highest Occupied Molecular Orbital) and gained in the LUMO (Lowest Unoccupied Molecular Orbital) as shown in Figure 3.5.

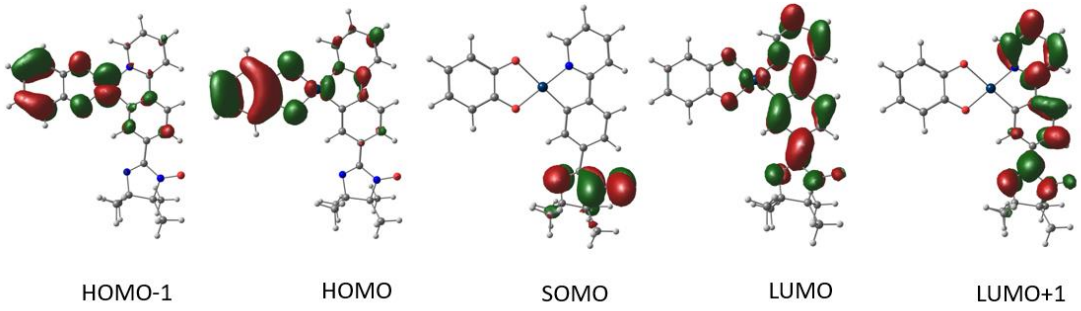

Figure 3.6: DFT computed frontier molecular orbitals for $[(PpyIN)Pt(Cat)]^{1-}$.

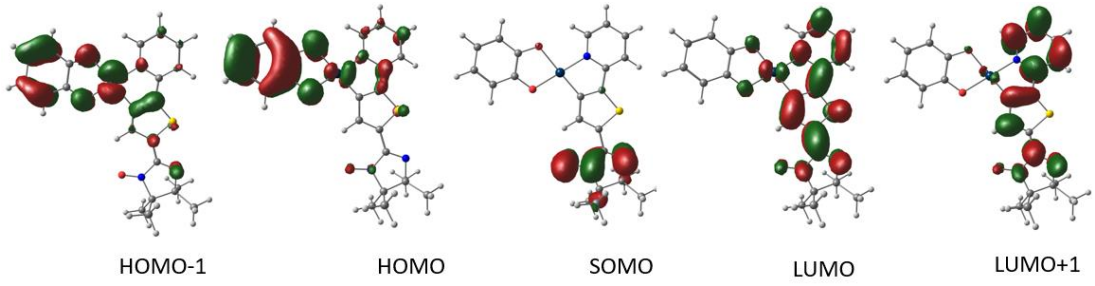

Figure 3.7: DFT computed frontier molecular orbitals for $[(TpyIN)Pt(Cat)]^{1-}$.

Figure 3.6 and Figure 3.7 show the DFT computed frontier molecular orbitals, including the SOMO (Singly Occupied Molecular Orbital). The presence of the SOMO leads to the paramagnetic doublet ground state configurations in these radical elaborated molecules.

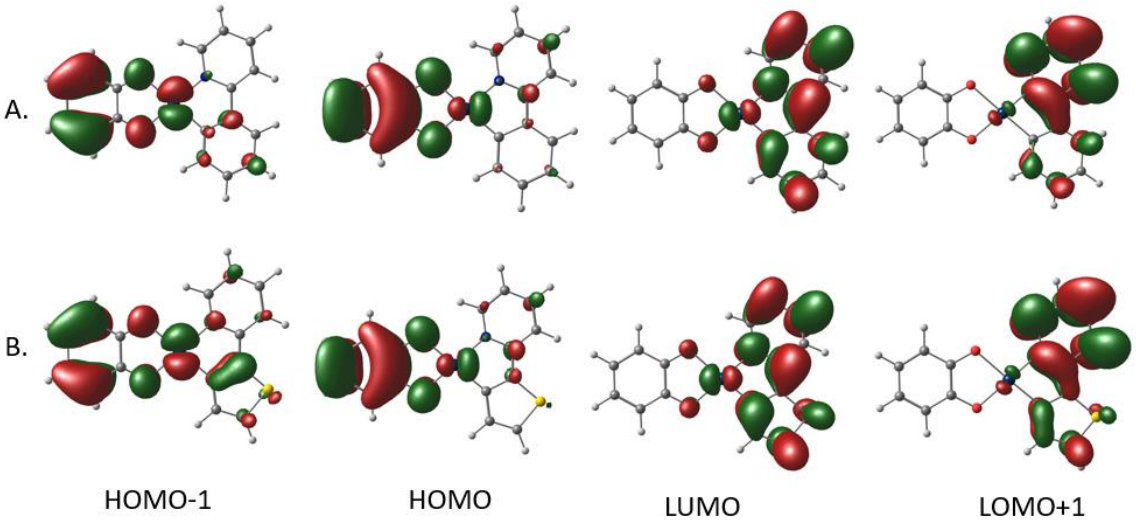

Figure 3.8: DFT computed frontier molecular orbitals of the parent complexes A: $[(Ppy)Pt(Cat)]^{1-}$, B: $[(Tpy)Pt(Cat)]^{1-}$.

SOMO is absent in the parent complexes, and this leads to diamagnetic singlet ground state configurations.

3.4 EPR Spectra

Room temperature X-band EPR spectra for the radical-elaborated cyclometalated platinum catecholate complexes have been collected in dichloromethane solution. The room temperature EPR spectra of these radical elaborated cyclometalated CAT complexes show the characteristic features of the iminonitoxide radical, with no evidence of hyperfine coupling to the ^{195}Pt I=1/2 nucleus. All EPR data have a characteristic seven-

line pattern with intensity ratios of 1:1:2:1:2:1:1 due to the interaction of a single unpaired electron with two nonequivalent nitrogen nuclei (Figure 3.9 and Figure 3.10).

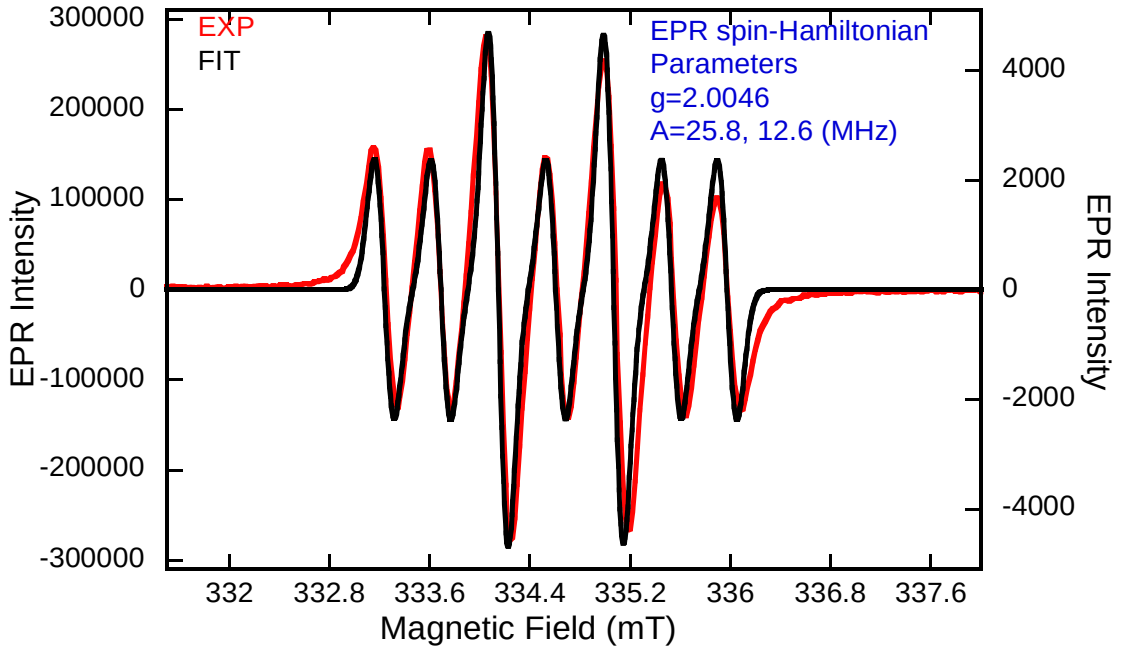

Figure 3.9: Room temperature X-band EPR spectrum of $[(PpyIN)Pt(Cat)]^{1-}$ in DCM (red) and corresponding spectral simulation (black).

EPR spectral simulations for these complexes (Figure 3.9 and Figure 3.10) yield an isotropic g values and hyperfine coupling constants which are similar to that of the free iminonitroxide radicals[16,17]. The g-value for $[(PpyIN)Pt(Cat)]^{1-}$ was found to be 2.0046 and the hyperfine interactions with two non-equivalent nitrogen nuclei were determined to be 25.8 MHz and 12.6 MHz. Similarly, the g-value for $[(TpyIN)Pt(Cat)]^{1-}$ was found to be 2.0046 and the hyperfine interactions with two non-equivalent nitrogen nuclei were determined to be 25.9 MHz and 13.1 MHz. Thus, these data indicate that the radicals do

not dramatically interact with the chromophore in the ground state configuration due to the near free-ion g-values and lack of any observable Pt hyperfine coupling. Spin densities were computed from optimized the ground state doublet molecules and show the presence of negative spin density on the methine carbon of the iminonitroxide radical (Figure 3.11).

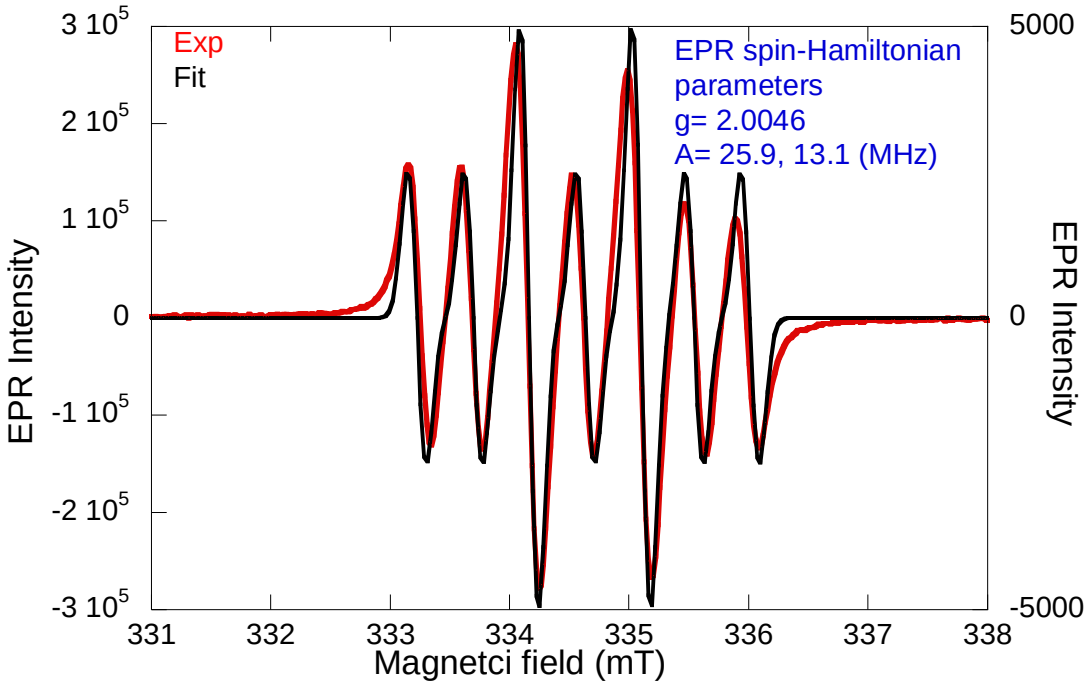

Figure 3.10: Room temperature X-band EPR spectrum of $[(TpyIN)Pt(Cat)]^{1-}$ in dichloromethane (red), and corresponding spectral simulation (black).

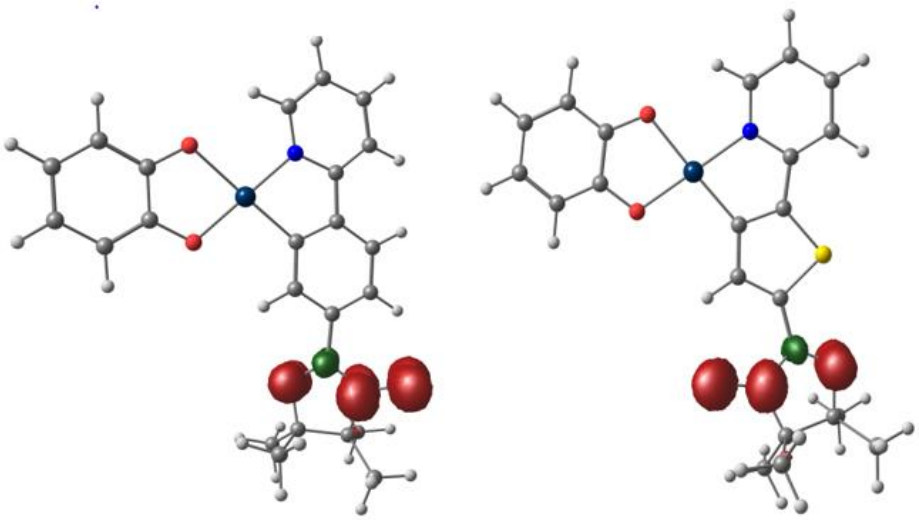

Figure 3.11: DFT computed spin densities for $[(PpyIN)Pt(Cat)]^{1-}$ and $[(TpyIN)Pt(Cat)]^{1-}$ at 0.0031 contour values. Positive spin density (red) and negative spin density (green).

3.5 Emission Spectra and Lifetimes

Steady state emission spectra have been collected for $[(PpyIN)Pt(Cat)]^{1-}$ and $[(PpyIN)Pt(Cat)]^{1-}$ complexes at room temperature in dichloromethane (DCM) solutions. The sample solutions were degassed by purging using a flow of nitrogen gas for fifteen minutes. Both the radical elaborated cyclometalated square planar Pt(II) catecholates are found to be emissive in DCM solutions.

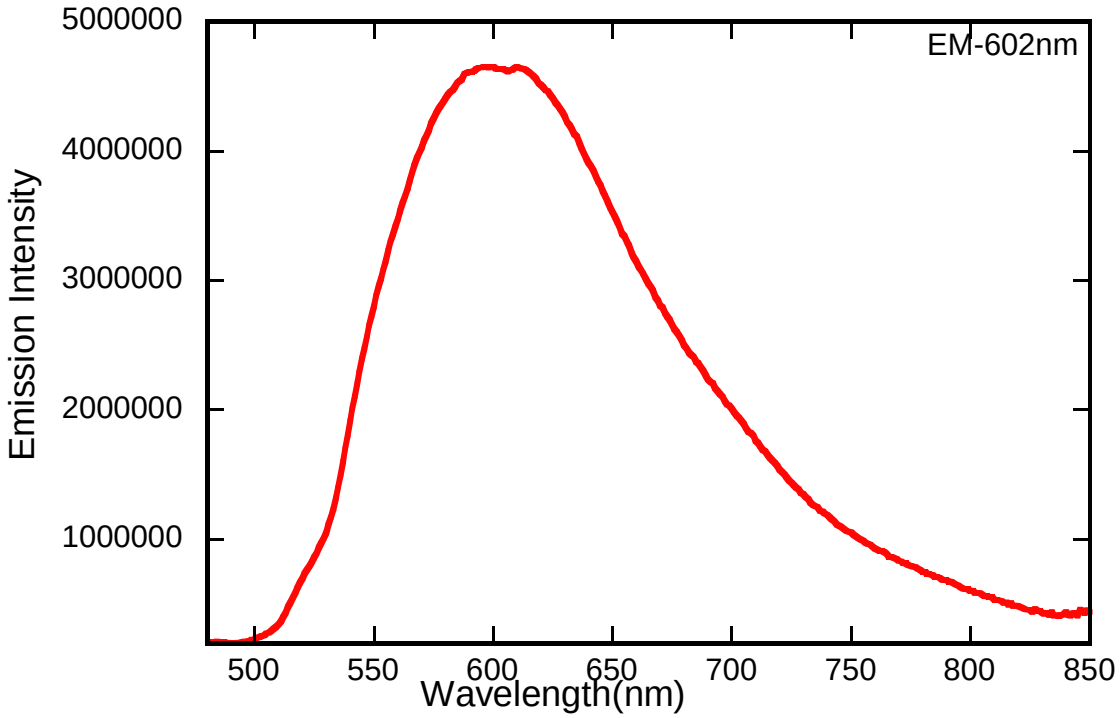

Figure 3.12: Room temperature steady state emission spectrum of $[(PpyIN)Pt(Cat)]^{1-}$ in degassed DCM using 450 nm excitation.

The room temperature emission spectrum of the $[(PpyIN)Pt(Cat)]^{1-}$ complex has an emission maximum at 602 nm (Figure 3.12; lifetime data in Figure 3.13) while that of the $[(TpyIN)Pt(Cat)]^{1-}$ complex has its maximum at 648 nm (Figure 3.14; lifetime data in Figure 3.15). The emission maximum of platinum catecholate complex with 2-thienylpyridine as a cyclometalating ligand is red shifted relative to the analogous catecholate complex with 2-phenylpyridine as a cyclometalating ligand. The room temperature emission spectrum for $[(PpyIN)Pt(Cat)]^{1-}$ has broad structureless features while the room temperature emission spectrum of $[(TpyIN)Pt(Cat)]^{1-}$ has some vibronic features.

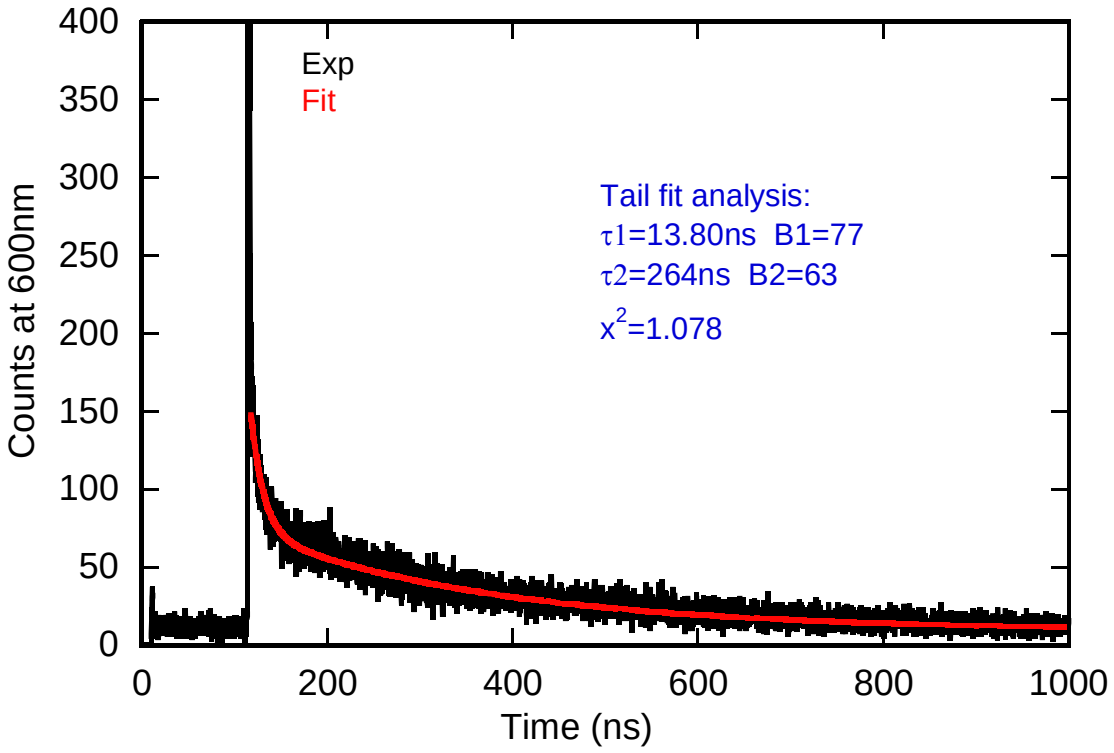

Figure 3.13: Room temperature emission decay for $[(PpyIN)Pt(Cat)]^{1-}$ in degassed DCM using a 450 nm diode laser.

When we measured the emission decays of these two complexes in dichloromethane solutions at room temperature, the lifetimes of both of these catecholate complexes were best fit with a bi-exponential decay expression. EPR spectra were collected just before the luminescence decay data collection, ensuring no degradation of the radical fragment. The bi-exponential excited-state decay rate could be from complex photophysical behavior, dimer formation, or aggregation induced emission.

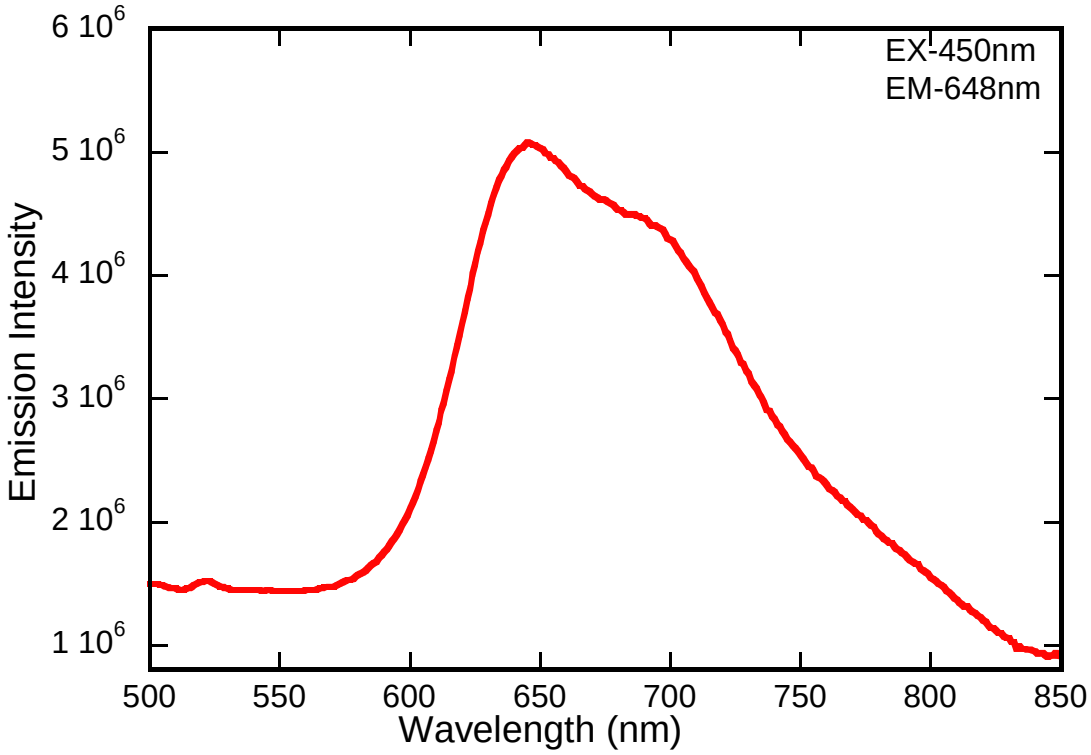

Figure 3.14: Room temperature steady state emission spectrum of $[(TpyIN)Pt(Cat)]^{1-}$ in degassed dichloromethane using 450 nm excitation.

The Ghedini group has reported photophysical properties of anionic cyclometalated Pt(II) square planar catecholate complexes, where they are using tetrabromo catecholate as the donor ligand[10]. They have found that these molecules are weakly emissive in DMSO solution with bi-exponential decays. This group has reported that the source of bi-exponential excited-state decays of their anionic cyclometalated catecholate complexes could be a possible result of aggregate formation.[10]

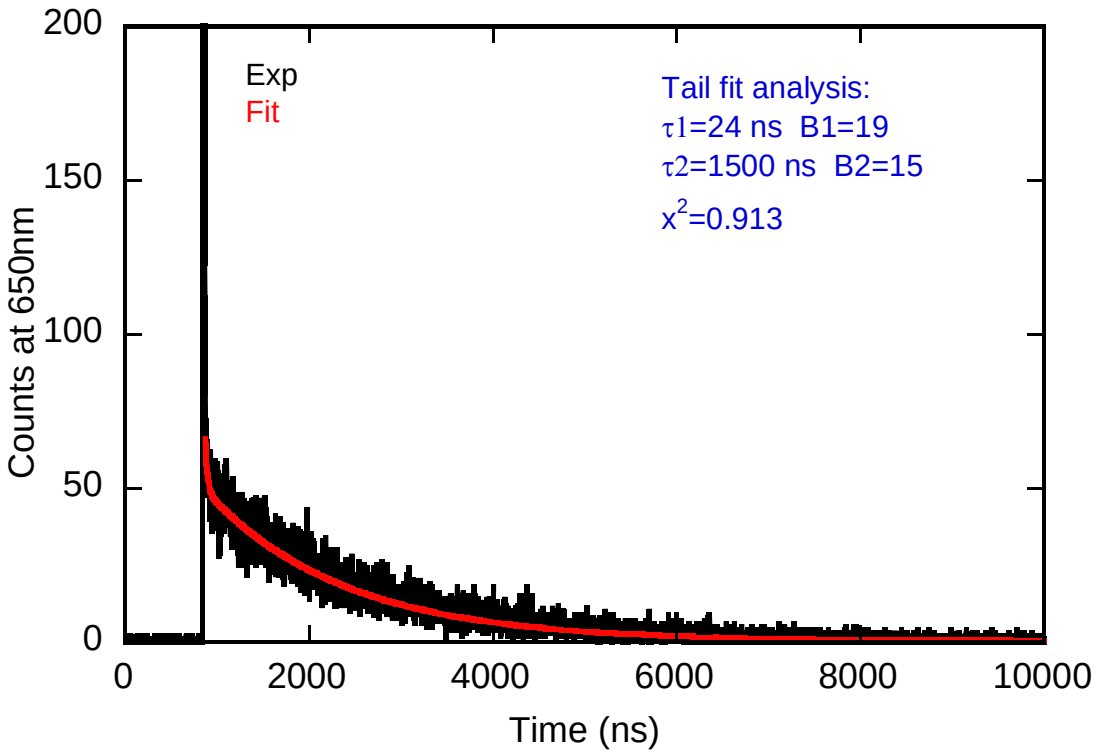

Figure 3.15: Room temperature emission decay for $[(TpyIN)Pt(Cat)]^{1-}$ in degassed dichloromethane using a 450nm diode laser.

We have also collected 77K emission spectra for both the $[(PpyIN)Pt(Cat)]^{1-}$ and $[(TpyIN)Pt(Cat)]^{1-}$ complexes in butyronitrile. The emission spectrum of $[(PpyIN)Pt(Cat)]^{1-}$ in butyronitrile at 77K has vibronic features with maximum at 560 nm upon excitation at 450 nm (Figure 3.16).

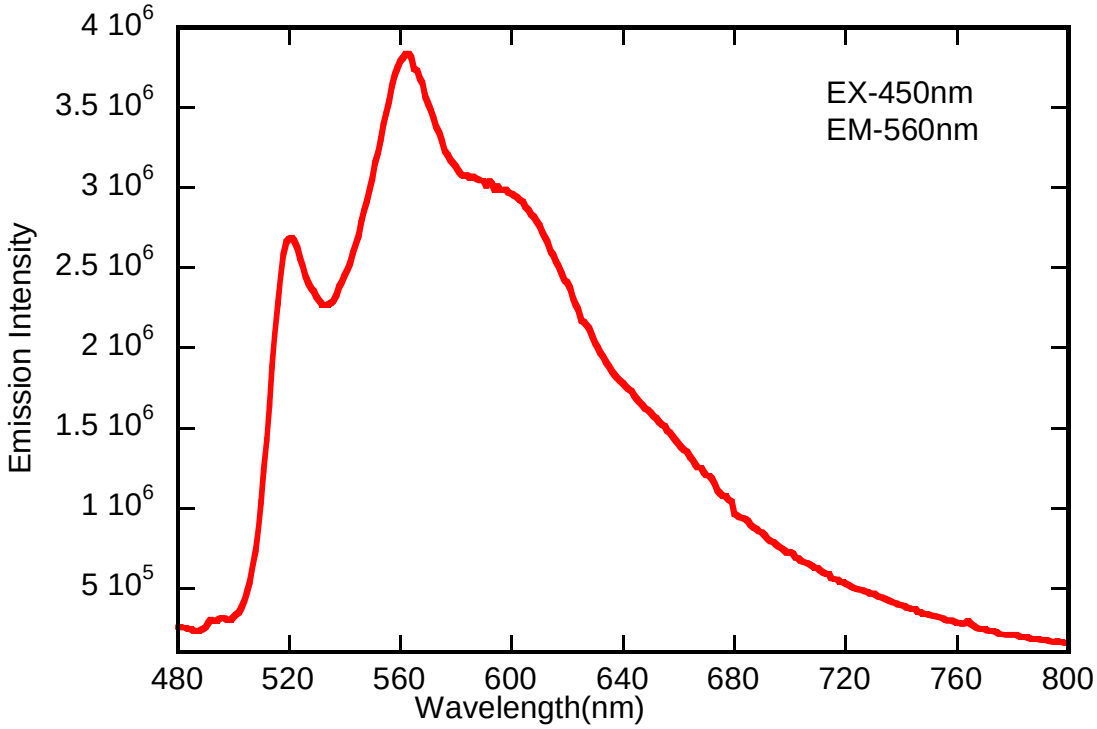

Figure 3.16: Emission spectrum of $[(PpyIN)Pt(Cat)]^{1-}$ at 77K in degassed butyronitrile, using 450 nm excitation .

The emission spectrum of $[(TpyIN)Pt(Cat)]^{1-}$ in butyronitrile at 77K has vibronic features with maximum at 625 nm upon excitation at 450 nm. Emission spectra of both $[(PpyIN)Pt(Cat)]^{1-}$ and $[(TpyIN)Pt(Cat)]^{1-}$ complexes are blue shifted when temperature is reduced to 77K (Figures 3.16 and 3.18; lifetime data in Figures 3.17 and 3.19).

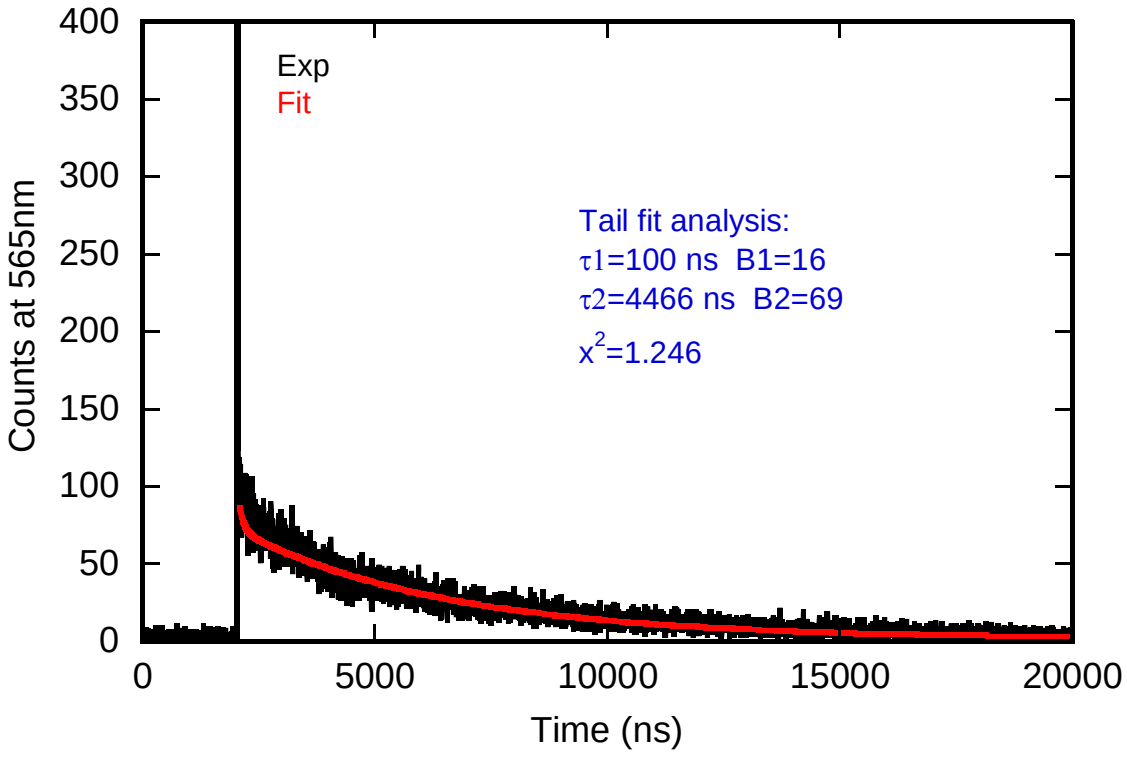

Figure 3.17: Emission decay for $[(PpyIN)Pt(Cat)]^{1-}$ at 77K in degassed butyronitrile, using a 450 nm diode laser.

Their emission lifetimes were also measured when the temperature was cooled down to 77K . The photoluminescence decay rates for both $[(PpyIN)Pt(Cat)]^{1-}$ and $[(TpyIN)Pt(Cat)]^{1-}$ were best fit with bi-exponential decay expressions (Figure 3.15 and Figure 3.17). Both the short and long lifetime components of both complexes became longer when the temperature was lowered to 77K in a butyronitrile glass.

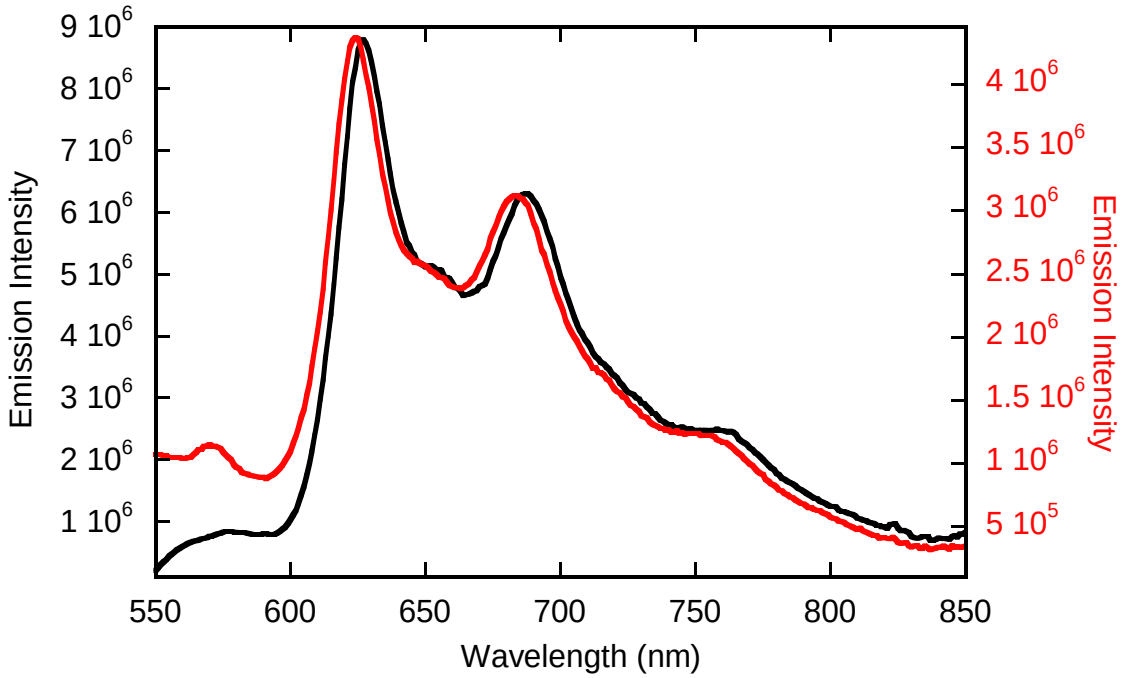

Figure 3.18: Emission spectra of $[(TpyIN)Pt(Cat)]^{1-}$ at 77K in degassed butyronitrile, using 450 nm (red) and 510 nm (black) excitation.

We also checked for emission from the free ligands used in the synthesis of these complexes in order to rule out the presence of any ligand impurity. These free ligands are emit in the near IR region, and we could not measure their lifetimes. Their lifetimes should be faster than the instrument response time (~600ps). Their emission spectra are presented in Appendix D. Thus, the bi-exponential excited-state decay rate could be from impurity, complex photophysical behavior, dimer formation, or aggregation induced emission.

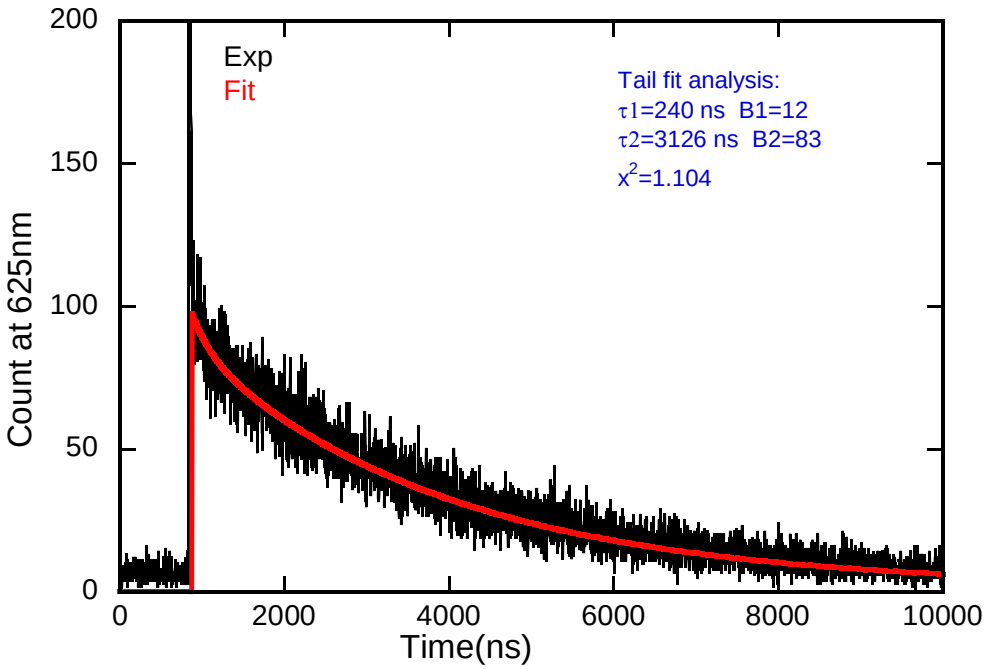

Figure 3.19: Emission lifetime for $[(TpyIN)Pt(Cat)]^{1-}$ at 77K in degassed butyronitrile using a 450nm diode laser.

The relative quantum yields of both $[(PpyIN)Pt(Cat)]^{1-}$ and $[(TpyIN)Pt(Cat)]^{1-}$ were calculated where emission intensities of these complexes and a standard were measured using the same set of spectral parameter (e.g., monochromator) settings. The quantum-yield standard used was tris(bipyridine)ruthenium(II)chloride $[Ru(bpy)_3Cl_2]$ and it was freshly prepared in acetonitrile solvent. In this method, we used the integrated intensities of our standard and our complexes to calculate the quantum yields. We assumed that the standard and the complexes with identical absorbances at the same excitation wavelengths could absorb a similar number of photons.

The quantum yield of $[Ru(bpy)_3]^{++}$ is 0.095 in acetonitrile under degassed conditions at room temperature and the counter anion effect is considered to be negligible[14]. The quantum yield expression and details were discussed previously in Chapter 2. The integrating sphere method for quantum yield evaluation was not applicable for our radical elaborated complexes because of their small quantum yield values. Hence, we measured relative quantum yields using $[Ru(bpy)_3Cl_2]$ as a reference sample, and the results are given in a Table 3.1 below.

Compound	Quantum yield (ACN)
$[(PpyIN)Pt(Cat)]^{1-}$	2.95×10^{-4}
$[(TpyIN)Pt(Cat)]^{1-}$	3.82×10^{-4}

Table 3.1: Quantum yields of $[(PpyIN)Pt(Cat)]^{1-}$ and $[(TpyIN)Pt(Cat)]^{1-}$ in acetonitrile solution

3.6 Discussions and Future Directions

The iminonitroxide elaborated catecholate derivatives of cyclometalated square planar Pt(II) complexes with two different cyclometalating ligands Ppy, (2-Phenylpyridine) and Tpy (2-Thienylpyridine), were synthesized and characterized. The radicals were attached to the acceptor side (cyclometalating ligand) of these donor-acceptor complexes to study the effect of a radical substituent on the molecule's excited state properties, not on the donor side as in earlier studies.[18,19,20]

Similar to radical-elaborated cyclometalated dithiolate derivatives discussed in Chapter 2, these radical-elaborated cyclometalated catecholates are found to be emissive in solution. Thus, the emissive nature of these radical appended complexes also indicates a rare example of emission from a Kramer's spin system.[21] The emission quantum yields of these catecholate derivatives are less than the respective dithiolate derivatives (presented in Chapter 2). The emission decay rates of these catecholate derivatives were best-fit using bi-exponential functions. Both the short and long components of the emission decay rates for these catecholates were longer than the emission decays rates of similar dithiolate derivatives discussed in Chapter 2. The emission decay rates of the longer components for both catecholates are in the microsecond range. The excited state manifold will have triradical character with one spin localized on the radical, one spin localized on the cyclometalating ligand (LUMO), and one spin localized on the donor ligand (HOMO). Thus, there will be pairwise exchange interactions in the excited state manifold. The exchange interaction between iminonitroxide and the cyclometalating ligand will be the one to control the D_{sing} and D_{trip} mixing through an EISC mechanism.[18,19,20,22,23] CASSCF calculations showed larger D_{trip} (trip-doublet) and quartet energy gaps compared to the cyclometalated dithiolate derivatives. These complexes should easily be able to access the quartet state because of the large spin orbit coupling effect.

The CASSCF calculation also shows that quartet lies below D_{trip}, which suggests that there is ferromagnetic exchange coupling between the chromophore and the radical moiety.

State	Multiplicity	Energy (cm^{-1})
GS	2	0
1	4	10051.6
2	2	10583.2
3	2	11910.1

Table 3.2: CASSCF(3,3) transition energies for $[(PpyIN)Pt(Cat)]^{1-}$ complex.[24]

State	Multiplicity	Energy (cm^{-1})
GS	2	0
1	4	10026.4
2	2	10575.8
3	2	12132.9

Table 3.3: CASSCF(3,3) transition energies for $[(TpyIN)Pt(Cat)]^{1-}$ complex.[24]

The energy gaps between D_{trip} and quartet for $[(PpyIN)Pt(Cat)]^{1-}$ and $[(TpyIN)Pt(Cat)]^{1-}$ obtained from the CASSCF calculations are 531.6 cm^{-1} and 549.4 cm^{-1} respectively (Table 3.3). Based on these energy gaps and the emission decay times, we can assume that these molecules likely decay from both the D_{trip} and quartet states, but

the dominant decay pathway is from the quartet state. The quartet to ground doublet state relaxation process is a spin forbidden process, while relaxation from the D_{trip} to the doublet ground state is a partially spin allowed process. Based on the above assumption, we can propose the following decay mechanism for radical-elaborated cyclometalated platinum catecholate complexes.

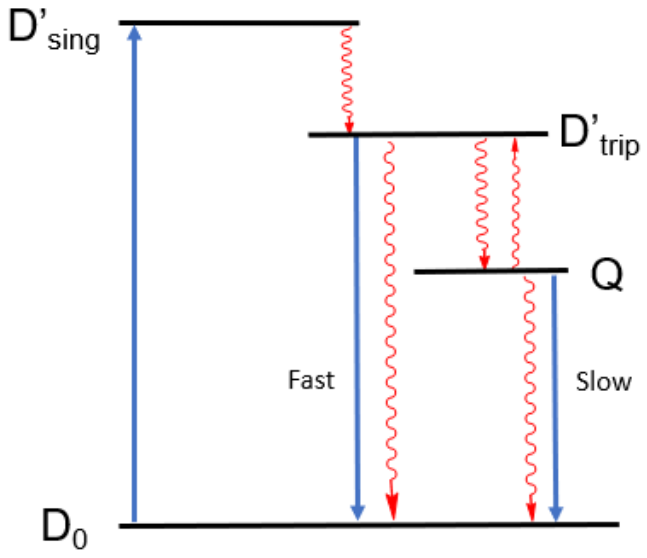

Figure 3.20: A schematic diagram for the proposed decay mechanism for radical-elaborated cyclometalated platinum catecholates.

We also performed CASSCF calculations to determine the energy gap between D_{trip} and quartet for (PpyIN)Pt(acac), where acac is a diketonate ligand. The energy gap between D'trip and quartet from the calculation is 1,935 cm^{-1}. This acac complex is also found to be emissive and has longer emission lifetime than these catecholate and dithiolate complexes. Parent molecules of this acac complex were extensively studied[4,15],

and their lowest lying emitting state was described having MLCT character. When we have donor groups such as dithiolates and catecholates, we found that LL'CT character is dominant and MLCT is reduced, and lifetime gets shorter. We measured the shortest emission decay rates for our cyclometalated platinum dithiolates compared to the catecholates and the diketonate analogs. Thus, LL'CT character, magnetic exchange coupling, and the energy gap between D_{trip} and quartet are controlling the lifetimes of these cyclometalating platinum complexes.

Because of the radical elaboration, these cyclometalated Pt(II) catecholate complexes are expected to be MCD active, and hence a detailed analysis of the doublet excited manifold can be performed using the MCD results coupled with theoretical calculations in the future. Due to the paramagnetic nature of these complexes, they can be studied by TREPR to obtain insight into spin polarization effects.

3.7 References

1. Ziegler, M.; Zelewsky A. V.; Charge-Transfer Excited State Properties of Chiral Transition Metal Coordination Compounds Studied by Chiroptical Spectroscopy Coordination Chemistry Reviews, **1998**, 177, 257-300.

2. Maestri M.; Sandrini, D.; Balzani V.; Chassot, L.; Jolliet, P.; and Zelewsky A.V. Luminescence of ortho-metallated platinum(II) complexes. Chemical Physics letter, **1985**,122, 375-379.

3. Kozhevnikov, D. N.; Kozhevnikov, V. N.; Shafikov, M. J.; Prokhorov A. M.; Bruce, D. W, and Williams, J. A.; Phosphorescence vs Fluorescence in Cyclometalated Platinum(II) and Iridium(III) Complexes of (Oligo)thienylpyridines. Inorg. Chem. **2011**, 50, 3804-3815

4. Yersin, H.; Rausch, A. F.; Czerwieniec, R.; Hofbeck.; Fisher, T.; The triplet state of organo-transition metal compounds. Triplet harvesting and singlet harvesting for efficient OLEDs. Coordination Chemistry Reviews, **2011**, 255, 2622-2652.

5. Kozhevnikov, D. N.; Kozhevnikov, V. N.; Ustinova, M. M.; Santoro, A.; Bruce, D. W.; Koenig, B.; Czerwieniec, R.; Fisher, T.; Zabel, M. and Yersin, H.; Synthesis of Cyclometallated Platinum Complexes with Substituted Thienylpyridines and Detailed Characterization of Their Luminescence Properties. Inorg. Chem. **2009**,48,4179-4189.

6. Goss, Carol H. A.; Henderson, W.; Wilkins, A. L.; Evans, C.; Synthesis, characterization and biological activity of gold(III) catecholate and related complexes. J. organometallic Chemistry, **2003**, 2, 194-201

7. Szerb, E. I.; Ionescu, A.; Godbert, N.; Yadav, Y. J.; Talarico, A. M. and Ghedini, M.; Anionic cyclometallated iridium (III) complexes containing substituted bivalent *ortho*-hydroquinones. Inorg. Chem. Com. **2013**,37, 80-83.

8. Hirani, B.; Li, J.; Djurovich, P. I.; Yousufuddin, M.; Oxgaard, J.; Persson, P.; Wilson, S. R.; Bau, R.; Goddard III, W. A. and Thomson, M. E. Cyclometallated Iridium and Platinum Complexes with Noninnocent Ligands. Inorg. Chem. **2007**, 46, 3865-3875

9. Moussa, J.; Loch, A.; Chamoreau, L.; Esposti, A. D.; Bandini, E.; Barbieri, A. and Amouri, H. Luminescent Cyclometalated Platinum Complexes with π-Bonded Catecholate Organometallic Ligands. Inorg. Chem. **2017**, 56, 2050-2059

10. Ricciardi, L.; La Deda, M.; Ionescu, A.; Godbet, N.; Aiello, I. and Ghedini, M. Anionic cyclometallated pt(II) square-planar complexes: new sets of highly luminescent compounds. Dalton. Trans. **2017**, 46, 12625-12635

11. Sesolis, H.; Moussa, J.; Gontard, G.; Utand, A.; Gullo, M. P.; Barberi, A. and Amouri, H. A unique class of neutral cyclometalated platinum(II) complexes with π-bonded benzenedithiolate: synthesis, molecular structures and tuning of luminescence properties. *Dalton Trans. Comm.* **2015**, 44, 2973-2977

12. Julia, F.; Jones, P.G.; Gonzalez-Herrero, P. Synthesis and photophysical Properties of Cyclometalated Platinum(II) 1,2-Benzenedithiolate Complexes and Heterometallic Derivatives Obtained from the Addition of [Au(PCy_3)]+ Units. *Inorg. Chem*. **2012**, 51, 5037-5049.

13. Brooks, J.; Babayan, Y.; Lamansky, S.; Djurovich, P.I.; Tsyba, I.; Bau, r.; and Thompson, M.E. Synthesis and Characterization of Phosphorescent Cyclometalated Platinum Complexes. *Inorg. Chem.* **2002**, 41, 3055-3036

14. Suzuki, K.; Kobayashi, A.; Kaneko, S.; Takehira, K.; Yoshihara, T.; Ishida, H.; Shiina, Y.; Oishi, S.; Tobita, S.; Reevaluation of absolute luminescence quantum yields of standard solutions using a spectrometer with an integrating sphere and a back-thinned CCD detector. Phys. Chem. Chem. Phys. **2009**, 11, 9850–9860

15. Xing, Y., Liu, C. and Li, J. Photostable trifluoromethyl-substituted platinum(II) emitters for continuous monitoring of molecular oxygen. *J. Mater. Chem. C*. **2015**, 3, 2166-2174

16. Nishida, S.; Morita, Y.; Kobayashi, T.; Fukui, K.; Ueda, A.; Sato, K.; Shiomi, D.; Takui, T. and Nakasuji, K. Spin delocalization on curved π-system: Corannulene with iminonitroxide. *Polyhedron*. **2005**,24,2200-2204.

17. Fidan, I.; Onal, E.; Luneau, D.; Ahsen, V. and Hirel, C. Synthesis and Straightforward Quantification Methods of Imino Nitroxide-Based Hexaradical Archtecture on a Cyclotriphosphagene Scafold. *Inorg. Chem.* **2016,55,** 11447-11453.

18. Stein, B. W.; Tichnell, C. R.; Chen, J.; Shultz, DA and Kirk, ML. Excited State Magnetic Exchange Interactions Enables Large Spin Polarization Effects; *J. Am. Chem. Soc.* **2018**, 140, 2221-2228

19. Tichnell, C.R.; Daley, D.R.; Stein, B.W.; Stultz, DA.; Kirk, M L., and Danilov, E.O.; Wave Function Control of Charge-Separated Excited-State Lifetimes. *J. Am. Chem*. *Soc*. **2019**, 141, 9,3986-3992

20. Stein, B.W. The Electronic Structure of the Pyranopterin Dithiolene Cofactor and Radical Reporters of Excited state Interactions. Disseration, **2015**.

21. Cho, E.; Coropceanu, V. and Breadas, J.-L. Organic Neutral Radical Emitters: Impacts of Chemical Substitution and Electronic-State Hybridization on the Luminescence Properties. *J. Am. Chem*. *Soc.* **2020**, 142, 17782-17786.

22. Kirk, M. L.; Shultz D, A.; Chen, J.; Hewitt, P.; Daley, D.; Paudel, S.; Est, A. Vd. Metal Ion Control of Photoinduced Electron Spin Polarization in Electronic Ground States. *J. Am. Chem. Soc*. **2021**, 143, 10519-10523.

23. Teki, Y.; Excited-State Dynamics of Non-Luminescent and Luminescent π-Radicals. *Chem. Eur. J*. **2019,** 25, 1-18.

24. The Orca 4.0.0.2 software program was used for CASSCF computations. The input files were generated using the molecular builder function in the Gaussview 03 software. The CASSCF(3,3) method where a 3-electron-in-3-orbital (HOMO, SOMO and LUMO) active space was considered.

Chapter 4

Excited State Properties and Solvatochromism of Square Planar Platinum (II) Bipyridine-Napthalene-1,2-diol Complex

4.1 Background

Platinum(II) dimine catecholates have been studied as attractive candidates for many light-driven applications such as sensitizers in dye-sensitised solar cells, chemosensors, etc.[1,2,3,4,5]. Many catechol ligands have already been studied with many other transition metal ions such as Ru(II), Os(II), etc. for their rich electrochemistry that derives from the non-innocent behavior of the ligand which also includes oxidized semiquionone and quinone forms. However, diimine platinum catecholate chemistry has been given limited attention[1,3,6,7]. An advantate is that the photophysical and elecrochemical properties of diimine Pt(II) complexes can easily be tuned by ligand modifications.

Mixed-ligand Pt(II) diimine systems are mostly nonemissive in solution at room temperature due to the prescence of low lying ligand field "d-d" metal centered states.[8] These low-lying metal centered d-d states increases the efficiency of nonradiative decay processes[8]. To overcome the problem of efficient non-radiative dacay pathways, two major strategies have been applied. The first strategy is to raise the energy of the metal centered d-d states by introducing strong ligand field ligands such as chelating ligands (cyclometalating ligands)[9,10]. The second technique is to change the charge-transfer character of emissive excited states via modification of ligands by tuning to longer

lifetime or higher quantum yields.[8] Moussa et al. reported that diimine platinum catecholate (O,O) is non-luminescent in degassed solutions at room temperature but luminescent at 77K in a 1:4 ethanol-methanol mixture[8].

Earlier studies in our lab involved diimine Pt dioxolenes where simple diimine platinum catecholate was observed to be non-luminiscent due to the high effective symmetry (C_{2v}) of the complex (Figure 4.1)[9]. However, when one of the donor atoms was changed for O to S or Se, then anisotropic covalency induced the rotation of the metal d orbital towards the softer heteroatom and enhanced the spin orbit coupling effect.

$$K_{isc} \propto < S_n|L_x|T_n >^2 / \Delta E_{st}{}^2 \qquad 4.1$$

Thus, the intersystem crossing rate is increased by increasing the spin-orbit matix element in the numerator and by decreasing the energy gap between singlet and triplet states.

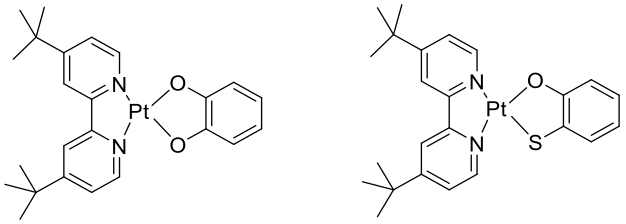

Figure 4.1: Non-emissive (O, O) complex (left) and emissive (O, S) complex (right).

The photophysical behavior of these two molecules can be understood by the Jablonski diagram as shown in Figure 4.2.

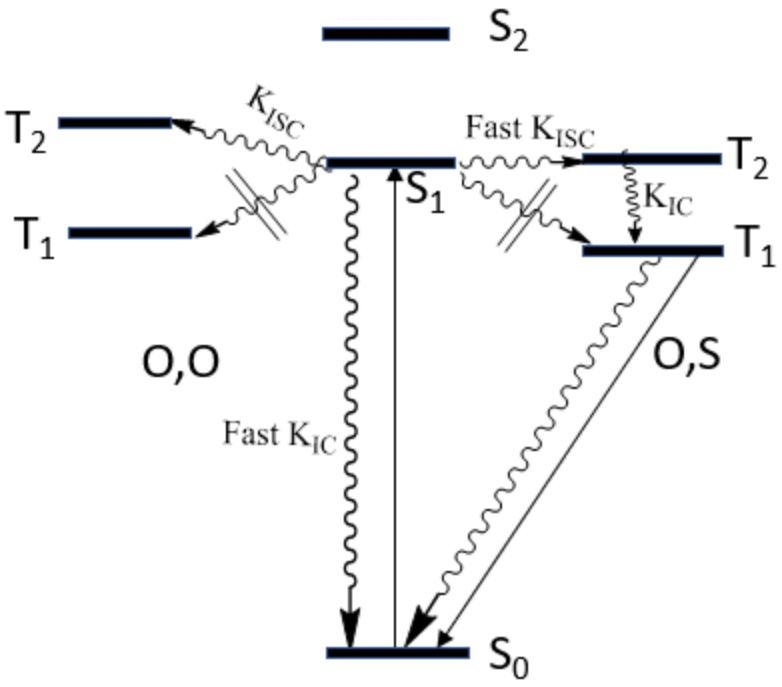

Figure 4.2: Jablonski diagram showing the photophysical properties for (O, O) and (O, S) complexes. This system was previously studied by Yang *et al.* in our research lab.[11,12]

In this case, the LL'CT charge transfer band does not change significantly with changing the donor atom but the lifetime of the excited state changes dramatically. The (O,O) system does not access the triplet state as there is no spin-orbit matrix element that effectively connects the S_1 and T_1 states. So, for the (O,O) complex there is rapid nonradiative deexcitation to ground state, while for (O, S) ISC occurs providing access to the triplet excited state.

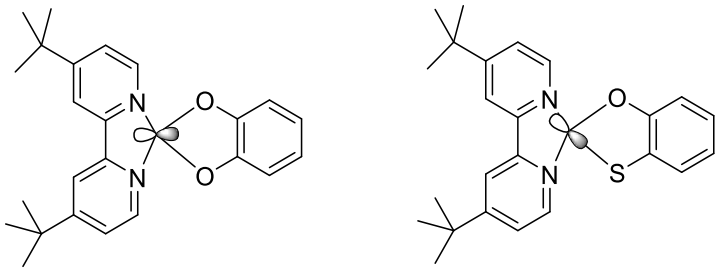

Figure 4.3: A diagram showing metal d-orbital rotation in the (O, S) complex, but no orbital rotation in (O,O). [11,12]

The (O, S) molecule has a rotation of the d(xz) orbital in the HOMO directed toward the softer donor atom, while there is no rotation in the LUMO, which is localized on the bpy ligand. Hence, based on the heteroatom dependency of singlet-triplet energy gaps and anisotropic covalency, the (O, O) molecule is observed to be non-luminescent in nature.

Here, we are changing the electronic structure of the donor ligand from 1,2-dihydroxy-benzene to 1,2-dihydroxy-naphthalene in order to tune the photophysical properties of the diimine platinum catecholate complex. The addition of one benzene ring to the donor ligand gives an extended conjugation to the donor ligand and creates an unsymmetrical donor as well.

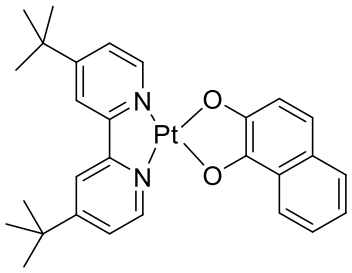

Figure 4.4: Molecular structure of Pt(II) diimine with naphthalene-1,2-diol as the donor ligand.

4.2 Synthesis and Characterization

First, the dichloro precursor was prepared by heating the mixture of 4,4'-di-tert-butyl-2,2'-bipyridine with potassium tetrachloroplatinate in 1:1 equivalent in 3M hydrochloric acid solution. This is an already established method in our lab for synthesizing the dichloro derivative of Pt(II) diimine complexes.[11,12] The dichloro precursor was then subjected to the next reaction with naphthalene-1,2-diol in the presence of a base to obtain the desired product. The complex was purified by column chromatography and collected in good yield as a bluish black solid that was soluble in most organic solvents. A detailed synthetic procedure and characterization data are given in the experimental procedure section (Appendix B). Starting materials are commercially available from Sigma-Aldrich and were used in the reaction directly.

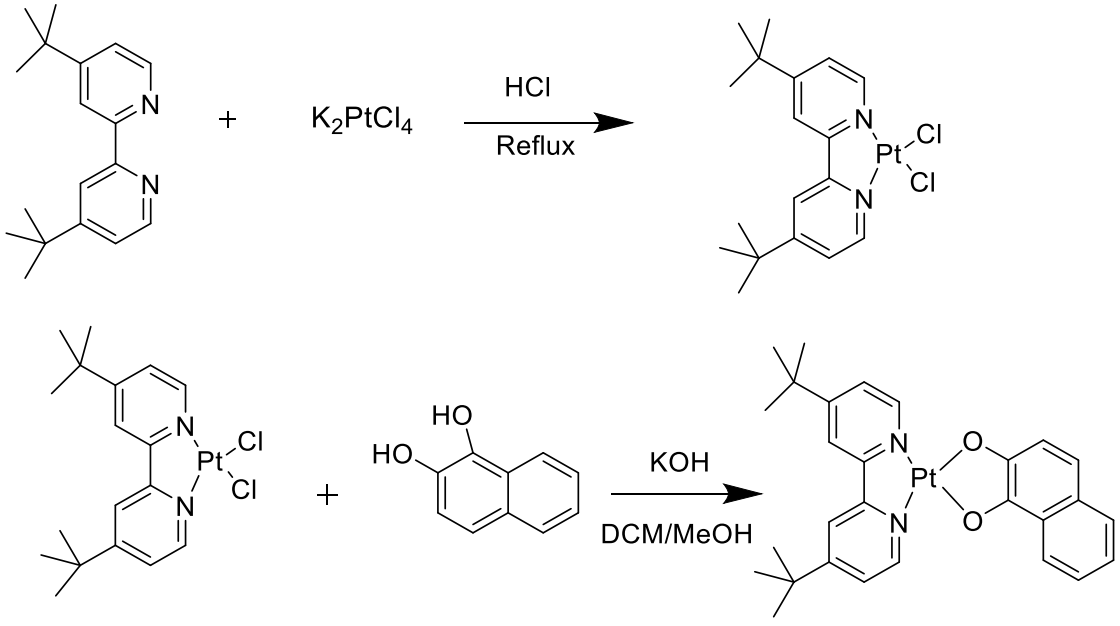

Figure 4.5: Scheme for the synthesis of (bpy)Pt(ND).

4.3 Electronic Absorption Spectra

The electronic absorption spectrum was collected in dichloromethane solution at room temperature and is shown in Figure 4.6 as a function of energy. The room temperature absorption spectrum shows a structureless broad band at 16,600 cm^{-1} (610 nm) with an extinction coefficient of 12,600 $M^{-1}cm^{-1}$ in dicloromethane (Figure 4.6). This lowest energy band is characterised as the LL'CT band since this band is absent in the dichloro precursor.

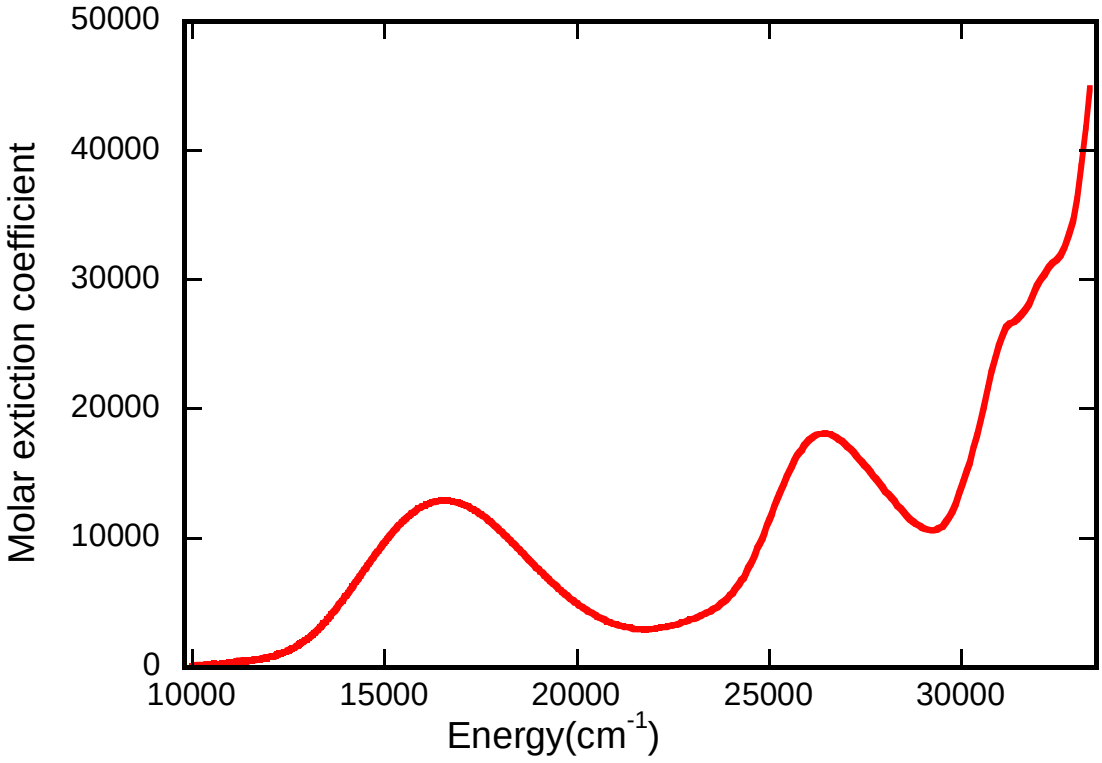

Figure 4.6: Room temperature electronic absorption spectrum of (bpy)Pt(ND) in dichloromethane.

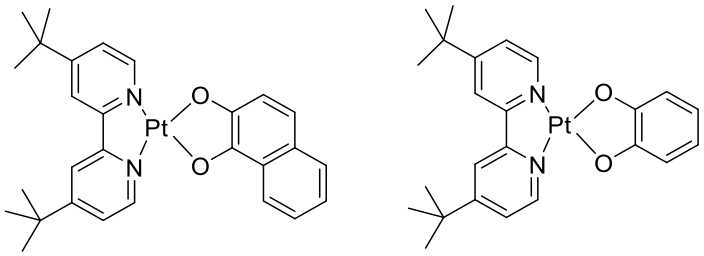

Figure 4.7: Molecular structures of (bpy)Pt(ND) and (bpy)Pt(Cat).

The energy of the lowest energy absorption band for (bpy)Pt(ND) is not significantly different from that of (bpy)Pt(Cat), but the this band in (bpy)Pt(ND) is more intense than that observed for (bpy)Pt(Cat) (Figure 4.8). Based on DFT and TD-DFT calculations, the lowest energy absorption band in the visible region can be assigned as LL'CT in character.

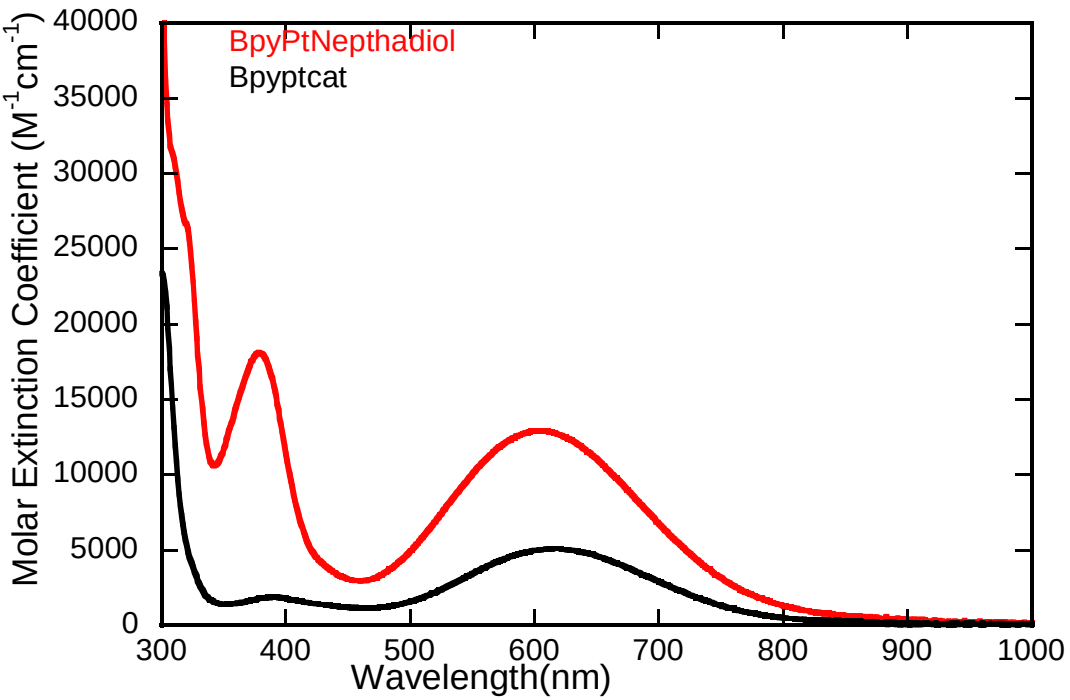

Figure 4.8: An overlay of electronic absorption spectra of (bpy)Pt(Cat) (black) and (bpy)Pt(ND) (red) in dichloromethane solution at room temperature.

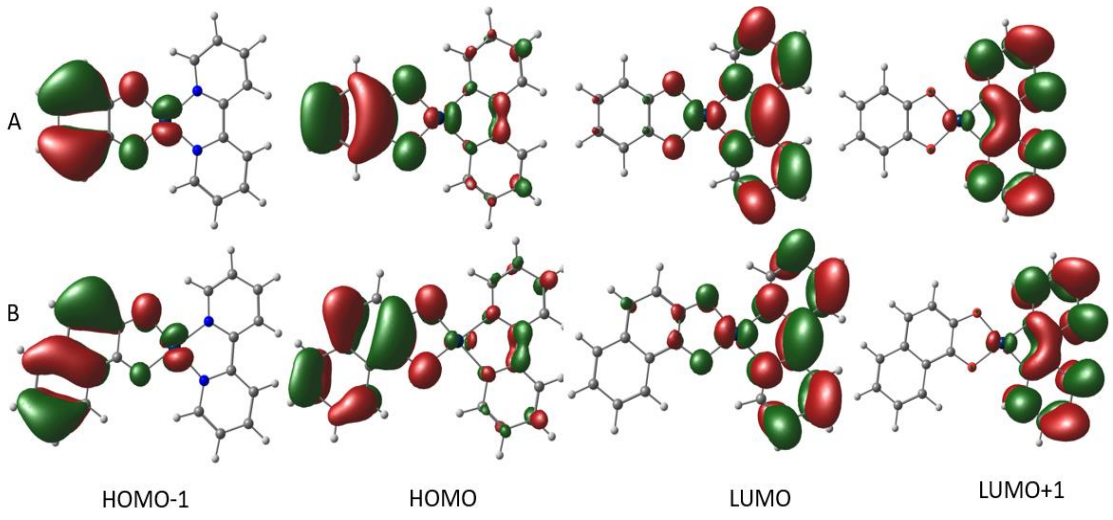

Figure 4.9: Frontier molecular orbitals of A. (bpy)Pt(Cat) and B. (bpy)Pt(ND) at the same contour values (0.0031).

4.4 Emission Spectra and Lifetime Measurements

A room temperature steady state emission spectrum has been collected in methanol solution. The sample solution was degassed by purging with a flow of nitrogen gas for fifteen minutes. The (bpy)Pt(ND) complex was found to be emissive in degassed methanol solution when it is excited at 450 nm (Figure 4.10).

The (bpy)Pt(Cat) complex with the catecholate ligand is non-emissive at room temperature, but when this catecholate ligand is replaced by napthalene-1,2-diol, the (bpy)Pt(ND) complex becomes emissive. The emissive properties of this complex likely derive from breaking the high effective C_{2V} symmetry present in (bpy)Pt(Cat) coupled with the extended delocalization within the HOMO of the donor ligand.

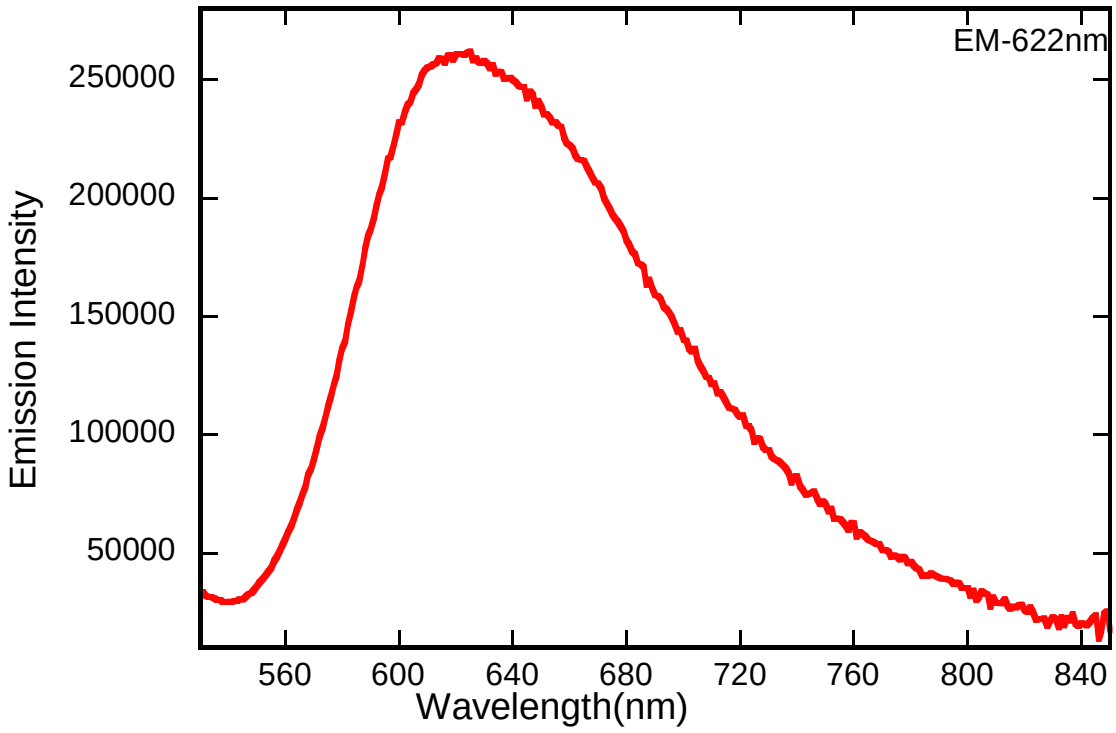

Figure 4.10: Steady state room temperature emission spectrum for (bpy)Pt(ND) in degassed methanol using 450 nm excitation.

We also measured the emission decay rate of this molecule and emission decay rate was best fit by a bi-exponential expression with a short component of 1.31 ns and long component of 5.72 ns as seen in Figure 4.11.

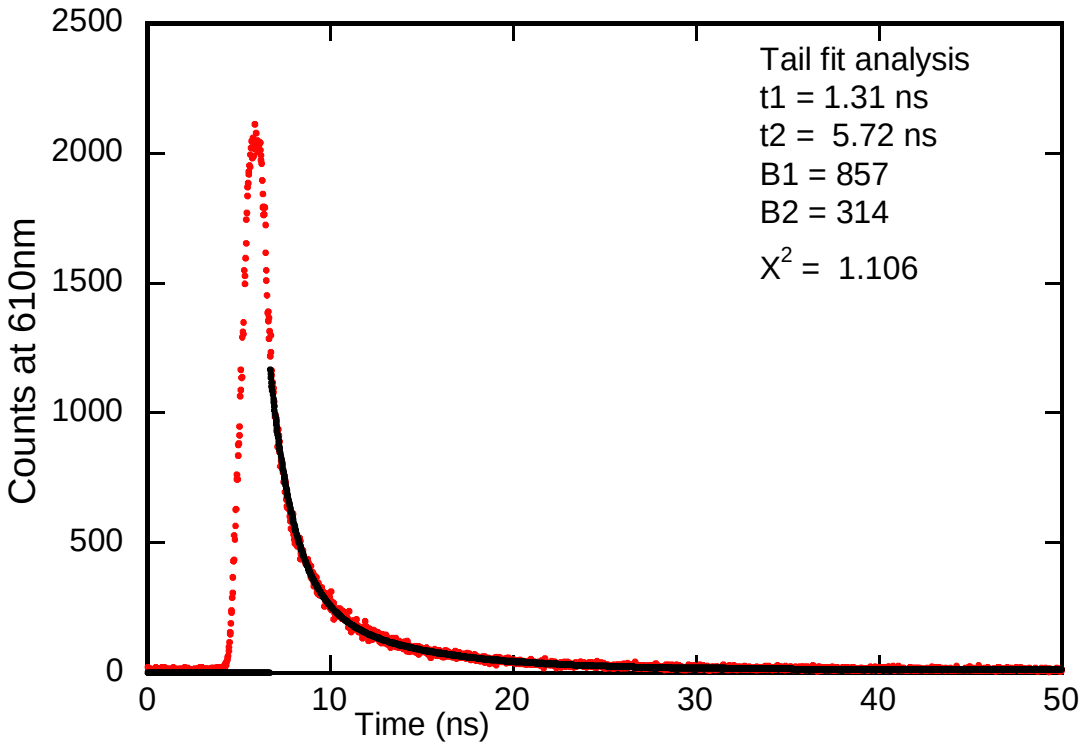

Figure 4.11: Room temperature emission decay rate of (bpy)Pt(ND) in degassed methanol at 610 nm using a 450 nm diode laser.

4.5 Solvatochromism

Solvatochromism is the character of a molecule (e.g., organic dye) where a color change is observed when it interacts with solvents of different polarities. Positive solvatochromism is a red shift (bathochromic shift) with increasing solvent polarity while negative solvatochromism is characterized by a blue shift with increasing solvent polarity and *vice versa*. Solvatochromism of a compound is observed in its absorption and emission spectra as changes in the band energies, band intensities, and band shapes. The changes in the color of the solution and the energy of the charge transfer absorption bands in different solvents of different polarities are the indications of solvatochromic behavior in molecules. In these systems, the ground state and excited state dipole moments of a molecule are different, and hence they interact differently with solvents of different polarities in order to stabilize the molecules. Thus, solvatochromism can give ground and excited state dipole moment estimations.[14] Pt(II) catecholates are known to show negative solvatochromism, *i.e.* the energy band shifts to lower energy (higher wavelength) with less polar solvents[2,13,14]. The electronic absorption spectra of this molecule was collected in different solvents of different polarities (Table 4.1).

Solvents	ʎmax (nm)
Toluene	705
THF	655
CH2Cl2	610
Acetone	600

DMSO	570
CH3CN	560
MeOH	525

Table 4.1: Wavelength maxima of the LL'CT charge transfer bands for (bpy)Pt(ND) in different solvents.

The positions of the lowest energy absorption bands in seven different solvents show that this molecule is displaying negative solvatochromism (red shift with less polar solvent). The lowest energy absorption maximum is blue shifted with increasing polarity, from toluene at 705 nm to 525 nm in methanol (Figure 4.12). The blue shift of the band maxima with increasing polarity indicates that this complex has a polar ground state and less polar excited state.

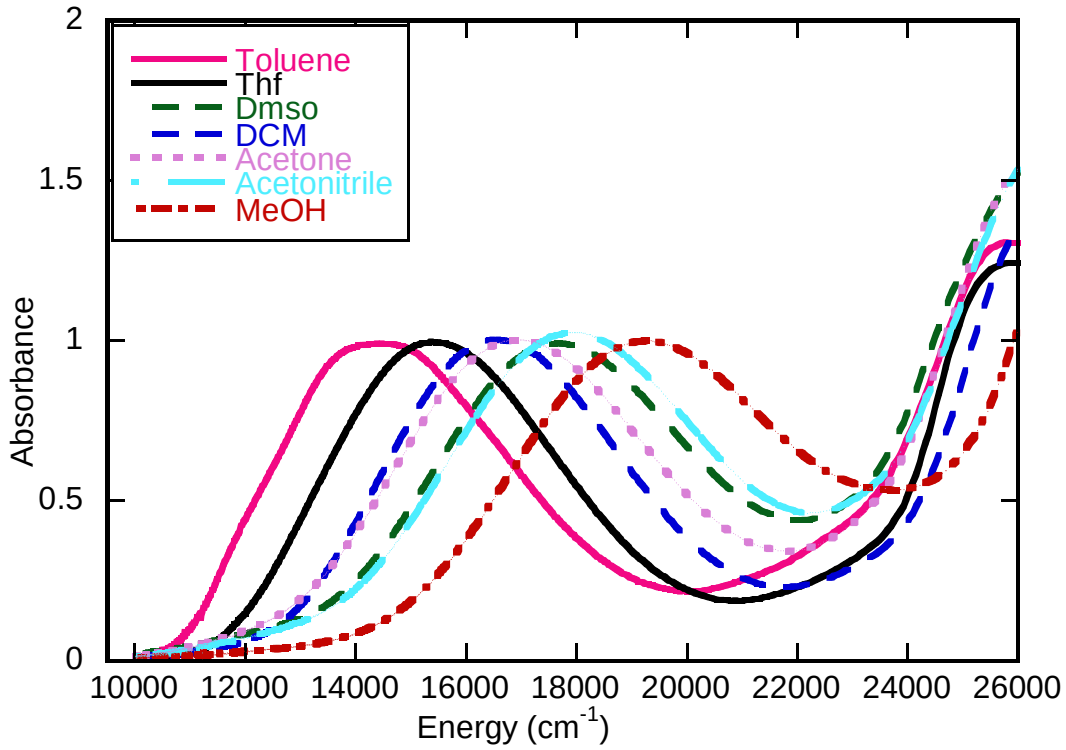

Figure 4.12: An overlay of electronic absorption spectra for (bpy)Pt(ND) in different solvents.

A linear correlation is found between the energy of the charge-transfer band and the solvent polarity parameter. The slope of the plot of the energy of the lowest absorption band versus solvent parameter is the value of the solvatochromic shift (4,311 cm^{-1}) as shown in Figure 4.13. The solvent parameter data were obtained from reference 6. Only the lowest energy absorption band (charge transfer band) of this complex is highly solvatochromic, while other absorption bands are observed to shift less.

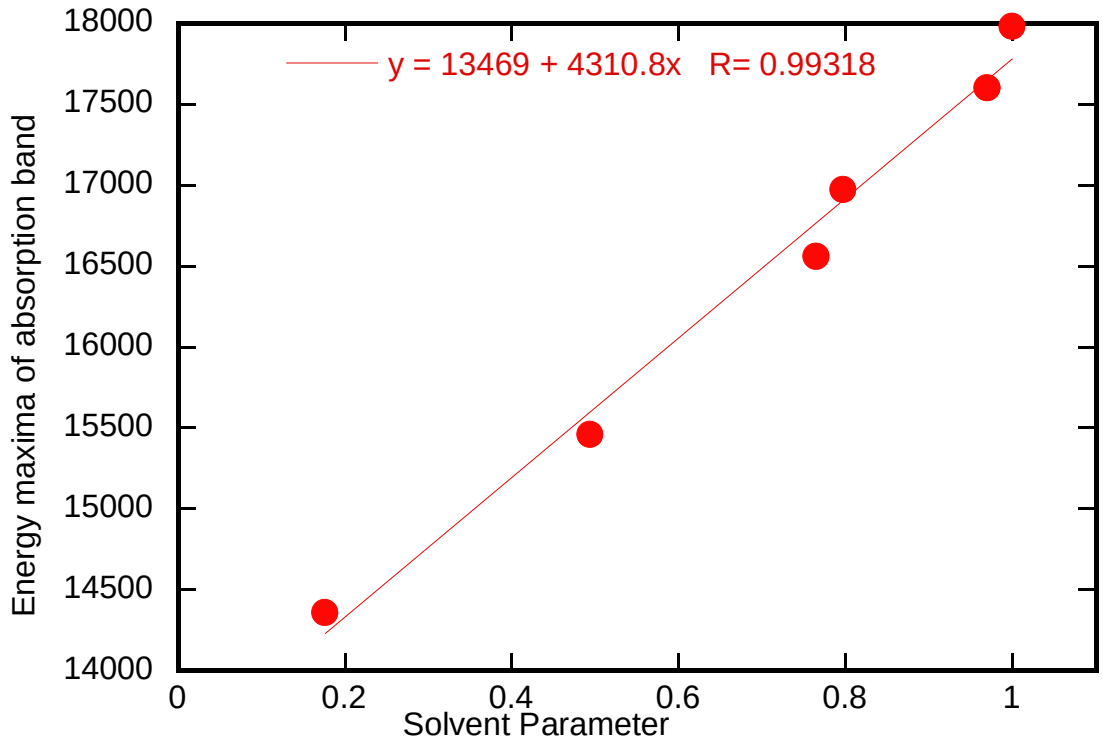

Figure 4.13: A linear correlation plot of the energy of LL'CT charge transfer maxima versus solvent parameter for (bpy)Pt(ND).

4.6 Discussion and Future Directions

The (bpy)Pt(ND) complex has been synthesized and characterized by mass spectrometry, NMR, and elemental analysis. The lowest energy band at 610 nm can be assigned as an LL'CT transition based on the our computations and the results of similar molecules studied previously in our lab. Here, changing the donor ligand from 1,2-dihydroxybenzene to 1,2-dihydroxynaphthalene does not significantly change the energy of the charge transfer band, but does increse the exctinction coefficient of this band with a molar absoptivity of ~12,500 $M^{-1}cm^{-1}$. This change of the donor ligand from 1,2-dihydroxy benzene to 1,2-dihydroxynaphthalene also changes the excited state

properties and molecule in that it becomes emissive in nature. TDDFT calculations on (bpy)Pt(ND) suggests that the lowest singlet/triplet (S_1/T_1) transition is a HOMO to LUMO and the next lowest singlet/triplet (S_2/T_2) transition is dominated by a HOMO to LUMO+1 one-electron promotion. The T_3 and T_4 transitions can be assigned as HOMO-1 → LUMO. In these (bpy)Pt(Cat) and (bpy)Pt(ND) systems, the LUMOs are predominantly localized on the diimine ligands and these orbitals possess the C_{2v} character of the free ligand. However, the HOMO and HOMO-1 of (bpy)Pt(ND) are not symmetric, and hence the mixing of d-orbital character increases the nonradiative ground state recovery rate. The CASSCF method was used to calculate the SOC matrix element between lowest triplet states (T_1) and the electronic ground state (S_0) for (bpy)Pt(Nd) along with (bpy)Pt(O,O), (bpy)Pt(O,S) for comparision purposes. We have applied an intensity-weighted average lifetime for (bpy)Pt(ND) in the table below [15].

Compounds	SOC-Matrix Element	LL'CT Energy	Lifetime
(bpy)Pt(O,O)	0 cm^{-1}	16,880 cm^{-1} (592 nm)	0.6 ns
(bpy)Pt(ND)	9.83 cm^{-1}	16,600 cm^{-1} (610 nm)	4.0 ns
(bpy)Pt(O,S)	67.01 cm^{-1}	17,750 cm^{-1} (564 nm)	46 ns

Table 4.2: Calculated SOC matrix elements that connect the lowest triplet states (T_1) and the electronic ground states (S_0), using CASSCF(4,3) method.[16]

Here, the CASSCF calculated matrix element for (bpy)Pt(ND) is nonzero but is very small. The (bpy)Pt(ND) complex has a very small SOC matrix element that connects the lowest triplet state (T_1) and the electronic ground state (S_0) and, shorter lifetime compared to (bpy)Pt(O,S), but a longer lifetime when compared to that of (bpy)Pt(Cat). This CASSCF calculation is showing a increasing trend of lifetimes with increasing SOC matrix elements. Finally, future work will focus on the effects of a radical substituent on photophysical properties of this molecule (Figure 4.14).

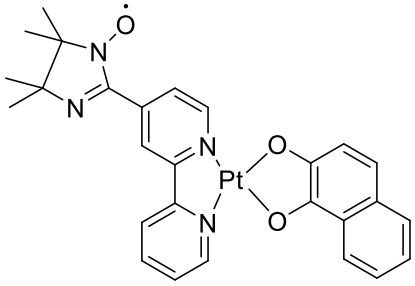

Figure 4.14: A proposed radical appended complex.

4.7 References

1. Best, J.; Sazanovich, I G.; Adams, H.; Bennett, R.D.; Davies, E.S.; Meijer, A.J.H.M.; Towrie, M.; Tikhomirov, S.A.; Bouganov, O.V.; Ward, M.D and Weinstein J.A. Structure and Ultrafast Dynamics of the Charge-Transfer Excited State and Redox Activity of the Ground State of Mono- and Binuclear Platinum(II) Diimine Catecholate and Bis-catecholate Complexes: A Transient Absorption, TRIR, DFT and Electrochemical Study. *Inorg. Chem*. **2010** , 49, 10041-10056

2. Scattergood, P.A.; Jesus,P.; Adams, H.; Delor,M.; Sazanovich, I. V.; Burrows, H.D. Serpa, C.; and Weinstein, J. A. Exploring excited states of Pt(II) diimine catecholates for photoinduced charge separation. *Dalton Trans*. **2015**, 44, 11705-11716

3. Geary,E.A.M.; Hirata, N., Clifford, J.; Durrant, J.R.; Parsons, S.; Dawson, A.; Yellowlees, L.J.; and Robertson, N. Synthesis, structure and properties of [Pt(2,2-bipyridyl-5,5-dicarboxylic acid)(3,4-tolunedithiolate)]: tuning molecular properties for application in dye-sensitised solar cells. *Dalton Trans*. **2003**, 3757-3762

4. Chakraborty, S. Platinum chromophore-based systems for photoinduced charge separation : A molecular design approach for artificial photosynthesis. *Inorg. Chem.* **2005**, 44, 6865-6878

5. Wadas, T. J.; Wang, Q-M.; Kim, Y.-J.; Flaschenreim, C.; Blanton, T. N. and Eisenberg, R. Vapochromism and its Structural Basis in a Luminescent Pt(II) Terpyridine-Nicotinamide Complex. *J Am. Chem. Soc*. **2004**, 126, 16841-16849

6. Shavaleev, N. M.; Davies, E. S.; Adams, H.; Best, J. and Weinstein J. A. Platinum(II) Diimine Complexes with Catecholate Ligands Bearing Imide Electron-Acceptor Groups: Synthesis, Crystal Structure, (Spectro)Electrochemical and EPR studies , and Electronic Structure. *Inorg. Chem*. **2008**, 47, 1532-1547

7. Moussa, J.; Chamoreau, L.-M.; Esposti, A. D.; Gullo, M. P.; Barbieri, A. and Amouri, H. Tuning Excited States of Bipyridyl Platinum(II) Chromophores wth π-Bonded Catecholate Organometallic Ligands: Synthesis, Structure, TD-DFT Calculations, and Photophysical Properties. *Inorg. Chem*. **2014**, 53, 6624-6634

8. Weinstein, J.A.; Tierney, M. T.; Davies, E.S.; Base, K.; Robeiro, A. A.; Grinstaff, M. W. Probing the Electronic Structure of Platinum(II) Chromophores: Crystal Structures, NMR Structures, and Photophysical Properties of Six New Bis- and Di-Phenolate/Thiolate Pt(II) Diimine Chromophores. *Inorg. Chem*. **2006** , 45, 4544-4555

9. Furuta, P.T.; Deng, L.; Garon, S.; Thompson M. E. and Frechet. J. M. J. Platinum-Functionalized Random Copolymers for Use in Solution-Processible, Efficient, Near-White Organic Light-Emitting Diodes. *J Am. Chem. Soc*. **2004**,126,47, 15388-15389

10. Shavaleev, N. M.; Bell, Z. R.; Easun, T. L.; Rutkaite, R.; Swanson, L. and Ward, M. D. Complexes of substituted derivatives of 2-(2-pyridyl)benzimidazole with Re(I), Ru(II) and Pt(II): structures, redox and luminescence. *Dalton Trans*. **2004**, 3678-3688

11. Yang, J.; Kersi, D.K.; Giles, L. J.; Stein, B. W.; Feng, C.; Tichnell, C. R.; Shultz D. A. and Kirk, M. L. Ligand control of donor-acceptor excited -state lifetimes. *Inorg. Chem*. **2014**, 53,4791-4793.

12. Yang, J.; Kersi, D.K.; Richers, C. P.: Giles, L. J.; Dangi, R.: Stein, B. W.; Feng, C.; Tichnell, C. R.; Shultz D. A. and Kirk, M. L. Ground State Nuclear Magnetic Resonance Chemical Shifts Predicts Charge-Separated Excited State Lifetimes. *Inorg. Chem*. **2018**, 57, 13470-13476.

13. Kamath, S. S.; Uma, V. and Srivastava, T.S. Neutral mixed-ligand complexes of Platinum(II) and Palladium (II) with α-diimine and dioxolenes. *Inorganica. Chimica Acta*. **1989**, 166, 91-98.

14. Cummings, S. and Eisenberg, R. Tuning the Excited-State Properties of Platinum (II) Diimine Dithiolate Complexes. *J. Am. Chem. Soc*. **1996**, 118, 1949-1960

15. Ito, A; Kobayashi, N. and Teki, Y. Low-Energy and Long-Lived Emission from Polypyridyl Ruthenium(II) Complexes Having a Stable-Radical Substituent. *Inorg. Chem*. **2017**, 56, 3794-3808.

16. The Orca 4.0.0.2 software program was used for CASSCF computations. The input files were generated using the molecular builder function in the Gaussview 03 software. The reduced spin orbit matrix elements (SOC matrix element) that connect the lowest triplet states and the electronic ground states were computed using CASSCF (4,3) method where a 4-electron-in-3-orbital (HOMO-1, HOMO and LUMO) active space was considered.

Appendices

Appendix A:

Experiments and Methods

A.1 Reagents : All the starting materials were purchaged from the commercial sources and used them directly without further purification. Potassium Tetrachloroplatinate(II) , 1,2-Benzenedithiol, 2-Ethoxyethanol, Tetrabutylammonium chloride, Lead(IV) oxide, 2-Phenylpyridine, 2-(2-thienyl)pyridine, GR ACS Anhydrous Methanol were purchased from Sigma-Aldrich.

A.2 Elemental Analysis: Elemental analysis were done by Robertson Microlit Laboratories.

A.3 High Resolution Mass Spectra : Most of the mass spectra were collected at University of New Mexico Mass Spectrometry Facility , Department of Chemistry and Chemical Biology. The mass spectra at UNM Mass Specrometry Facility were collected on Xevo G2 XS Quadrupole Time-of-Flight spectrometer coupled with Acquity UPLC H-Class plus Ultra Performance LC System . We also collected mass spectra from The University of Texas at Austin Mass Spectrometry Facility.

A.4 Electronic Absorption Spectra: Elecronic absorption spectra were collected on Hitachi U-4100 UV-Vis-NIR double beam spectrophotometer with 1 cm pathlength quartz cuvette. This spectrophotometer capable of scanning 250 and 3300nm wavelength region was calibrated with reference to the 656.10 nm line of deuterium. All absorption data

were collected using a 2.0 nm slit width. All absorption data were collected in 1 cm pathlength quartz cells and solution samples were prepared by dissolving the sample in respective solvents.

A.5 Electron Paramagnetic Resonanace (EPR): EPR spectra were collected on a Bruker EMX X-band EPR spectrometer with associated Bruker magnet control electronics and microwave bridges. Fluid solution X-band EPR data were collected using a microwave power of 20 dB or 30 dB. Sample solutions were prepared by dissolving the sample in dichloromethane at room temperature. The room temperature EPR data for ligands and complexes were simulated in MATLAB in the EasySpin program.

A.6 Nuclear Magnetic Resonance (NMR) Spectra: NMR were collected on Avance II 300 MHz NMR spectrophotometer. Chemical shift is referenced to Tetramethyl silane at 0.0 delta.

A.7 Time Resolved Electron Paramagnetic Resonance(TR-EPR) Spectra: TR-EPR spectra in dichloromethane were collected on Bruker EPR 200D-SRC X-band Spectrophotometer. These experiments were performed in collaboration with Prof. Art Van der Est, Department of Chemistry, Brock University, Canada.

A.8 Photoluminescence and Emission Lifetime measurements: photoluminescence and life time measurements were performed on an Edinburgh Instruments FLS980 Fluorimeter. The instrument response time for the FLS980 Fluorimeter is 0.6 ns. For lifetime measurements of solution samples, EPL-450 Picosecond pulsed diode laser with pulse width 92.8 ps was used. For 77K photoemission and lifetime measurements in liquid

nitrogen, samples were dissolved in butyro-nitrile and degassed for 15 minutes by purging a flow of nitrogen gass. The degassed samples were kept in a liquid nitrogen dewar throughout the measurements.

A.9 Variable Temperature Emission and Photoluminescence Lifetimes: Variable temperature emission and photoluminescence lifetimes of cyclometalated platinum dithiolates in polystyrene thin films (solid-solution form) were performed on Edinburgh Instruments FLS 980 Fluorimeter and Oxford cryostat.

Polystyrene thin film samples were prepared by dissolving the samples and the polystyrene beads in dichloromethane solvent. This mixture was then cast slowly over the glass slide. These films were allowed to dry for one day before being removed from the glass slide and then stored in the glove box for a few days. The thin films were mounted into the sample holder insert for an Oxford cryostat. The cryostat was placed inside an Edinburg FLS 980 fluorimeter and a transferline for liquid helium was connected to it. After the sample was properly secured to the end of the sample rod, it is inserted into the cryostat perpendicular to the beam path. The sample chamber was pumped and purged with helium before a helium tank was connected to the cryostat. The variable temperature photoemission measurements were performed using an Oxford temperature controller after the thin film samples were thermally equilibrated for a few minutes at the target temperature. A flash lamp was used for the emission lifetime measurements.

Appendix B

Synthetic Procedures and Characterization

B.1 $Bu_4N[(Ppy)Pt(bdt)]$

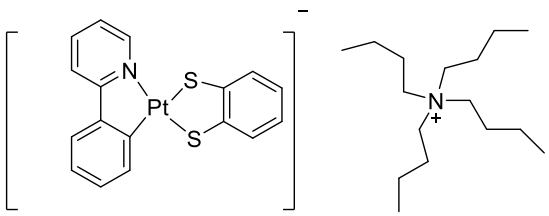

Synthetic procedure for this compound is based on the procedure described by Julia et. al. First, the precursor for this compound was synthesized. Potassium tetracholroplatinate(II) (0.5mmol, 207.5mg) and 2-phenylpyridine (1.2mmol, 186mg) were taken in a long neck flask and purged with nitrogen three times. Then, through a needle, the degassed 3:1 mixture of ethoxyethanol and water was added to the reaction mixture and heated at 80^0C for two days. After 2 days, water was added and yellow/orange precipitate was filtered. It was dried in air, and followed by in vacuum. This solid was washed several times with diethyl ether, cold DCM, and this precursor was directly used for the next step without further purification. This procedure was followed for the synthesis of precursors for all other cyclometalated complexes.

The precursor (108mg, 0.20mmole considering as monomer structure) was taken in a 100ml round bottom flask and degassed dichloromethane(20ml) was added to it. 1,2-Benzenedithiol (32mg , 0.22mmole) , Tetrabutylammonium chloride (61mg , 0.22mmol) and potassium hydroxide (25mg, 0.44mmol) in a 50ml round bottom flask and degassed 6 ml methanol was added to it . This solution was added to the flask containing the

precursor solution . The reaction mixture slowly turned to reddish orange in color over two hours at room temperature under nitrogen. Solvent was evaporated, the remaining solid was dissolved in DCM and filtered. The filtrate was evaporated to half and hexane was added to initiate precipitation of product. This precipitate was washed with diethyl ether and crystallized in diethylether/ DCM solution. Yield was 65% . High-resolution MS (ESI), [M]- : 489.0060; ^{1}H NMR (300 MHz, $CDCl_3$, TMS, 25^{0}C): δ = 9.25 (d, 1H), 7.96 (d, 1H), 7.70 (t,1H), 7.62 (d, 1H),7.48 (d, 1H), 7.43,(m, 1H), 7.34(m, 1H), 7.02(m, 2H), 6.91 (m, 1H), 6.58 (m, 2H), 2.93 (m, 8H), 1.04 (m, 8H), 0.97(m, 8H), 0.67 (m, 12H) . Proton NMR was consistent with the literature reported data.

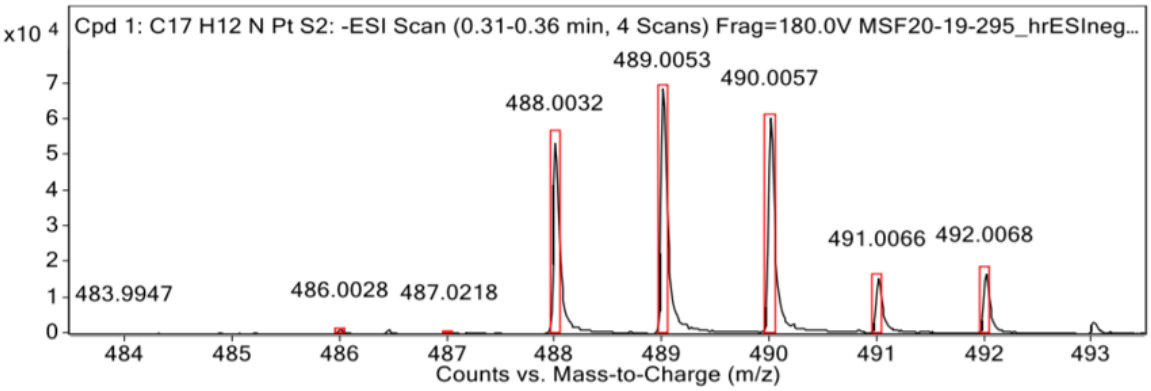

Figure B1: MS isotope pattern for [(Tpy)Pt(bdt)]$^{1-}$ complex

B.2 Bu_4N[(Tpy)Pt(bdt)]

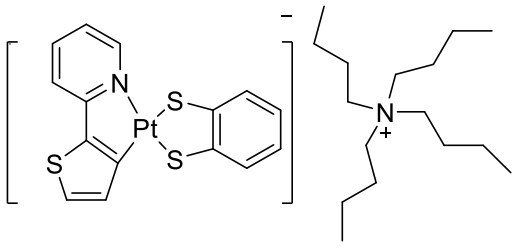

First, precursor was prepared by heating potassium tetrachloro platinate with 2-2.2 equivalents of 2-(2-thienyl)pyridine in a 1:3 mixture of water and 2-ethoxyethanol at 80^0C for two days, and a resulting yellow-orange solid was filtered, and dried in air. It was an insoluble solid and washed with diethyl ether, folllowed by cold dichloromethane and used for the next step without further purification.

This precursor (220mg, 0.40) in dichloromethane and a mixture of 1,2-Benzenedithiol (62mg , 0.44mmole) , Tetrabutylammonium chloride (122mg , 0.44mmol) and potassium hydroxide (49mg, 0.88mmol) in anhydrous methanol were mixed, and the reaction mixture color changed gradually to reddish orange color. The reaction was run for two hours, and solvent was then evaporated. The solid was then dissolved in dichloromethane and filtered. The filtrate was evaporated to one half, and hexane was added to initiate precipitation of product. This solid was washed several times with cold diethyl ether and chloroform. It was then crystallized in diethyl ether/dicholomethane solution and dried. Yield was 60%. High-resolution MS (ESI), [M]- : 494.9614; ^{1}H NMR (300 MHz, CDCl3, TMS, 250C): δ =9.03(d,1H), 7.58 (t, 1H), 7.49-7.46 (m, 2H), 7.35-7.32 (m, 2H), 6.73 (t, 1H), 6.60-6.57 (m, 3H), 2.70 (m, 8H), 1.095(m, 8H), 0.95 (m,8H), 0.68(m, 12H).

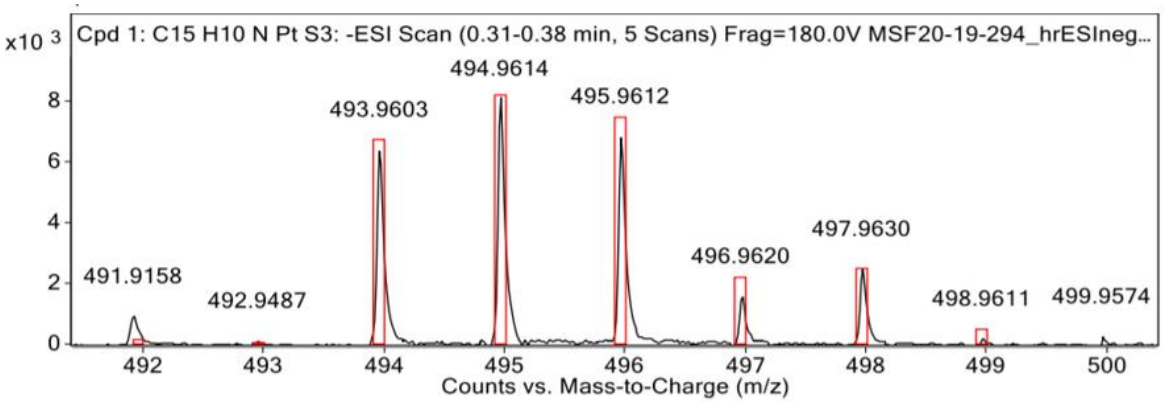

Figure B2: MS isotope pattern for $[(Ppy)Pt(bdt)]^{1-}$ complex.

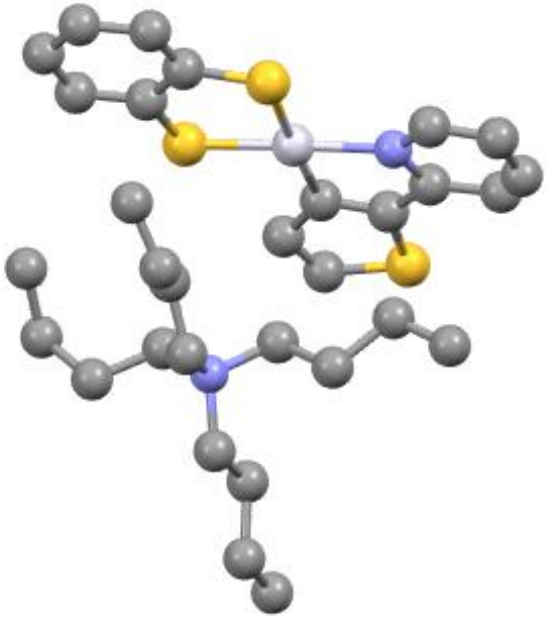

Figure B3: Crystal structure for $[(Tpy)Pt(bdt)]^{1-}$ complex (Crystallography at UNM facility).

B.3 Bu_4N[(PpyIN)Pt(bdt)]

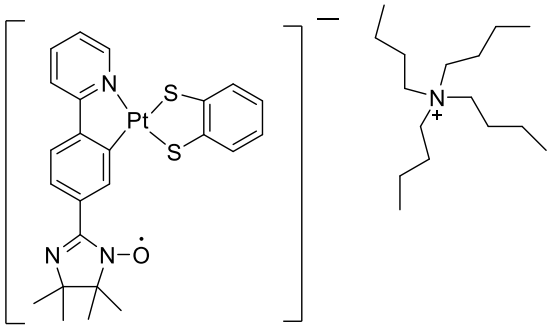

First, radical elaborated ligand (PpyNN) was synthesized. 4-(2-pyridyl) Benzaldehyde (PpyCHO) was mixed with 1.2 equivalents of BHA [(2,3-dimethyl-2,3-bis(hydroxyamino)butane] in anyhyrous methanol in a 50 ml round bottom flask and stirred for 4 days at room temperature . The volume of the solution was reduced and solid was filtered and washed several times with DCM to get a white solid. This solid was directly used for next reaction. This white solid was reacted with excess Pb(IV) oxide overnight to get a blue solution. It was filtered and a blue solution was evaporated off.The product was purified by column chromatography with 1:1 ethylacetate /hexane solvent mixture and collected as blue crystalline solid. The product was characterized by Mass and EPR specroscopy.

The precursor was synthesized as mentioned above by heating the mixture of potassium tetrachloroplatinate and cyclometalating ligand in a 3:1 ratio of 2-ethoxyethanol and water for 2 days and collected as yellowish orange solid. The precursor (60mg , 0.057mmole calculated as dimer formation) in dichloromethane and a mixture of 1,2-Benzenedithiol (16mg), tetrabutylammonium chloride (32mg) and potassium hydroxide (8mg) in anhydrous methanol were mixed and reaction mixture color was changed gradually to reddish orange color. The reaction was run for two hours and solvent was

evaporated. The solid was dissolved in dichloromethane, and filtered. The filtrate was evaporated to one half and hexane was added to get the precipitate. This solid was washed several times with cold diethyl ether and chloroform. It was then subjected to alumina column with 2% methanol and dichloromethane mixture.Yield was 33%. ESI MS : [M]- 628.093; EPR (X-Band, DCM, 298K): g= 2.0045, a_N= 25.8 MHz and 12.6MHz. Elemental analysis : calculated for $C_{40}H_{59}N_4OPtS_2.CH_2Cl_2$: C 51.51, H 6.43, N 5.86 found: C 51.38, H 5.94, N 5.63

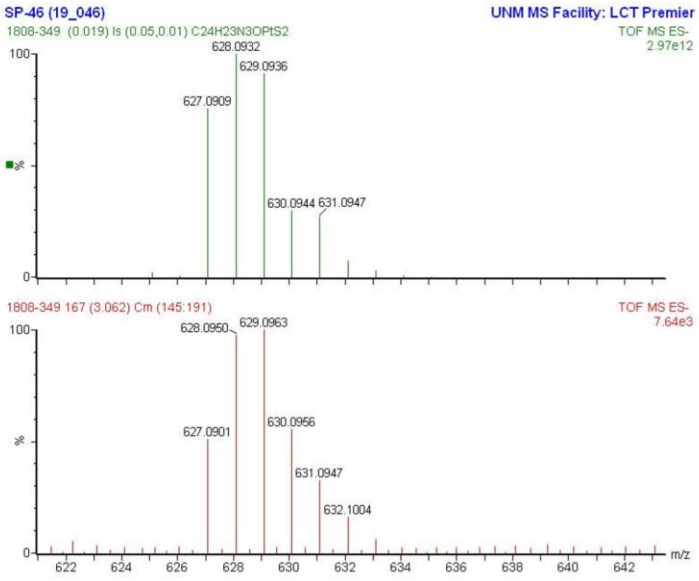

Figure B4: Mass spectra for $[(PpyIN)Pt(bdt)]^{1-}$ complex. Isotope pattern (computed above and experimental below)

B.4 Bu_4N[(PpyIN)Pt(Cat)]

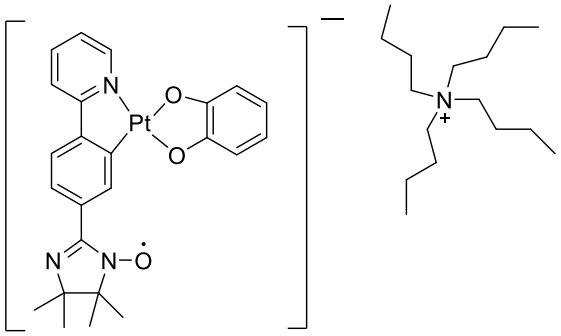

The precursor was synthesized by heating the mixture of Potassium tetracholroplatinate and cyclometalating ligand (PpyNN) in a 3:1 ratio of 2-ethoxyethanol and water for 2 days and collected as yellowish orange solid. The precursor (60mg , 0.057mmole calculated as dimer formation) in dichloromethane and a mixture of catechol (13mg), Tetrabutylammonium chloride (32mg) and potassium hydroxide (8mg) in anhydrous methanol were mixed and reaction mixture color was changed gradually to reddish orange color. The reaction was run for two hours and solvent was evaporated. Then, solid was disolved in dichloromethane and filtered. The filtrate was evaporated to one half and hexane was added to get the precipitate. This solid was washed several times with cold diethyl ether and chloroform. It was then subjected to alumina column with 2% methanol and dichloromethane mixture. Yield was 30%. ESI MS: [M]- 596.139; EPR (X-Band, DCM, 298K): g= 2.0046, a_N= 25.8 MHz and 12.6MHz. Elemental analysis: calculated for $C_{40}H_{59}N_4O_3Pt.CH_2Cl_2$: C 53.30, H 6.65, N 6.06 found: C 53.54, H 6.92, N 6.20

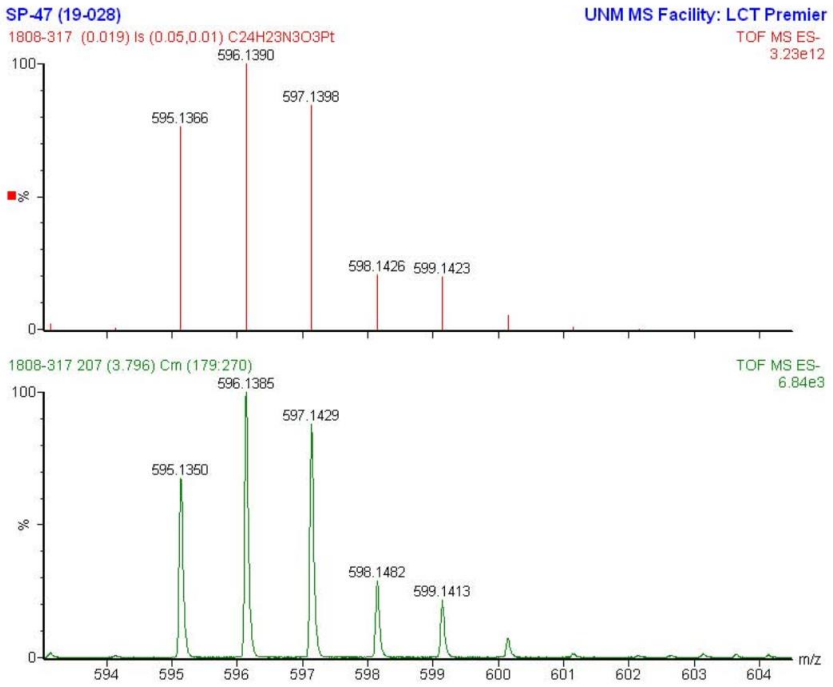

Figure B5: Mass spectra for $[(PpyIN)Pt(Cat)]^{1-}$ complex. Isotope pattern (computed above and experimental below)

B.5 Bu_4N[(TpyIN)Pt(bdt)]

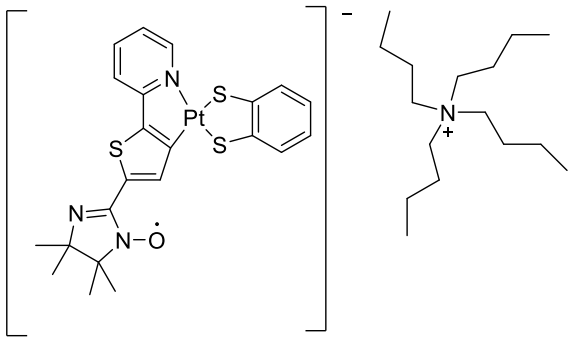

First, radical elaborated ligand (TpyNN) was synthesized. 5-(Pyridin-2-yl)thiophen-2-carboxyaldehyde (TpyCHO) was mixed with 1.2 equivalents of BHA [(2,3-dimethyl-2,3-bis(hydroxyamino)butane] in anyhyrous methanol in a 50 ml round bottom flask and stirred for 4 days at room temperature . The volume of the solution was reduced and solid

was filtered and washed several times with DCM to get a white solid. This solid was directly used for the next reaction. This white solid was reacted with excess Pb(IV) oxide overnight to get a green blue solution. It was filtered and the remaining solution was evaporated.The product was purified by column chromatography with 1:1 ethylacetate /hexane solvent mixture and collected as blue-green crystalline solid. The product was characterized by Mass and EPR spectroscopy.

The precursor was synthesized as mentioned above by heating the mixture of potassium tetrachloroplatinate and cyclometalating ligand in a 3:1 ratio of 2-ethoxyethanol and water for 2 days and collected as yellowish orange solid. The precursor (65mg , 0.06mmole calculated as dimer formation) in dichloromethane and a mixture of 1,2-Benzenedithiol (17.5mg), Tetrabutylammonium chloride (34mg) and potassium hydroxide (14mg) in anhydrous methanol were mixed and reaction mixture color changed gradually to red-orange color. The reaction was run for two hours and solvent was evaporated. Then, solid was disolved in dichloromethane and filtered. The filtrate was evaporated to one half and hexane was added to get the precipitate. This solid was washed several times with cold diethyl ether and chloroform. It was then subjected to alumina column with 2% methanol and dichloromethane mixture.Yield was 36%. ESI MS: [M]- 635.0574 ; EPR (X-Band, DCM, 298K): g= 2.0045, a_N= 25 MHz and 13 MHz, and elemental analysis : calculated (%) for $C_{38}H_{57}N_4OPtS_3.CH_2Cl_2$: C 48.69, H 6.18, N 5.82; found: C 49.12, H 6.21, N 5.56.

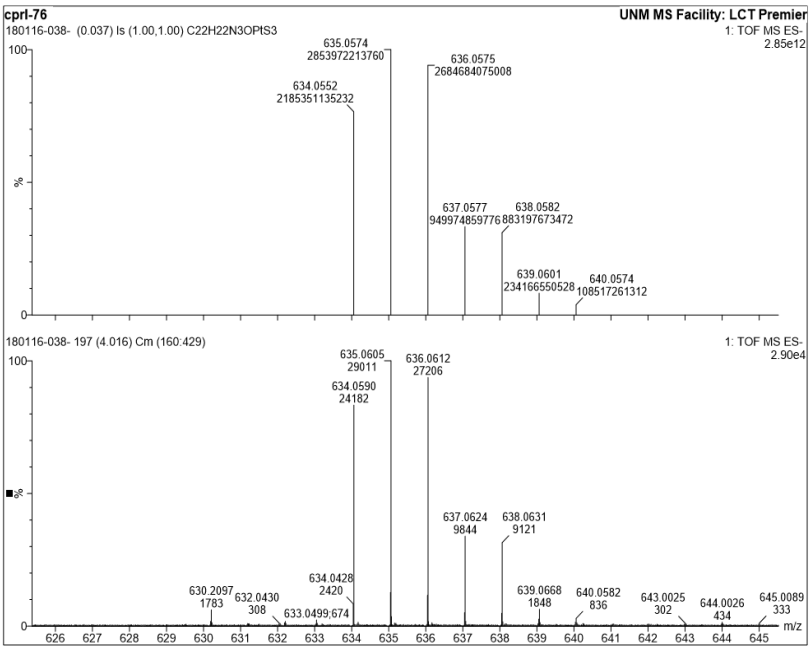

Figure B6: Mass spectra of $[(TpyIN)Pt(bdt)]^{1-}$: Isotope pattern (Computed above and experimental below)

B.6 $Bu_4N[(TpyIN)Pt(Cat)]$

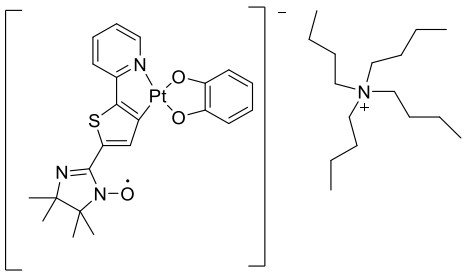

The precursor was synthesized as mentioned above by heating the mixture of potassium tetrachloroplatinate and cyclometalating ligand (TpyNN) in a 3:1 ratio of 2-ethoxyethanol and water for 2 days and collected as yellowish orange solid. The precursor (65mg , 0.06mmole calculated as dimer formation) in dichloromethane and a mixture of catechol

(13.2mg), Tetrabutylammonium chloride (34mg) and potassium hydroxide (14mg) in anhydrous methanol were mixed and reaction mixture color changed gradually to orange color. The reaction was run for two hours and solvent was evaporated. Then, solid was disolved in dichloromethane and filtered. The filtrate was evaporated to one half and hexane was added to get the precipitate. This solid was washed several times with cold diethyl ether and chloroform. It was then subjected to alumina column with 2% methanol and Dichloromethane mixture. Yield was 29%. ESI MS: $[M]^-$ 603.103 , EPR (X-Band, DCM, 298K): g= 2.0046, a_N= 26 MHz and 13 MHz, and Elemental analysis : calculated (%) for $C_{38}H_{57}N_4O_3PtS.CH_2Cl_2$: C 50.37, H 6.40, N 6.02 found: C 49.99, H 6.12, N 5.57.

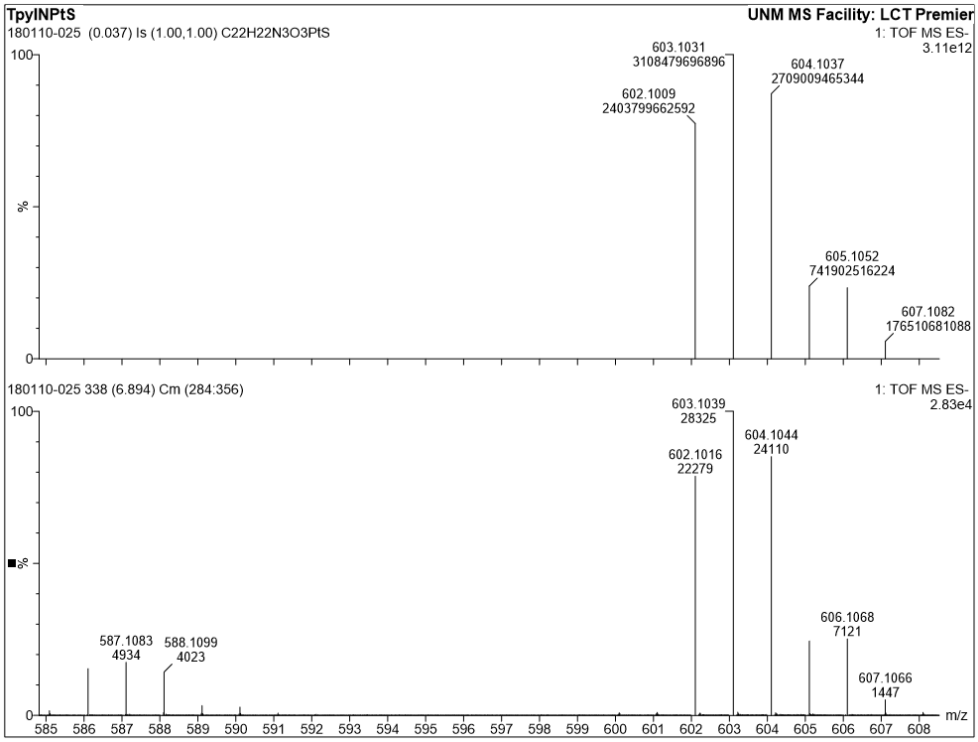

Figure B7: Mass spectra of $[(TpyIN)Pt(Cat)]^{1-}$: Isotope pattern (Computed above and experimental below)

B.7 (bpy)Pt(ND)

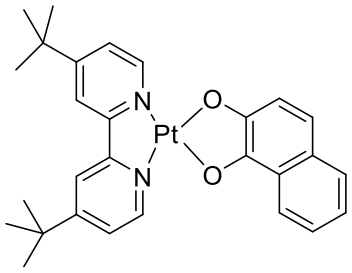

First, (t-Bu_2bpy) Pt(Cl_2), was prepared according to literature procedures. 4,4'-di-tert-butyl-2,2'-bipyridine (0.2 mmol) and potassium tetrachloroplatinate (0.2mmol) were mixed in a RB flask with 20ml (3MHCl) and refluxed overnight. A bright yellow precipitate was collected, filtered, and dried. It was then washed with water, ethanol, diethyl ether and hexane. It was used for the next reaction without further purification.

A mixture of 1,2-Naphthalenediol (0.5 mmol, 80mg) and potassium hydroxide (1.2 mmol, 67mg) were mixed in a flask with 1:1 mixture of degassed methanol and dichloromethane and stirred for 30 mins. This mixture was mixed with one equivalent of (t-Bu_2bpy) Pt(Cl_2) in dry methanol and refluxed for one day. Reaction mixture was cooled to room temperature and hexane was added to get the precipitate. This crude solid was subjected to column chromatography and eluted with 2% methanol in dichloromethane. Product was collected as blue-black solid. Yield was 60%. ESI-MS(m/z): calculated for$C_{28}H_{30}N_2O_2Pt$: 621.20 found: 621.19 $[M]^+$. ^1H NMR (300 MHz, $CDCl_3$, TMS, 25^0C): δ = 9.15 (d, 1H), 9.05(d,1H), 9.62 (d, 1H) , 7.52(S, IH), 7.42 (d,2H), 7.31 (m , 2H), 7.28 (m, 2H), 7.02 (m, 2H),

1.44 (s, 9H), 1.35 (s, 9H); Elemental analysis: calculated (%) for $C_{28}H_{30}N_2O_2Pt$: C 54.10, H 4.86,N 4.51 found C 54.07, H 4.71, N 4.21.

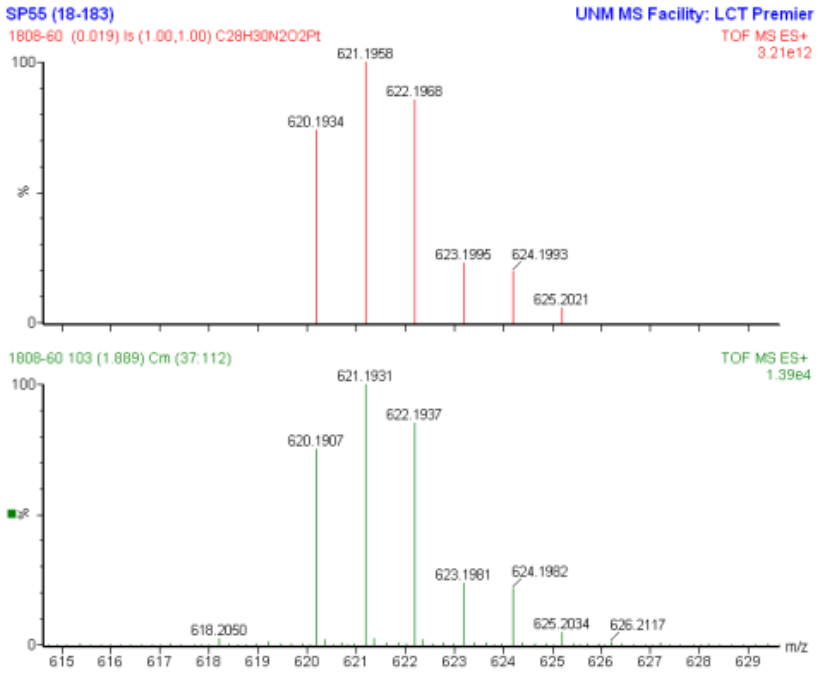

Figure B8: Mass spectra of (bpy)Pt(ND): Isotope pattern (Computed above and experimental below)

B.8 BHA [(2,3-dimethyl-2,3-bis(hydroxyamino)butane]

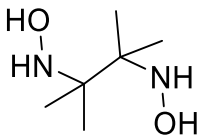

BHA was synthesized following a reported procedure (J. Org. Chem. 2014,69,475). A mixture of aluminium foil (4.25mmol, 115mg) and 3% aqueous mercuric chloride (2.5ml , 0.28mmol) was stirred for 5 mins at room temperature. Then, liquid was removed and

solid portion was washed with water and THF three times. This aluminium amalgam was covered with 10ml THF and 1ml water and cooled to 0^0C. 2,3-dimethyl-2,3-dinitrobutane (0.149g, 0.85mmol) in 12 ml THF was added to it and stirred for 2 hours. It was filtered on celite and the filtrate was evaporated to get white solid. It was washed with cold methanol to get the product (61%). This is used as precursor for the synthesis of radical ligand.

Appendix C

Computational

DFT and TDDFTcalculations were done using a hybrid functional, B3LYP, and TZVP basis set for the all atoms in the complexes. For CASSCF calculations the Zeroth Order Relativistic Approximations (ZORA) was used for the transition metals for all complexes. For all radical-elaborated complexes, the spin unrestricted B3LYP hybrid functional was employed using the ORCA 4.0.0.2 program package. The molecule builder function in the Gaussview 03 software package was used in generation of input files for all calculations.

XYZ-coordinates:

$[(PpyIN)Pt(bdt)]^{1-}$

```
* xyz -1 2 (charge and Multiplicity)

  C       0.980033      3.154186      0.018450
  C       3.323982      2.927038      0.063443
  C       3.507613      4.299868      0.060446
  C       2.380895      5.136836      0.034173
```

C	1.123369	4.551877	0.013521
H	4.170397	2.238797	0.083764
H	4.520667	4.702584	0.078697
H	2.488923	6.223023	0.031049
H	0.225983	5.171111	-0.005684
C	3.942164	-2.070989	-0.019020
C	5.126009	-2.836434	-0.050020
C	2.693784	-2.744655	-0.010672
C	5.084987	-4.227455	-0.070919
H	6.084737	-2.311496	-0.057347
C	2.667998	-4.153046	-0.031505
C	3.847022	-4.891723	-0.061587
H	6.016358	-4.798550	-0.094913
H	1.698396	-4.658164	-0.024179
H	3.805841	-5.983357	-0.078158
N	2.101060	2.345152	0.041664
Pt	1.752122	0.329110	0.035618
C	-0.145665	1.000030	0.032196
C	-1.342872	0.263940	0.042882
C	-0.271085	2.425277	0.007685
C	-2.606151	0.878972	0.005948
H	-1.312155	-0.827255	0.076335
C	-1.536267	3.044170	-0.026863
C	-2.697969	2.290192	-0.038468
H	-1.617716	4.134419	-0.050022
H	-3.671989	2.772388	-0.087176
C	-3.794610	0.018236	0.052482
C	-6.077249	-0.611393	-0.041676
C	-5.117985	-1.814931	0.257810
N	-5.053703	0.417959	-0.442875
N	-3.808824	-1.191982	0.544286
O	-5.386081	1.517412	-0.993110
C	-7.092368	-0.794233	-1.163366
H	-7.848907	-1.536269	-0.869196
H	-7.596739	0.162575	-1.358454
H	-6.621532	-1.124925	-2.097198
C	-6.778416	-0.048431	1.204977
H	-7.225852	0.922679	0.947528
H	-7.576467	-0.721329	1.549421
H	-6.068311	0.105206	2.028776
C	-4.904958	-2.723355	-0.968867
H	-4.101437	-3.435763	-0.738881
H	-5.815791	-3.287468	-1.221732
H	-4.591269	-2.140826	-1.846287
C	-5.537892	-2.681241	1.447469
H	-6.512528	-3.162958	1.270814
H	-4.785428	-3.468316	1.595682

```
  H      -5.594533     -2.099738      2.375939
  S       1.187998     -1.848200      0.021982
  S       4.003633     -0.325530      0.006000
*
```

[(TpyIN)Pt(bdt)]$^{1-}$

```
* xyz -1 2

  Pt     -1.791092      0.330667     -0.005692
  C       0.203426      0.543316     -0.000578
  N      -1.655503      2.393473      0.030616
  S      -4.121465      0.220756      0.000542
  S      -1.732176     -1.914610     -0.041049
  C      -0.365004      2.907220      0.050252
  C      -2.692805      3.258470      0.037729
  C      -2.531852      4.635967      0.064713
  C      -1.231586      5.169404      0.086207
  C      -0.153223      4.299493      0.078871
  C       0.625243      1.884461      0.034450
  S       2.353970      2.082172      0.050659
  C       2.553728      0.346263      0.008810
  C       1.332820     -0.319172     -0.017225
  C       3.904496     -0.161996      0.012197
  N       4.975432      0.586131      0.138106
  C       6.168246     -0.261805     -0.072192
  C       5.663509     -1.728460      0.166177
  N       4.197912     -1.530182     -0.121136
  C       6.221076     -2.816470     -0.743702
  C       5.751696     -2.181082      1.632416
  C       6.624522     -0.022233     -1.524873
  C       7.286900      0.181734      0.873717
  O       3.394013     -2.506770     -0.251163
  C      -4.463078     -1.491856     -0.020622
  C      -3.404742     -2.436939     -0.038214
  C      -3.707229     -3.813303     -0.053161
  C      -5.025580     -4.257433     -0.050820
  C      -6.075860     -3.323656     -0.033800
  C      -5.792835     -1.961449     -0.019235
  H      -2.881392     -4.529529     -0.066421
  H      -5.239284     -5.328787     -0.062067
  H      -7.114493     -3.663167     -0.031726
```

```
  H      -6.603906     -1.228880     -0.005667
  H      -3.683177      2.800427      0.020695
  H      -3.413471      5.277067      0.068604
  H      -1.071717      6.249123      0.107677
  H       0.872345      4.672197      0.093826
  H       1.277973     -1.405777     -0.050338
  H       6.118553     -2.562101     -1.805549
  H       5.671920     -3.752038     -0.567354
  H       7.284757     -2.987631     -0.522734
  H       5.155690     -3.096490      1.755084
  H       5.352052     -1.414561      2.310113
  H       6.791446     -2.396781      1.917009
  H       8.191626     -0.431884      0.738360
  H       6.978322      0.128203      1.925028
  H       7.543366      1.228036      0.655583
  H       7.554550     -0.563303     -1.758243
  H       5.847841     -0.325388     -2.240703
  H       6.801440      1.053523     -1.661795
*
```

[(PpyIN)Pt(Cat)]$^{1-}$

```
* xyz -1 2
  C       1.368187     -2.953127     -0.026789
  C       3.684280     -2.457510     -0.035123
  C       4.014656     -3.803107     -0.032710
  C       2.986694     -4.759908     -0.026939
  C       1.667631     -4.322900     -0.023664
  H       4.430597     -1.661348     -0.037859
  H       5.065263     -4.094720     -0.034995
  H       3.216797     -5.826827     -0.025000
  H       0.845682     -5.039852     -0.018815
  C       3.755622      2.023636      0.018982
  C       4.887435      2.860926      0.050325
  C       2.451701      2.622429      0.010260
  C       4.740937      4.250706      0.069374
  H       5.876332      2.394973      0.058261
  C       2.323611      4.020305      0.028851
  C       3.463067      4.830169      0.058827
  H       5.628741      4.888012      0.093159
  H       1.319170      4.450544      0.020661
  H       3.354789      5.917403      0.073993
  N       2.399461     -2.026973     -0.032608
  Pt      1.899844     -0.118323     -0.029275
  C       0.097870     -0.903197     -0.041291
  C      -1.130825     -0.225191     -0.054373
```

```
  C       0.060806     -2.333952     -0.027760
  C      -2.355490     -0.916028     -0.030809
  H      -1.144600      0.865760     -0.077079
  C      -1.164135     -3.025013     -0.010087
  C      -2.365347     -2.331552     -0.001271
  H      -1.183791     -4.118747      0.002528
  H      -3.313057     -2.864393      0.037337
  C      -3.594793     -0.126310     -0.071769
  C      -5.903635      0.371505      0.028293
  C      -5.013600      1.633132     -0.245955
  N      -4.825413     -0.606646      0.409823
  N      -3.671768      1.091077     -0.545368
  O      -5.101878     -1.740335      0.931025
  C      -6.927655      0.476131      1.152259
  H      -7.725164      1.180800      0.873946
  H      -7.377086     -0.511330      1.328119
  H      -6.475305      0.812418      2.093239
  C      -6.573658     -0.202656     -1.230465
  H      -6.968941     -1.201087     -0.992842
  H      -7.405725      0.433784     -1.564108
  H      -5.854885     -0.302937     -2.055181
  C      -4.850771      2.523931      1.001504
  H      -4.096638      3.292633      0.785103
  H      -5.793725      3.021856      1.275783
  H      -4.493277      1.940399      1.861300
  C      -5.487478      2.501939     -1.413516
  H      -6.491255      2.914502     -1.224416
  H      -4.786642      3.338968     -1.539897
  H      -5.507476      1.942154     -2.356850
  O       3.828636      0.698780     -0.002225
  O       1.385945      1.811522     -0.012696
*
```

[(TpyIN)Pt(Cat)]$^{1-}$

```
* xyz -1 2
  Pt     -1.959047      0.152545     -0.012740
  C      -0.025328      0.475233     -0.028592
  N      -1.972570      2.139840     -0.029137
  C      -0.735891      2.784498     -0.037137
  C      -3.100602      2.886517     -0.031032
  C      -3.077212      4.273388     -0.040461
  C      -1.839060      4.940524     -0.048329
  C      -0.672736      4.187738     -0.046425
  C       0.330460      1.840653     -0.035467
```

```
  S       2.042553     2.123427    -0.041347
  C       2.329467     0.393948    -0.037470
  C       1.142764    -0.332929    -0.033626
  C       3.701068    -0.048764    -0.026656
  N       4.742717     0.736416     0.096809
  C       5.971283    -0.061217    -0.100814
  C       5.528606    -1.545897     0.146165
  N       4.058205    -1.411153    -0.149839
  C       6.135050    -2.615507    -0.754096
  C       5.630029    -1.983752     1.615986
  C       6.426794     0.187316    -1.552044
  C       7.062310     0.437586     0.849910
  O       3.296612    -2.416024    -0.280031
  C      -4.287846    -1.437480     0.027775
  C      -3.186561    -2.349460     0.026657
  C      -3.423621    -3.731263     0.045989
  C      -4.735487    -4.220940     0.066822
  C      -5.817994    -3.332029     0.068249
  C      -5.596791    -1.949807     0.048839
  H      -2.564344    -4.406753     0.044460
  H      -4.910899    -5.299556     0.081951
  H      -6.841342    -3.716175     0.084686
  H      -6.431102    -1.243054     0.049892
  H      -4.026800     2.308964    -0.024076
  H      -4.019491     4.821719    -0.041607
  H      -1.793472     6.030995    -0.055833
  H       0.307588     4.667678    -0.052303
  H       1.131254    -1.420583    -0.037304
  H       6.025320    -2.373644    -1.818152
  H       5.627480    -3.573151    -0.572257
  H       7.204300    -2.738857    -0.528615
  H       5.080178    -2.927083     1.743200
  H       5.190178    -1.233788     2.287147
  H       6.677659    -2.146247     1.906749
  H       7.991519    -0.141565     0.730607
  H       6.745408     0.383789     1.898642
  H       7.279277     1.490581     0.622042
  H       7.381841    -0.313499    -1.773029
  H       5.670263    -0.155491    -2.271524
  H       6.556942     1.268683    -1.696565
  O      -4.012234    -0.132554     0.009680
  O      -1.942441    -1.838715     0.007378
*
```

(bpy)Pt(ND)

```
* xyz 0 1
  C      -5.395649      0.879486     -0.181242
  C      -4.010104      1.025441     -0.224937
  C      -3.454633      2.289616     -0.234982
  C      -4.298855      3.402355     -0.200908
  C      -5.662405      3.212041     -0.158204
  C      -6.115942     -0.380013     -0.165797
  C      -5.539348     -1.648804     -0.192332
  C      -6.347068     -2.768652     -0.173371
  C      -7.733798     -2.604665     -0.127719
  C      -8.260649     -1.332207     -0.102757
  H      -3.378433      0.149348     -0.250675
  H      -2.380897      2.413845     -0.268752
  H      -3.902939      4.407844     -0.207407
  H      -6.374175      4.025751     -0.130238
  H      -4.464250     -1.749459     -0.227627
  H      -5.909869     -3.757548     -0.193690
  H      -8.399671     -3.455628     -0.111658
  H      -9.322570     -1.131422     -0.067314
  N      -7.474128     -0.240986     -0.121166
  N      -6.203766      1.980379     -0.148447
  Pt     -8.159300      1.626463     -0.087468
  C     -10.821555      2.348288      0.002911
  C     -12.237981      2.327877      0.048788
  C     -10.129033      3.556876     -0.012642
  C     -12.978603      1.124000      0.065983
  C     -12.934040      3.577217      0.078531
  C     -10.825440      4.780370      0.016912
  C     -14.350000      1.145947      0.110659
  H     -12.439687      0.186512      0.043129
  C     -14.346475      3.557027      0.124288
  C     -12.196684      4.788150      0.061475
  H     -10.255474      5.701109      0.003630
  C     -15.042663      2.374032      0.140158
  H     -14.876508      4.502457      0.146887
  H     -12.735746      5.727353      0.084316
  O     -10.095197      1.219665     -0.027054
  O      -8.786128      3.502547     -0.056660
  H     -16.124943      2.380686      0.175348
  H     -14.906397      0.216702      0.123429
*
```

Appendix D

Cyclometalating ligands

(PpyNN and TpyNN ligands)

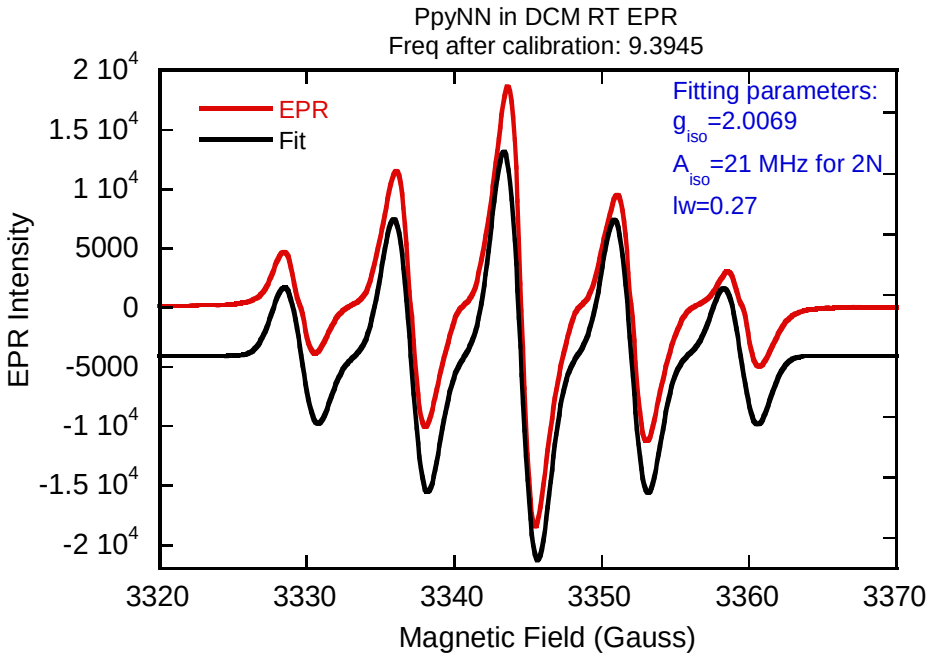

Figure D1: Room temperature X-band EPR spectra of PpyNN in DCM

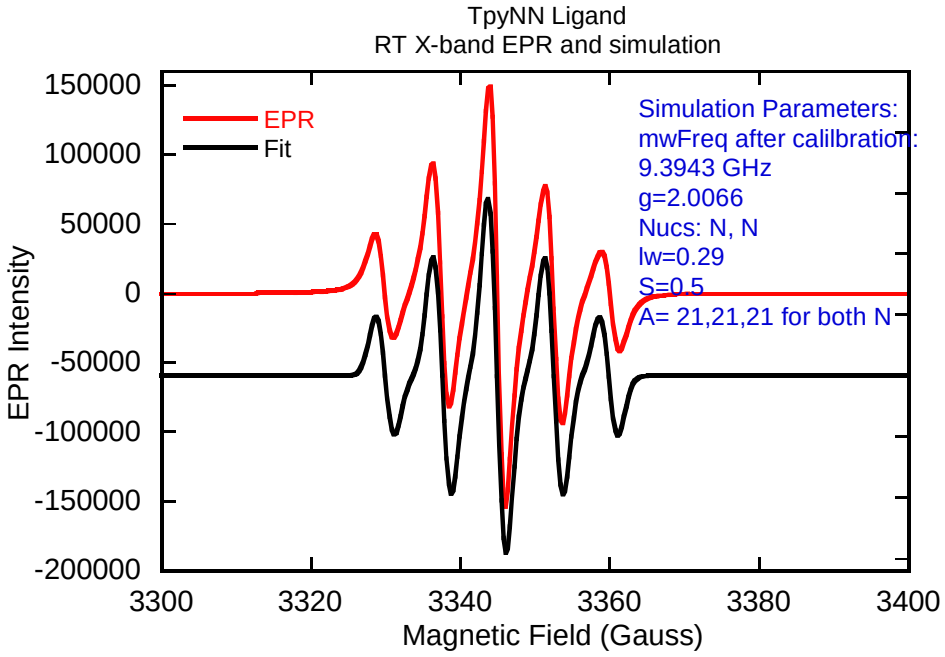

Figure D2: Room Temperature X-band EPR spectra of TpyNN in DCM

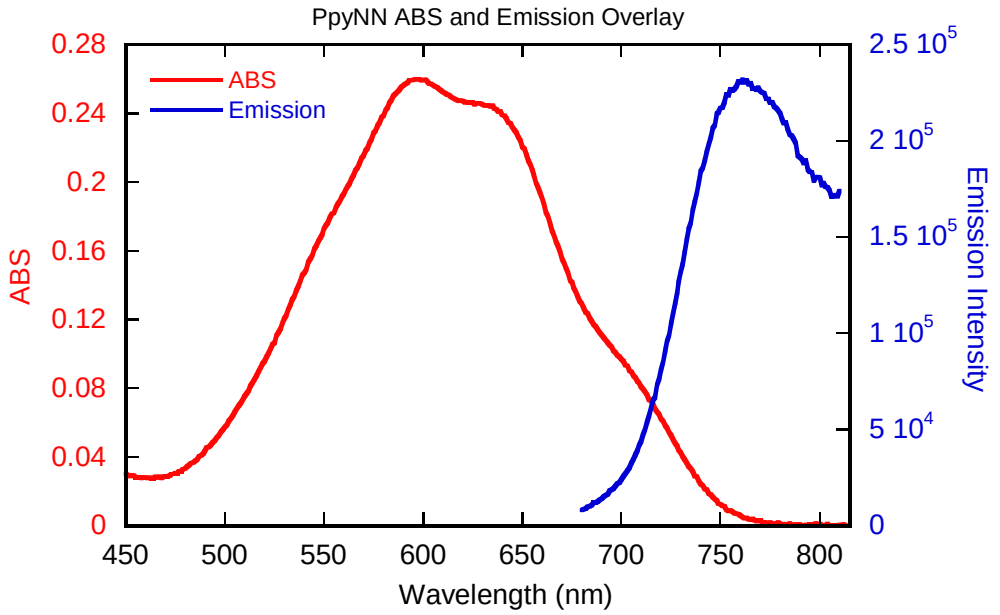

Figure D3: Room temperature absorption and emission overlay of PpyNN in DCM

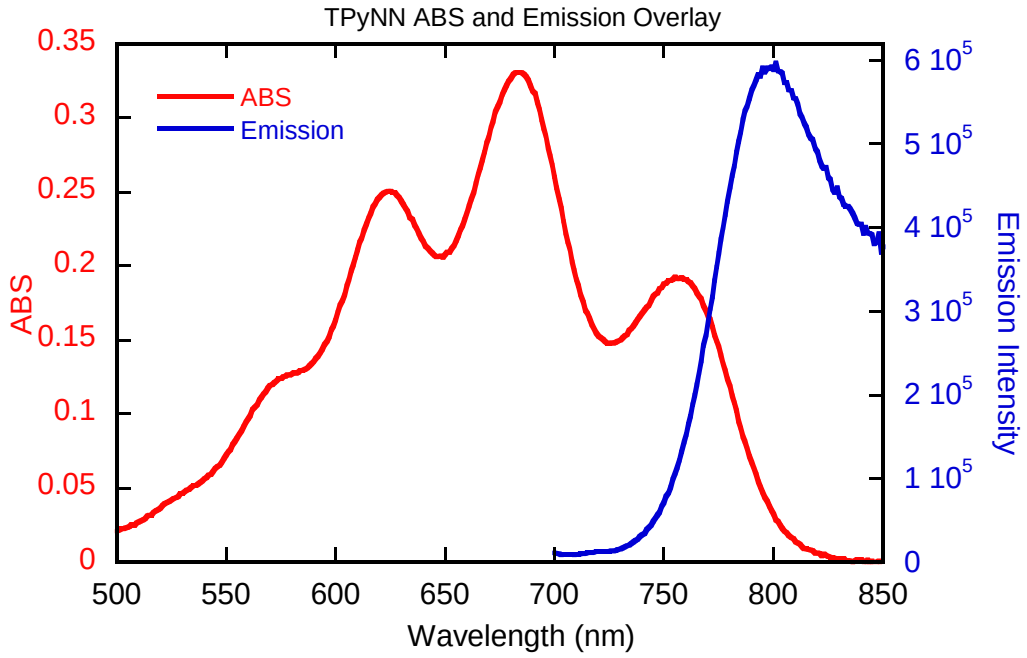

Figure D4: Room temperature absorption and emission overlay of TpyNN in DCM

Appendix E

UV-Vis and Emission data of platinum complexes.

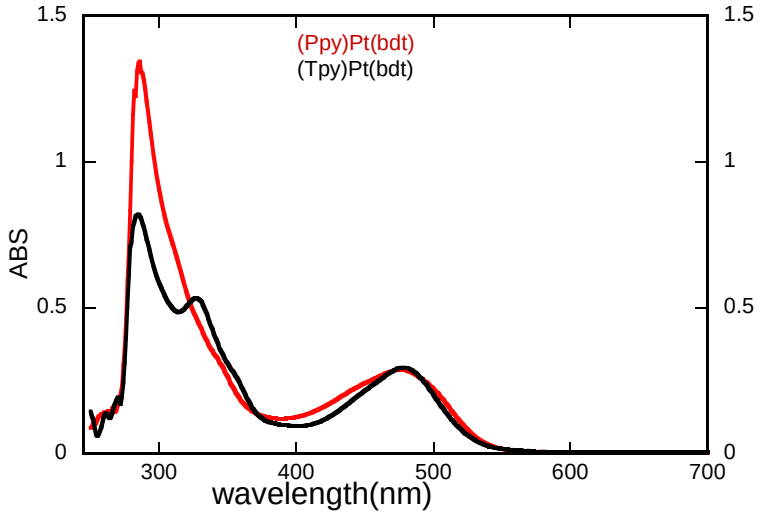

Figure E1: Overlay of RT absorption spectra of $[(Tpy)Pt(bdt)]^{1-}$ (black) and parent $[(Ppy)Pt(bdt)]^{1-}$ (red) .

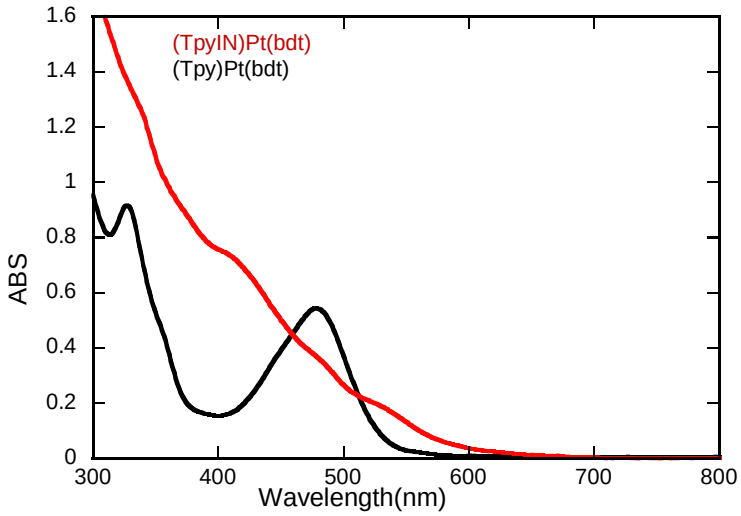

Figure E2: Overlay of RT absorption spectra for parent molecule $[(Tpy)Pt(bdt)]^{1-}$(black) and radical elaborated molecule $[(TpyIN)Pt(bdt)]^{1-}$ (red).

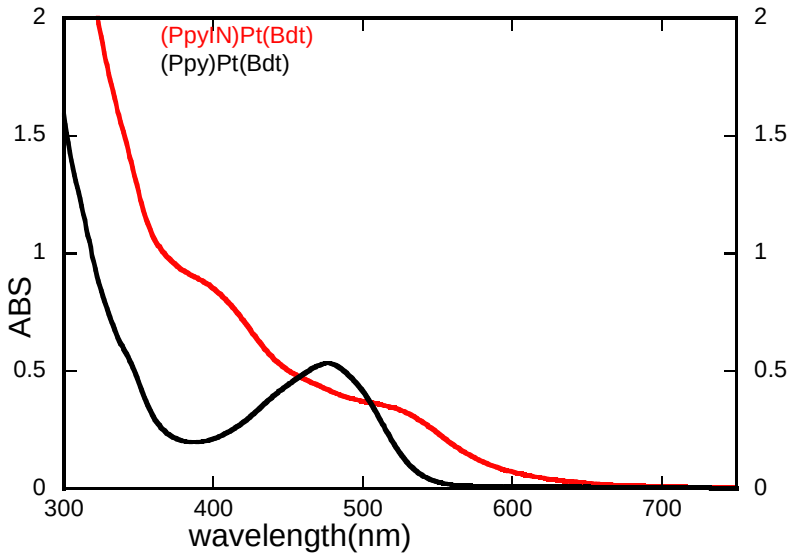

Figure E3: Overlay of RT absorption spectra for parent molecule $[(Ppy)Pt(bdt)]^{1-}$ (black) and radical elaborated molecule $[(PpyIN)Pt(bdt)]^{1-}$ (red).

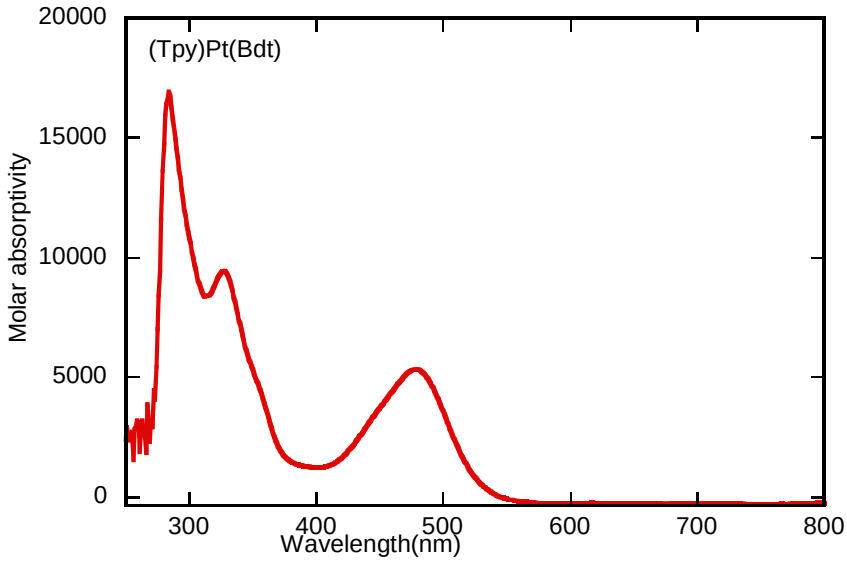

Figure E4: Room temperature absorption spectrum of Parent $[(Tpy)Pt(bdt)]^{1-}$

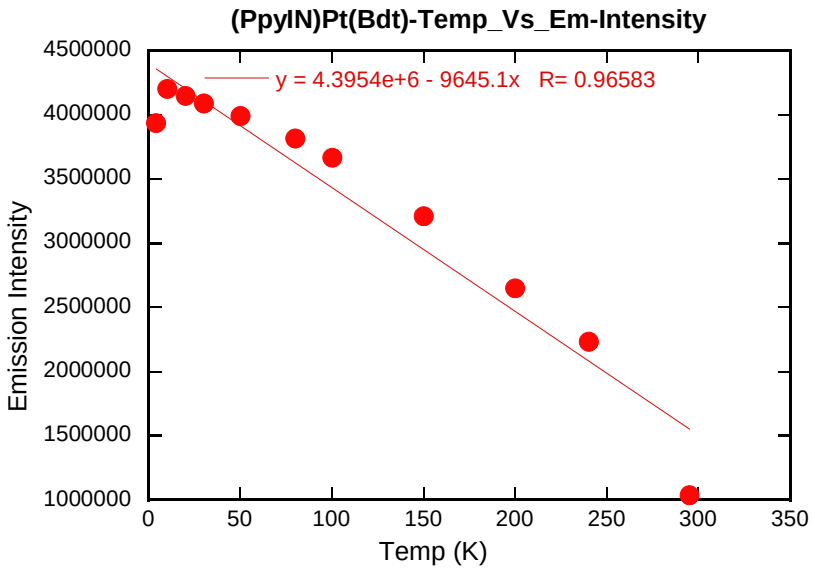

Figure E5: Emission intensity vs Temperature plot for $[(PpyIN)Pt(bdt)]^{1-}$ in a polystyrene thin film.

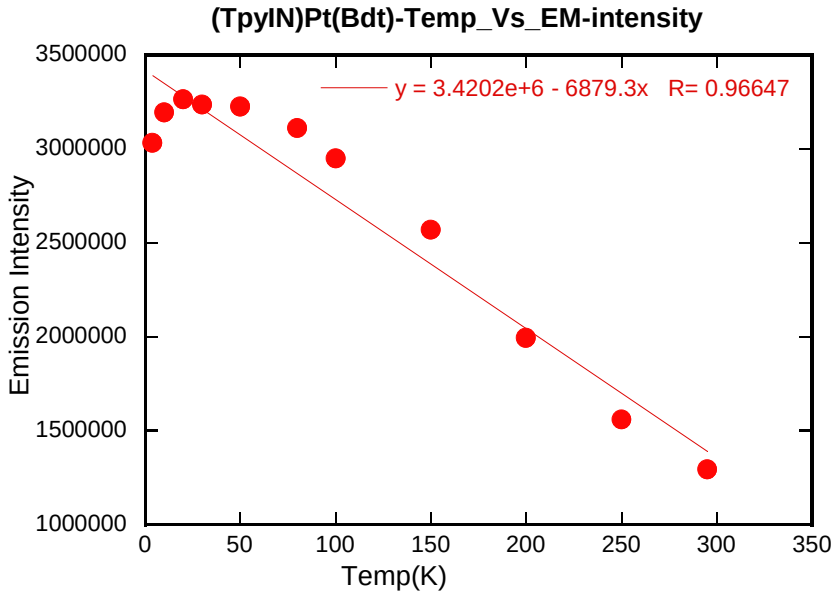

Figure E6: Emission intensity vs Temperature plot for $[(TpyIN)Pt(bdt)]^{1-}$ in a polystyrene thin film.